CRANFIELD INSTITUTE OF TECHNOLOGY

SCHOOL OF INDUSTRIAL AND MANUFACTURING SCIENCE

PhD Thesis

ACADEMIC YEAR 1991/2

JULIET M. EVANS

THE EFFECT OF NICKEL PLATING ON HYDROGEN EMBRITTLEMENT OF HIGH STRENGTH STEEL.

SUPERVISOR M. J. ROBINSON

JULY 1992

ACKNOWLEDGEMENTS

The author would like to express thanks to Mike Robinson who supervised her work for this thesis. His help, advice and support were highly valued.

Thanks are also due to Chris Smith and Peter Lane for helpful and interesting discussion, and to their employers, the Defence Research Agency, for the support of this project.

Many technical and support staff at Cranfield have given valuable assistance during the author's time at the School of Industrial and Manufacturing Science and she is grateful for many kindnesses shown and help given. In particular, the author would like to express her gratitude to Freda Parsons who was responsible for the preparation of this thesis.

Finally, acknowledgement is due to family and friends for their encouragement, forbearance and support over the past few years.

ABSTRACT

The microstructure of high strength steel is susceptible to delayed failure caused by the absorption of hydrogen produced either during cathodic charging or electroplating. When 0.8%C and AISI 4340 steel are subjected to constant load testing, a wide range of failure times is observed. By applying Weibull statistics small changes in experimental parameters such as heat-treatment are detected readily and are explained in the terms of hydrogen trapping at microstructural defects.

During the electroplating of steel in a double-cell, quantitative measurements are made of the amount of hydrogen permeated. Current densities are measured in the range 2 - 40 $mAcm^{-2}$ and it is shown that, although the lowest current density produces the most mechanically sound plate, it also causes the largest amount of hydrogen absorption. The nickel deposit is found to act as a reservoir for reversibly trapped hydrogen allowing diffusion to continue into the steel after the cessation of plating.

Permeation measurements were taken on AISI 4340 steel using an electrochemical probe developed from the Barnacle Electrode. The effects of cathodically charging and electroplating with nickel are compared. Exposure of the steel to the atmosphere is shown to have an important influence on the hydrogen content after a period of time due to a limited occurrence of corrosion. Various post-plating treatments are commonly used to remove a damaging concentration of hydrogen and the quantitative effects of such treatments are described.

Finally, a mathematical model is proposed which explains the reason for the wide spread of delayed failure times. It is found that if the stress intensity necessary to initiate a crack is known and, provided either the nominal stress or the crack size is known, it is possible to calculate either the allowable defect size or the allowable stress below which cracking is not expected to occur.

CONTENTS

LIST OF FIGURES

LIST OF TABLES

CHAPTER ONE.

INTRODUCTION

Despite hydrogen being one of the most studied elements, the mechanism by which it influences the mechanical properties of iron and steel is still not fully understood.

It is known that hydrogen may enter steel from several sources during manufacture and preparation for use when it is exposed to many processes including chemicals, pickling, welding, corrosion, cathodic protection, electroplating and other processes. Mechanical damage may be caused by the presence of, or interaction with, this hydrogen; damage which may be classified into four main areas as suggested by Fontana and Green (Corrosion Engineering)- blistering, decarburization (removal of carbon from steel), attack (the interaction between hydrogen and component of an alloy at high temperatures) and embrittlement.

The hydrogen exists in the metal in two distinguishable forms. The first, usually present in high concentrations, may be innocuous as it is trapped at grain boundaries, dislocations, interstitial atoms and carbide interfaces. It is believed that the second form, mobile interstitial hydrogen, can diffuse to internal defects and sites of high triaxial stress where it may be responsible for hydrogen embrittlement by influencing the fracture mechanism (Townsend, 1981).

Embrittlement is known to occur mainly in high strength steels, such as AISI 4340 which is used in the aerospace industry. The tendency for embrittlement, which increases with the hydrogen content of the metal, is linked with the fact that high strength steels are subjected to

high stresses, thus cracking is likely to occur more rapidly.

A common de-embrittling treatment for electroplated steel is to bake for several hours in the range 150 - 200°C whereupon promotion of removal of hydrogen from the surface occurs by permeation. However, depending on the temperature, some of the reversibly trapped hydrogen may become mobile, diffuse to sites of significant internal defects, and cause more damage (Robinson and Sharp, 1986). The same de-embrittling treatment for cathodically charged steel, such as AISI 4340, results in lower susceptibility to fracture as the baking time increases (See Figure 1.1 - reproduced from Fontana and Green).

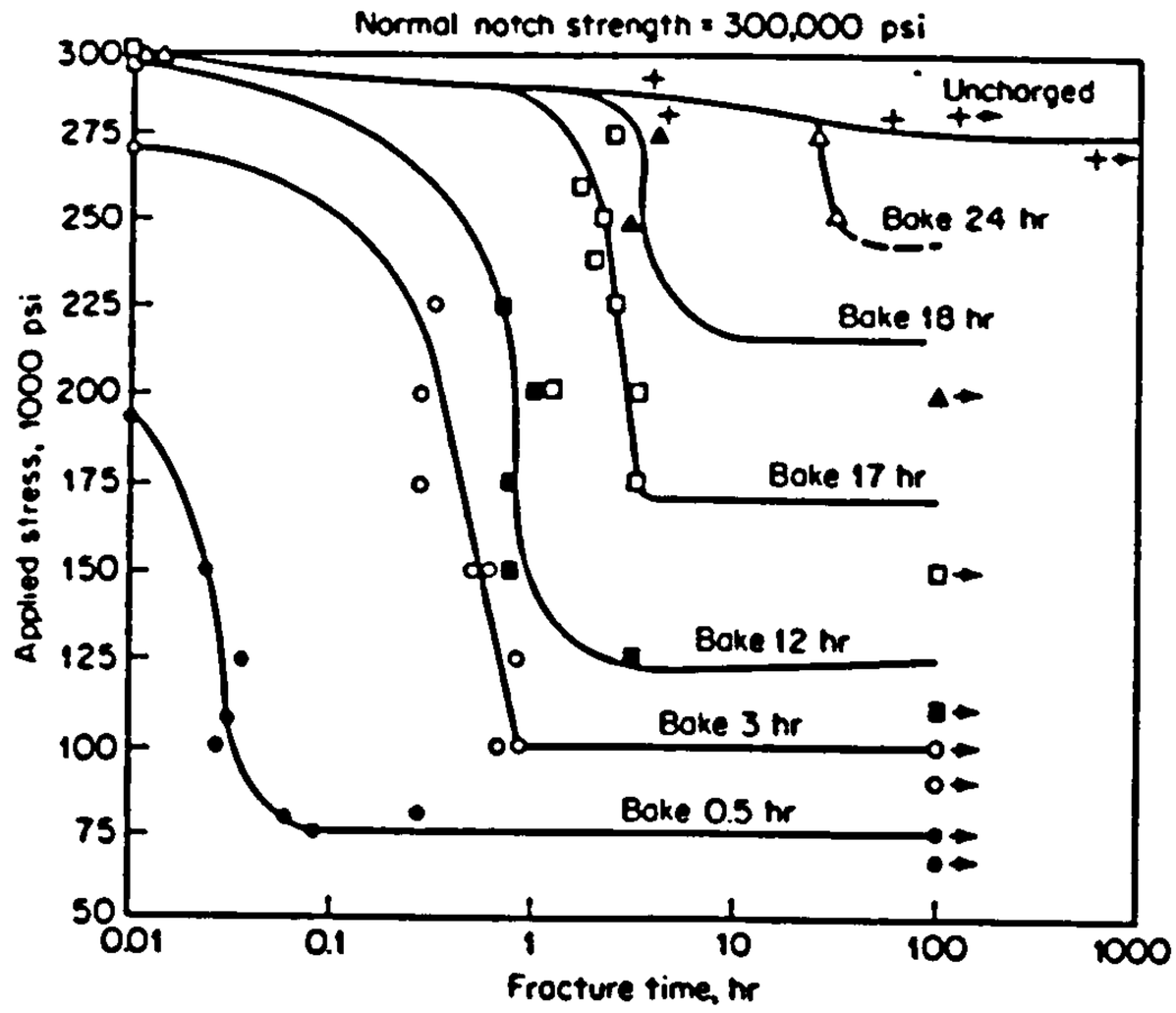

FIG. 1.1 Static fatigue curves for various hydrogen concentrations obtained by baking AISI 4340 steel at 300°F

Electroplating processes generally have a current efficiency in the range of 90 - 95% in terms of the mass of metal deposited. Whilst the electroplating, or cathodic charging current is being passed, hydrogen is discharged and some enters the metal. Cathodic charging of steel results in the ingress of high concentrations of hydrogen

whereas nickel plating is not generally considered to be a cause of severe hydrogen embrittlement when compared with plating with cadmium or with cathodic charging.

However, embrittlement can occur and this thesis investigates various aspects of the effects of heat-treatment, cathodic charging, electroplating and post-plating baking on hydrogen absorption and embrittlement in high strength steels.

Constant load testing continues work done previously by Robinson and Sharp (1986) on a high carbon (0.8%) steel and adapts their techniques for use with AISI 4340 (0.4%C) steel. Weibull plots display the distribution of failure times indicating the probability, P_s, of a specimen surviving for a specific time. Materials were tested in the as-quenched condition and stressed to 90% σ_f. The effects of cathodic charging in sulphuric acid and plating for 2 hours at 5 $mAcm^{-2}$ in a nickel single salt solution are compared.

The current density used during electroplating is shown to have an important influence on the amount of hydrogen absorbed by the metal. Permeation studies indicate that within the typical range of plating conditions it is clear that the lower current densities are responsible for promoting greater hydrogen absorption.

These permeation studies fall into two sections: the first series looked at the permeation transients obtained during and after nickel plating a low carbon (0.04%) steel shim using the double-cell technique pioneered by Devanathan and Stachurski in 1962. Also investigated were the permeation of hydrogen produced by cathodically charging the shim and the hydrogen permeated when plating nickel sheet with nickel. Surface hydrogen

concentrations, C_0, were compared for electroplating and cathodic charging, enabling determination of the susceptibility of steel to embrittlement after being subjected to a range of heat treatment conditions.

The second series used the novel variation of the Barnacle Electrode first used by Nanis in 1964 and then further developed at Cranfield by Hudson as part of his M.Sc thesis and details were published by Robinson and Hudson in 1990. This improved electrochemical hydrogen probe has been developed to allow in situ measurements to be made of the concentration of mobile lattice hydrogen present in steel components. This enabled work to be done directly with the 2 mm thick AISI 4340 steel sheet which was subjected to four main treatments involving quenching, tempering, plating and post-plating baking. Comparisons were made of the various concentrations of hydrogen before and after different treatments, both in the plate and the steel substrate, and after differing methods of storage.

Finally, mathematical modelling was also carried out using various fracture mechanics and diffusion equations to see if it was possible to make predictions from simple experimental results. Two equations linking hydrogen concentration with the stress intensity necessary to initiate a crack have been published and the model fits that used by Yamakawa et al (1984). From the modelling it was found that if the stress intensity necessary to initiate a crack is known and provided either the nominal stress or the crack size is known, it is possible to calculate either the allowable crack size or the allowable stress below which cracking is not expected to occur.

CHAPTER TWO
LITERATURE SURVEY

2.1 MECHANISMS

2.1.1 Introduction

Hydrogen may enter a steel from several sources such as corrosion, welding, electro-plating and excessive cathodic protection. Mechanical damage caused by the presence of, or interaction with hydrogen, is observed in four main ways: blistering, decarburisation, chemical hydrogen attack and embrittlement.

The terms hydrogen embrittlement, hydrogen induced cracking, hydrogen assisted cracking and hydrogen induced stress corrosion cracking are often considered as synonymous since they relate to similar, if not identical, processes.

It is a well known fact that steels and other alloys contain various defects, other than dislocations, which interact with dissolved hydrogen entering the metal during different kinds of treatment. High strength steels are susceptible to hydrogen embrittlement, a phenomenon which is well known but not completely understood. Several theories as to the mechanism of hydrogen embrittlement have been proposed but there is no general consensus other than that there seems to be a combination of factors which, in themselves, depend upon individual circumstances prevailing at the time.

Stress corrosion cracking of high strength steels was reviewed by B.F. Brown (1971) and he takes the view that in high strength steels stress corrosion cracking occurs by a hydrogen embrittlement mechanism. However, corrosion is

an essential step in that it generates the hydrogen necessary to cause the embrittlement (Fontana and Green). In other alloys hydrogen embrittlement is not thought to occur and the crack grows by a localised corrosion reaction alone (e.g. stress corrosion cracking of austenitic stainless steel).

It is possible to differentiate between mechanisms of hydrogen embrittlement and stress corrosion cracking by cathodically polarising the material. If failure occurs by hydrogen embrittlement the cracking is increased due to the increased hydrogen absorption at the lower potentials.

One of the special characteristics of hydrogen embrittlement is its prevalence at room temperature. Rhines (1971) identifies two types of hydrogen embrittlement:

a. Loss of elongation, or reduction in area, by reason of the development of internal cavities which reduce the effective cross-section of the metal and cause it to succumb to rupture as a network instead of as a single coherent ductile bar;

And b. A change of mechanical properties of the metal, bringing about a reduction in the stress necessary to induce fracture and localising the concurrent plastic deformation of the metal as a whole.

Elements of both types of processes are likely to be involved in any specific instance of hydrogen embrittlement.

McIntyre states that in high strength steels, hydrogen concentrations of less than 1 ppm by weight can produce

both brittle and ductile failure. This is a lower value than that quoted by Steigerwald et al (1959,1960) who were of the opinion that 5 ppm was the minimum concentration. On testing hydrogen charged specimens, hydrogen embrittlement manifests itself as any or all of reductions in tensile ductility, tensile strength, notch tensile strength and as delayed failure under sustained load. Yield strength and true fracture stress are virtually unaffected by hydrogen. At temperatures above 0°C, the value of $K_{i_{scc}}$ increases progressively with increased temperature and the same effect is observed with decreasing temperature, i.e. at 0°C $K_{i_{scc}}$ is a minimum.

There are seven main theories concerning the mechanism of hydrogen embrittlement. Briefly titled, they are as follows:

1. Hydride induced cracking (Gahr et al; Hirth; Gilman)
2. Internal hydrogen pressure (Zappfe and Sims)
3. Proton-dislocation interaction (Bastien and Azou)
4. Hydrogen adsorption (Petch and Stables)
5. Lattice decohesion (Troiano; Oriani)
6. Segregation (Rice)
7. Hydrogen induced slip softening (Beachem)

2.1.2 Mechanisms of Hydrogen Embrittlement

2.1.2.1 Brittle Hydride Induced Cracking

Westlake (1969) suggested that hydrides could form ahead of a crack tip which would result in lattice embrittlement as the hydride is of lower strength. After such a phase has contributed to crack propagation it redissolves. Brittle hydride could conceivably be formed by contact of hydrogen with metal and thus provide a

constantly growing cracking medium. However, despite many sensitive means for detecting an iron hydride being applied over many years, no positive evidence of the existence of an iron hydride has been found. Holzworth and Louthan (1968) found that electrolytically charged hydrogen can induce a type of martensite formation but no hydride. Rhines (1970) believed that hydrogen cracking is merely a localised plastic flow to produce a new surface along suitably oriented grain boundaries. Supporting this view, Louthan found metallographic and electron microscope evidence of shear emanating from the crack tip and proceeding at 45° to the cracking direction on one side only of the crack. Closely analogous to the case of liquid metal cracking, it was also noted that hydrogen cracks are nearly always clean and shiny as they follow grain boundaries. This argues against hydrogen reacting with metal other than to reduce surface tension.

In general, no hydride phases have been detected in steel although Fidelle (1988) stated that iron hydride was very unstable under normal conditions. However, it is not clear if he had actually observed the hydride. Hydrides are thought to play a key role in stress corrosion cracking of non-ferrous alloys. Gahr et al (1977) suggested that hydrides provide initiation sites for fracture but they do not play a significant role in crack propagation.

Baronowski (1972) found that there was no stable hydride for iron at low pressures of less than 2 GPa. However, Hirth (1980), suggested that such a model could apply on an atomic scale. Gilman (1977) proposed that it was thermodynamically possible for the formation of a surface hydride near the tip of a crack in iron which will suppress the glide of dislocations which, in turn, will suppress crack blunting. This will tend to prevent stress relaxation and thus provide favourable conditions for

embrittlement.

2.1.2.2 Internal Hydrogen Pressure

In 1941, Zappfe and Sims postulated that the embrittlement of steel results from the high internal pressures generated by the formation of molecular hydrogen within voids or fissures. Hancock and Johnson (1965), among others, showed that crack propagation occurring in dry hydrogen at sub-atmospheric pressures demonstrated that such a mechanism could not be general. Tien et al (1976) indicated that large dislocation transport of hydrogen could lead to supersaturation and hence large internal pressure, even when the external pressure is low. However, Johnson and Hirth (1976) used a predictive model to suggest that, in practice, supersaturation would be small. This theoretical prediction was later confirmed experimentally by West and Louthan (1979) who also pointed out that many hydrogen assisted crack related phenomena had been rationalised in terms of hydrogen transport by dislocations and hydrogen embrittlement could be explained without any localised hydrogen enhanced deformation.

More recent work in 1983 by Grundy, Davies and Ryder suggests that hydrogen gas pressure exerted at oxide inclusions could result in embrittlement and subsequent failure.

2.1.2.3 Proton-Dislocation Interaction

This model, proposed by Bastien and Azou (1951), follows on from the pressure theory of Zappfe and Sims. The model considers that hydrogen is transported by interstitial proton diffusion, or by dislocations through proton-dislocation interaction. It is then collected at defects as super-saturated hydrogen gas which exerts high

pressure. The high pressure causes tri-axial stress around the defect which, in turn, assists crack development, despite there being no plastic deformation which would be necessary in the lattice decohesion model.

The proton-dislocation model was investigated by Tien et al (1976) and Johnson and Hirth (1976) and more recently in 1983 by Nair et al who have developed more quantitative models which require exact data of the energy binding hydrogen with various traps, since the interest is in how many hydrogen atoms can be transported by dislocations to areas of high tri-axial stress. It is suggested that hydrogen is trapped as anions in strong trapping, but as atoms in weak trapping. i.e. hydrogen will destroy metal bonds by absorbing dissociated electrons. It is believed that embrittlement develops as metal bonds are destroyed.

2.1.2.4 Hydrogen Adsorption (Surface Energy)

The surface energy theory is based on the Griffith theory that when a crack grows, strain energy is released but new surface energy is created. This implies that a crack will grow when the strain energy released is greater than the new surface energy. Petch and Stables (1952) suggested that the adsorption of hydrogen by a newly formed fracture surface lowers the surface energy and, in turn, the Griffith stress required for brittle fracture. Fast fracture is not affected by hydrogen but, where crack propagation is slow, hydrogen adsorption can take place and lower the stress intensity necessary for fracture. The crack will be unstable and will propagate at the rate determined by the supply of hydrogen.

Williams and Nelson (1970) used this model to explain certain crack growth in high strength steel and were able to account in an approximate way for the pressure and

temperature dependence on the rate of growth of cracks.

The evidence suggesting hydrogen assisted cracking is a surface or near-surface effect is contrary to the slip theory of Beachem (1972) but Hirth (1980) suggested that adsorption could still occur as a crack tip mechanism in a more complex over-all process although he disputed a completely brittle surface energy controlled crack process since Lynch (1979) showed it greatly underestimated the work of fracture. Hirth also states that the model cannot account for discontinuous cracking as indicated by sonic emissions, that it cannot explain why the tendency for delayed failure can be reversed on stress removal (Robinson and Sharp 1986), and why oxygen not only fails to promote cracking but stops the hydrogen effect.

2.1.2.5 Lattice Decohesion Theory

Troiano (1960) suggested that the existence of large elastic stresses in the vicinity of the crack tip implies conditions which are thermodynamically favourable for the accumulation of hydrogen and that the hydrogen would produce a weakening of the cohesive Fe-Fe bond by the formation of a Fe-H bond.

Oriano and Josephic (1972) and Oriani (1977) investigated this theory. Oriani postulated the hypothesis that hydrogen concentrates at regions which are able to support elastic stresses approaching those of the cohesive strength of the iron lattice and reduce the Fe-Fe bond strength such that the maximum cohesive force is lowered. He suggested that this only occurs when the highly stressed regions are within a few atomic spaces of the crack tip.

Figure 2.1 (reproduced from Oriani, 1987) is a theoretical depiction of a concentration/strain relationship from the Hookean region to that of infinite separation. It shows why it is reasonable to expect very large hydrogen concentrations in elastically strained regions of the lattice where the stress corresponds to significant proportion of Young's modulus. The second part of the figure shows how the increasing hydrogen concentration is expected to affect the cohesive strength of the lattice.

The existence of large concentrations of hydrogen at the crack tip has been supported experimentally by Lacombe et al (1973).

Oriani assumes that a critical concentration of hydrogen is required below which no cracking occurs. If this is the case, the experimental evidence suggests that such concentrations can only be achieved within a few atom spacings of the crack tip.

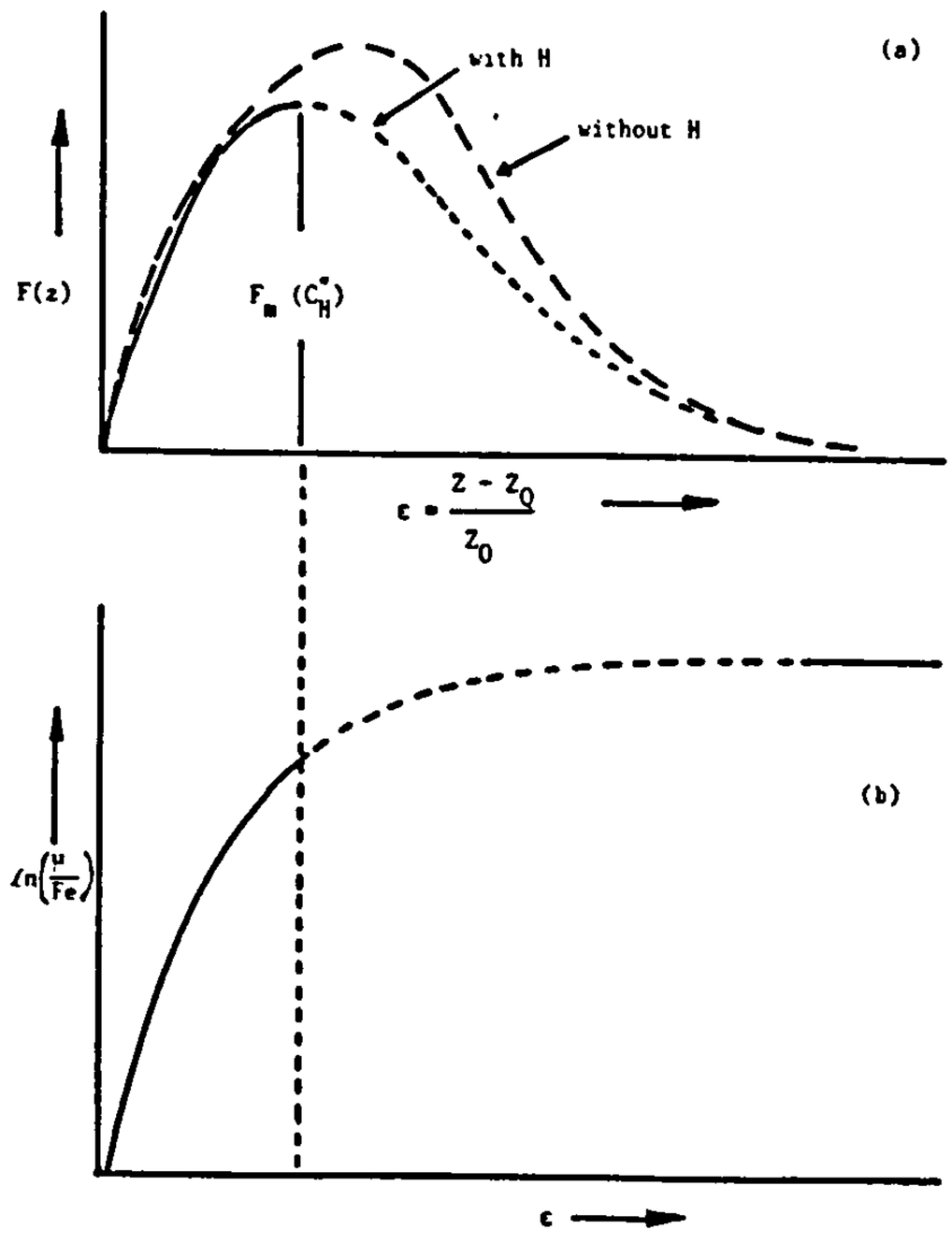

FIG. 2.1 Theoretical Depiction of a Concentration/Strain Relationship from the Hookean Region to that of Infinite Separation.

The lattice decohesion theory seems to explain successfully failure under constant load behaviour of high strength steel but does not give a satisfactory reason for hydrogen induced fracture under dynamic fatigue conditions.

The most direct investigation of the validity of the decohesion model is that of Vehoff and Rothe (1983). They could conceive of only two candidates for the observed fracture mechanism; micro-cleavage (H-aided decohesion) and H-aided microvoid formation ahead of the crack tip (Lynch, 1981). They dismiss the latter because no evidence of microvoids could be found. In fact, Lynch also concludes that neither surface energy nor near-surface cohesive bond energy arguments were supported by his findings. However, Oriani (1987) agrees it is extremely difficult to devise a feasible experiment to measure the cohesive force between iron atoms with which a very large (H/Fe >1/10) amount of atomic hydrogen is dissolved. He concludes that competent theoretical investigations allow one to be confident that dissolved hydrogen does increase the force resisting the co-linear separation of iron atoms so that the basic postulate of the decohesion model is supported by theory.

2.1.2.6 Segregation

Pollock, in a paper given in Beijing, 1988, refers to work done by Rice (1977) and, also in the same year, Kerns et al who suggested that when high strength steel is under stress, environmental hydrogen is adsorbed at areas where the air-formed oxide film is broken by the applied stress. The adsorbed hydrogen can do one or more of three things:

a. weaken the surface layer of the steel to induce subcritical cracking.
b. diffuse to regions of maximum triaxial stress ahead of the crack.

c. diffuse to a defect where an increment of subcritical crack growth will occur once a critical concentration of hydrogen is reached.

Whichever mechanism is operative, removal of the environment stops the generation of hydrogen and eliminates the possibility of future sub-critical cracking.

Rice and Thompson (1974) made two assumptions for tensile decohesion:

(i) dislocations do not normally intersect with crack tips; and
(ii) voids do not form ahead of cracks so fracture surfaces should not be dimpled.

However, these assumptions may not be valid as they are surely the basis of the slip assisted mechanism of stress corrosion cracking.

Unfortunately for the researchers, Lynch, in the paper mentioned in the previous section (Lynch, 1981) found that neither of these assumptions were satisfied in his work on aluminium, nickel, titanium and ferrous alloys, and he concluded that crack growth in embrittling environments (as well as in inert surroundings) occurs, or is accompanied, by plastic flow.

2.1.2.7 Hydrogen Induced Slip Softening

Beachem (1972 and 1977) proposed four interactions which could account for many phenomena encountered in stress corrosion cracking and hydrogen assisted cracking.

(a) On evolution of hydrogen it is either absorbed at the surface of the metal where it diffuses to defects

during electrolytic charging, or it becomes part of a corrosion reaction and enters the metal at a crack tip.

(b) Pure molecular hydrogen gas dissociates at clean forming surfaces and enters the metal. Some of the hydrogen will immediately form molecules again but some atoms will be absorbed before recombination.

(c) Hydrogen diffuses to regions of high triaxial stress within the metal.

(d) The presence of hydrogen dissolved in the ferrite matrix aids the deformation of the matrix.

Beachem supported the first three points with experimental evidence and suggests that they are more concerned with the supply of hydrogen to the critical regions, whereas the final point is the crucial interaction determining the susceptibility to cracking.

By observing increases of plasticity and the lowering of torsional flow stress in material degraded by hydrogen, Beachem suggested that the role of hydrogen is to increase the movement of dislocations along the slip planes. He argued that the formation, growth and coalescence of microvoids as the fracture mode during hydrogen assisted cracking distracts the attention away from embrittlement mechanisms and towards microscopic plasticity. Such a softening mechanism has also been observed by Gibala (1977).

A schematic representation of Beachem's fracture process is shown in Figure 2.2. At high stress intensity,(a) large volumes are plastically deformed at the crack tip, assuming that there is sufficient hydrogen concentration. The inclusions present in the plastic region act as initiation sites for void nucleation and thus the fracture process is characterised by microvoid coalescence. At

intermediate stress intensity, there is a decrease in plastic zone size and so there are fewer initiation sites.(b) Microvoid coalescence does not occur and instead, a lower energy quasi-cleavage mode of propagation occurs where the combined effect of stress intensity and hydrogen concentration is enough to drive the necessary plastic deformation.

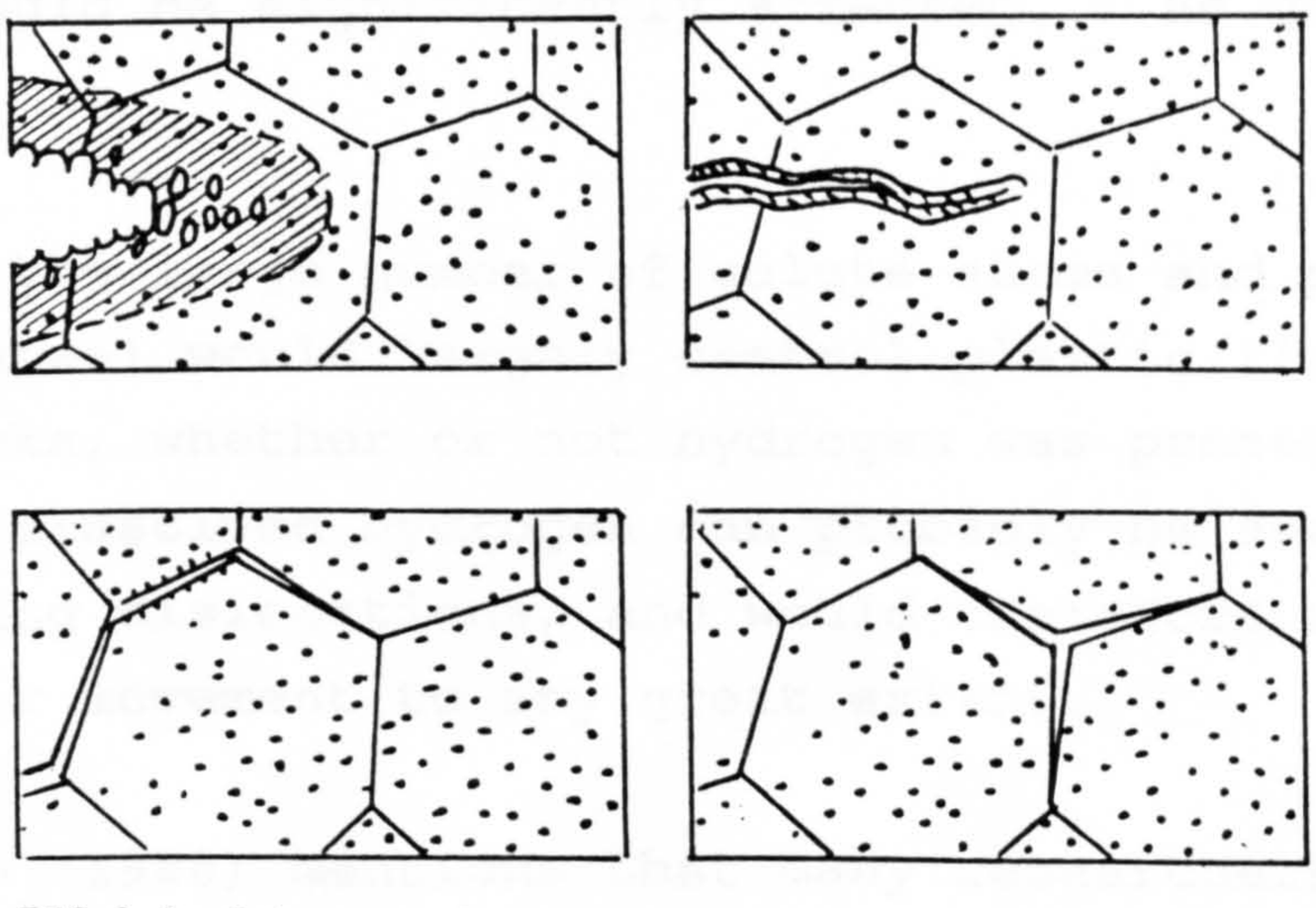

FIG 2.2 Schematic Representation of Beachem's Fracture Process

As cracks elongate, further growth occurs by the still lower plastic deformation processes of intergranular fracture which may eventually require assistance from internal pressurisation effects of molecular hydrogen.(c)(d) This model is able to account for the fracture surface appearance and fracture surface properties of quenched and tempered steel.

Whilst dislocation motion is established, with softening behaviour including enhanced screw dislocation mobility and dislocation injection at surfaces, it should be recalled that Hirth (1977) emphasised that hardening effects are also observed, and that the idea of slip

softening is not universally accepted. Should hydrogen and dislocations be required to initiate a crack at an inclusion, then enhanced dislocation motion would be a contributing factor to an overall process rather than a model in itself as proposed in earlier sections.

Lynch (1979) argued that dissolved hydrogen would be unlikely to influence slip to such an extent that crack growth would be significantly affected. He gave two reasons:

a) the large number of solute atoms and precipitates in steel would largely control plastic flow ahead of cracks, whether or not hydrogen was present, and
b) dissolved hydrogen can probably be swept along by moving dislocations, and would therefore not restrict their movement to any great extent.

Iino (1988) mentions that many researchers in recent years have been interested in different hydrogen-dislocation interaction as important precursors of hydrogen induced embrittlement. For instance, Pei, Liu and Chen (1988) suggest that hydrogen atoms, driven by a stress field, diffuse to and enrich in the vicinity of dislocation pile-ups, decreasing the elastic distortion energy of the dislocations, which, in turn, promote more dislocations and merge into a giant dislocation: thus a brittle crack could form and result in hydrogen induced cracking. Iino also sees a progression from the pressure theory of Zappfe and Sims to the lattice decohesion model proposed by Troiano, Oriani and others, via the adsorption hypothesis, whilst Beachem's slip theory combines the proton-dislocation model with plastic deformation accelerating hydrogen influx into the crack tip region. Iino considers that, although the segregation hypothesis is not currently fashionable, it could be considered to give the deepest insight into

possible hydrogen effects on the fracture mode.

Various theories at times are contradictory. For instance, lattice cohesion seems to explain the static fatigue behaviour of high strength steel, but under dynamic conditions, the theory is felt to be inappropriate as it would require a process of hydrogen transport by dislocations if it is to successfully interpret the rapid extension of hydrogen induced fracture.

Hirth (1980) in his general overview of the effects of hydrogen on the properties of iron and steel also refers to contradictory theories: for instance Beachem (1972), Bernstein and Thompson (1976) and Kimura and Matsui (1979) all suggest that hydrogen softens iron, yet Adair and Hook (1972) and Asano et al (1973) suggest that hydrogen hardens iron.

Hydrogen has little effect on the yield stress of high strength steel but reduces the ductility and the critical stress intensity for crack propagation (Bernstein 1970, Oriani, 1978 and Thompson and Bernstein, 1979). Due to the higher strength level and the greater susceptibility to degradation, hydrogen induced failure is at lower stress levels characterised by reduced plasticity, and the corresponding fractography is that of quasi-cleavage or brittle cleavage (Beachem, 1972) - see Figure 2.2.

First found by Johnson et al (1958) for notched, tensile specimens of quenched and tempered AISI 4340 steel and afterwards confirmed by Lee et al (1979) and Oriani and Josephic (1979), cracking initiated internally in the region of maximum triaxial stress and maximum principal normal stress near the elastic-plastic boundary in precharged specimens. The cracks propagate initially in a Mode I manner (see Figure 2.3 taken from Hirth 1980 (figure

18 page 884) but Lee et al (1979) showed that a Mode I - Mode II crack transition can occur with the Mode II crack connecting the Mode I crack to the surface. Troiano (1960) had noted that the hydrogen would be attracted to the triaxial stress region, however, Pressouyre and Bernstein (1979) predicted that the presence of traps weaker than interface traps tends to decrease the propensity for cracking by preventing the hydrogen from reaching the inclusions or second phase particles more likely to initiate cracking.

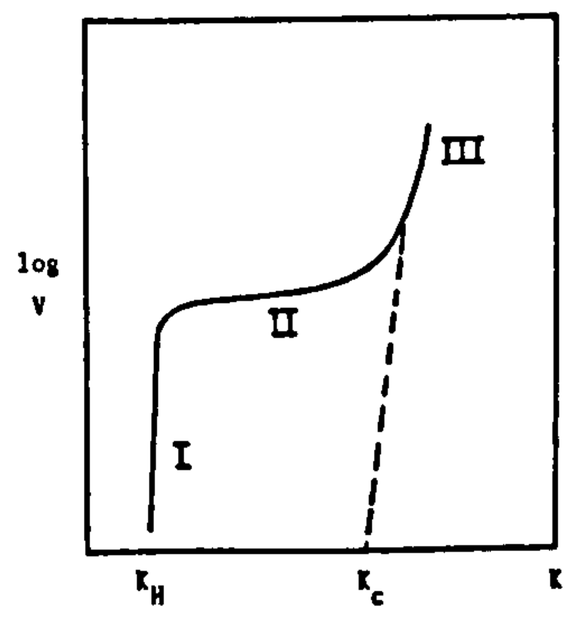

FIG. 2.3 Form of crack velocity-mode I stress intensity plot for crack growth under sustained load. K_H is the threshold stress intensity in the presence of hydrogen and K_c is the critical stress intensity for initiation of crack propagation in air. Region I is characterized by intergranular cracking, region II by transgranular ductile rupture by hole growth, region III by mixed mode tearing and quasi-cleavage and sometimes by crack branching and tortuosity.

2.1.3 Summary

Two mechanisms of cracking have been suggested to be operative in high strength steels. Dependent upon conditions, these were hydrogen embrittlement and a dissolution mechanism referred to as active path corrosion. Particularly since the work of Brown (1971) it has been accepted generally that failure can be accounted for in terms of hydrogen embrittlement.

Opinion seems to favour the absorption and decohesion models for iron-based alloys, the models being largely based on the hydrogen affected reduction of the surface

energy and cohesive strength of iron respectively. The model suggested by Oriani requires the build up of stress ahead of the crack tip, causing an accumulation of hydrogen at that region. Troiano suggested that the stress concentrations were approximately three times the yield strength, whereas Oriani believes that stresses as large as E/10 could exist. It is difficult to accept that stress of this magnitude could be reached in steel before plastic deformation takes place. However, Oriani argues that the lifetime of these highly stressed regions is sufficient for hydrogen assisted cracking to occur.

The position of the embrittlement site is in dispute. Troiano suggests that the site is ahead of the crack tip at approximately 1 - 2 times the diameter of the crack: he also proposes that cracking is discontinuous. Oriani, on the other hand, postulates that continuous cracking can occur at the highly stressed sites within a few atomic diameters of the crack tip.

Oriani's model differs from the adsorption model only in the choice of embrittlement site. Unfortunately, the adsorption model is faced with the serious difficulty of explaining how a brittle crack can propagate at low velocities without becoming blunted by plastic deformation of the steel.

The hydride model put forward by Gilman is speculative and there is no experimental evidence to support such a mechanism in steel.

Oriani (1987) regards cohesion and localised slip models as complementary with both manifesting a somewhat different aspect of the same disturbance of the Fe-Fe bond caused by hydrogen. Indeed, a complex process composed of several allied mechanisms would account for many observed

energy and cohesive strength of iron respectively. The model suggested by Oriani requires the build up of stress ahead of the crack tip, causing an accumulation of hydrogen at that region. Troiano suggested that the stress concentrations were approximately three times the yield strength, whereas Oriani believes that stresses as large as E/10 could exist. It is difficult to accept that stress of this magnitude could be reached in steel before plastic deformation takes place. However, Oriani argues that the lifetime of these highly stressed regions is sufficient for hydrogen assisted cracking to occur.

The position of the embrittlement site is in dispute. Troiano suggests that the site is ahead of the crack tip at approximately 1 - 2 times the diameter of the crack: he also proposes that cracking is discontinuous. Oriani, on the other hand, postulates that continuous cracking can occur at the highly stressed sites within a few atomic diameters of the crack tip.

Oriani's model differs from the adsorption model only in the choice of embrittlement site. Unfortunately, the adsorption model is faced with the serious difficulty of explaining how a brittle crack can propagate at low velocities without becoming blunted by plastic deformation of the steel.

The hydride model put forward by Gilman is speculative and there is no experimental evidence to support such a mechanism in steel.

Oriani (1987) regards cohesion and localised slip models as complementary with both manifesting a somewhat different aspect of the same disturbance of the Fe-Fe bond caused by hydrogen. Indeed, a complex process composed of several allied mechanisms would account for many observed

degradation phenomena, but much further work needs to be done experimentally to observe crack tip processes at the atomic level, and improved calculations are needed for atomic measurements of crack tips. However, with regard to the embrittlement site, Page and Gerberich (1982) have suggested it is dependent on whether the critical hydrogen concentration is residual or introduced from the environment.

Louthan and McNitt (1977) discuss the relationship between the test techniques utilised and proposed embrittlement mechanisms and conclude that, as none of the proposed mechanisms taken singly appears to be compatible with all the observations noted, either there is no universal embrittlement mechanism or a new theory must be developed.

However, despite all the theories, Floreen observed that, whilst hydrogen cracking is an ever-present danger, it is well known and procedures developed in production and employment of steels reduce the hazards to an acceptable level. More recently, Hsiao (1988) suggested using silicon and titanium, elements which strongly bond with hydrogen, as a measure to combat hydrogen induced cracking by trapping hydrogen, and Paatsch (1988) is looking at thermal alloying techniques which would ensure that out-gassing hydrogen and de-embrittling baking would occur simultaneously during alloying.

2.2 DIFFUSION COEFFICIENTS FOR HYDROGEN IN STEEL AND NICKEL

In a study of transients for hydrogen in metals, Gileadi, Fullenwider and Bockris (1966) observed that hydrogen diffused via the lattice and not along the grain boundaries. Bockris (1977) later states that, considering

that metal contains normal lattice sites as well as trapping sites, it is clear that diffusion between trapping sites does not occur by direct jump but has an intermediate stage of diffusion through lattice sites. Devanathan et al (1963) showed that permeation through plated and unplated AISI 4340 steel was much slower than that through ARMCO iron and they quoted:

$$D = 2.0 \times 10^{-7} cm^2 s^{-1}$$

Bockris (1977) found that the value of D could vary considerably, but he concluded that detailed comparison between the results obtained by various workers suggested that the diffusion coefficient for hydrogen in steel could be determined to +/-12% and that the value for hydrogen in iron did not depend on stress. When Kiuchi and McLellan surveyed the published values in 1982, they found a diversity in hydrogen diffusion coefficients from various laboratories according to the different methods used. In the same year (1982) Mansfield et al, experimenting with the Barnacle Electrode, assumed the value to be 2.5 x $10^{-7} cm^2 s^{-1}$ for AISI 4340 steel.

Unfortunately, values obtained for nickel vary considerably. Matusiewicz and Duquette (1985) found the diffusion coefficient of hydrogen through nickel to be 7.10 x $10^{-10} cm^2 s^{-1}$ at 300K. Indeed in 1988, the coefficient was taken to be 7 x $10^{-10} cm^2 s^{-1}$ at 300K. In 1990, Harris and Latinision calculated that the grain boundary diffusion coefficient for nickel was 3.3 x $10^{-12} m^2 s^{-1}$ (ie.3.3 x $10^{-8} cm^2 s^{-1}$) at 30°C which was approximately 40 times that for lattice diffusion; i.e. a value of approximately 8 x $10^{-10} cm^2 s^{-1}$. They noted that, in a high purity material, annealing will eliminate many of the highest energy grain boundaries which are believed to be the pathways of least resistance for hydrogen diffusion.

Pyun and Oriani (1989) measured D to range from 4 to 9 x $10^{-9}cm^2s^{-1}$.

Archer and Grant in 1984 used the double-cell method to obtain a range of diffusion coefficients for nickel, 1 to 5 x $10^{-10}cm^2s^{-1}$ at room temperature; the lower values were found for unannealed cold-rolled nickel. They also found that electro-formed nickel foils gave anomalously high diffusion coefficients (circa $10^{-9}cm^2s^{-1}$). These anomalies were possibly due to small voids and electrolytic inclusions which would render electro-formed nickel foils unsuitable for permeation work.

Fortunately for the purpose of this thesis, Yamakawa et al (1984) found that D for hydrogen appears to be independent of thickness in layers of nickel 100 to 1000 angstroms and consequently the rate of permeation is controlled by the iron specimen. This means that for the permeation experiments the diffusion coefficient for nickel need not be known but it did become important when using the probe to investigate hydrogen depletion rates in nickel plate and in AISI 4340 steel.

More recently, in 1988, Paatsch investigated the possible avoidance of embrittlement by thermal alloying techniques:

a) alloying base material with a nickel plated layer,
b) alloying a nickel with a zinc layer or a copper with a nickel layer,

both being plated on to a steel substrate. In both cases, hydrogen caused by the plating process is outgassed during the alloying treatment occurring simultaneously with the de-embrittlement baking.

Paatsch found that a hydrogen barrier is built up if an austenitic iron-nickel alloy is formed by treating about 10 minutes at 850°C. This reduces D from about $10^{-7}cm^2s^{-1}$ for the as-plated specimen to values lower than $10^{-10}cm^2s^{-1}$. D remains constant below an annealing temperature of about 600°C.

Figures 2.4 and 2.5 (reproduced from Paatsch, 1988) illustrate the diffusion behaviour of nickel and iron as a function of heat treatment and the relationships between hydrogen diffusion coefficient and microhardness of plated nickel foils against heat treatment.

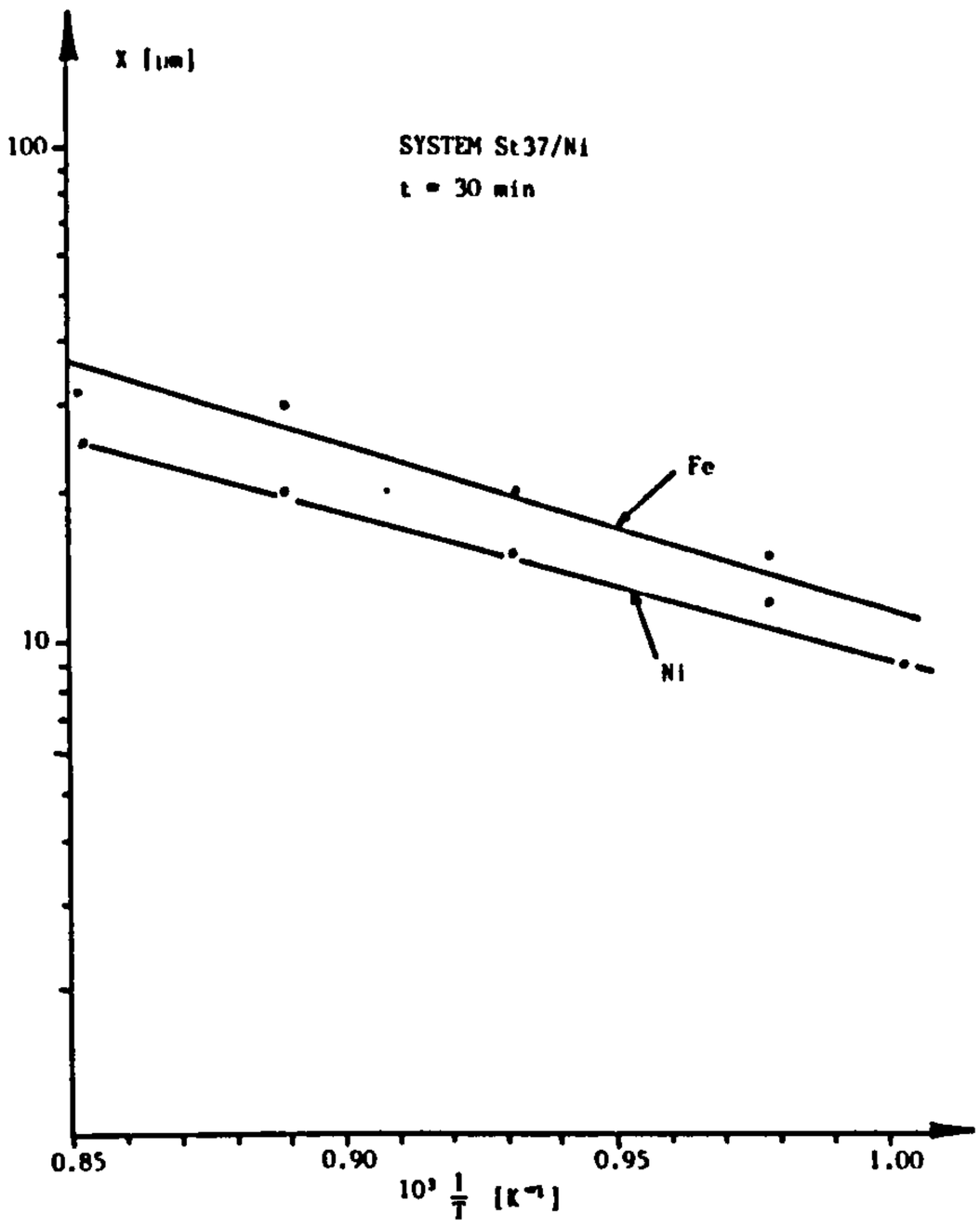

FIG. 2.4 Diffusion behaviour of Nickel and Iron as a Function of Heat Treatment

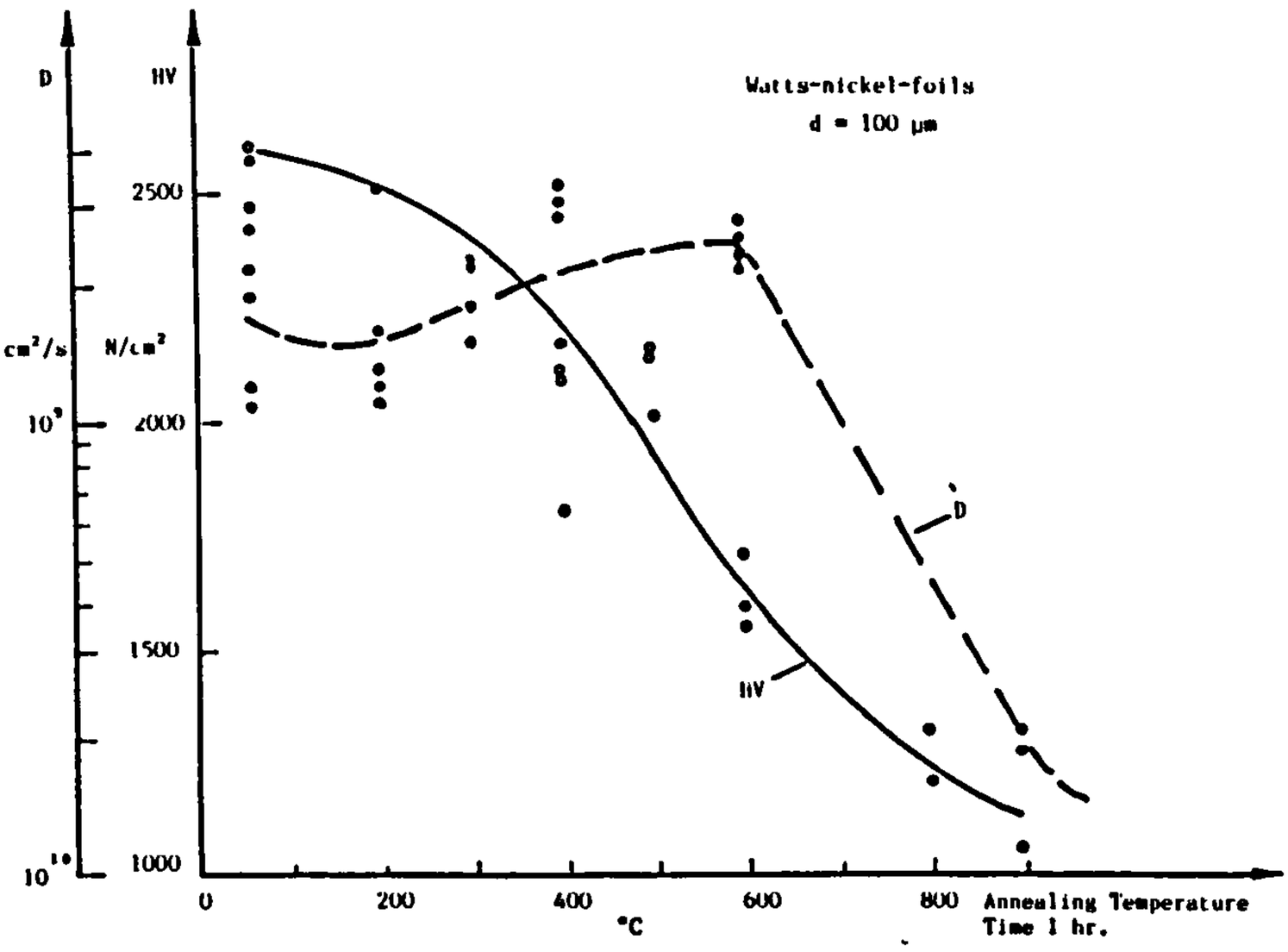

FIG. 2.5 Hydrogen Diffusion Coefficient D and Microhardness HV of Plated Ni- foils vs. Heat treatment Temperature.

2.3 THE ROLE OF STRESS IN HYDROGEN ASSISTED CRACKING

Steigerwald et al (1959, 1960) showed that the initiation of localised cracking in hydrogenated high strength steel was dependent on the development of a critical hydrogen concentration and relatively insensitive to the magnitude of the applied stress. They confirmed that the delayed failure testing advocated by Johnson, Morlet and Troiano (1958) was the most sensitive means of detecting hydrogen embrittlement since it allows the maximum time for hydrogen diffusion during a test.

Steigerwald et al described the nature of the delayed failure, using four parameters (see Figure 2.6)

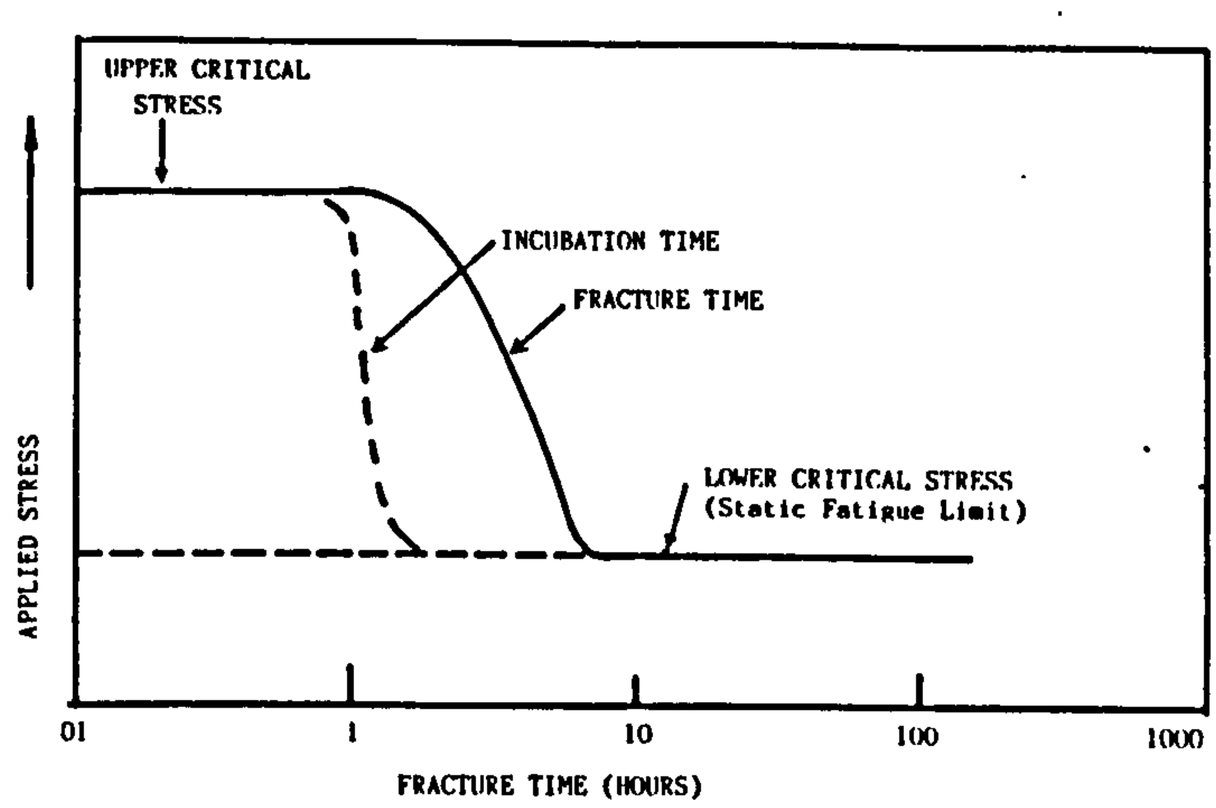

FIG. 2.6 Schematic Representation of Static Fatigue Characteristics of a Hydrogenated High Strength Steel

The upper critical stress corresponds to the rupture stress in conventional notch tensile testing. The lower critical stress is the stress below which no delayed failure will occur. The incubation period is the time required for the formation of the first crack and the fourth parameter is the failure time. An increase in hydrogen content, notch acuity or strength level of the material increases the susceptibility for delayed failure

by decreasing all three of the latter parameters.

Johnson et al (1958) had already shown that a uniform hydrogen distribution is present after 30 minutes and that the baking time in excess of that figure could be used as an effective measure of regulating the hydrogen content.

Tests done by Steigerwald et al indicated that below approximately 5 ppm of hydrogen no embrittlement occurs but when this critical figure was exceeded, a rapid decrease of ductility was encountered. They stated that above a particular threshold stress, the conditions necessary for localised cracking were essentially dependent only on the development of a critical hydrogen content.

Smialowski (1962) showed that hydrogen is not uniformly distributed across sections of iron and nickel specimens after prolonged electrolytic charging. Hydrogen accumulates in the surface metal layer and is not driven by diffusion into deeper layers; and certainly in the case of nickel, the formation of a phase rich in hydrogen occurs, containing 0.7 hydrogen atoms per nickel atom. This phase is unstable and starts to decompose once the polarising current has been interrupted, but both its formation and disintegration are influenced by structural defects and impurities present in the samples. Therefore the depth of penetration of hydrogen into the cathode is limited and controlled by the chemical potential of atomic hydrogen which is, in turn, dependent on the current density and the cathodic poison used, by the structure of the metal sample and by the presence of impurities in it.

He continues to state that the presence of an impermeable metal coating renders the evolution process of hydrogen from the interior of the base metal more difficult and, in practice, this may aggravate the effects of

embrittlement and delayed failure of electroplated steels.

Strecker, Ryder and Davis (1969) carried out delayed failure tests on unnotched specimens and treated the results statistically, finding that the failure frequency conformed to an exponential distribution, and that the scatter in failure times could be treated as a stochastic process defined as the probability system generated by time where the state of the system at time, t, is dependent on chance.

Further work by the same authors, published in 1975, produced evidence for the occurrence of two separate stages in the evolution of hydrogen in cold-worked steel. These evolution stages are associated with traps of different binding energies for hydrogen. Robinson also observed that at low stresses there was an additional initiation step which he believes to be due to formation of internal voids of sufficient size for the threshold intensity to be exceeded.

Johnson et al (1958) suggested that after an incubation period for crack initiation, instantaneous fracture will occur when the applied stress is sufficient to initiate a crack over an appreciable volume of the specimen cross-section. They verified the existence of the incubation period by showing that the notch tensile stress is not reduced by stressing for times less than the incubation period and supported this view by metallographic study of specimens where cracks were not observed unless the time under load exceeded the incubation time. They stated that the critical hydrogen concentration necessary for crack initiation is a constant for a given stress.

Zakroczymski (1985) showed that strain did not materially affect the transportation of hydrogen in nickel

and that the diffusion coefficient was not affected by plastic deformation. This agrees with the work done by Bockris (1977) and by Gerberich, Gary and Lessar in the same year; the latter group supported neither the surface energy theory nor cohesive bond arguments. Zakroczymski found that the production of dislocations by plastic deformation enhances hydrogen trapping and consequently, if accelerated hydrogen transport does occur, it is overcome by this trapping.

2.4 THE ROLE OF STRUCTURE IN HYDROGEN ASSISTED CRACKING

Xian et al (1988) discussed the different forms of traps in low carbon steels, including cold deformation, precipitated phases and inclusions. They found that physical reactions, e.g. the influence of local lattice deformation, are insensitive to temperature changes, whereas chemical reactions, e.g. gaining or losing electrons, were very sensitive to changes of temperature.

Grundy, Davies and Ryder (1983) suggested that from observations of fractographs, fracture initiated at oxide inclusions and that crack growth occurred in one step with little or no sub-critical crack growth; whereas Oriani (1977) and Nelson and Williams (1977) showed that Stage I crack growth responds in a few seconds to changes in pressure of a gaseous environment, and that branching could occur. In the same paper, Grundy et al produced a modified Weibull distribution of failure times and suggested that this illustrated that delayed failure and rising stress hydrogen embrittlement were two facets of the same effect.

Referring to work published by Shubinsky, Davies and Ryder (1982) which demonstrated susceptibility to

embrittlement by gaseous hydrogen environments is a function of austenitic grain size, Ryder, Grundy and Davies (1982) suggested that structure rather than strength is more important in controlling susceptibility to hydrogen embrittlement. Indeed, they showed that embrittlement was most severe in extremes of grain sizes i.e. the finest and coarsest grain sizes and that minimum embrittlement occurred for grain sizes in the range 30 to 80 μm. They conclude that carbide-matrix interfaces appear to act as non-hydrogen trapping sites and that coarse austenitic grain sizes appear to reduce hydrogen embrittlement by providing interfaces that promote branch cracking.

Garber, Bernstein and Thompson (1981), Beachem (1972), Thompson (1979) and Kosco and Thompson(1982) had already observed the intereffect of structure and susceptibility to hydrogen embrittlement.

In 1987 Lucas and Robinson assessed the significance of defects within a structure. They state that defects below the size of about 60 μm would be difficult to detect and so that it is possible that in a corrosive environment cracks could initiate and propagate from these sites. If hydrogen is generated solely at the surface of the specimen, sufficient time must be allowed for the hydrogen to diffuse to the mid-section and for a sufficient concentration to be reached. Crank (1956) calculated that a period of L^2/D was necessary for this condition to be reached.

In 1988, Hirose et al suggested that as the inclusion content increases, K_{th} increases, implying that resistance to hydrogen assisted cracking was heightened by the presence of inclusions. They identified three possible factors:

a. Decrease in hardness with the increase in inclusions.
b. Local relaxation of plane-strain condition at the crack tip, due to separations of inclusion-matrix interfaces, and
c. Reduction and delay in concentration of hydrogen at the crack tip due to hydrogen trapping at inclusions.

They concluded that 'c' was the most likely factor.

Lucas and Robinson, working on BS 4360 Grade 50D steel, showed that the relationship between K_{th} and C_0 was of the form

$$K_{th} = 91.2e^{-0.49\,Co}$$

whereas Yamakawa et al (1984), using AISI 4340 steel, found the relationship to be

$$K_{iscc} = 17.0C_H^{-0.160}$$

Both sets of researchers agree that K_{iscc} is a function of the hydrogen content and their differing equations relate to particular types of steel with defined heat treatment. For instance, the BS 4360 steel was quenched and tempered and had high hardness which caused susceptibility to hydrogen embrittlement. (Lower hardness would cause lower susceptibility). However, K_{iscc} did not depend on the presence of cathodic polarisation; K_{iscc} depends on C_0 and this is controlled by the potential.

Thomson and Lin (Fundamentals of Fracture) comprehensively review and analyse cracking and fracture mechanisms, considering bond energies and methods of fracture in various materials. They state that grain boundary effects often predominate and are always

potentially important since grain boundaries provide an easy path for fracture.

2.5 SLOW STRAIN RATE TESTING

Slow strain rate techniques can provide a quantitative measure of either susceptibility to environment assisted fracture (Rice, 1977 and Kearns et al, 1977) or to internal hydrogen embrittlement (Troiano, 1959) in high strength AISI 4340 steel. Pollock (1988) working on aircraft materials showed that although plating prevents the escape of hydrogen from steel, should the plate become damaged or degraded then exposure to maintenance chemicals etc over a long period of time, the cumulative build up of hydrogen could ultimately lead to delayed failure. Pollock's work was mainly on aluminium and cadmium coatings, but nickel too has a low hydrogen diffusivity and the effects are likely to be comparable.

2.6 ELECTROPLATING

2.6.1 Introduction

As Bidmead and Davies (1978) wrote in their overview of electrodeposition in engineering practice, nickel electrodeposits are tough, strong, ductile and have good wear and corrosion resistance in many environments, making nickel a good protective covering on steel. However, hydrogen pick-up during plating is a major source of hydrogen embrittlement and consequently great care and attention should be taken in using proper plating baths and by careful control of the plating current. Defence Standards (Def Stan) covering various aspects of electroplating are available:

Def Stan	03-01	1975	Electrodeposition of Nickel and Chromium.
	03-2/2	1984	Cleaning and Preparation of Metal Surfaces
Def Stan	03-4		Pre-treatment and Protection of Steel Parts.
B.S	1224:1970		Electroplated Coatings of Nickel and Chromium.
DTD	905A	1955	Nickel Plating (Heavy)

These include surface preparation, methods of plating and post-plating heat treatment which is commonly used to remove hydrogen. These Standards were relevant to the high strength steels used in the aircraft industry.

2.6.2 Hydrogen Uptake During Plating

For a coating to be an effective barrier it has to be continuous, relatively thick (although 8 μm is the normal thickness) and resistant to permeation of hydrogen. The quantity of hydrogen taken up by a high strength steel is strongly influenced by the plating process and the structure of the coating. Mahklouf and Sisson Jnr (1990) investigated cadmium plated AISI 4340 steel and found that, as with nickel plating, the rate of absorption during plating reaches a maximum in the initial stages and then stabilises as the deposit forms a barrier against entry. The application of an initial high current density accelerates the plating during the initial period of plating and leads to a decrease in hydrogen entry. This decrease is due to the impervious barrier that develops at the high current density and is retained during subsequent plating at lower current densities.

Dini and Johnson (1977) discussed how current density and temperature affected deposit appearance and composition. They were talking about a zinc/nickel alloy which was later investigated by Kamitani et al (1985) who found that if the nickel content ranged between 8 and 15 percent, it was possible to plate high strength steel parts without hydrogen embrittlement, thus avoiding any heat treatment process. For this to occur, anodic autocleaning and an inhibitor in the acid dip were used instead of the normal electro-cleaning and pickling. This work makes an interesting comparison with that of Paatch's thermal alloying technique.

A fraction of the hydrogen generated at the surface of steel during the preparation for and electro-plating with nickel is absorbed by the substrate. Although post-plating baking can relieve embrittlement by simply driving mobile hydrogen out of the steel, Townsend (1981) demonstrated that relief can also occur by an alternative mechanism of driving the mobile species into internal trap sites. His determination of the total hydrogen content by high temperature extraction also included the non-mobile hydrogen and so did not provide a reliable indication of delayed failure susceptibility. In practice, this meant that other methods (e.g. delayed failure tests or direct measurement of mobile hydrogen) should be employed to test for susceptibility to hydrogen embrittlement.

Zakroczymski (1982), using specimens of various sizes and shapes, not just membranes, realised that the total hydrogen would include, not just diffusible hydrogen, but also that related to diverse traps and unstable metal hydrides. Using an electrolytic cell, potentiostat and an ammeter, he reasoned that the electrochemical measurement of the hydrogen desorption rate from a metal compared with the measured diffusion rate would make it possible to

estimate what proportion was related to trapped hydrogen.

Early work on diffusion of hydrogen through cathodically charged or electroplated steel used the double-cell technique of Devanathan and Stachurski. A diagram of the experimental set-up is to be found in Chapter 3, Figure 3.10, and the technique is described in Section 3.4.1. Several experimenters used a palladium film on one side of the membrane: Manalotos and LeCoze (1988) said that by placing the layer on the passive exit side it should be possible to give an indication of the amount of irreversibly trapped hydrogen by comparing successive permeation curves. Unfortunately, they found that their experimental results did not fit the theoretical curves.

In 1989, Pyun and Oriani used a palladium film on the entry side of the specimen to minimize surface contamination and to eliminate surface impediments for hydrogen entry. They found that, should the metal be unpassivated, both sides should be coated with palladium otherwise passivation at the exit side would occur. Their results indicated that hydrogen transport through passivated specimens is retarded by oxide films, very severely in the case of iron. This implies that the transport of hydrogen in steel is controlled mainly by the oxide, and through passivated nickel by both the oxide and the metal.

With or without a palladium coating, the sensitivity of the double-cell method reveals details in the permeation of metals susceptible to hydrogen embrittlement. Bockris found there were several disadvantages to this technique:

a. If the metal is too thick, the time involved is too long, whereas if the metal is too thin, pinholes may exist.

b. If there are surface oxide films on the evolution side, some hydrogen will be spent reducing it.

c. There will be some anodic dissolution on the throughput side which could be obviated by coating with palladium on the anodic side. If the coating is sufficiently thin, there will be no resistance to the throughput of hydrogen whilst protecting the iron from dissolution.

d. Impurities in the anode cell could cause problems.

However, on the positive side, he found the technique to be easy to use and inexpensive. A range of 10^{-4} to 10^{-13}moles cm^2sec^{-1} can be measured on the same apparatus and the boundary conditions are fixed and tested by the method.

Although, previously, stress corrosion cracking had been associated with anodic dissolution and hydrogen assisted cracking associated with the way hydrogen permeates through the lattice, Bockris (1977) believes there is an increasing amount of evidence which decreases the sharpness of the boundaries and extends the realm in which the hydrogen mechanism of cracking becomes applicable.

It is interesting to note that Robinson and Sharp in 1986 found that post-cathodic charging heat treatment in 0.8%C steel could increase the susceptibility to failure by allowing the diffusion of hydrogen to the most significant internal defects which act as large incipient crack sites. However, this may be a non-typical example as this type of steel is not commonly used for aircraft components.

2.6.3 The Hydrogen Probe

The degree of embrittlement is a function of the rate of entry of hydrogen into the bulk lattice from the adsorbed state. Consequently, it is necessary to have methods of detecting low concentrations of hydrogen. The double-cell technique pioneered by Devanathan and Stachursky measures the permeation rate through metal foils by imposing a diffusion gradient in the foil by cathodically producing hydrogen at one side whilst simultaneously removing the hydrogen from the other side by oxidising it.

$$H \rightarrow H^{+} + e^{-}$$

Both the hydrogen concentration and the diffusion coefficients can be calculated from the permeation current-time transients as will be seen in Chapters 4 and 5.

A better procedure from the time and equipment requirements is to obtain the hydrogen concentration from the shape of the current-time transient obtained by using a Barnacle Electrode, which is a variation of the permeation method in which use is made only of the oxidation process to determine the hydrogen concentration. A potential is imposed on the surface of the part which is made the anode of an electrochemical cell, causing mobile hydrogen in the part to emerge and be oxidised at the surface.

The Barnacle Electrode was first made by Nanis in 1964 and then improved by Gileadi and Fullenwider (1966). They used a silver/silver oxide electrode to obtain a current-time transient from which, knowing the diffusion coefficient and assuming the thickness is sufficient to obtain a uniform hydrogen concentration profile to be obtained. Berman, Beck and DeLuccia (1974) noted that the

diffusion coefficient was measured from the hydrogen permeation transient analysis of thin foils, and they considered the concentration profile to be uniform for most structures of sufficient thickness. The diffusion equations to be solved are shown below:

$$\frac{J}{ZF} = -D\left(\frac{\delta C}{\delta x}\right) \qquad [1]$$

$$\left(\frac{\delta^2 C}{\delta x^2}\right) - \frac{1}{D}\left(\frac{\delta C}{\delta t}\right) = 0 \qquad [2]$$

where J = permeation current density
Z = number of electrons involved in the oxidation reaction
F = Faraday's constant
D = diffusion coefficient of hydrogen in iron
C = concentration of hydrogen
t = time
x = distance

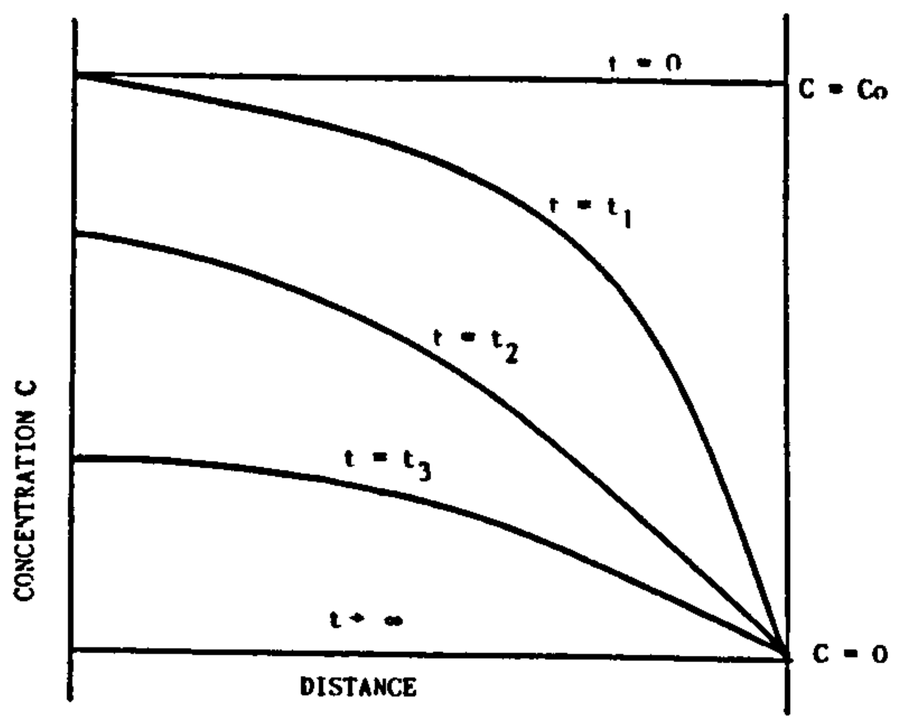

$$\frac{\delta C}{\delta X} = 0 \quad X = 0 \quad t \geq 0$$

$$C = 0 \quad X = L \quad t \geq 0$$

$$C = Co \quad 0 < X < L \quad t \geq 0$$

FIG. 2.7 Boundary Conditions for Barnacle Electrode Hydrogen Extraction

According to Berman, Beck and DeLuccia, Gileadi and Fullenwider used a Laplace transform solution of Equation 2 corresponding to the boundary conditions shown in Figure 2.7, and this results in the following when combined with Equation 1:

$$\frac{J}{ZF} = C_0 \left(\frac{D}{\pi t}\right)^{1/2} \left[1-\exp^{-\frac{L^2}{Dt}}+\exp^{-\frac{4L^2}{Dt}}\ldots\right] \qquad [3]$$

where C_0 = the maximum concentration of diffusable hydrogen
and L = the effective diffusion distance.

It is clear that for cases where $\exp^{-\frac{L^2}{Dt}} << 1$ all

exponential terms may be deleted and that the first term solution

$$\frac{J}{ZF} = C_0 \left(\frac{D}{\pi t}\right)^{1/2} \qquad [4]$$

i.e. provided D is known, a measurement of J at any time, t, will give the value for C_0. This should hold true for thicknesses in excess of 0.1 cm and for

$$t_{max} = \frac{L}{4D} \qquad [5]$$

where t_{max} is the time up to which C_0 may be calculated. Berman and his colleagues found that for a specimen of AISI 4340 steel 0.1 cm thick and D = 2.5 $x10^{-7}$ cm^2sec^{-1}, t_{max} was 100,000 seconds or approximately 30 hours.

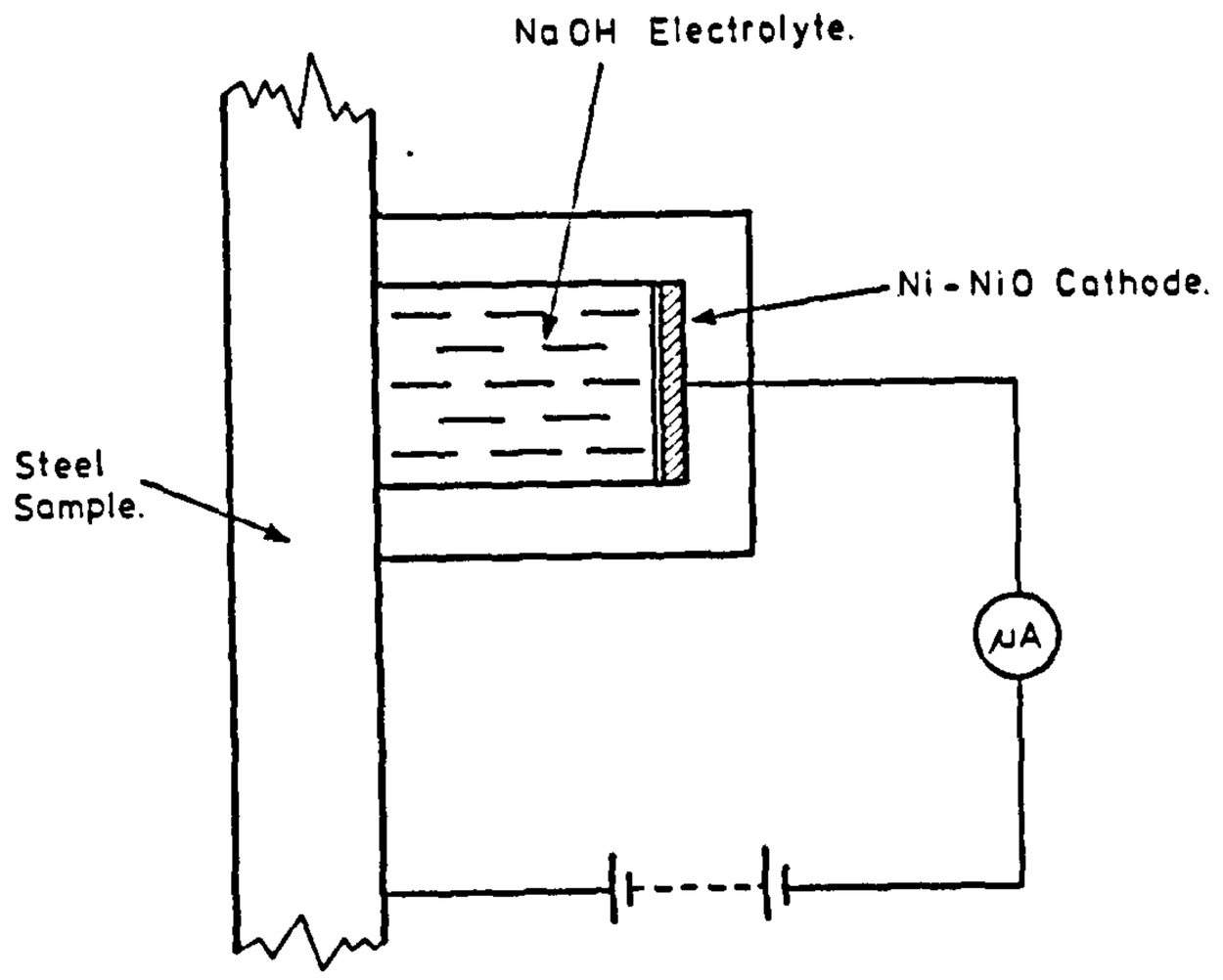

FIG. 2.8 Schematic diagram of the electrochemical hydrogen probe

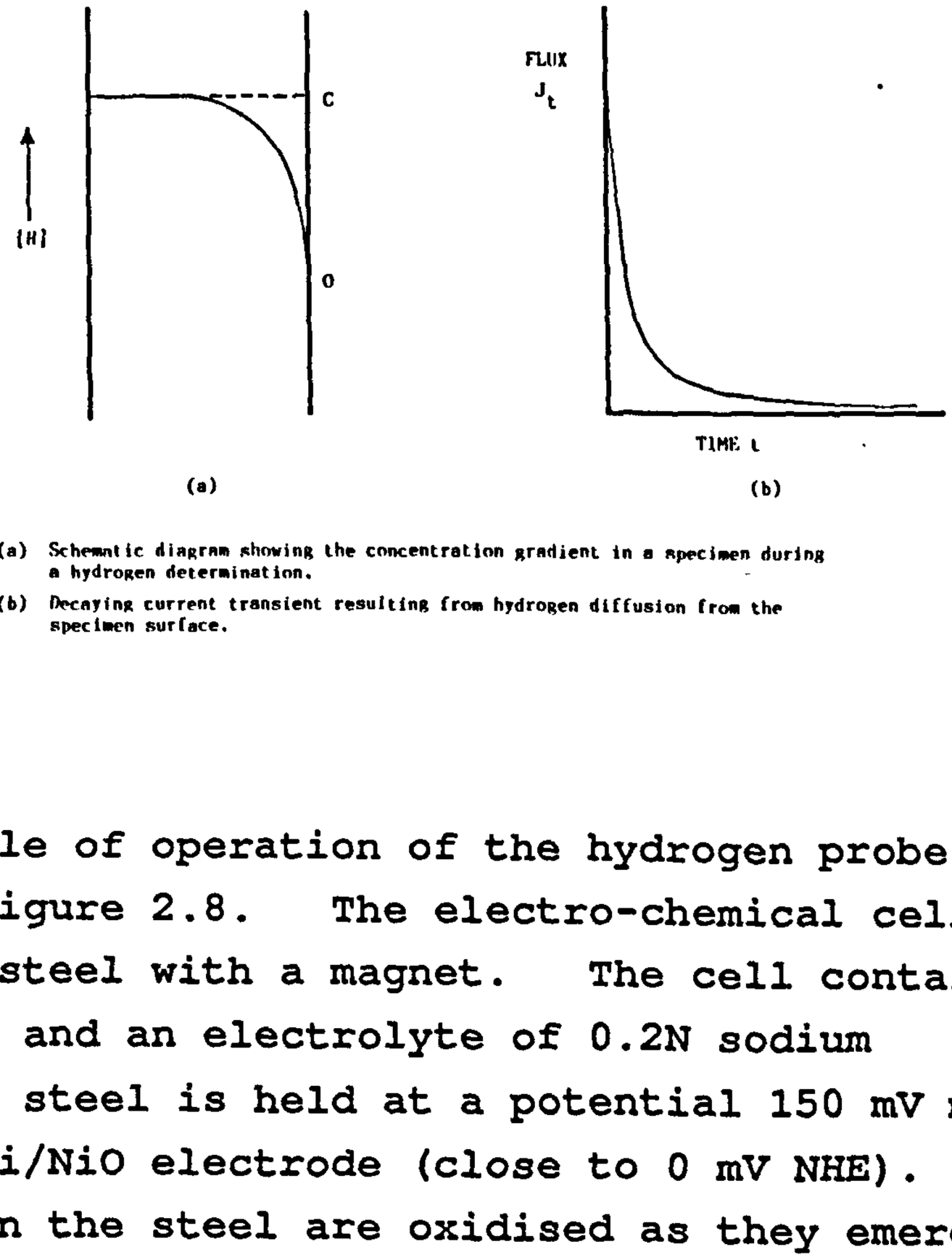

FIG.2.9 (a) Schematic diagram showing the concentration gradient in a specimen during a hydrogen determination.

(b) Decaying current transient resulting from hydrogen diffusion from the specimen surface.

The principle of operation of the hydrogen probe is illustrated in Figure 2.8. The electro-chemical cell is attached to the steel with a magnet. The cell contains a Ni/NiO electrode and an electrolyte of 0.2N sodium hydroxide. The steel is held at a potential 150 mV more noble than the Ni/NiO electrode (close to 0 mV NHE). Hydrogen atoms in the steel are oxidised as they emerge

from the surface under a concentration gradient and the oxidation current is measured using a zero resistance micro-ammeter.

The 0.2N sodium hydroxide solution maintains the steel in the passive condition such that oxidation of the iron does not contribute to the current measured.

The initial distribution of the hydrogen in the specimen is assumed to be uniform, but immediately the probe is connected, a decaying current transient is recorded as shown in Figure 2.9a and b. The flux, J_t is measured at time, t, from which the bulk hydrogen concentration can be measured using the equation above.

A graph of Log J_t plotted against Log t has a gradient of -½ and as will be seen in Chapter 4 - Results, the experimental results closely fit those predicted theoretically.

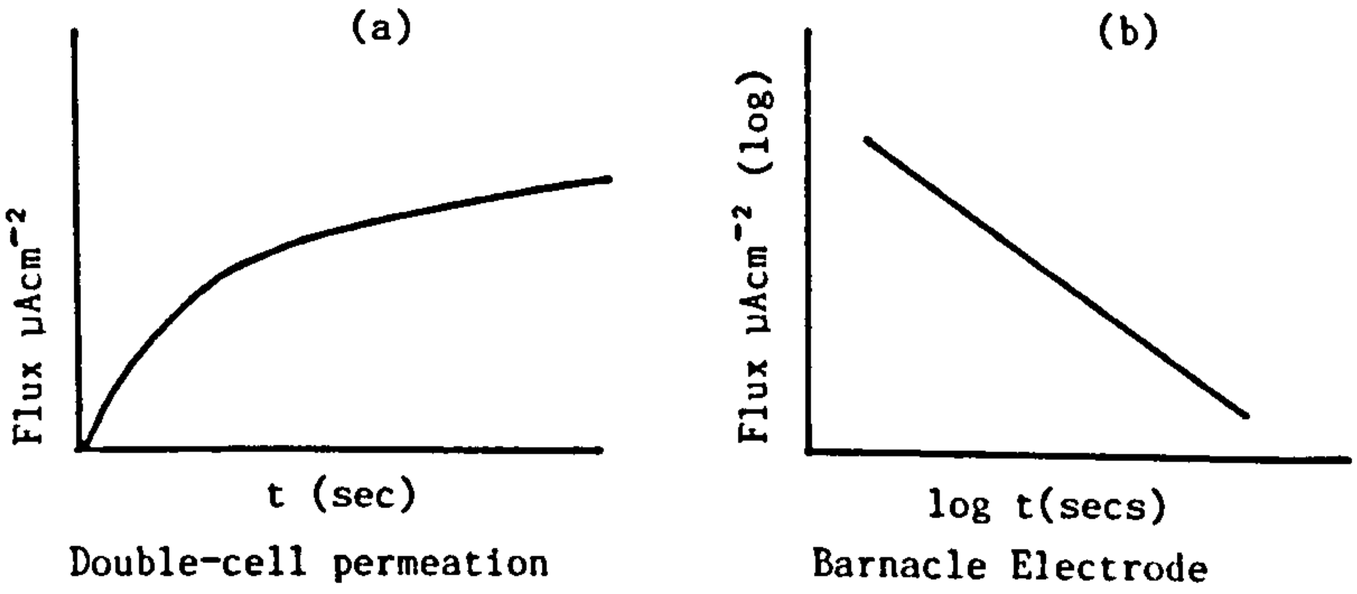

FIG, 2.10 Flux/Time Transients obtained using:
a) double-cell permeation
b) Barnacle Electrode

In decay, a continuous ionisation current is set up during and after charging, but using the Barnacle Electrode there is a distinct separation between charging and extraction phases. This leads to different shaped ionisation curves as shown in Figure 2.10.

From the permeation transients obtained using the double-cell method of Devanathan and Stachursky, the total hydrogen permeated is obtained from the area under the graph, whereas the hydrogen concentration value obtained using the probe is established from the flux value after 10 minutes.

Berman, Beck and DeLuccia (1974), using a nickel/nickel oxide electrode, found that times as short as 5 to 10 minutes after the initial extraction gave current values which could be used to distinguish between concentrations of hydrogen to less than 0.1 ppm in 1 mm thick specimens of AISI 4340 steel.

In 1979, Berman, DeLuccia and Mansfield described how the Barnacle Electrode works, using flat specimens. They found that sustained load failure data correlated with cathodically charged 150 mm flat tensile specimens of AISI 4340 steel; they also made measurements on cadmium plated specimens to determine the hydrogen content before and after de-embrittlement baking. They found that the hydrogen remaining after baking varied considerably depending on the porosity of the plate. Figure 2.11 shows typical Barnacle Electrode extraction transients.

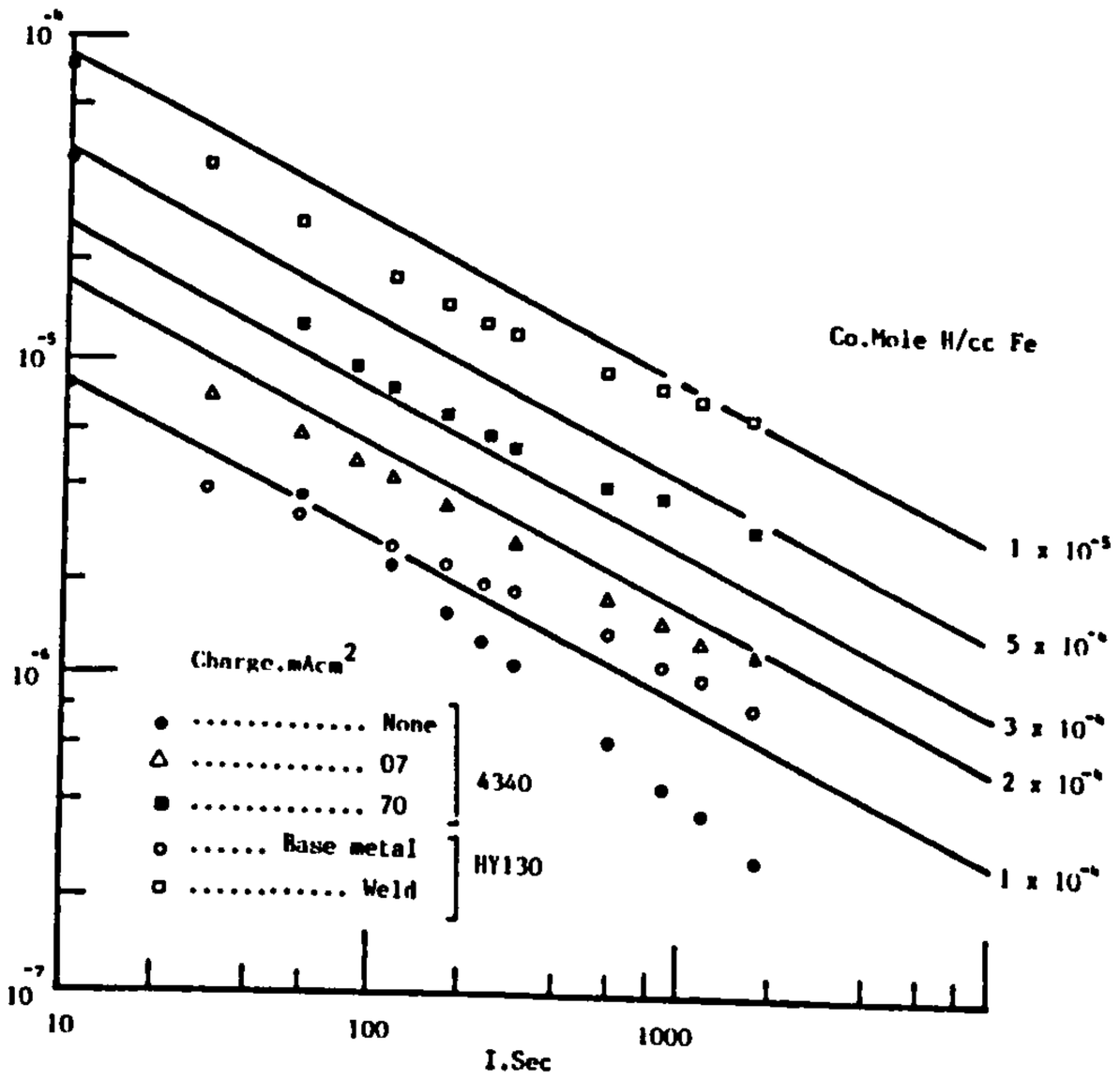

FIG. 2.11 Typical Barnacle Electrode Hydrogen Extraction Transients.

Using a highly sophisticated Lithium Nuclear Microprobe, Adler et al (1974) found very high concentrations, in excess of 200 ppm, [illegible] after plating D6AC steel. They found that the bake-out procedure following chromium plating was far more effective in reducing this concentration than the bake-out following cadmium plating when it did not reduce the concentration below 100 ppm. High trapping in cadmium was given as the reason for this.

In 1990, Robinson and Hudson published details of a further development of a new hydrogen gel-filled probe. This device is described in detail in Chapter 3 - Methods, Section 3.4.2.2., where it was used to show that exposure of steel to the atmosphere has an important influence on hydrogen over a period of time, causing a limited amount of corrosion to occur. This thesis will show that levels of hydrogen resulting from nickel plating are small compared with , those which arise from cathodic charging. Whereas there is a decrease of hydrogen on exposure to the atmosphere for cathodically charged steel, the low concentrations in nickel plated steel and unplated steel appeared to increase. The increase, sufficient to counter the effects of de-embrittling treatment, was possibly due to atmospheric corrosion.

CHAPTER THREE

METHODS

3.1 INTRODUCTION

This chapter divides into two main investigative areas:

a. Constant load testing
b. Hydrogen permeation experiments.

Although the two areas appear to be separate entities, the results of constant load testing after various heat-treatments affected the direction of the hydrogen permeation experiments.

3.1.1. Materials

0.8%C pearlitic cold-drawn steel wire, 1.63 mm. in diameter was used initially. Photomicrographs of this steel in the as-received condition, showing coarse lamellar carbides in the pearlite, and the quenched and tempered condition, can be seen in Figure 3.1a and b respectively.

2 mm AISI 4340 steel sheet was selected as an example of a high strength steel as used in aerospace applications. (Table 3.1- Analysis) Photomicrographs of this steel can be seen in Figure 3.2. It can clearly be seen that in the as-received condition, the steel is very fine-grained and the microstructure is difficult to define (Figure 3.2a) even at X 750 magnification, whereas the quenched condition shown in Fig. 3.2b is highly martensitic and the quenched and tempered at 200° C condition shown in Figure 3.2c still shows signs of the presence of martensite.

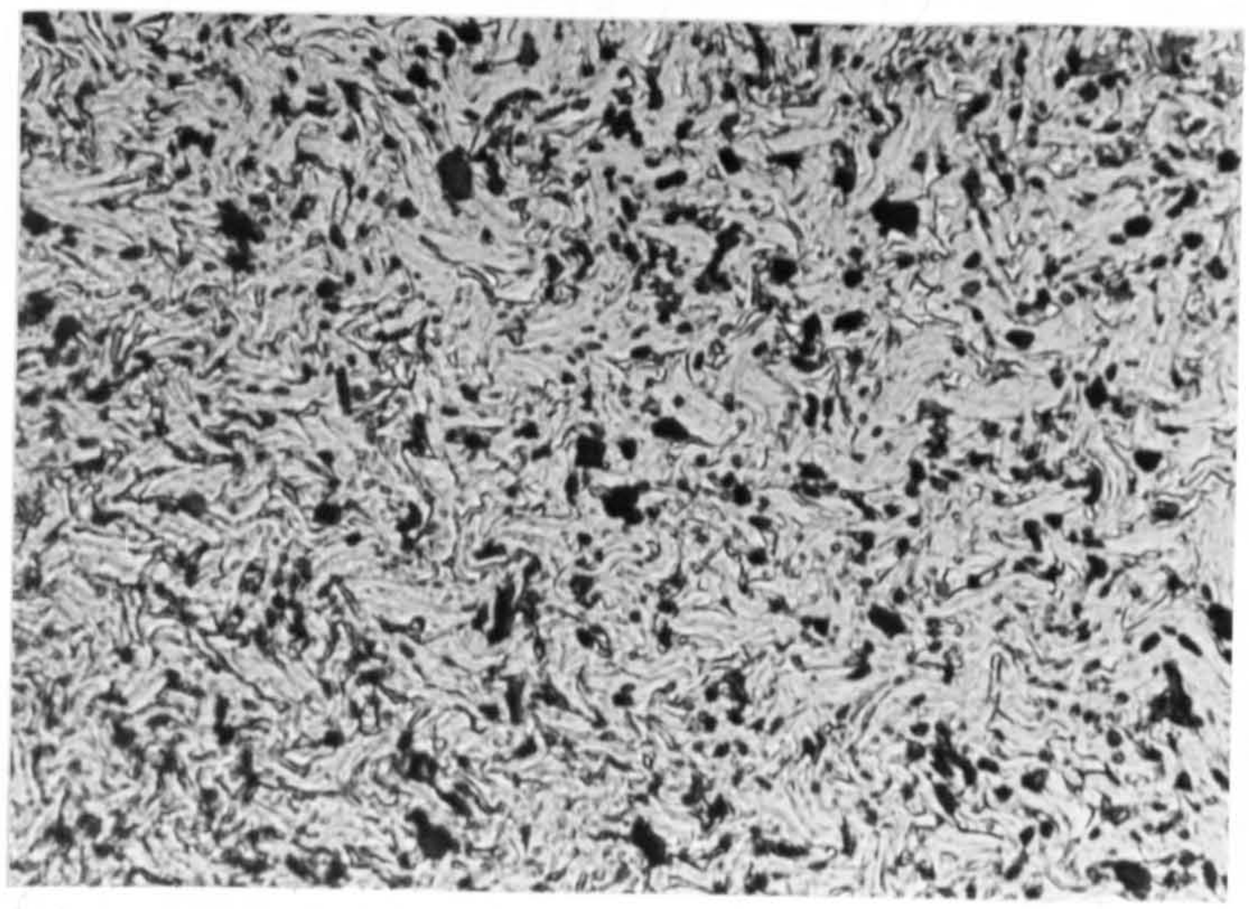

FIG. 3.1a. 0.8%c steel wire. As received. [Mag. x750]

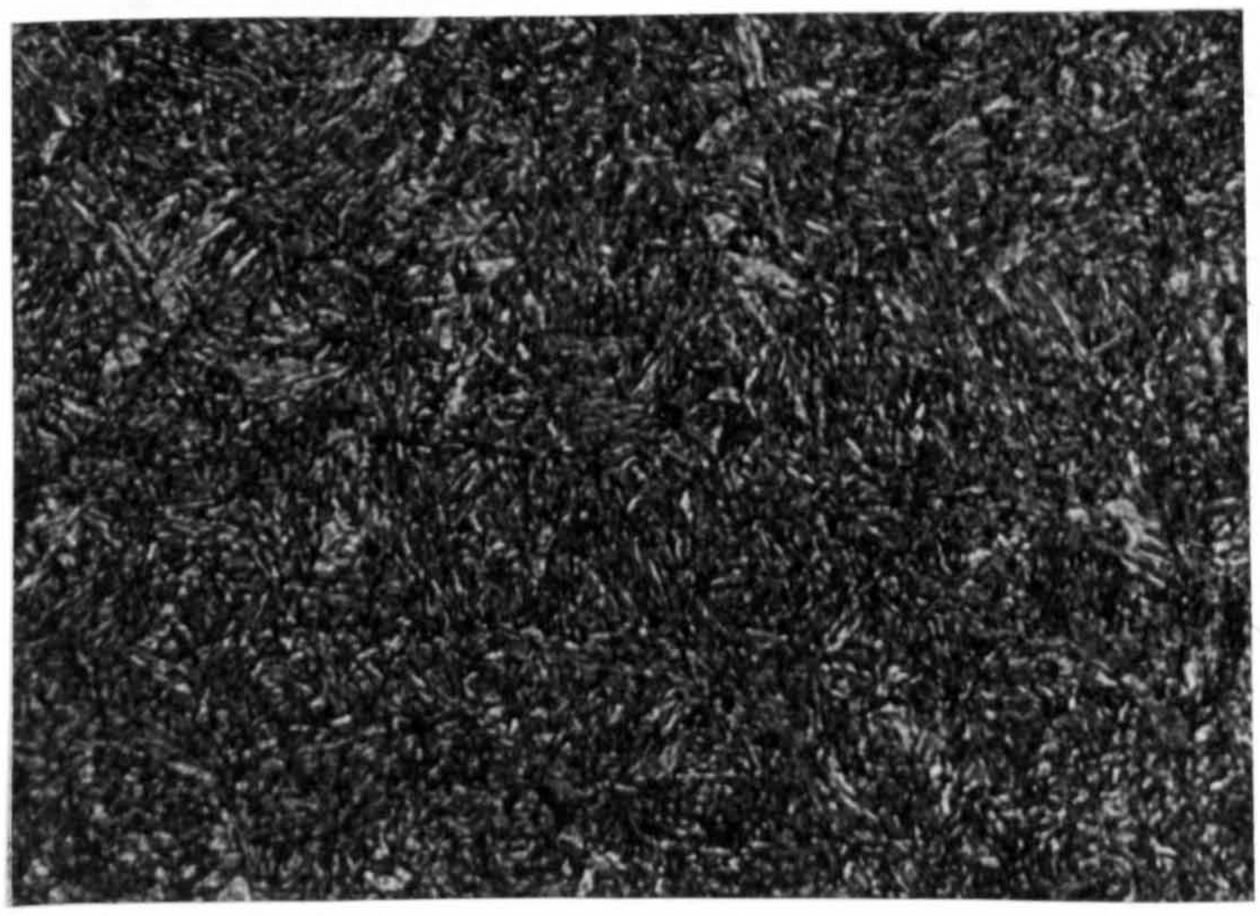

FIG. 3.1b. 0.8%C steel wire. Quenched and Tempered. [Mag. x750]

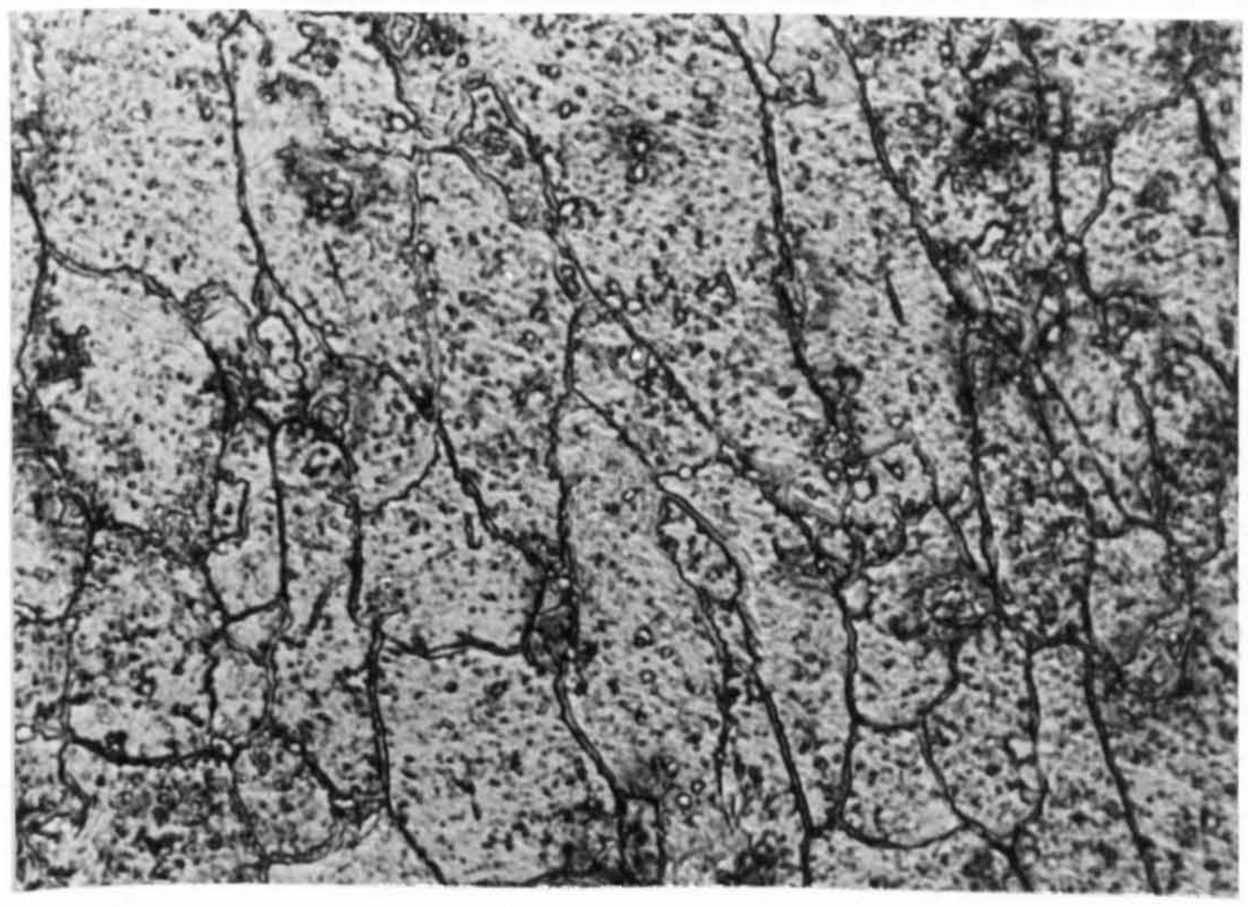

FIG. 3.3. 0.04%c steel foil [Mag. x750]

0.4% C

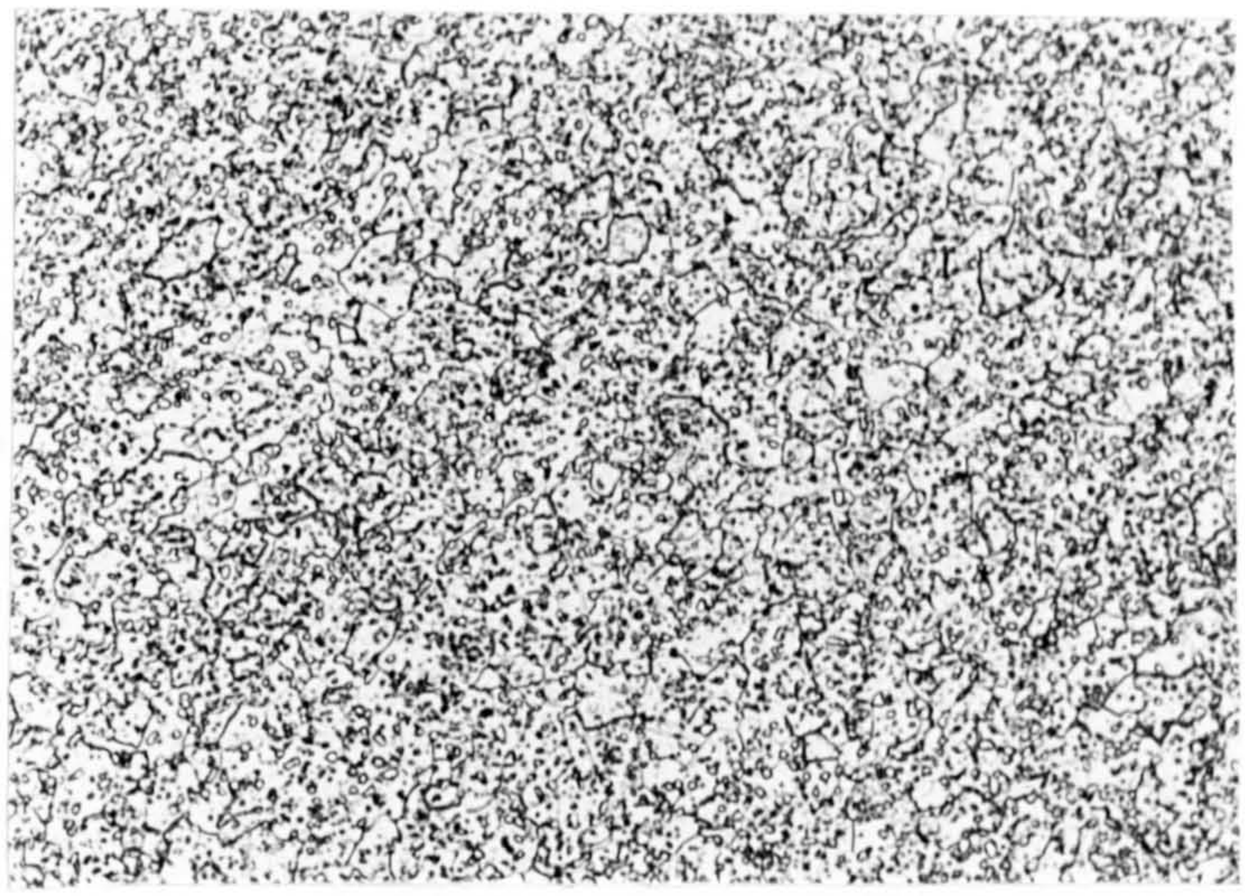

FIG 3.2a. AISI 4340 steel. As received. [Mag. x750]

FIG. 3.2b. AISI 4340 steel. Quenched. [Mag. x750]

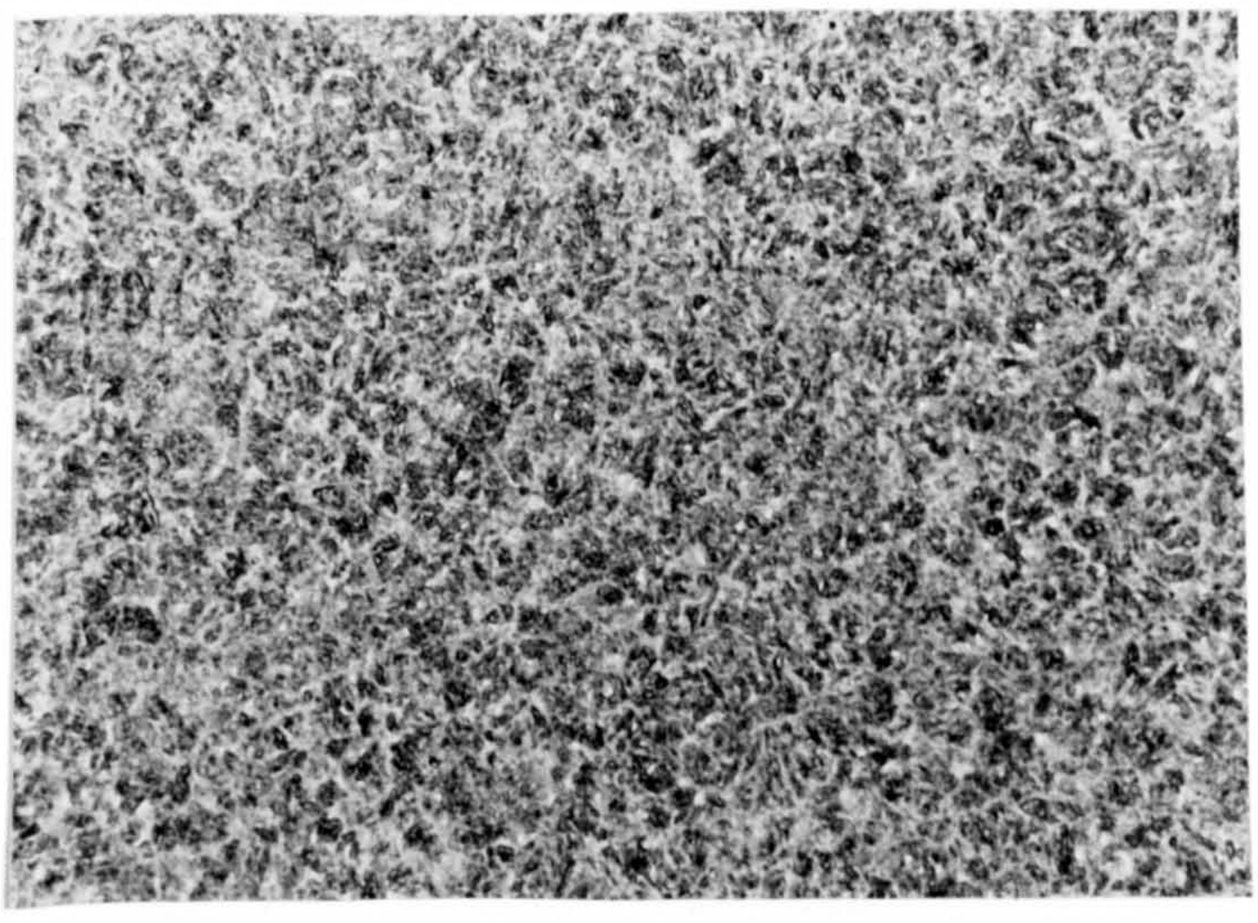

FIG. 3.2c. AISI 4340 steel. Quenched and Tempered. [Mag. x750]

TABLE 3.1 CHEMICAL ANALYSIS OF THREE TYPES OF STEEL

	SHIM	AISI 4340	WIRE
Carbon	0.04	0.38	0.80
Silicon	<0.02	0.36	0.26
Manganese	0.24	0.70	0.51
Phosphorus	0.008	0.008	0.015
Sulphur	0.012	0.005	0.018
Chromium	<0.010	0.82	0.05
Molybdenum	<0.030	0.22	0.03
Nickel	0.02	1.75	0.02
Aluminium	0.05	0.04	<0.010
Boron	<0.0005	<0.0005	<0.0005
Cobalt	<0.010	0.02	<0.010
Copper	0.04	0.04	0.04
Niobium	<0.10	<0.10	<0.10
Titanium	<0.010	<0.010	<0.010
Vanadium	<0.010	<0.010	<0.010
Tungsten	<0.040	<0.040	<0.040

0.04%C steel foil of thickness 57 μm. was used in the double-cell permeation experiments. The photomicrograph of this steel is shown in Figure 3.3. The specimen is rather over-etched but there is clear evidence of the heavy rolling which was used to produce such a thin sheet.

Table 3.1 shows the chemical analysis of each type of material.

3.2 BASIC METHODS

3.2.1 Heat Treatment

Work had already been done by Robinson and Sharp (1986) on 0.8%C steel. This was further tested and the investigation was extended to include the higher strength but lower carbon AISI 4340 steel. To investigate the effects of heat-treatment on the microstructure of the high strength AISI 4340 steel it was decided to use a water-cooled vertical furnace.

Figure 3.4 shows a schematic drawing of the water-cooled vertical furnace. The steel to be treated was attached by one of two methods to a central hollow tube which was suspended by copper wire. (The lengths of wire were simply tied directly on to the hollow tube, but the sheet specimens were hung from the specially designed rig shown in Figure 3.5). The furnace was then sealed, flushed through with argon and the steel specimens were heated in the argon atmosphere and held at 830°C for 30 minutes to ensure that the specimens were fully austenised. After this time, the copper wire was melted by a high current and the central tube, with its attached specimens, was dropped through the double diaphragm of aluminium foil and plastic film into a container of cold water. To achieve a good quench, it was found that no more than 24

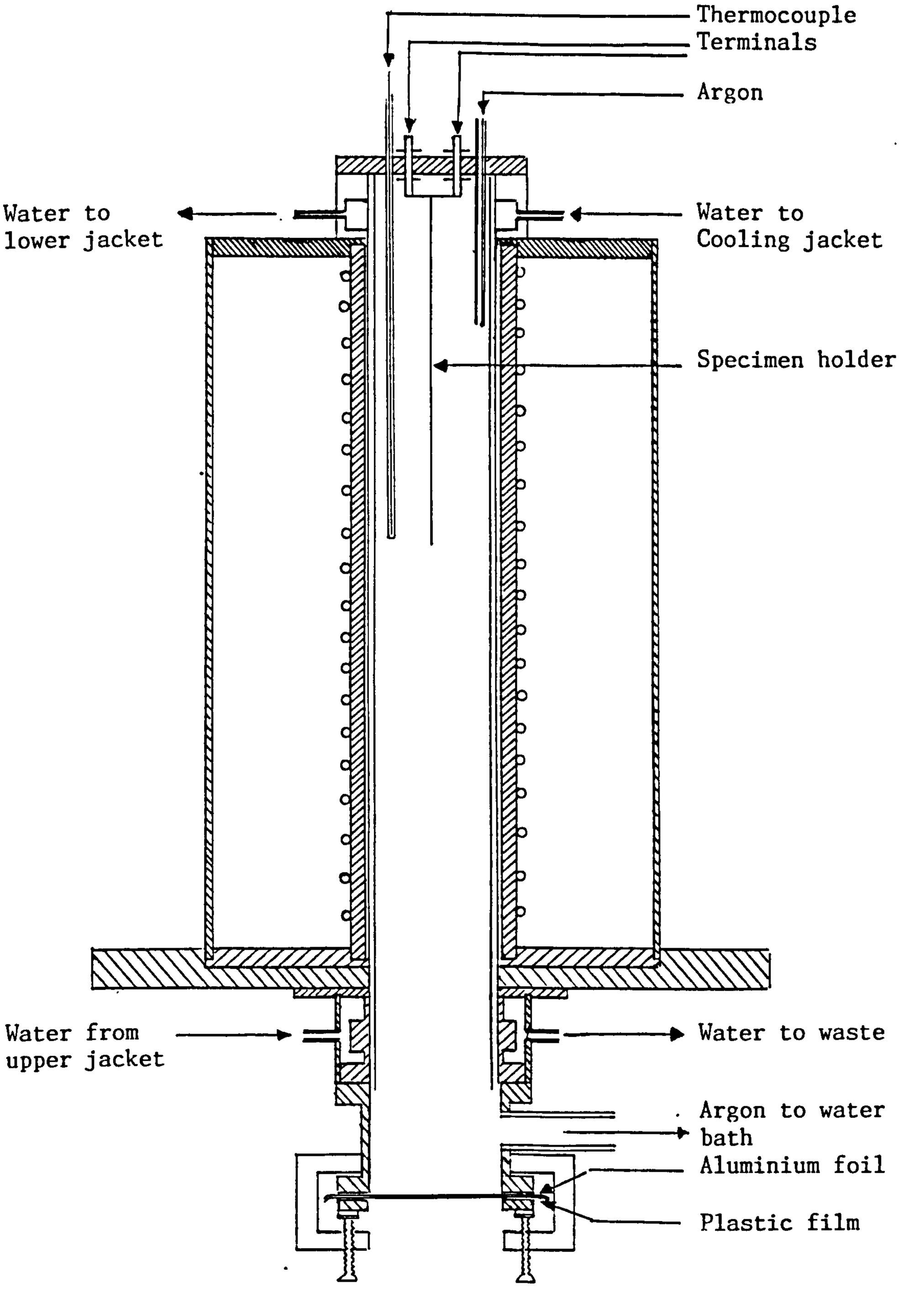

FIG. 3.4 Schematic drawing of the water-cooled furnace

ELECTRICAL CONNECTIONS

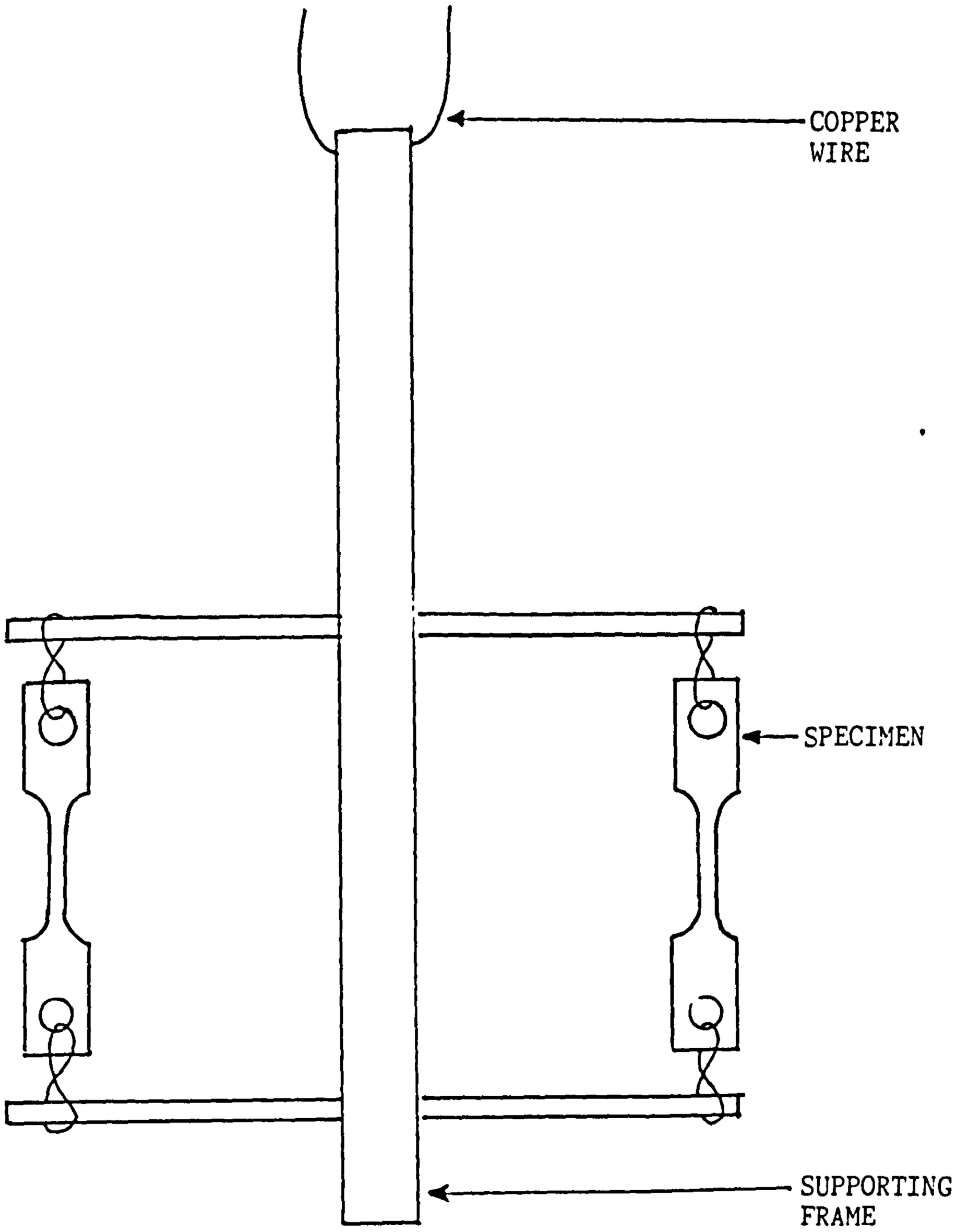

FIG. 3.5 Rig used for specimens in the vertical furnace

wires or 10 sheet specimens could be treated at the same time.

After quenching, it was found that the middle 20 cm of each wire was in a hardened martensitic condition, and so the rig for sheet specimens was designed to allow the entire specimen to reach the hardened condition.

Various groups of specimens were subjected to differing tempering conditions which included the following:

a. 1 hour at 200°C, 300°C, 350°C and 400°C.
b. 2 hours at 200°C, 300°C, and 400°C.
c. 20 hours at 200°C.
d. 2 hours after being placed in a cold furnace and taken up to 400°C.
e. 1 hour at 200°C followed by 1 hour at 400°C.

3.2.2. Cathodic Charging

Specimens were abraded to remove the surface oxide layer and thoroughly degreased using Gramasol. They were then mounted in the testing rig. Cathodic charging was carried out using a 4% sulphuric acid solution poisoned with 4 mgl^{-1} stannous chloride to promote ingress of hydrogen into the material under investigation. Charging occurred at 150 $mAcm^{-2}$ and, in the case of constant load testing, continued until failure of the specimen had occurred. During hydrogen permeation experiments, charging was carried out for a period of 2 hours.

3.2.3. Nickel Plating

The specimens were cleaned as in the previous section before they were mounted in the test-rig where they were nickel plated using a nickel - single salt plating solution at current densities ranging from 2 - 40 $mAcm^{-2}$.

The composition of the standard Watts single salt plating solution was as follows:

$NiSO_2.7H_2O$	105 gl^{-1}	NH_4Cl	15 gl^{-1}	
$NiCl_2.6H_2O$	15 gl^{-1}	H_3BO_4	15 gl^{-1}	pH 4.2

3.3 CONSTANT LOAD TESTING

A diagrammatic representation of the constant load testing rig is shown in Figure 3.6. The knife-edge fulcrum was situated so that the lever ratio was 10:1, enabling fewer weights to be placed on the pan. Specimens were fixed as appropriate and either cathodically charged, plated or simply dead-load tested at loads varying as percentages of the calculated ultimate tensile stress. An electric clock was fixed in series so that the clock stopped when the specimen fractured, enabling the time to failure to be noted.

The fracture stress of each series of specimens was measured using a Dennison tensile testing machine and hardness measurements were made using a Vickers Hardness testing apparatus.

Initial experiments were carried out on as-received 0.8%C cold-drawn steel wire which was 1.63 mm. in diameter. 30 cm lengths of this wire were wound round pulley wheels (as used by Robinson and Sharp, 1986) and cathodically charged whilst loaded at various weights.

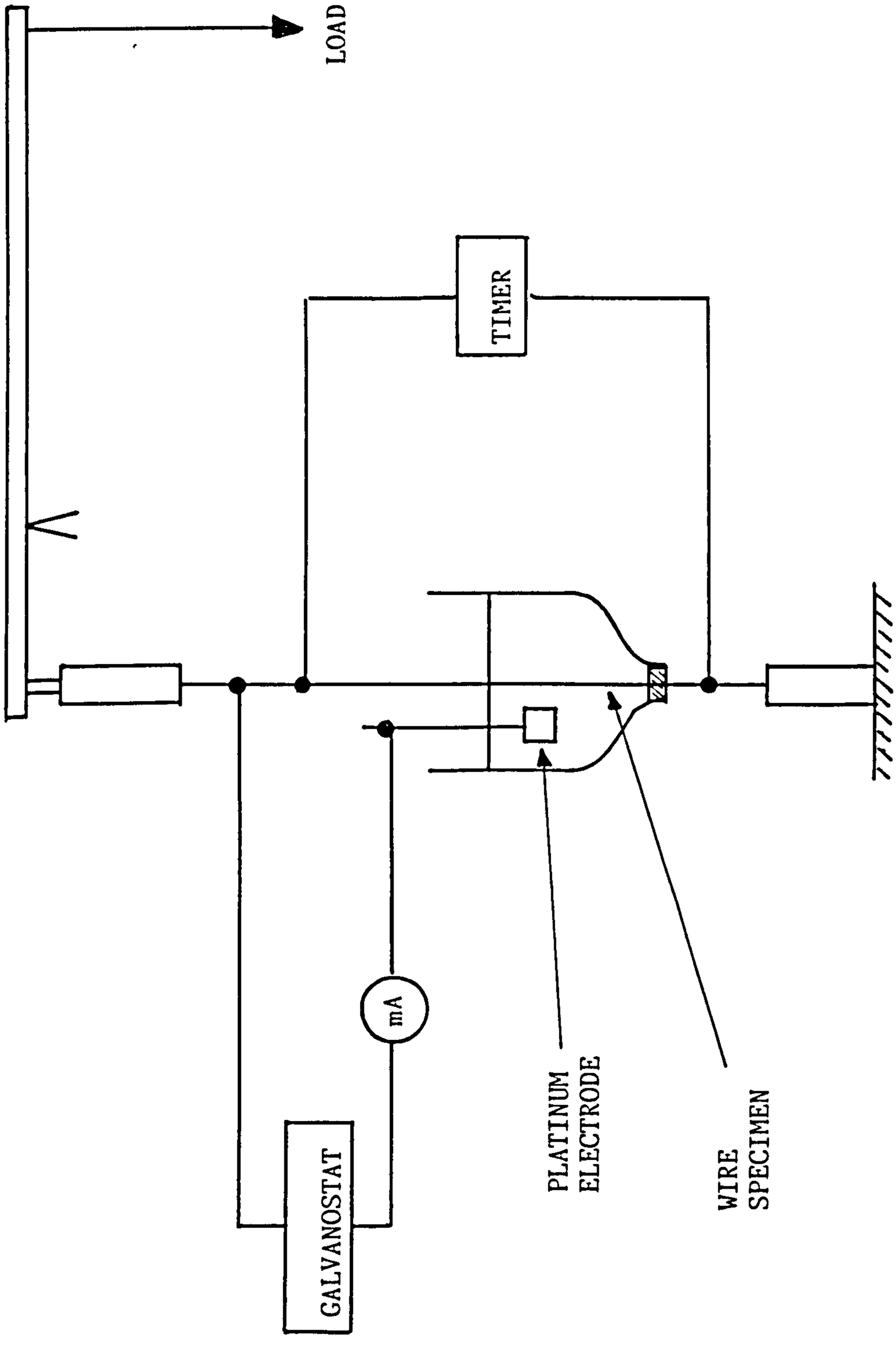

FIG. 3.6 Diagrammatic representation of the constant load testing rig.

Time to failure for each specimen was noted and the fracture surfaces of a selection of specimens were mounted for examination under a Scanning Electron Microscope. (S.E.M.).

Once the wires were heat-treated, they were in such a hardened condition that they could not be bent round the pulley wheels, therefore a new method of mounting had to be used. Hardened lengths were glued into cylindrical grips, using Loctite 638 adhesive, which was strong enough to hold the wire firmly, even though the stress applied was close to the fracture stress. The cell holding the liquid (either sulphuric acid or plating solution) was also modified. As the wire was much more rigid, it was possible to use a much smaller cell made from PTFE with part of a rubber bung, through which a hole had been drilled. The wire could be easily fed through the hole without necessitating the use of PTFE tape to ensure a watertight fit. The modified cell is shown in Figure 3.7.

Further modifications to the grip had to be made when the specimens were machined from 2 mm. AISI 4340 sheet, (see Figure 3.8.) and this configuration is shown in Figure 3.9.

3.4. HYDROGEN PERMEATION EXPERIMENTS

3.4.1. Double Cell Permeation

These experiments were based on the technique used by Devanathan and Stachurski (1962, 1963). This method is a very sensitive technique for measuring diffusion of hydrogen through steel. The hydrogen measured is not that which is kept innocuously in traps, but mobile hydrogen which can migrate to areas of potential crack initiation.

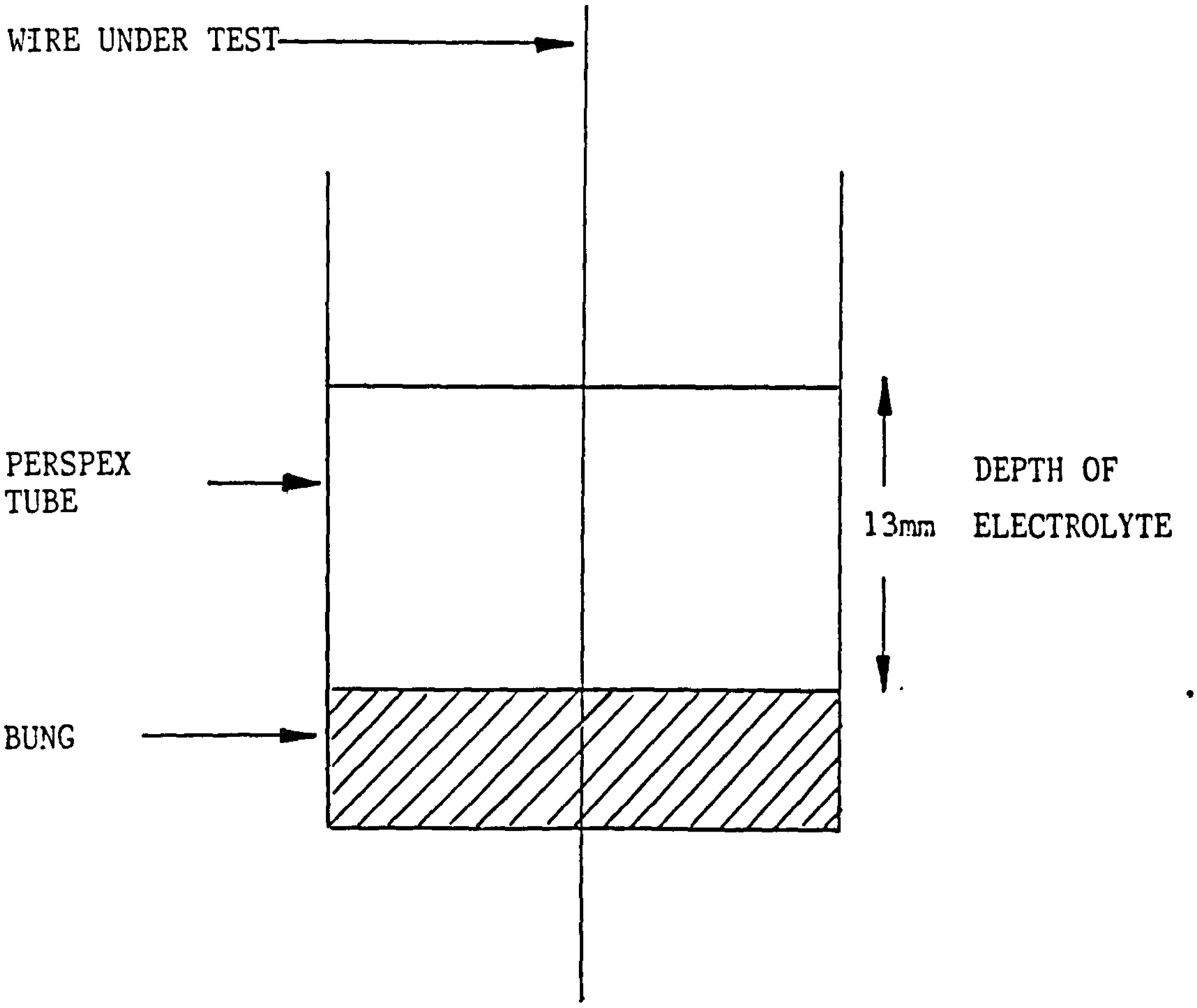

FIG. 3.7 Modified electrolyte cell

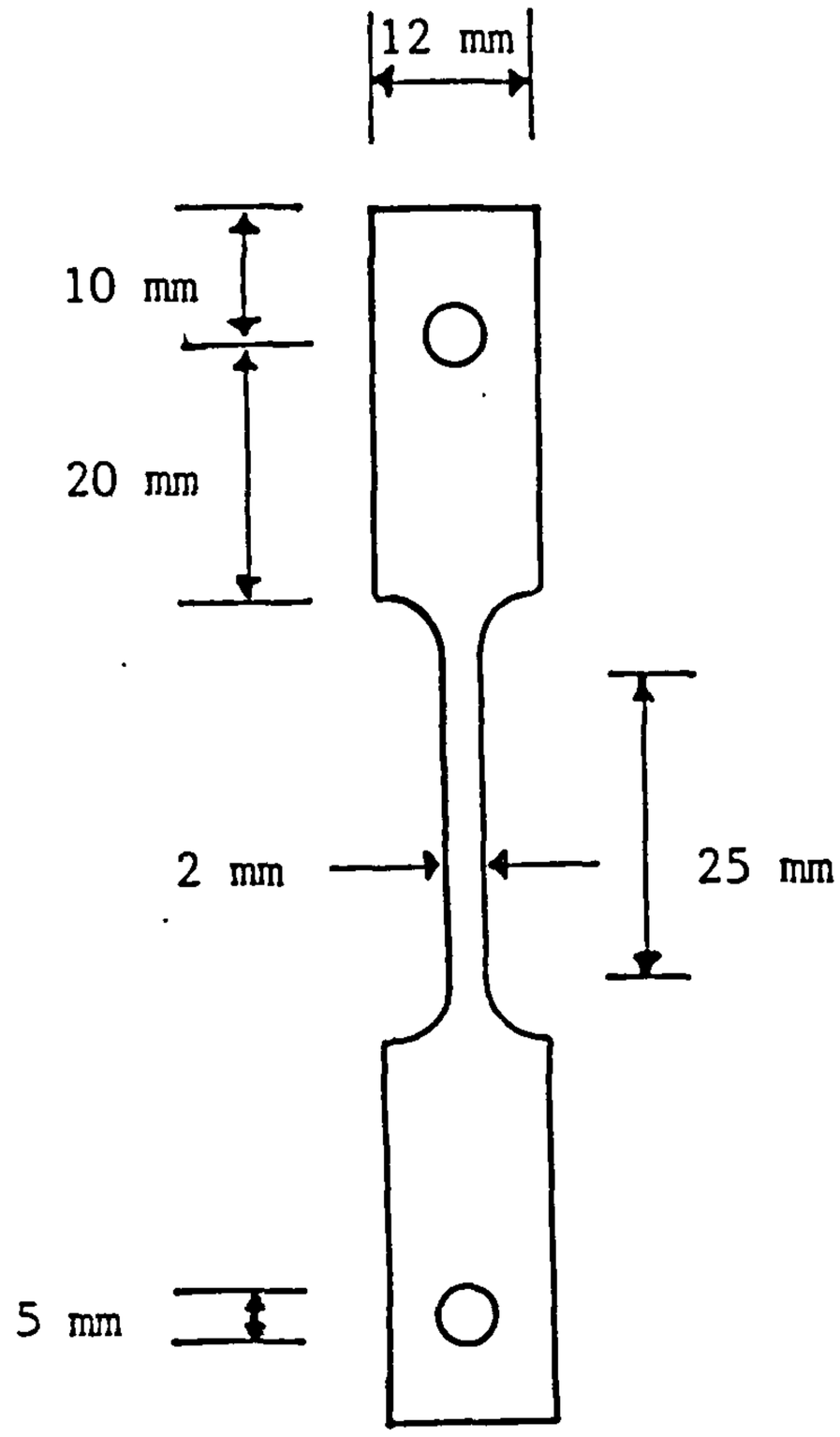

FIG. 3.8 Dimensions of sheet specimens machined from AISI 4340 steel.

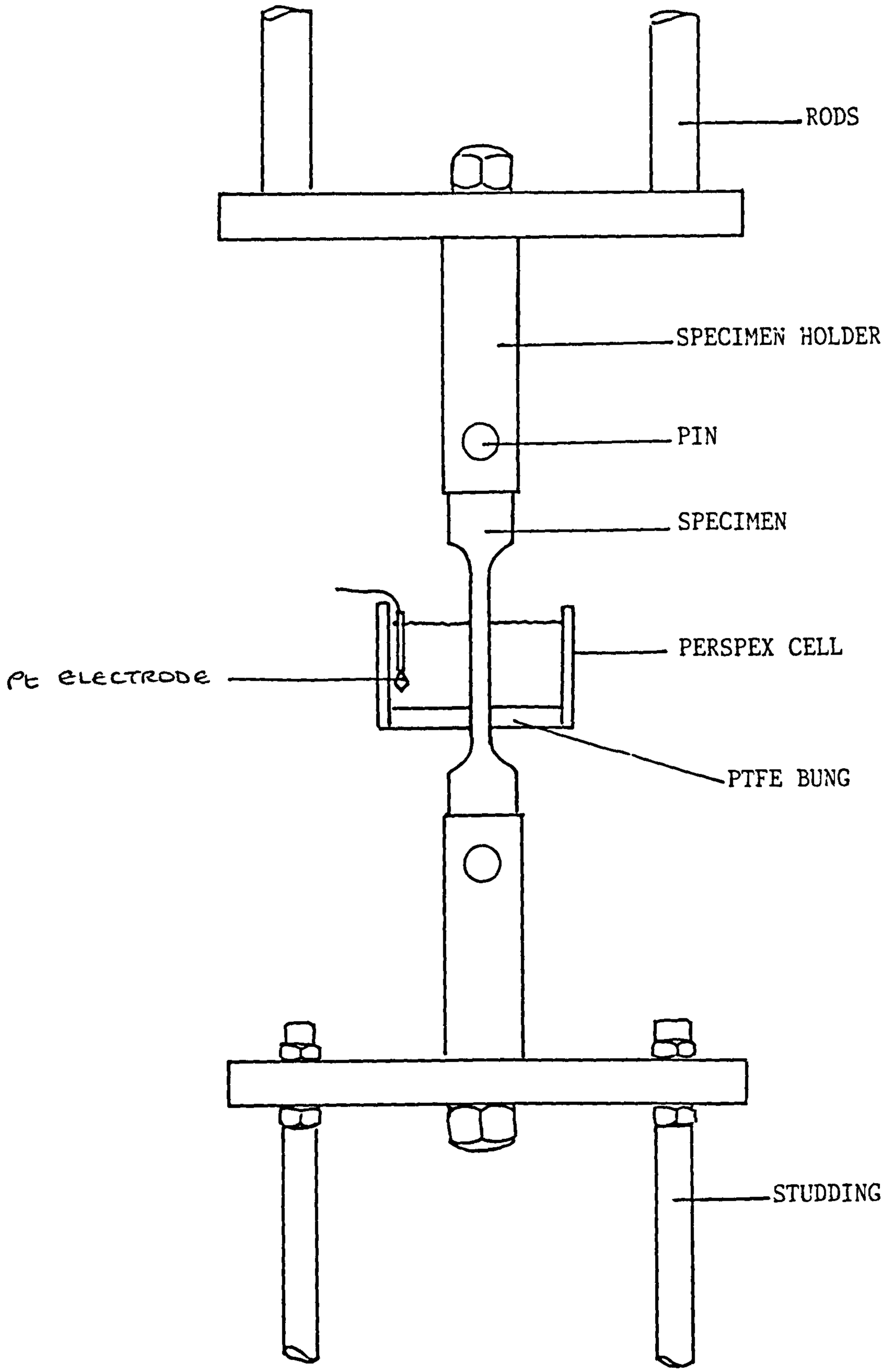

FIG. 3.9 Configuration for constant load testing of sheet specimens

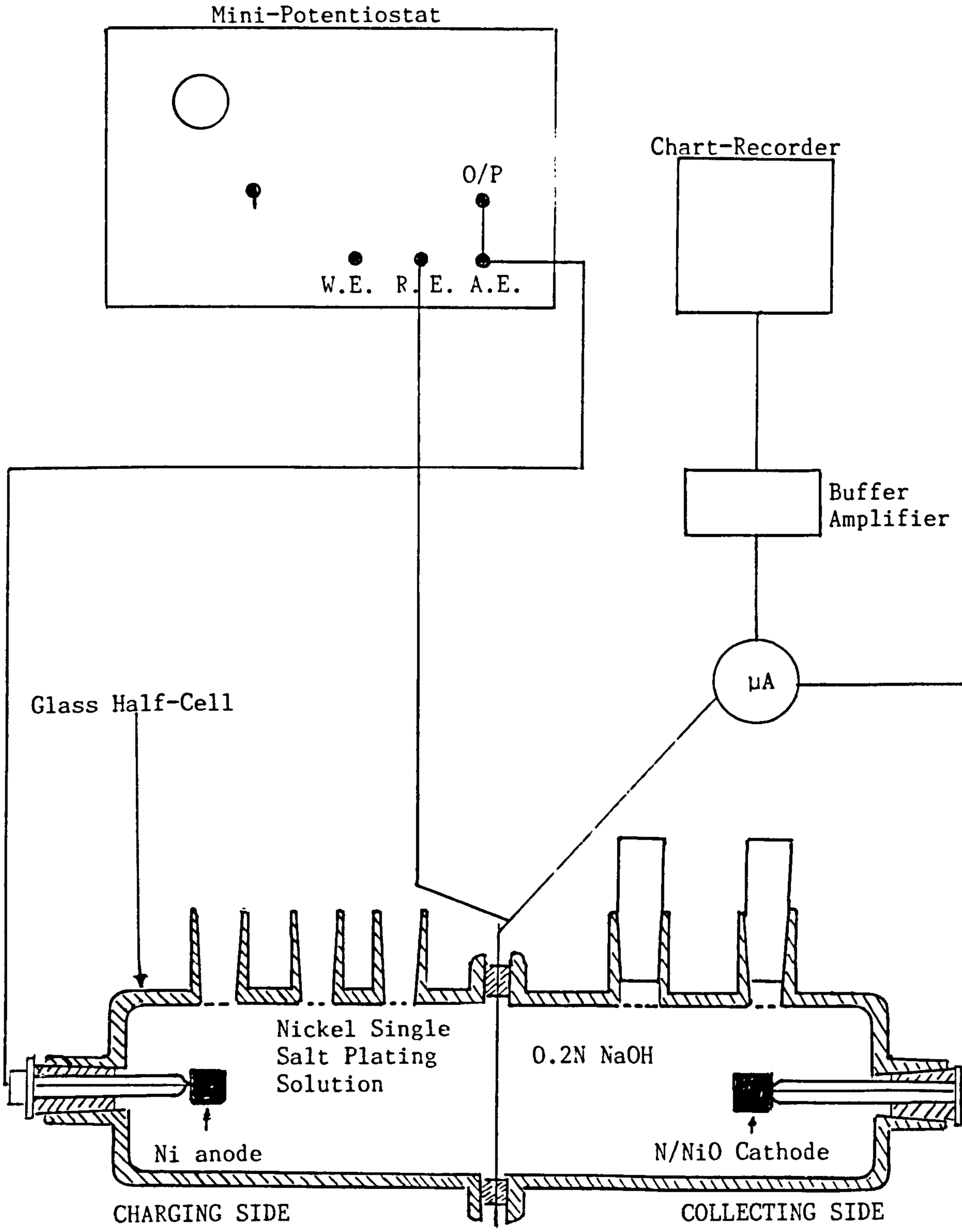

FIG. 3.10 Schematic representation of the double-cell apparatus

A diagrammatic representation of the apparatus is shown in Figure 3.10. It basically consists of two cells of cross sectional area 10 cm^2, separated by a metal membrane, which are clamped together. Each cell has its own independent circuitry with the metal membrane acting as a cathode in the left-hand cell, but as an anode in the right hand cell. The anode in the left-hand cell was made of anodised nickel/nickel oxide which had been anodised by charging in 10% sulphuric acid for 30 minutes at a current density of 15 $mAcm^{-2}$. (In the case of cathodic charging experiments, the anode was made of platinum). Hydrogen is generated by chemical action in the left-hand cell. The hydrogen diffuses through the metal membrane where it is depleted by electrolytic action in the right-hand cell. Depletion is measured using a very sensitive micro-ammeter and the microcurrent recorded can be used as an indicator of the rate of permeation of the hydrogen.

Since the flux is inversely proportional to the thickness of the specimen, the flux of hydrogen evolved at the surface of one side of a sheet specimen 2 mm. thick and permeating through to the other side, was too low to be easily recorded in laboratory experiments, and it was decided to use 57 μm. thick 0.04%C steel foil which would give higher readings. The breakthrough time for this steel was calculated to be less than 9 seconds, but, as the result of experimentation, it is believed to be approximately 100 seconds, and the diffusion coefficient is calculated to be about 2.8 x 10^{-8} cm^2sec^{-1}. Although the composition of this steel and its microstructure differs from AISI 4340 (see Figures 3.2 and 3.3) it was the hydrogen evolved in the plating process which was under investigation, and therefore the steel was only being used as a substrate for electroplating, and would not influence the concentration of hydrogen generated or detected. All experiments were conducted in a cabinet maintained at 25°C.

The steel foil was lightly abraded with fine, abrasive carborundum, thoroughly degreased with Gramasol, dried and placed between the two PTFE washers separating the two cells in the apparatus. Sodium hydroxide solution [0.2N] was placed in the right-hand cell and a potential of 150 mV. was applied, enabling hydrogen depletion to occur. Readings were taken on a microammeter placed in series, and once a minimum current had been reached, usually after being left overnight, nickel single-salt plating solution was placed in the left-hand cell. The specimen was then plated at a range of current densities. The recommended range for nickel plating is 5 - 20 $mAcm^{-2}$, so the investigations ranged over 2 to 40 $mAcm^{-2}$. In some instances, plating occurred in stagnant conditions and in others stirring took place. Plating was continued for two hours and the current was switched off although regular readings of the hydrogen flux permeation continued for a further 60 minutes. In one case, the specimen was coated with Lacomit, leaving only 1 cm^2 of steel exposed, then 4% sulphuric acid was placed in the left-hand cell and the steel was cathodically charged at 150 $mAcm^{-2}$.

3.4.2 The Gel-filled Hydrogen Probe Technique.

3.4.2.1. Introduction.

The double-cell method is very sensitive but it does have disadvantages which include:

1. The membrane must be very thin.
2. Setting up the apparatus with the appropriate solutions is very cumbersome.
3. The experiments must be conducted in a laboratory.

The Barnacle electrode had been developed by Berman, Beck and DiLuccia (1974) after a suggestion by Nanis(1964). This could be used on thicker specimens in situ, but still involved the use of liquid sodium hydroxide. An elegant, yet more simple probe was developed by Hudson in 1987 as an M.Sc. project at Cranfield using a 5 ml. syringe, sodium hydroxide gel and an annular magnet. It was this device that was used to investigate hydrogen permeation in high-strength AISI 4340 steel, heat-treated and/or plated with nickel, enabling comparisons to be made about the effectiveness (or otherwise) of de-embrittling treatment.

3.4.2.2. The Probe

A diagrammatic representation of the probe is to be seen in Figure 3.11. The body of the probe is a 5 cm^3 plastic syringe with the tip removed. A 2 cm. long incision was made along the length of the body and a piece of anodised sheet nickel 3 x 1.5 cm, with a tab 0.5 x 1.5 cm. (anodised as described above in 10% sulphuric acid, at a current density of 15 $mAcm^{-2}$ for 30 minutes) was wound into a cylinder and inserted into the syringe body with the tab protruding from the incision. It was this tab which formed the cathode. An annular magnet was then fixed over the end of the syringe and the surface which was to be placed on the specimen was covered in Araldite to act as insulation between the specimen and the magnet. Finally, the syringe was filled with 0.2N. sodium hydroxide gel. This gel was made by dissolving 2 gm. Agar in 50 ml. warm distilled water and mixing it with an equal volumes of 0.4N. sodium hydroxide.

The syringe was placed on the carefully cleaned specimen and the gel"injected" to form a good electrically conducting contact with the surface of the specimen.

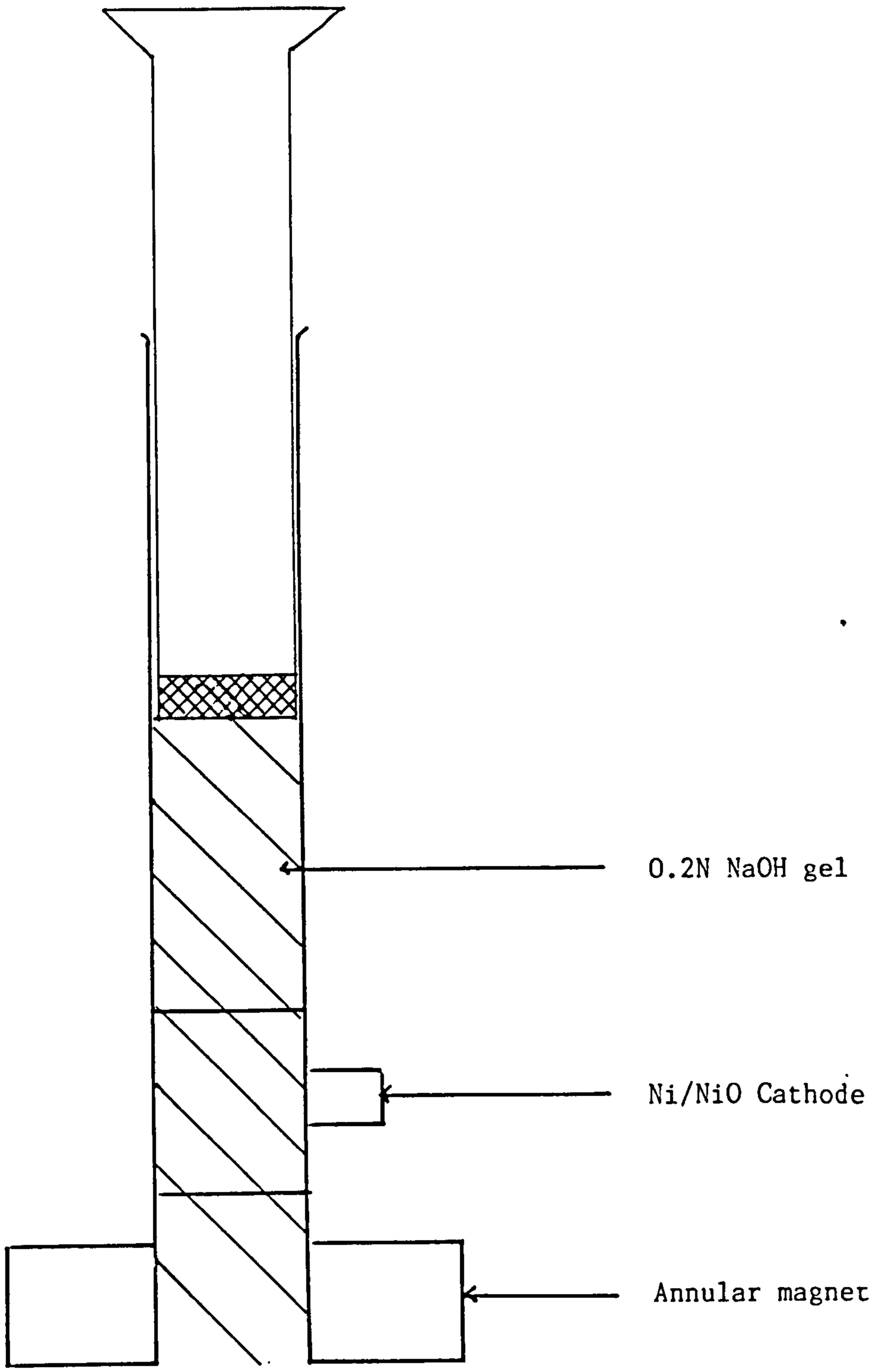

FIG. 3.11 The Hydrogen Probe

Electrical connections were made from the probe electrode and from the specimen to a current detecting meter which held the steel at a potential of 150 mV. compared with that of the nickel/nickel oxide electrode which was considered to be close to 0 mV. (NHE). As hydrogen atoms emerged from the surface under a concentration gradient, they were oxidised and the oxidation current was measured by a very sensitive microammeter.

The 0.2N sodium hydroxide solution maintains the steel in a passive condition, such that the oxidation of the iron does not contribute to the current measured.

The initial distribution of hydrogen in the specimen is assumed to be uniform as illustrated in Figure 2.9a. Immediately the probe is connected, a decaying current transient is recorded as shown in Figure 2.9b. The flux, J_t, measured at time, t, indicates the hydrogen concentration by using Bockris's equation:

$$J_t = F\,C\,\sqrt{(D/\pi t)}$$

where F is Faraday's constant and D is the diffusion coefficient of the material under investigation (in this case, steel). A graph of Log J_t plotted against Log t will have a gradient of -½ and an intercept of Log $FCD^{½}$.

Typical decay transients are shown in Figure 3.12 for .1%C steel, measured in the as-received condition and after cathodically charging in sulphuric acid. The solid lines on the graph represent the theoretical decay transients, calculated from Bockris's equation and correspond to hydrogen contents of 0.03, 0.2 and 0.5 ppm by weight. The experimental points lie parallel to the theoretical

transients, demonstrating that the experimental technique was valid and could be applied to similar specimens of

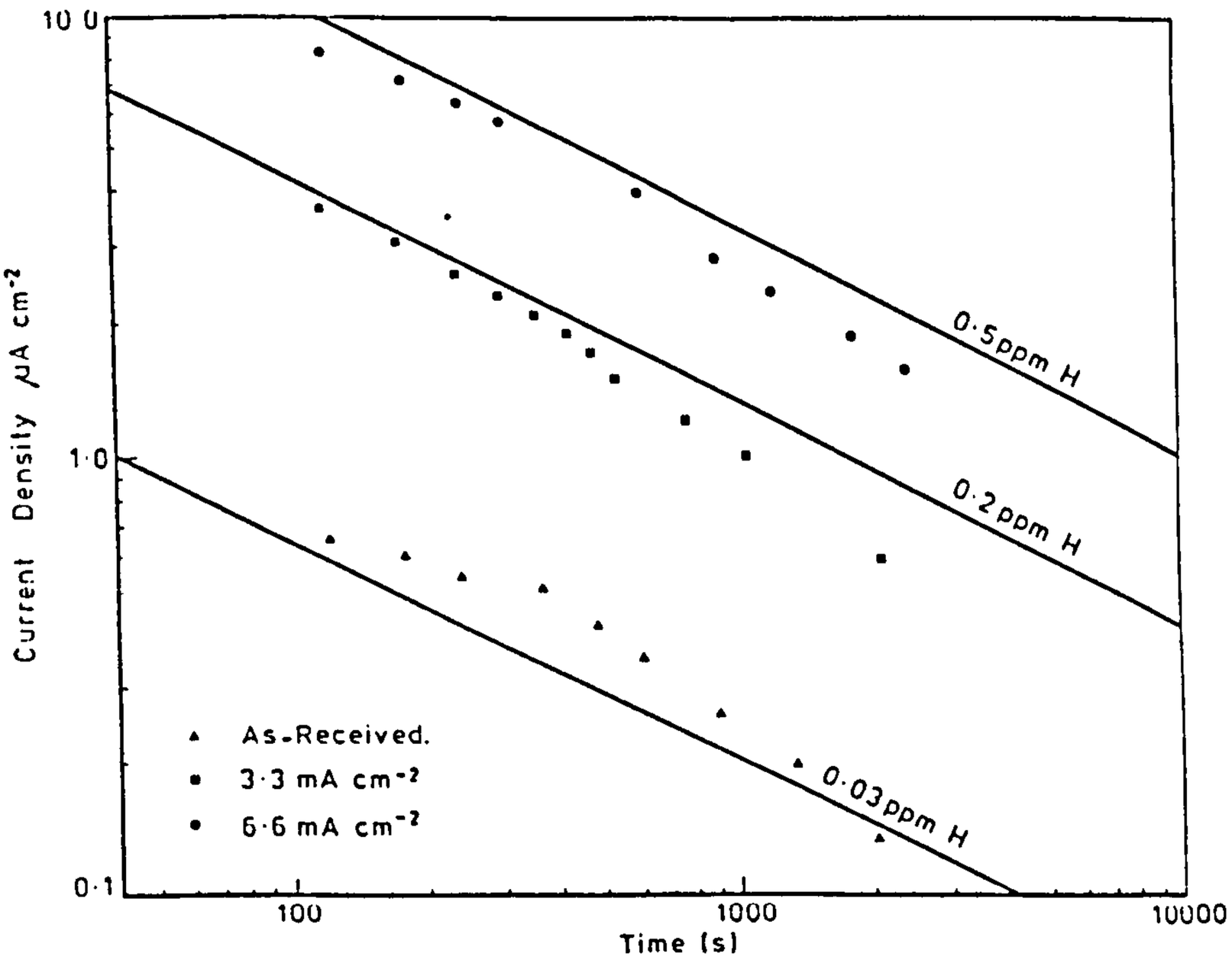

FIG. 3.12 Current transients for as-received and cathodically charged 0.1%C steel

AISI 4340 steel which had been either cathodically charged or nickel plated.

During depletion experiments it was found that variable gel consistency and the surface of the specimens could cause anomalous results; consequently, care was taken to refine experimental techniques to obtain consistency. The gel must be kept moist and constant pressure applied to the syringe plunger to ensure good electrical contact; whilst all the specimens needed to be carefully abraded and thoroughly degreased before each set of readings to obviate the erroneous results obtained in the presence of an oxide film.

Initial experiments were done on the machined specimens used in the constant load testing. In each case, the probe was placed on the specimen and the current

read at 60 second intervals for 15 minutes. Graphs were plotted for each specimen and the hydrogen concentration at 10 minutes was calculated. (The "bench-mark" of 10 minutes was chosen as it was felt that, by then , the characteristic initial rapid rate of depletion had slowed and settled down).

Four main conditions were assessed after the initial quenching heat-treatment (described in the previous section 3.2.1.). These were:

a. Tempered at 200°C.
b. Tempered and plated.
c. Tempered, plated and baked at 200°C for 2 hours.
d. Tempered, plated and baked at 200°C for 20 hours.

Later experiments were done on sheet specimens of 6 x 3 cm., enabling more measurements to be made on each specimen.

Effects of tempering, nickel plating, comparisons between hydrogen contents of plate and substrate and the effects of different methods of storage were all investigated. When comparing the contents of plate and substrate, the nickel was initially removed by abrasion. To assist in removing the nickel, further tests were performed in which the steel was coated with a thin layer of graphite prior to plating. The aim was to reduce the adhesion of the nickel to the steel whilst still maintaining good electrical conductivity. This technique was only partially successful and so a third series was performed where the nickel was removed by surface grinding. Care was taken when grinding slowly with the use of large volumes of coolant to avoid excessive heating of the steel, which would cause loss of hydrogen by diffusion. Eight hydrogen determinations were performed on the nickel on one

side of the sheet, and on the exposed steel substrate on the other. To study the redistribution of the hydrogen with time, further specimens were plated and then left for seven days prior to the nickel being ground off and the hydrogen contents of the nickel and the steel substrate determined.

The effects of different methods of storage were also investigated. Specific details of each type of experiment are to be found in Chapter Four - Results.

CHAPTER FOUR

RESULTS

4.1 CONSTANT LOAD TESTING

4.1.1. As Received 0.8% C. Wire

Table 4.1 shows the results obtained when fourteen specimens of as-received 0.8%C wire were cathodically charged under seven different loads. Load is expressed as a percentage of ultimate tensile stress (UTS) and the average time to failure (in seconds) is shown. Load against time to failure is plotted graphically in Figure 4.1. As to be expected, the higher the load, the shorter the time to failure.

TABLE 4.1. Times to Failure at Various Loads

Specimen	% UTS	Mean Time to Failure (sec)
1 2	84.7	483
3 4	97.0	170
5 6	85	245
7 8	69.4	601
9 10	57.9	1084
11 12	79.0	347
13 14	90.4	203

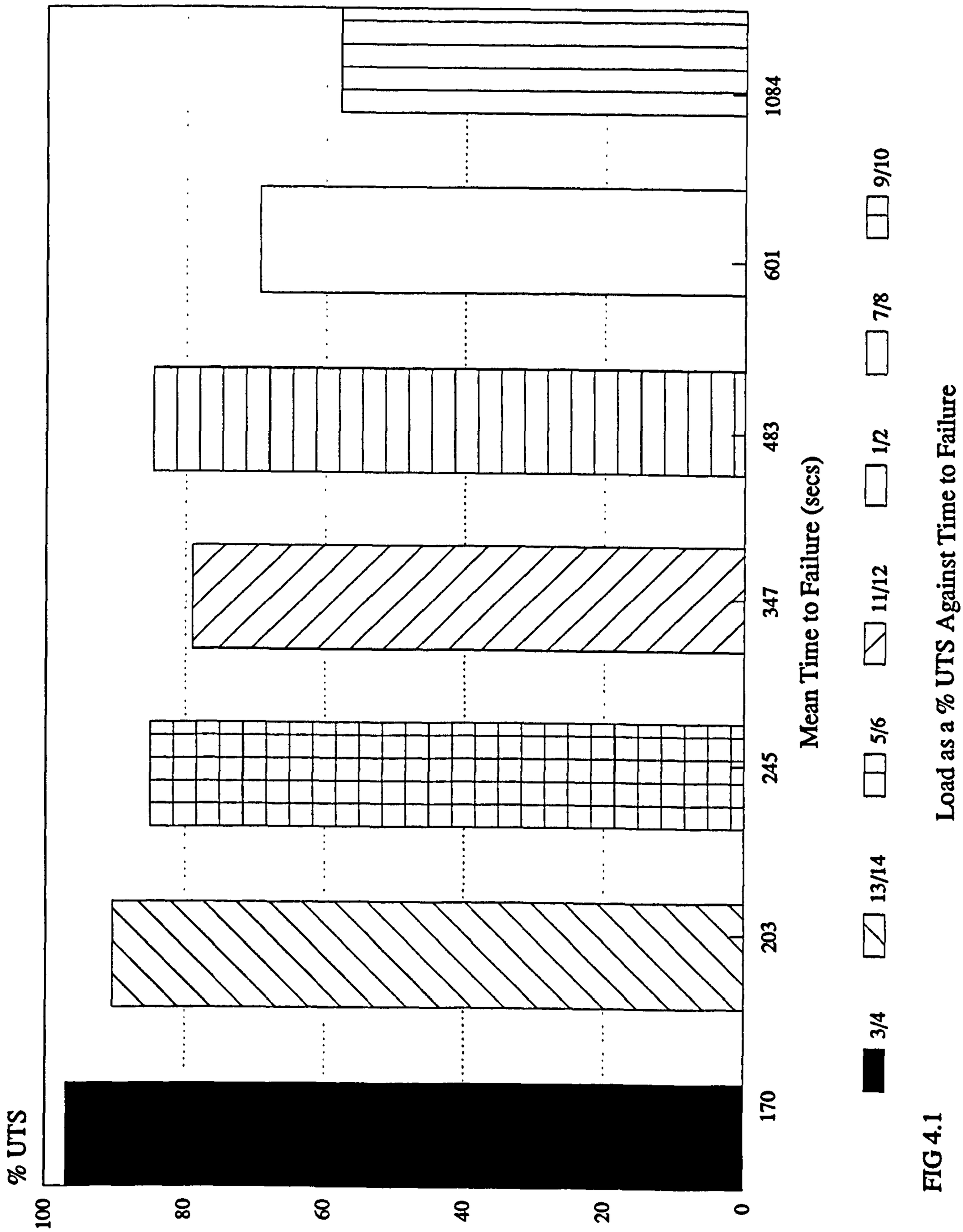
% UTS
100
80
60
40
20
0
Load as a % UTS Against Time to Failure
Mean Time to Failure (secs)
11/12
1/2
7/8
9/10
3/4
13/14
5/6
1084
601
483
347
245
203
170

FIG 4.1

The fracture surfaces of each of the specimens mentioned above were examined under a scanning electron microscope (SEM). Photographs were taken and, using tracing paper and counting squares, the extent of microvoid coalescence (MVC) was estimated for each specimen. Figure 4.2 consists of copies of SEM photographs of specimens fractured after each load value. Table 4.2 and Figure 4.3 show the data obtained, and from Figure 4.3 it can be seen that there appears to be a linear relationship between the load and the % MVC; the greater the load, the more extensive is the % MVC.

TABLE 4.2 % MVC Compared with % UTS

%UTS	%MVC
57.9 57.9	48.0 50.8
69.4 69.4	62.9 61.9
79.0 79.0	72.9 67.1
84.7 84.7	66.1 68.3
85.0 85.0	69.5 81.2
90.4 90.4	76.8 77.6
97.0 97.0	84.8 80.4

FIGURE 4.2 SEM PHOTOGRAPHS OF 0.8%C STEEL WIRE.
Fracture Surfaces after Various Loads

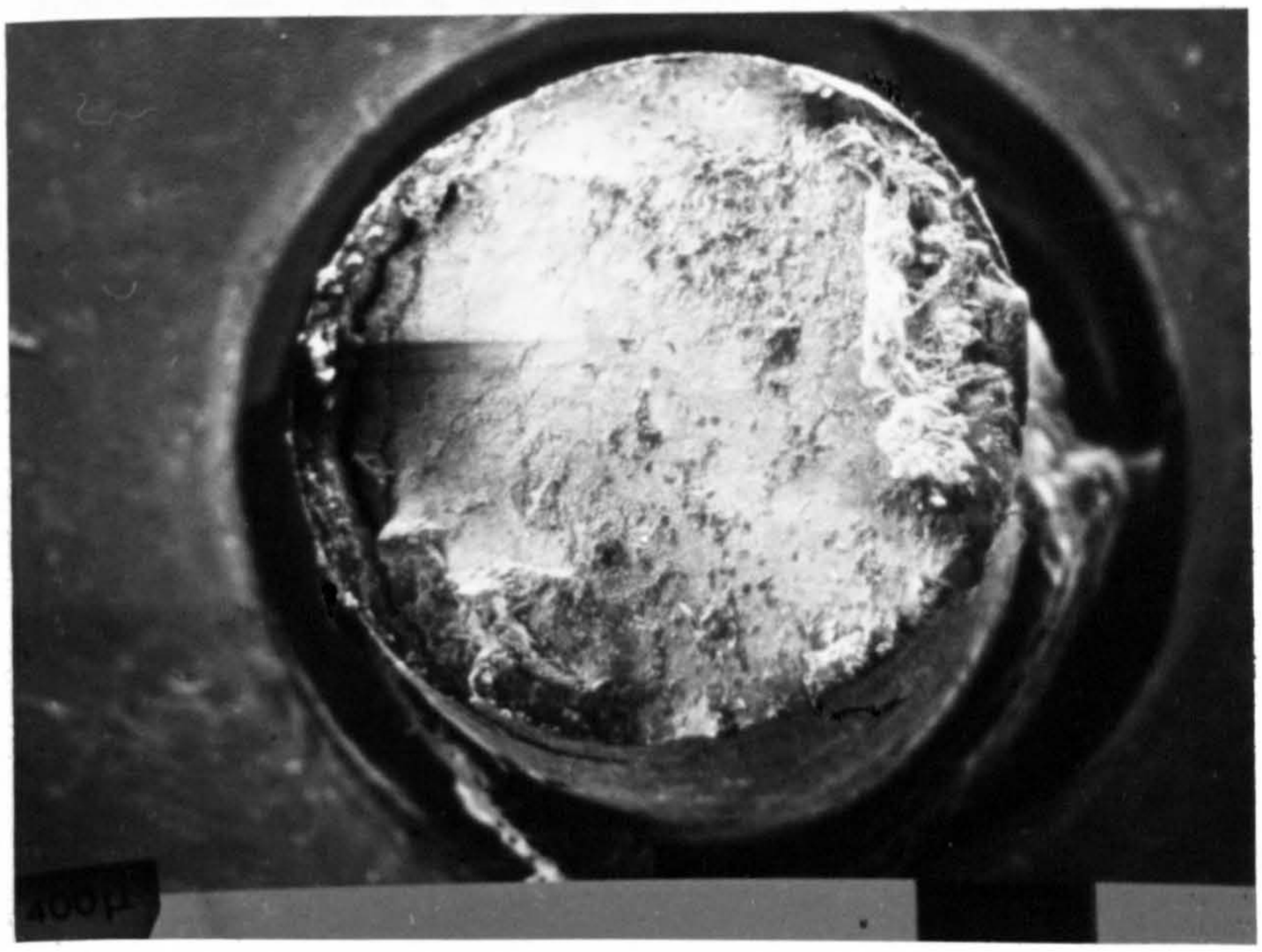

a. 97.2% UTS

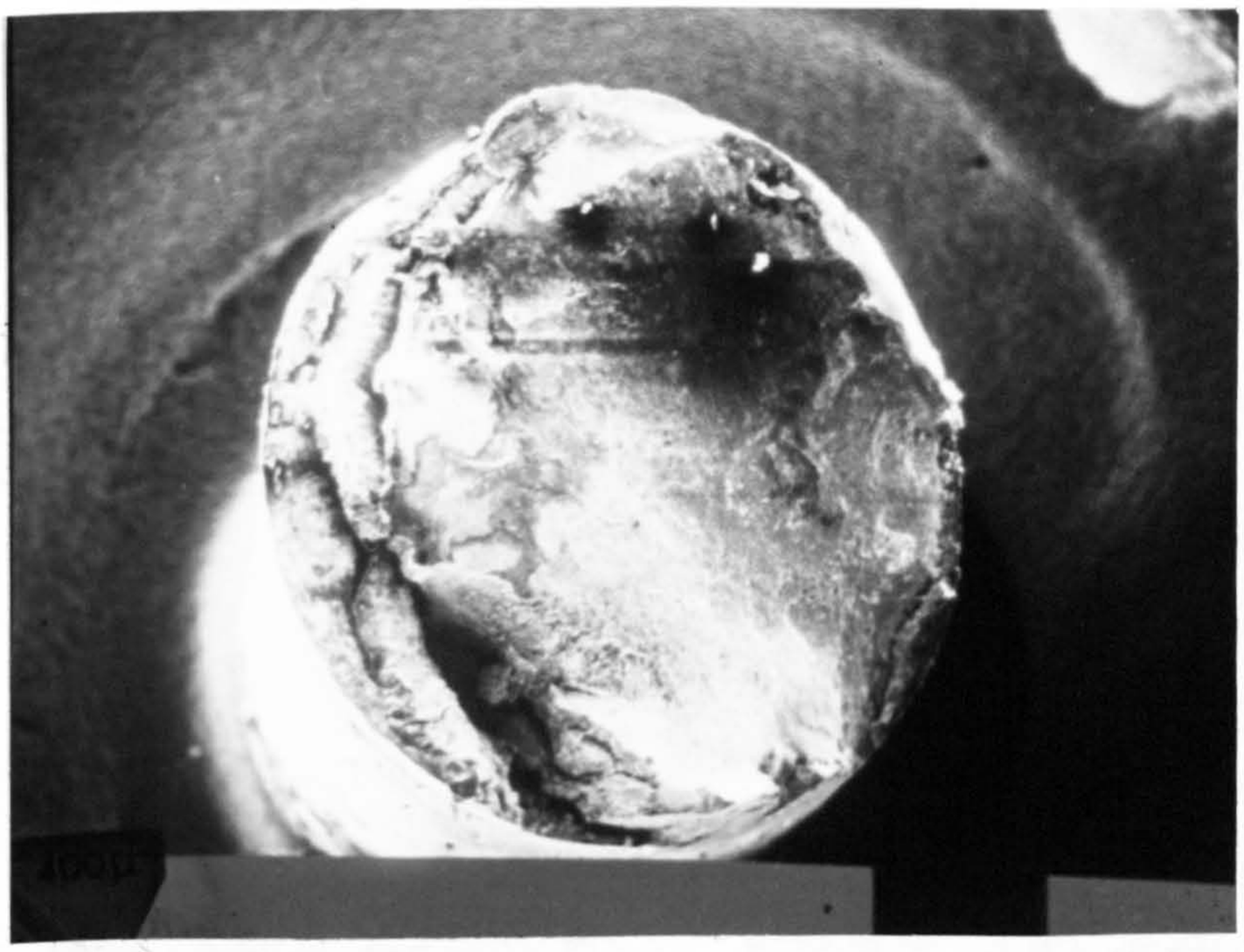

b. 84.7% UTS

FIGURE 4.2 Continued

c. 79.1% UTS

d. 69.4% UTS

FIGURE 4.2 Concluded

e. 57.9% UTS

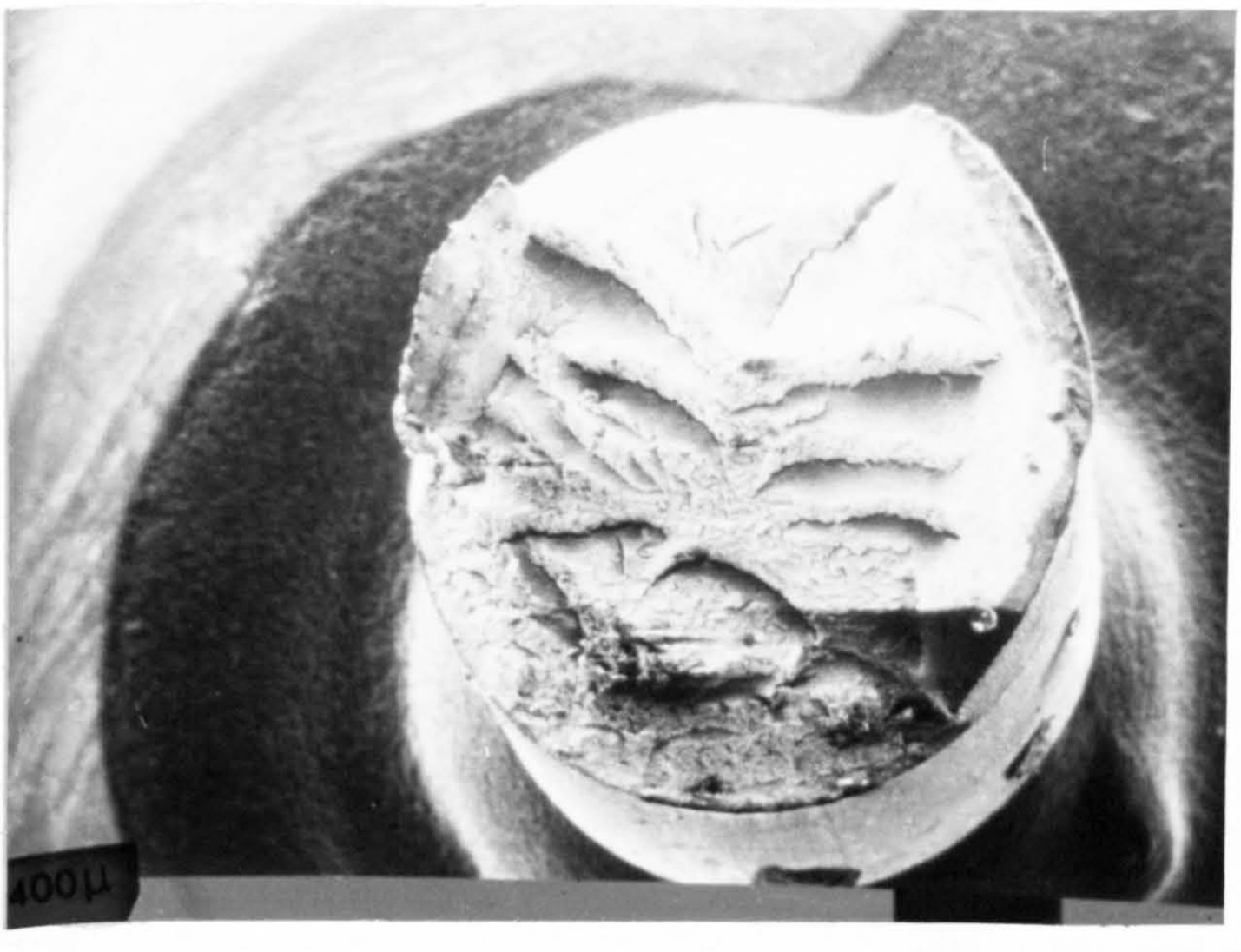

f. Another specimen loaded to 57.9% UTS.

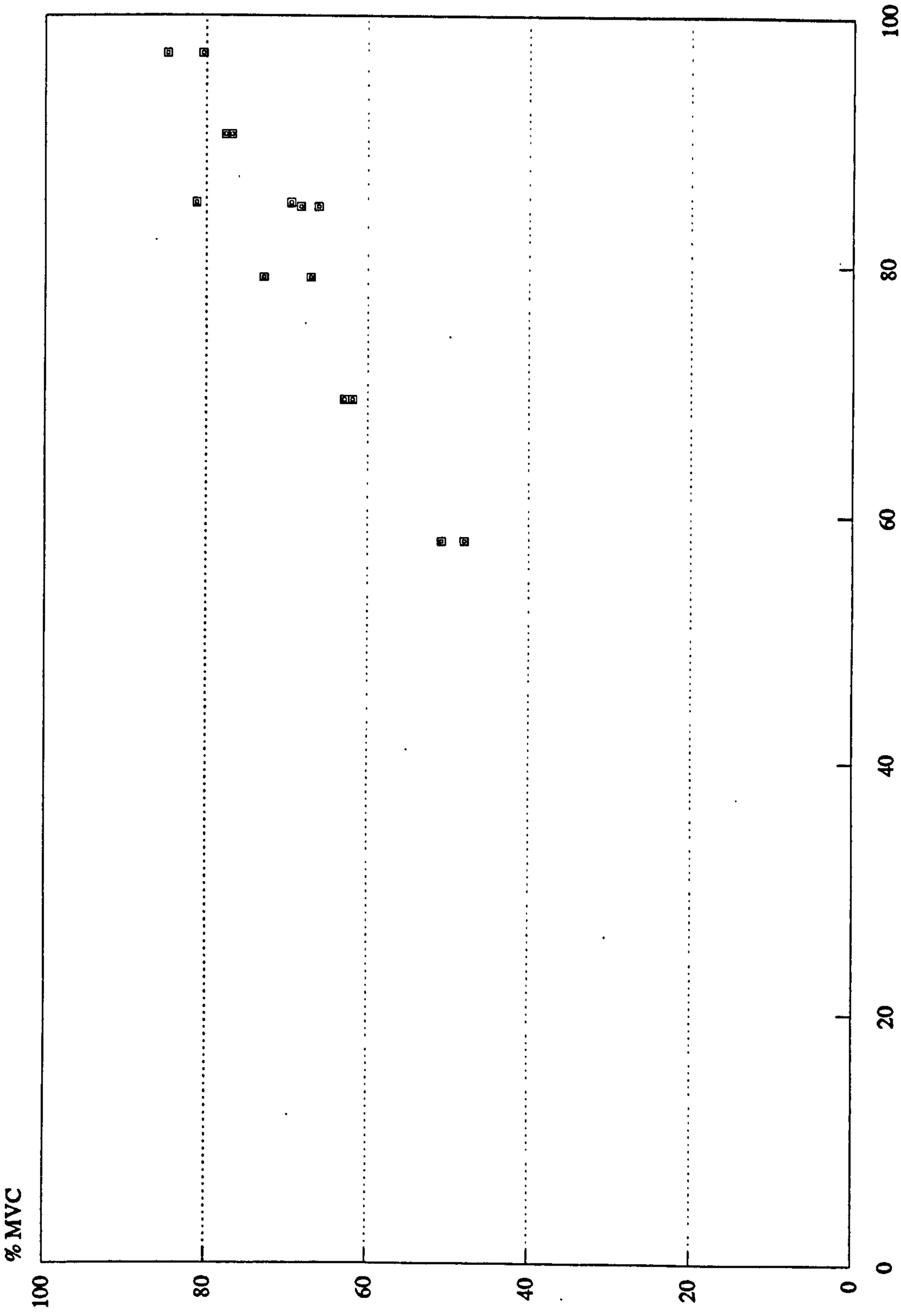
Relationship Between Applied
Load (% UTS) and Estimated (% MVC)
% UTS
0
20
40
60
80
100
% MVC
100
80
60
40
20
0

FIG. 4.3

TABLE 4.3 Summary of Heat Treatment Test Results

for 0.8% C wire

Test No.	Tempering Temperature (Degrees C)	Number of Specimens	Tensile Test		Hardness (V)
			Mean (lbs)	Range (lbs)	
As Rec'd					558, 575
HT 1	200	5	350	228-440	726, 732 739
	350	4	611	567-690	836, 762 762
	400	5	635	584-680	657, 590 605
HT 2	400*	8	558	530-596	294, 285 306
HT 3 (HT 2 Re-treated)	400**	8	550	516-598	420, 437
HT 4	400	5	523	476-560	503, 416
HT 5	400	5	560	464-623	478, 503 463, 463
HT 6	200,400	Mainly ductile failure			
HT 7	300	6	411	257-736	
	300*	4	369	258-520	
	350	5	616	546-670	
	400	6	528	516-544	
HT 8	350	4	306	304-308	
HT 9 (HT 8 Re-treated)	350	6	572	528-628	

* Tempered 2 hours
** Placed in cold furnace and taken up to temperature

4.1.2 Heat-treated 0.8%C Steel

Table 4.3 summarises the relevant mechanical data for the various types of heat-treatment. Hardness measurements were made on some batches but, as can be seen, the results were not consistent. It should also be noted that batches HT3, HT4 and HT5, which were all treated in the same fashion, gave very similar values.

From times to failure for wires heat-treated under a variety of conditions, and using Weibull Statistics, (see Appendix A- Statistical Methods) graphs were plotted showing the logarithm of the probability of survival (LnP_s) against time to failure. Figure 4.4 shows three survival plots for batches of specimens of 0.8%C steel tested at 80% UTS before and after heat-treatments which differed slightly.

a. As received.
b. Quenched and tempered at 350°C.
And c. Quenched and tempered at 400°C.

Initial failure times are very similar but condition (c) seems to give longer-lived specimens.

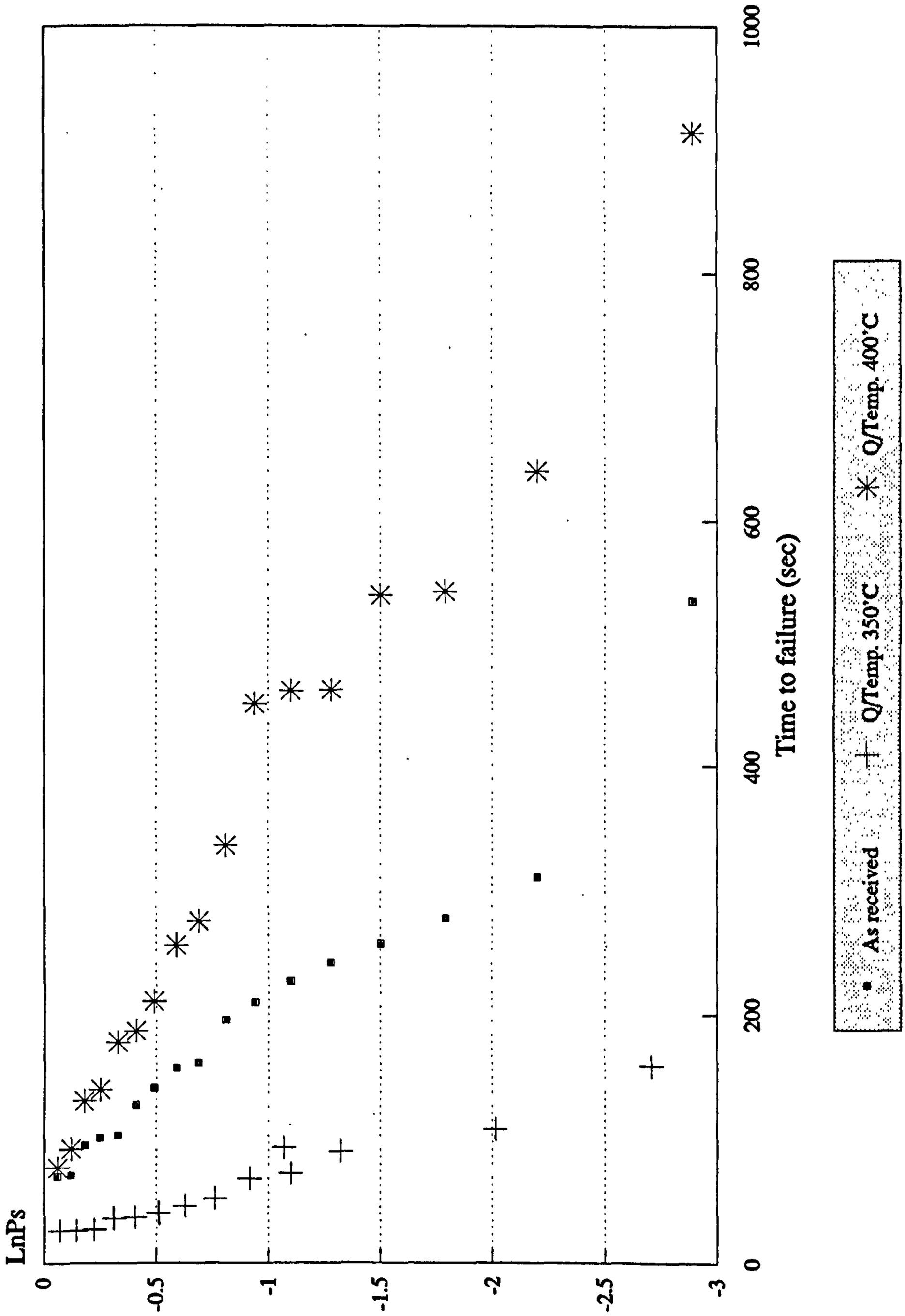

Probability of survival plots for 0.8%C steel tested at 80% σ_f showing the influence of heat-treatment.

FIG. 4.4

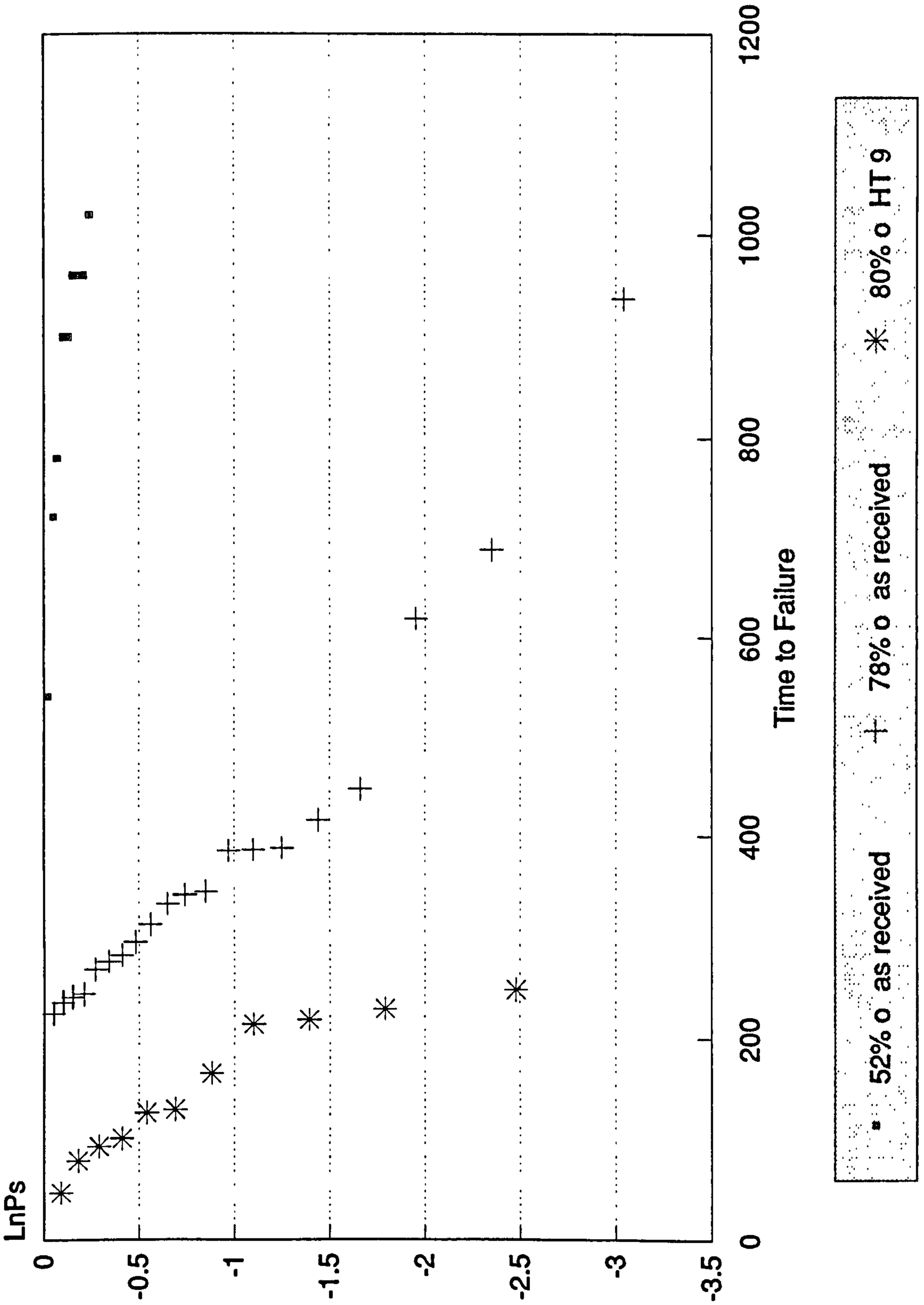

FIG. 4.4a LnPs against time to failure for 0.8%C steel under three different conditions

Attention has already been drawn to the fact that the mechanical properties and times to failure were very similar for the three batches of specimens numbered HT3, HT4 and HT5 (see Table 4.3), so a statistical test, Student's t-test, was performed. (Student's t-test is fully described in Appendix A- Statistical Methods.) The test confirmed that there was no significant difference between the sets of data and so the three batches could be considered as one. Results are shown in Table 4.4. All t values are well below the critical values for $t_{0.05}$.

Consequently, it was possible to draw a cumulative frequency distribution for HT3-5, and this is shown in Figure 4.5.

TABLE 4.4 t-TEST RESULTS FOR HT3, HT4, HT5, HT9

HT	t	$t_{0.05}$
3,4	1.524	2.201
3,5	0.451	2.201
4,5	1.236	2.306
3-5,9	1.357	2.06

calculated using the formula:

$$t = \frac{|m_1 - m_2|}{S\sqrt{\frac{1}{n_1} + \frac{1}{n_2}}}$$

$$v = n_1 + (n_2 - 2)$$

where:

$$s^2 = \frac{(n_1 - 1)\, S_1^2 + (n_2 - 1)\, S_2^2}{n_1 + (n_2 - 2)}$$

m = mean

s = standard deviation

n = number of specimens

v = degrees of freedom

$t_{0.05}$ = critical value of t at the 95% level

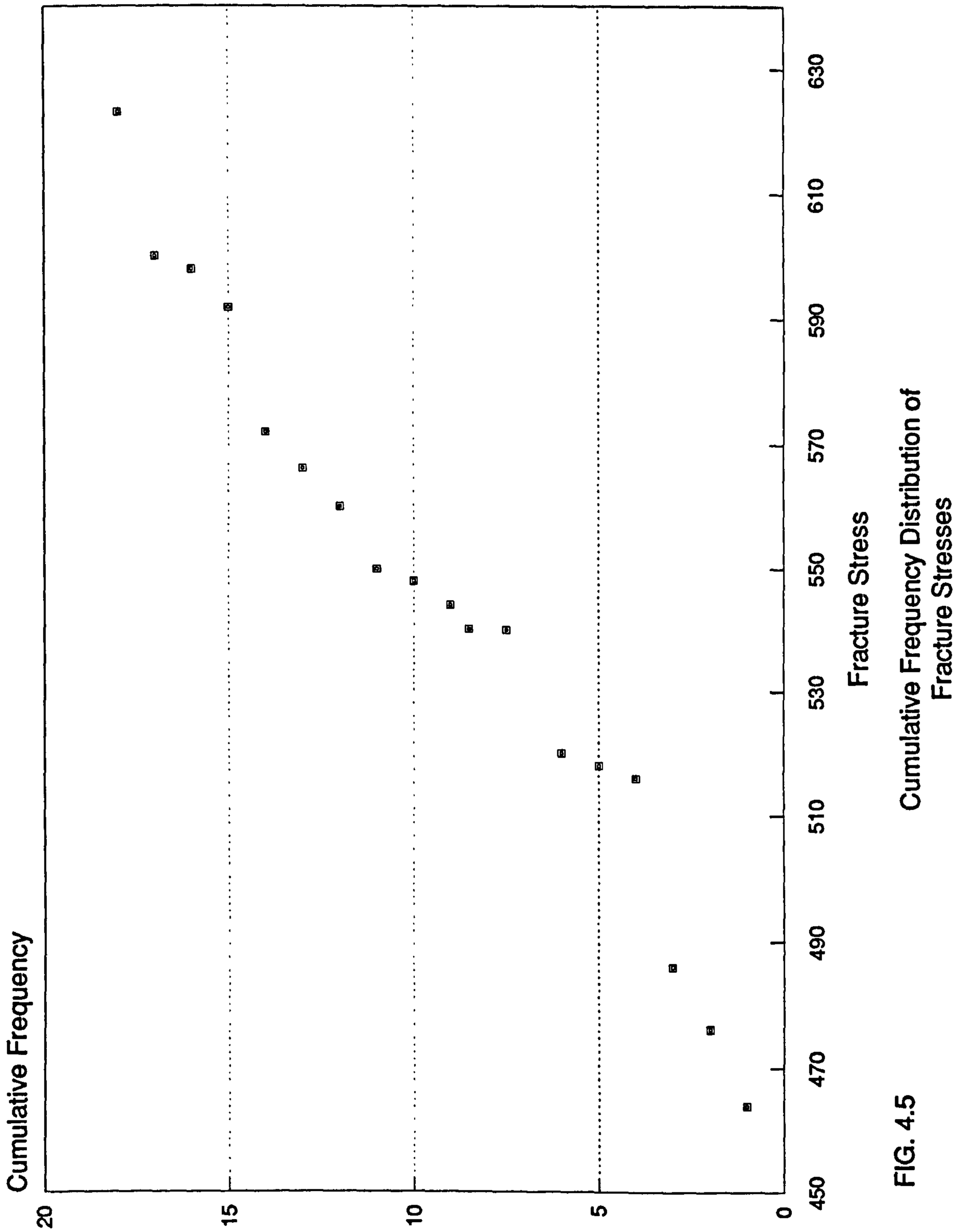
Cumulative Frequency
20
15
10
5
0
450
470
490
510
530
550
570
590
610
630
Fracture Stress
Cumulative Frequency Distribution of Fracture Stresses

FIG. 4.5

4.1.3. AISI 4340 steel

Similar probability of survival plots were drawn for AISI 4340 steel sheet loaded at 90% UTS. These directly compared the effects of cathodic charging at 150 $mAcm^{-2}$, with times to failure obtained whilst nickel plating at 5 $mAcm^{-2}$. These data are shown in Figure 4.6. It is immediately evident that cathodic charging causes more hydrogen absorption than electroplating with nickel and consequently cathodically charged specimens will fail much earlier.

Table 4.5 shows how times to failure for nickel plated specimens were converted to LnP_s. Times to failure were arranged in ascending order and expressed as P_f (the probability of failure) in the form "position in list divided by (number of specimens plus 1)". Probability of survival, P_s, is expressed as $1-P_f$ and finally, this fraction is converted to a natural logarithm.

Probability of Survival Plots for
AISI 4340 Tested at 90% σ_f.

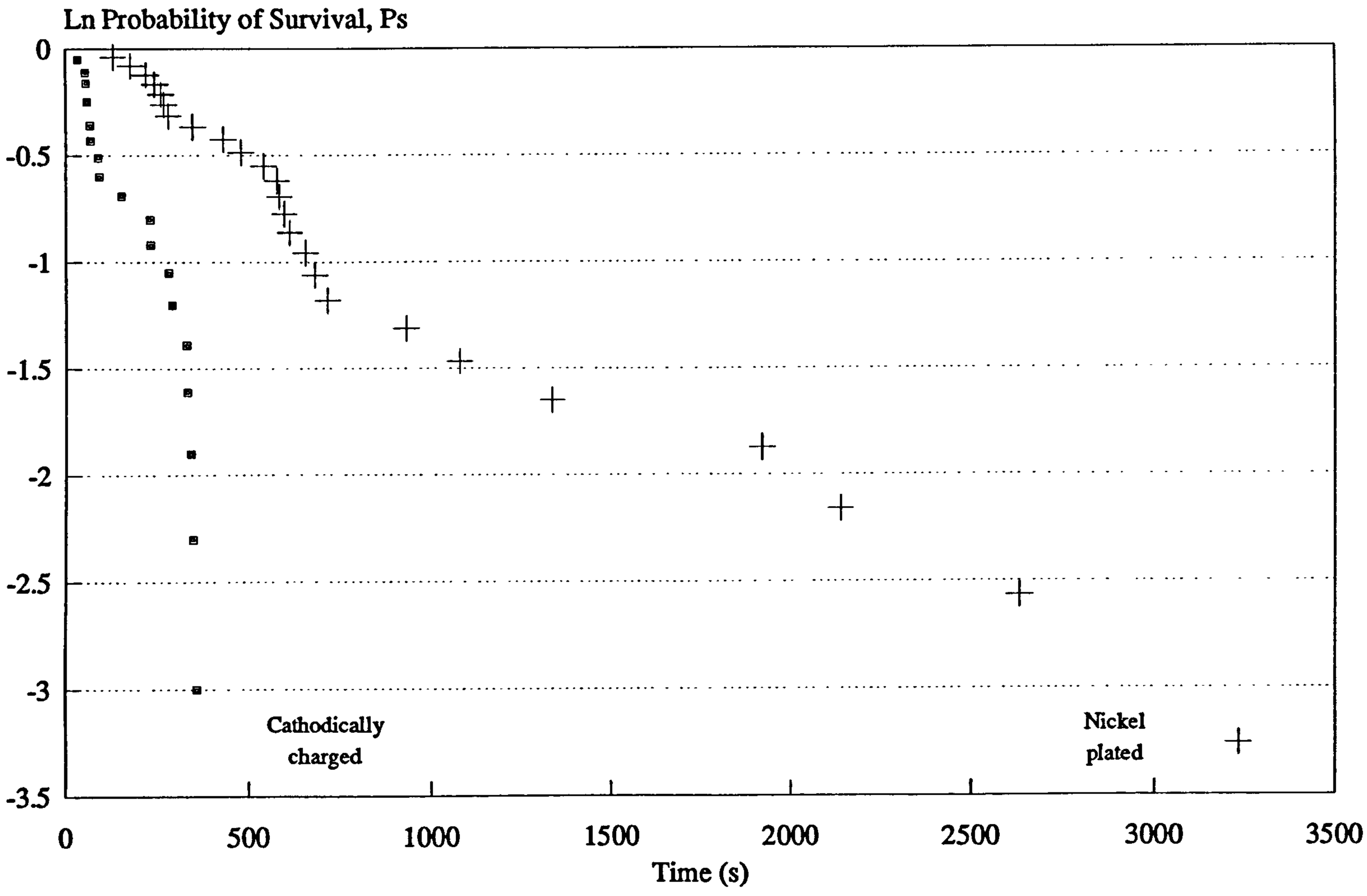

Fig. 4.6 Comparison of Effects of Cathodic Charging at 150 mA cm-2 and Nickel Plating at 5 mA cm-2.

TABLE 4.5. Time to Failure and Probability of Survival for Nickel Plated Specimens

Time to Failure (secs)	Nickel Plated		
	P_f	P_s	ln P_s
135	1/26	25/26	-0.04
183	2/26	24/26	-0.08
226	3/26	23/26	-0.12
249	4/26	22/26	-0.17
266	5/26	21/26	-0.21
274	6/26	20/26	-0.26
286	7/26	19/26	-0.31
351	8/26	18/26	-0.37
433	9/26	17/26	-0.43
481	10/26	16/26	-0.49
542	11/26	15/26	-0.55
580	12/26	14/26	-0.62
586	13/26	13/26	-0.69
600	14/26	12/26	-0.77
616	15/26	11/26	-0.86
661	16/26	10/26	-0.96
687	17/26	9/26	-1.06
721	18/26	8/26	-1.18
934	19/26	7/26	-1.31
1079	20/26	6/26	-1.47
1334	21/26	5/26	-1.65
1921	22/26	4/26	-1.87
2138	23/26	3/26	-2.16
2630	24/26	2/26	-2.57
3232	25/26	1/26	-3.26

4.2 HYDROGEN PERMEATION EXPERIMENTS

4.2.1 Double Cell Permeation Experiments

These results mainly consist of measurements of hydrogen flux over a period of time under certain conditions. During plating, some of the hydrogen liberated may be in the form of bubbles and some may be trapped in the deposit, whilst the rest will permeate through the steel. It is this permeated hydrogen that was measured throughout these experiments.

4.2.1.1 Effect of Plating Current Density

Figure 4.7 compares the hydrogen permeated (expressed as flux in μAcm^{-2}) when liberated over a period of time when nickel plating takes place at five different current densities. The recommended plating range is 5-20 $mAcm^{-2}$, so tests were made at 5, 10 and 20 $mAcm^{-2}$ and also included were tests at 2 and 30 $mAcm^{-2}$.

In all cases, once plating has started, there is a rapid initial increase in the amount of hydrogen being permeated. Theoretically, this should soon settle to a maximum "plateau" value. This is certainly evident when plating at 5 and 10 $mAcm^{-2}$ and the latter current density seems to be more effective at reducing hydrogen ingress. The upper end of the recommended range did not give the "plateau" effect and, on inspection, the specimen seemed to be heavily pitted with uneven coating. This was also evident on the specimens plated at 30 $mAcm^{-2}$ and 40 $mAcm^{-2}$ (the results are not shown for the latter specimen here but can be seen as Figure 5.6 in Chapter 5-Discussion p.145). This led to investigation of the effects of stirring whilst plating - see Section 4.2.1.3. p. 88

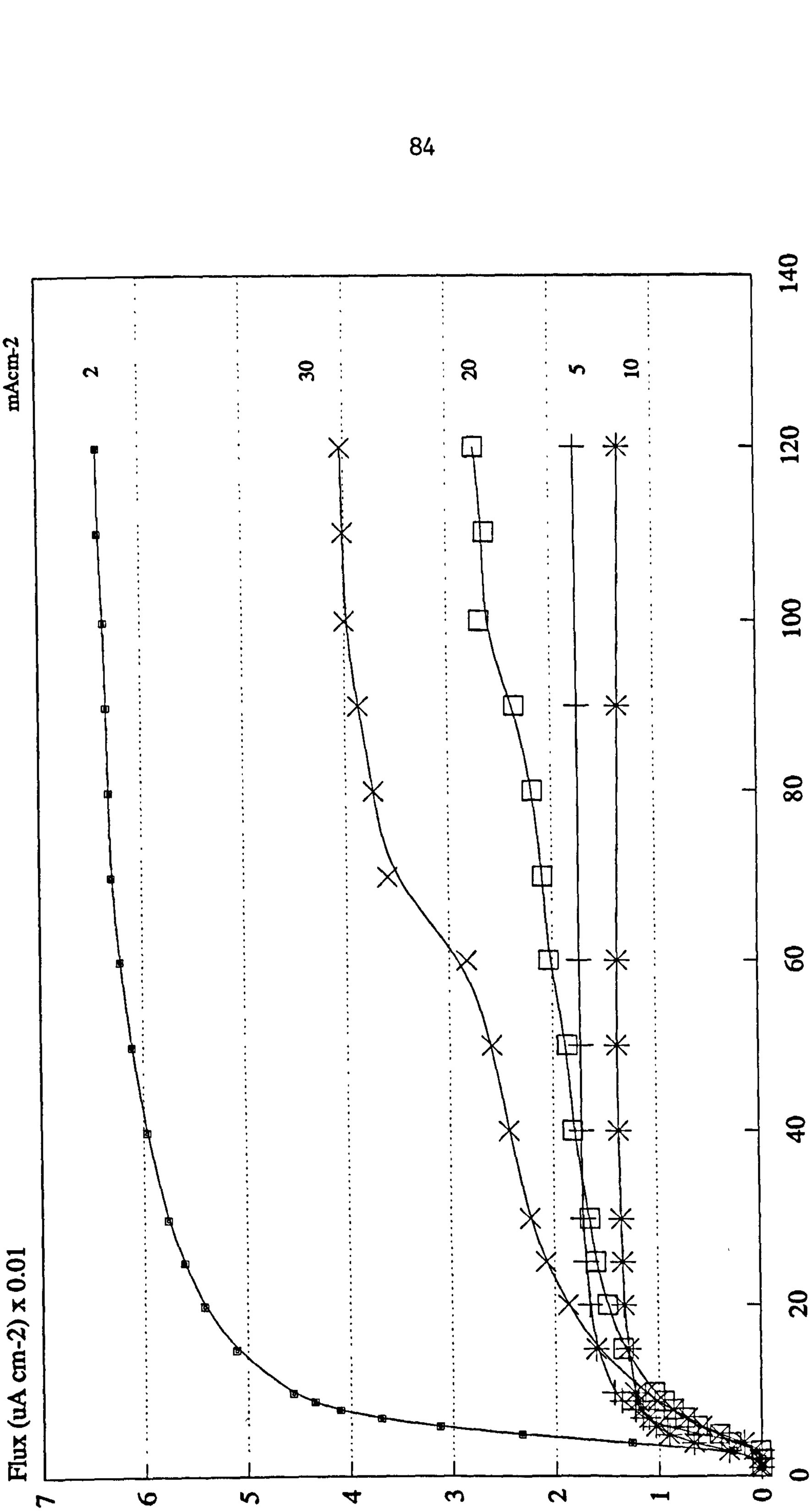

Hydrogen Permeation Curves for Nickel Plating at a Range of Current Densities.

FIG. 4.7

The lower plating current density of 2 $mAcm^{-2}$ did not seem to effectively prevent the permeation of hydrogen, possibly because the deposition of nickel was too slow, resulting in an insufficiently rapid deposition to prevent the ingress of hydrogen, or, more likely, the plating efficiency is much lower.

4.2.1.2 Absorption of Hydrogen after Cessation of Plating

It was anticipated that once plating had stopped, hydrogen permeation would rapidly decrease and the situation of no-permeation flux would rapidly ensue, but it was noted that, although slow depletion begins immediately, the steel appears to continue to permeate hydrogen, even though actually no hydrogen is being generated. Figure 4.8 denotes this quite clearly, showing the depletion after plating stopped, indeed, even after 51 hours, the hydrogen is still permeating through the steel. Figure 4.9 compares the permeation transients for specimens plated at 5 $mAcm^{-2}$ and 10 $mAcm^{-2}$. It is interesting to note that although the plateaux are roughly parallel, once plating has ceased, the depletion rate for the specimen , plated at the lower rate of 5 $mAcm^{-2}$ is much more rapid than that for the specimen plated at 10 $mAcm^{-2}$. Of course, after similar lengths of plating periods, the thickness of nickel plate for the 10 $mAcm^{-2}$ specimen will be double that of the 5 $mAcm^{-2}$ specimen but, theoretically the higher plating current density, with greater plating efficiency, should quickly form a coating which would protect the specimen from excessive hydrogen ingress.

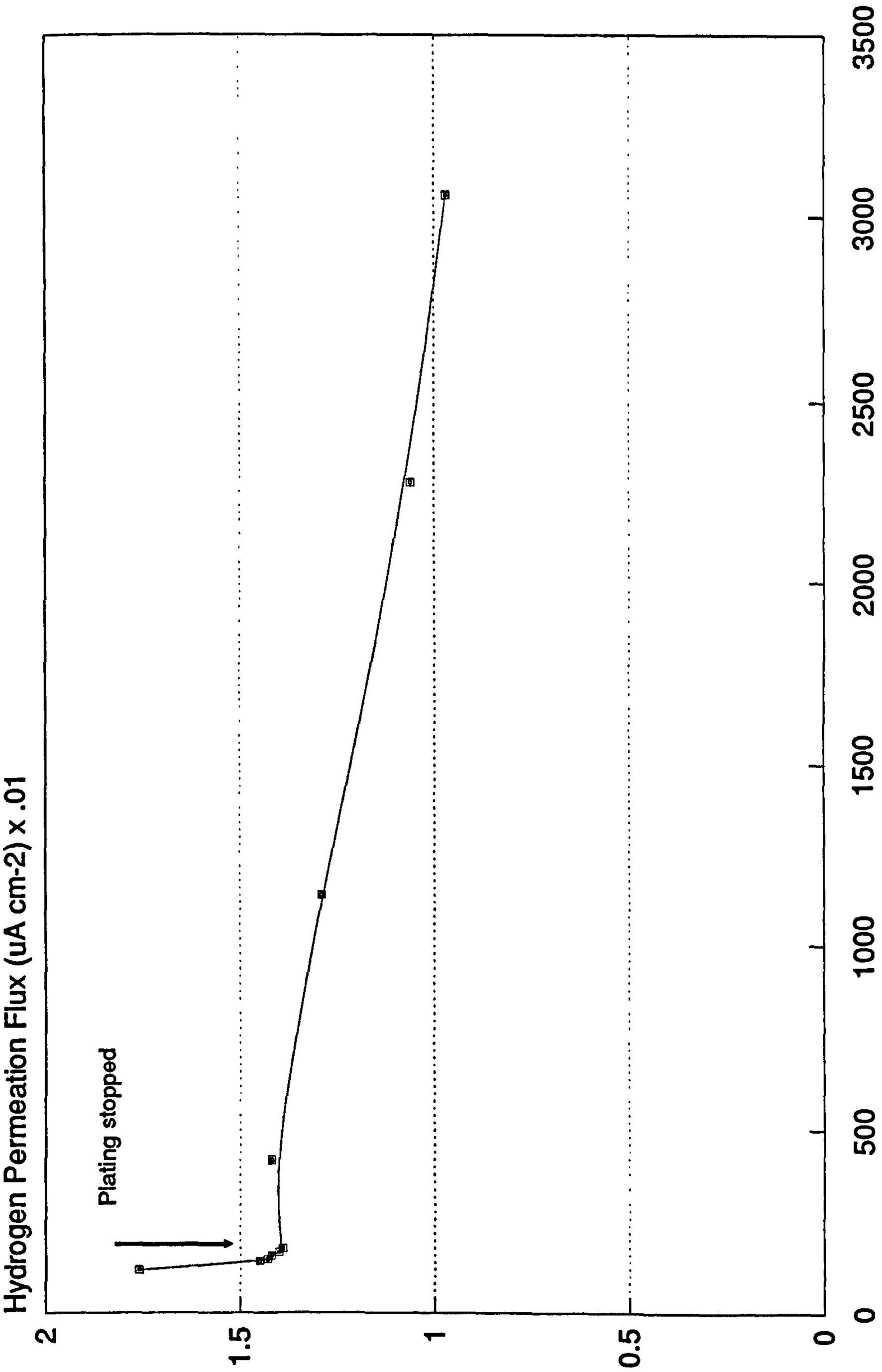

FIG. 4.8 Permeation Flux Curve Showing Continued Absorption of Hydrogen from the Nickel Deposit Following Electroplating.

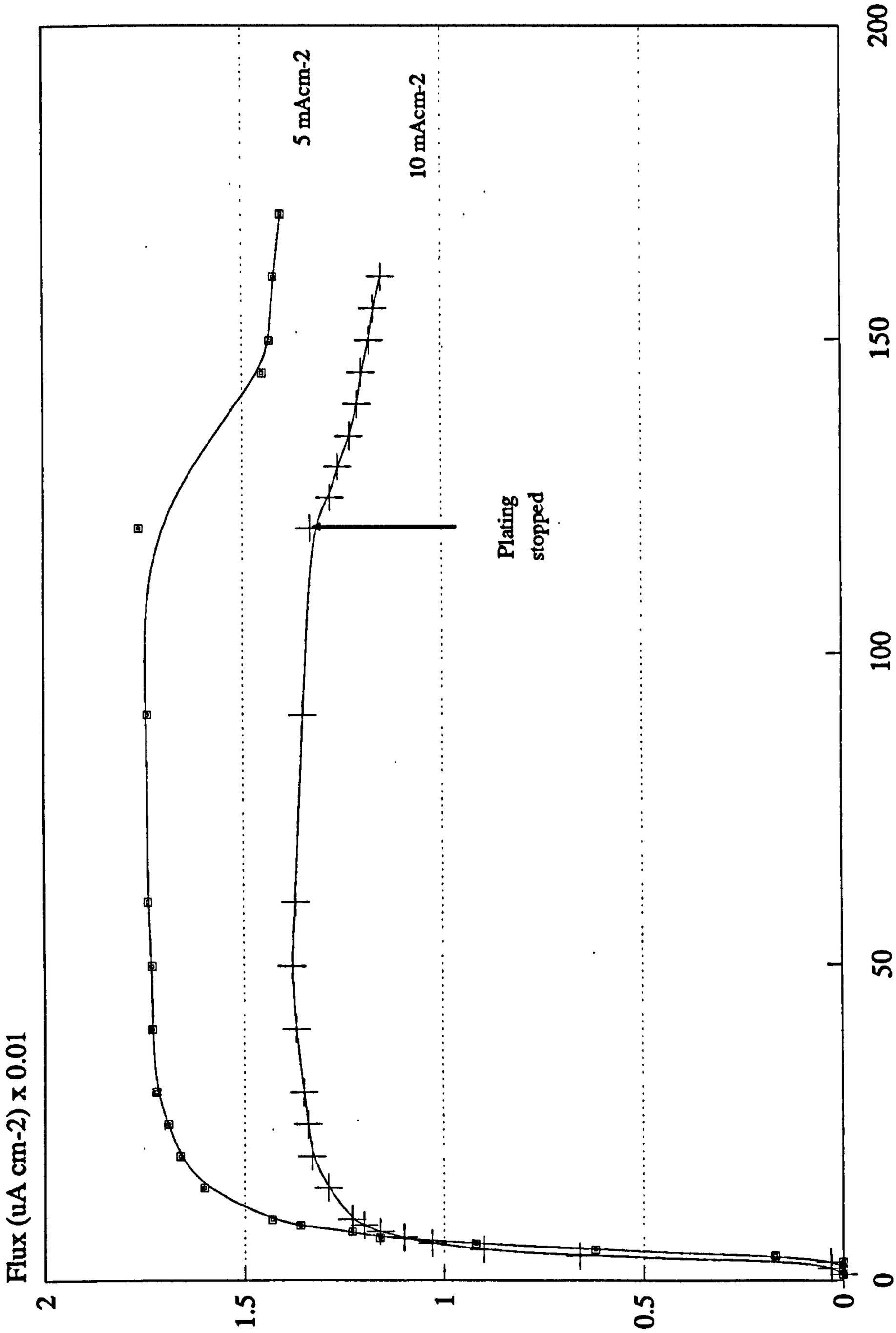
200
5 mAcm-2
10 mAcm-2
Plating
stopped
150
100
Time (mins)
50
Hydrogen Permeation flux curves for the
Electroplating of Nickel
Flux (uA cm-2) x 0.01
2
1.5
1
0.5
0
0

FIG. 4.9

4.2.1.3. The Effects of Stirring

It was noted that during plating, bubbles, presumably of hydrogen, appeared on the surface of the specimen. It was also noted that the plate deposited on specimens coated at the higher current densities of 20, 30 and 40 $mAcm^{-2}$ was heavily pitted.

Two questions posed themselves: (a) Did the presence of bubbles restrict the ingress of hydrogen? and (b) Was there some electro-chemical reaction occurring within the pits which would cause a continuous increase in the permeation of hydrogen?

Figure 4.10 shows the permeation transients for stirred plating at 5 $mAcm^{-2}$ and 10 $mAcm^{-2}$. Figure 4.11 directly compares stirred and unstirred solutions for a single current density. The slope of the flux/time curve is essentially the same as for unstirred solutions but stirring the plating solution to remove the bubbles does increase the amount of hydrogen permeating the steel.

Stirring seemed to have no effect on the formation of pits at the higher current densities, and no effect on the tensile stresses caused by the thicker plate on the 57 µm foil substrate.

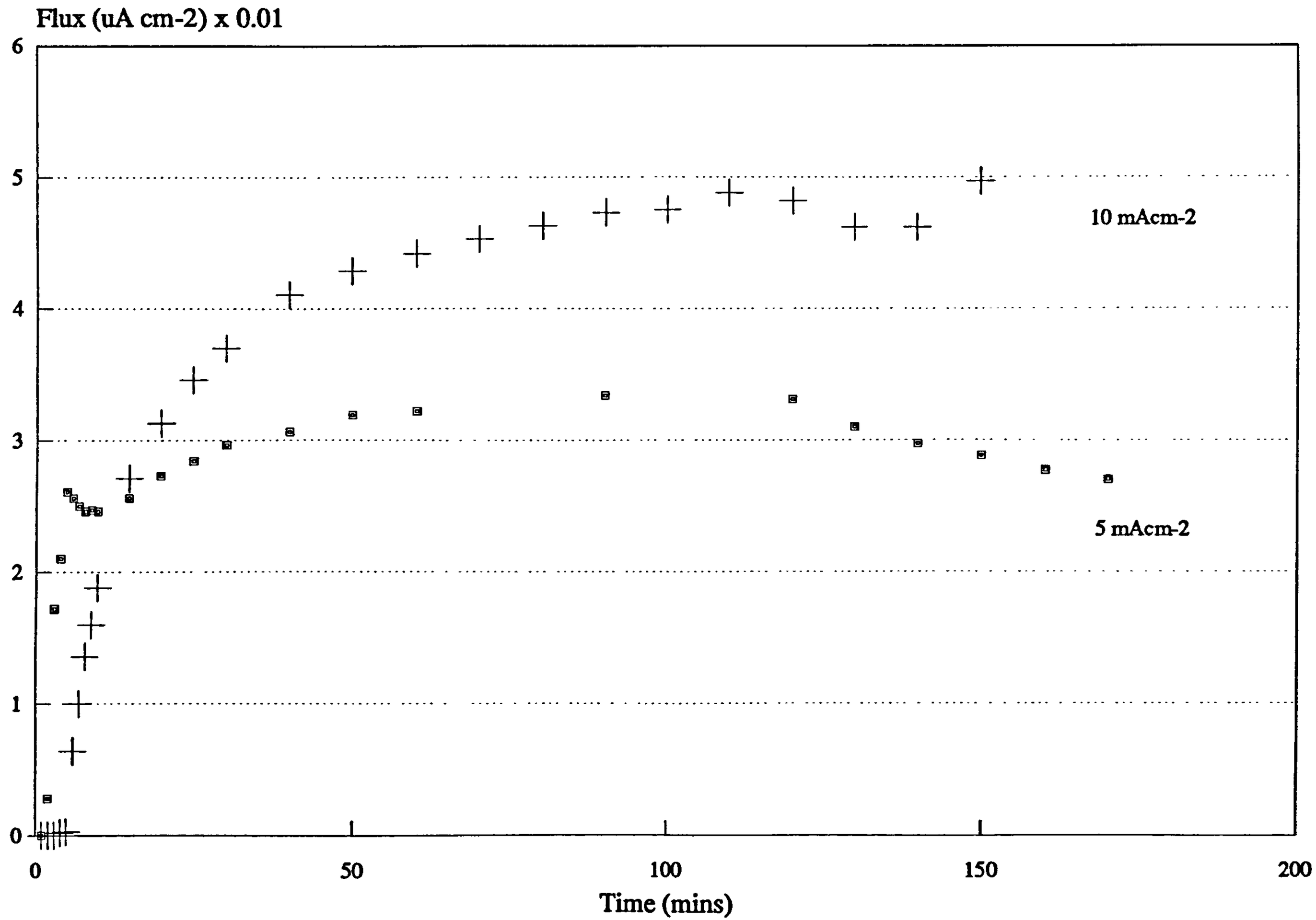

Fig. 4.10

Permeation Transients for Stirred
Plating at Different Current Densities

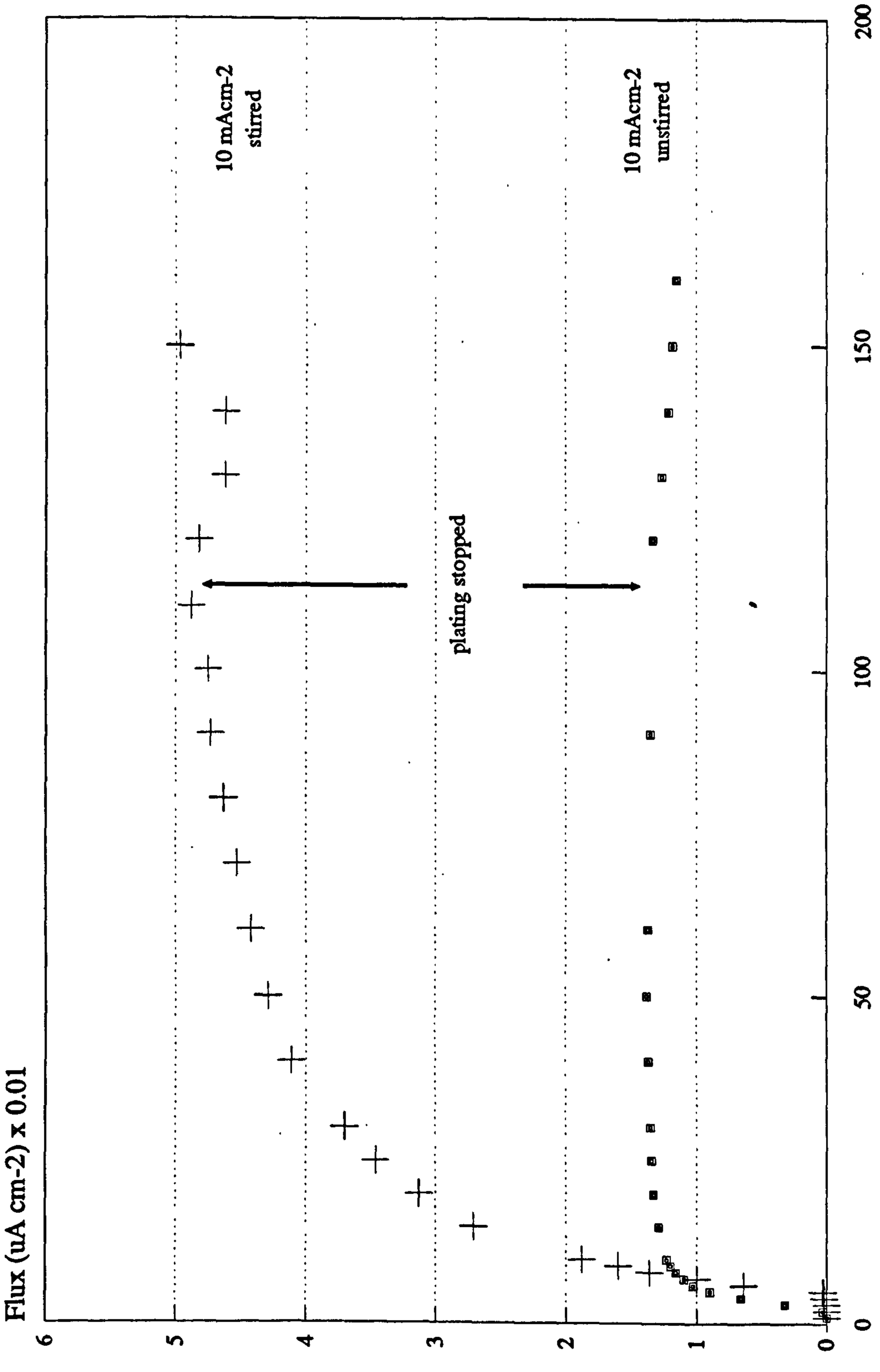

Permeation Transients showing the Effect of Stirring the Plating Solution on Hydrogen Absorption.

Fig. 4.11

4.2.1.4. Effect of Post-Plating Heat Treatment

Some specimens were plated at 5 $mAcm^{-2}$ for 2 hours, removed from the cell, subjected to post-plating heat treatment, replaced in the cell and then decay transients were measured. Figure 4.12 shows that specimens baked at 200°C for 2 hours gave a lower decay transient at first, indicating that post-plating baking does remove hydrogen from the plate.

4.2.1.5. Nickel Plating on Nickel Foil Substrate

Figure 4.13 shows the permeation transient obtained when nickel plating on an 80 μm nickel foil, which had been made by electro-depositing nickel on to a steel substrate until the nickel was of sufficient thickness to be easily separated from the substrate. It is interesting to note that the initial permeation showed a sharp increase at about one minute, possibly due to a massive influx of hydrogen through microscopic holes in the foil substrate. Once these holes were sealed by the nickel plate, then hydrogen depletion occurred in the normal way, levelling off at about 20 μAcm^{-2}.

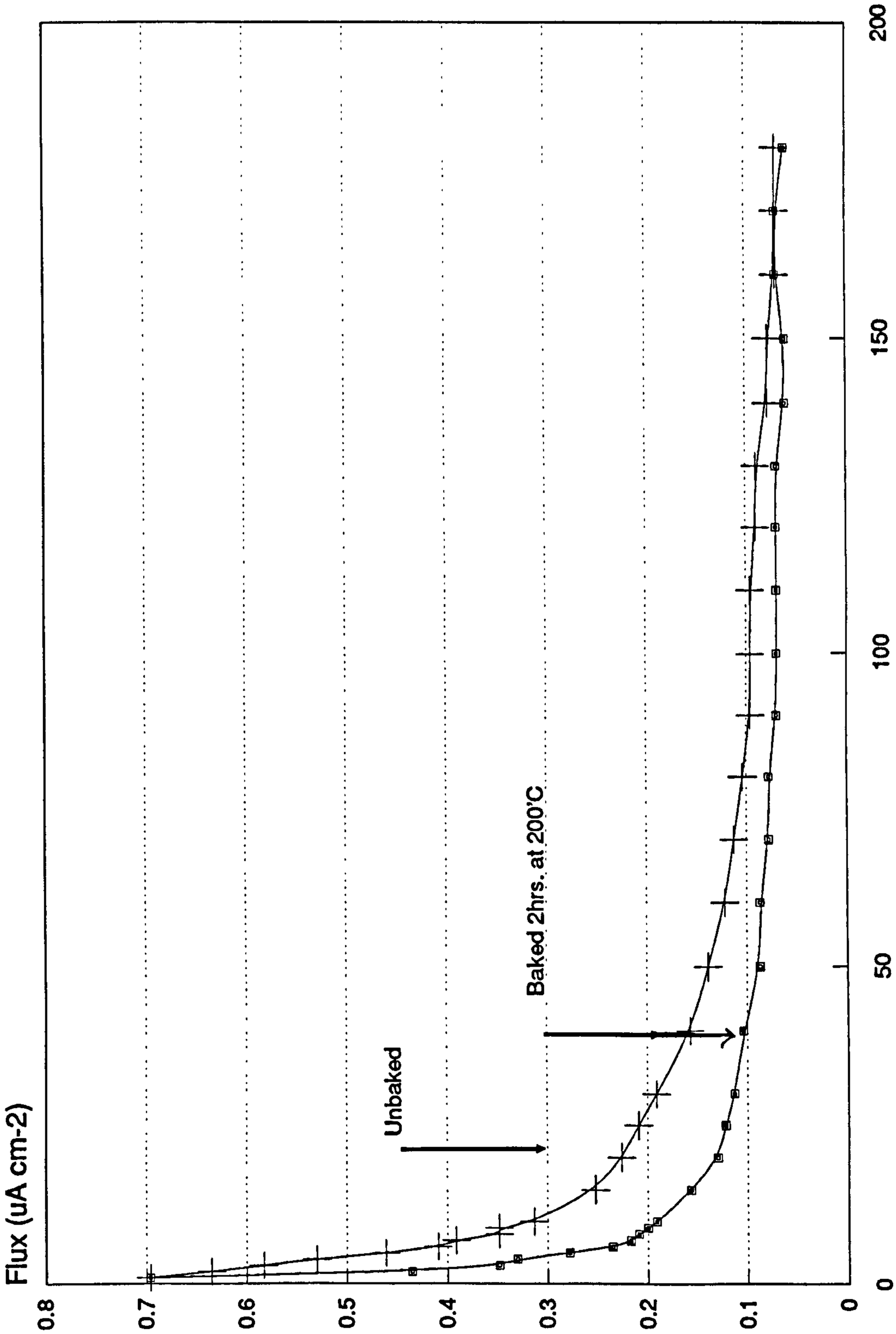
Flux (uA cm-2)
0.8
0.7
0.6
0.5
0.4
0.3
0.2
0.1
0
Unbaked
Baked 2hrs. at 200'C
0
50
100
150
200
Time (mins)
Decay Transients Showing the Effect of
Post Plating Heat-treatment.

FIG. 4.12

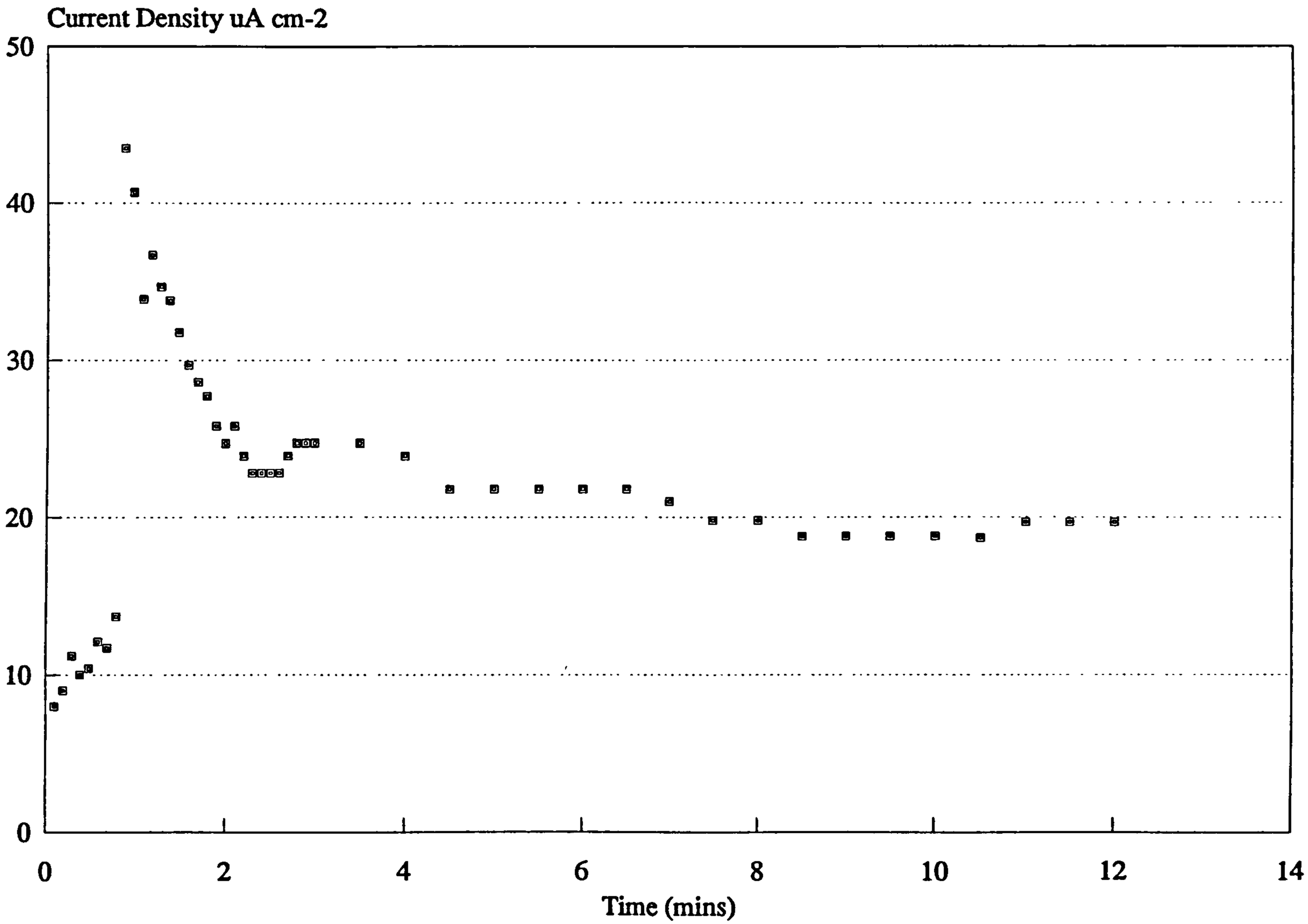

FIG. 4.13

Permeation Transient for Nickel Plating
at 5 mA cm-2 on a 57 um Nickel Foil

4.2.1.6. Cathodically Charged Steel

A piece of steel foil was coated with Lacomit, leaving a 1 centimetre square exposed. The left hand cell was then filled with 4% sulphuric acid and a current of 10 $mAcm^{-2}$ was applied. The charging lasted 2 hours whilst permeation transient readings were taken; the current was then switched off and readings were continued for another hour. The transient obtained is shown in Figure 4.14.

It will be noted that a considerable amount of hydrogen is evolved and permeated during charging compared to that permeated whilst nickel plating. Once the charging current is switched off, there is a rapid fall-off of hydrogen being permeated, but after about 10 minutes, more flux is being registered. It is likely that this increase is due to active corrosion of the steel by the sulphuric acid. Indeed, several attempts were initially made using a charging current of 150 $mAcm^{-2}$ (as used in constant load testing) but holes appeared in the steel foil after about 80 minutes, and so it was decided to use the less aggressive current of 10 $mAcm^{-2}$.

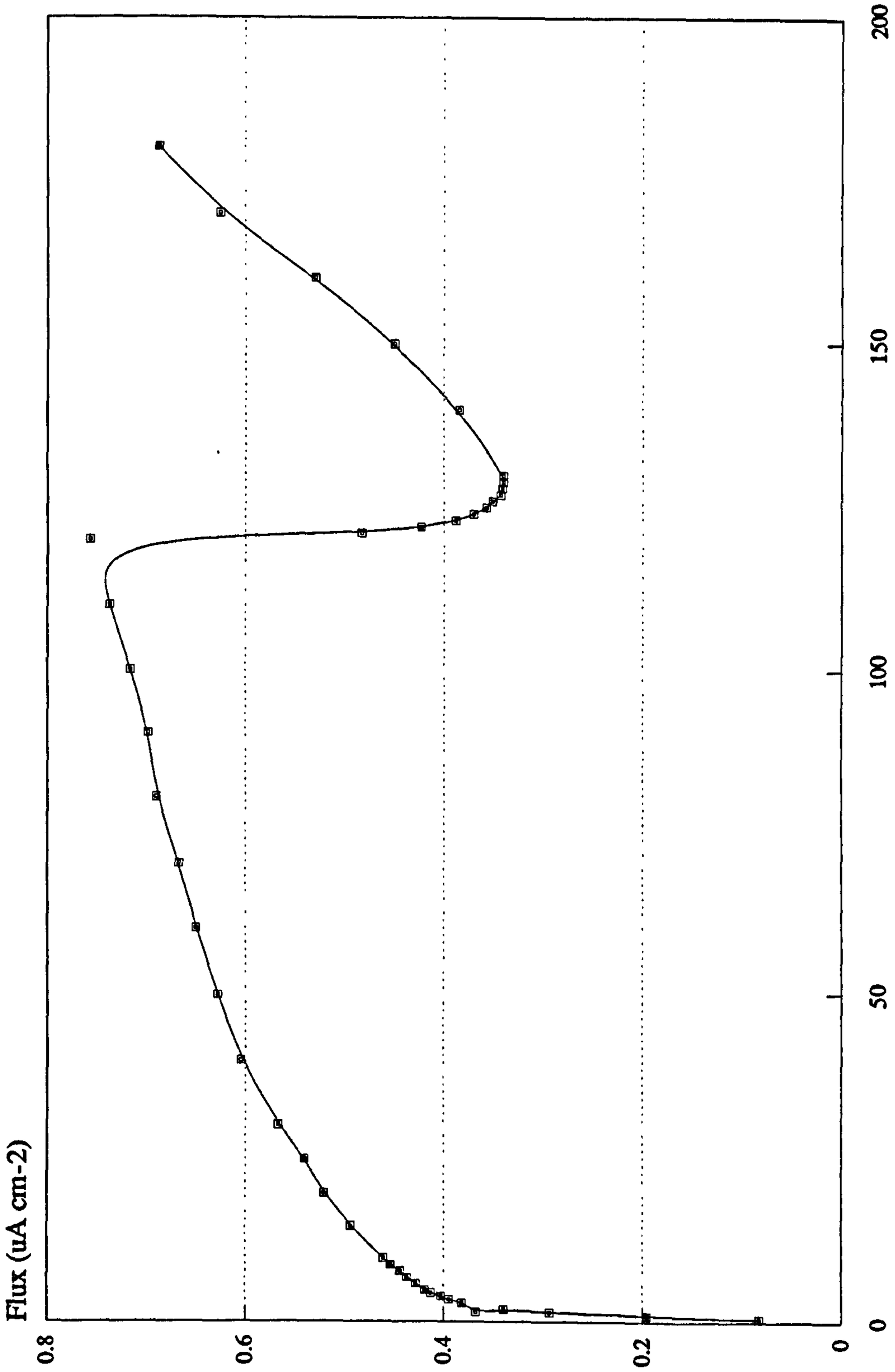

Permeation Transient obtained during and after Cathodically Charging at 10 mA cm2 in 4% Sulphuric Acid.

FIG. 4.14

4.2.2. Gel-filled Hydrogen Probe

4.2.2.1 Introduction

Four main treatments were used:-

(a) Quenched and tempered 2 or 20 hours at 200°C.
(b) Quenched, tempered as for (a) and then nickel plated for 2 hours at a current density of 5 $mAcm^{-2}$
(c) As for (b) and then baked a further 2 hours at 200°C.
(d) As for (b) and then baked a further 20 hours at 200°C.

To enable easy reference when looking at the figures in this section, code letters were assigned to each treatment as follows: (a) T, (b) TP, (c) TPB2, (d) TPB20. Treatments and codes are summarised in Table 4.6.

It was shown in Chapter 3 - Methods, that there were several series of experiments. In each case, measurements took place for a period of 15 minutes, and these were repeated several times some days later (precise details are noted as appropriate). It became evident that results needed to be displayed in two ways; first, separately for each specimen and then comparisons needed to be made between specimens that had been treated differently after plating but were at the same stage of time in the experiments.

Table 4.6 SUMMARY OF TREATMENTS AND CODES

T	Quenched and tempered 2 hrs at 200°C
TP	Quenched, tempered and Nickel Plated 2 hrs at $5mAcm^{-2}$
TPB2	Quenched, tempered, plated and baked 2 hrs at 200°C
TPB20	Quenched, tempered, plated and baked 20 hrs at 200°C

4.2.2.2 Effect of Post-exposure on Hydrogen Content using Tensile Specimens

Figures 4.15 to 4.18 show the effect of post-exposure on the hydrogen content of tempered, tempered and plated and tempered, plated and baked specimens. In each case, specimens were tempered for 20 hours. Each figure depicts the results obtained immediately after treatment and then after intervals of 8 and 13 days. Calculated hydrogen concentration values are also shown.

In each case the initial result is much lower than the values for 8 and 13 days, which tend to similar values. The quenched and tempered specimen (Figure 4.15) has an initial hydrogen concentration of 0.2 ppm, but after 13 days has settled to just under 1 ppm with the depletion rate gradient close to the theoretical value of-0.5. The tempered and plated specimen (Figure 4.16) showed a value of 2.0 ppm which was higher than that for the tempered specimen, and after 13 days the hydrogen concentration had settled to 9.1 ppm; tempered, plated and baked specimens similarly settled to 7.7 ppm and 10.2 ppm after 13 days, but the initial concentrations differ, as can be seen in Figures 4.17 and 4.18. A puzzling fact is, that the initial concentration for the 20 hour baked specimen is higher than that which has been baked for only 2 hours (2.3 ppm compared to 1.0 ppm); but the initial readings for the lower bake time took longer to settle down.

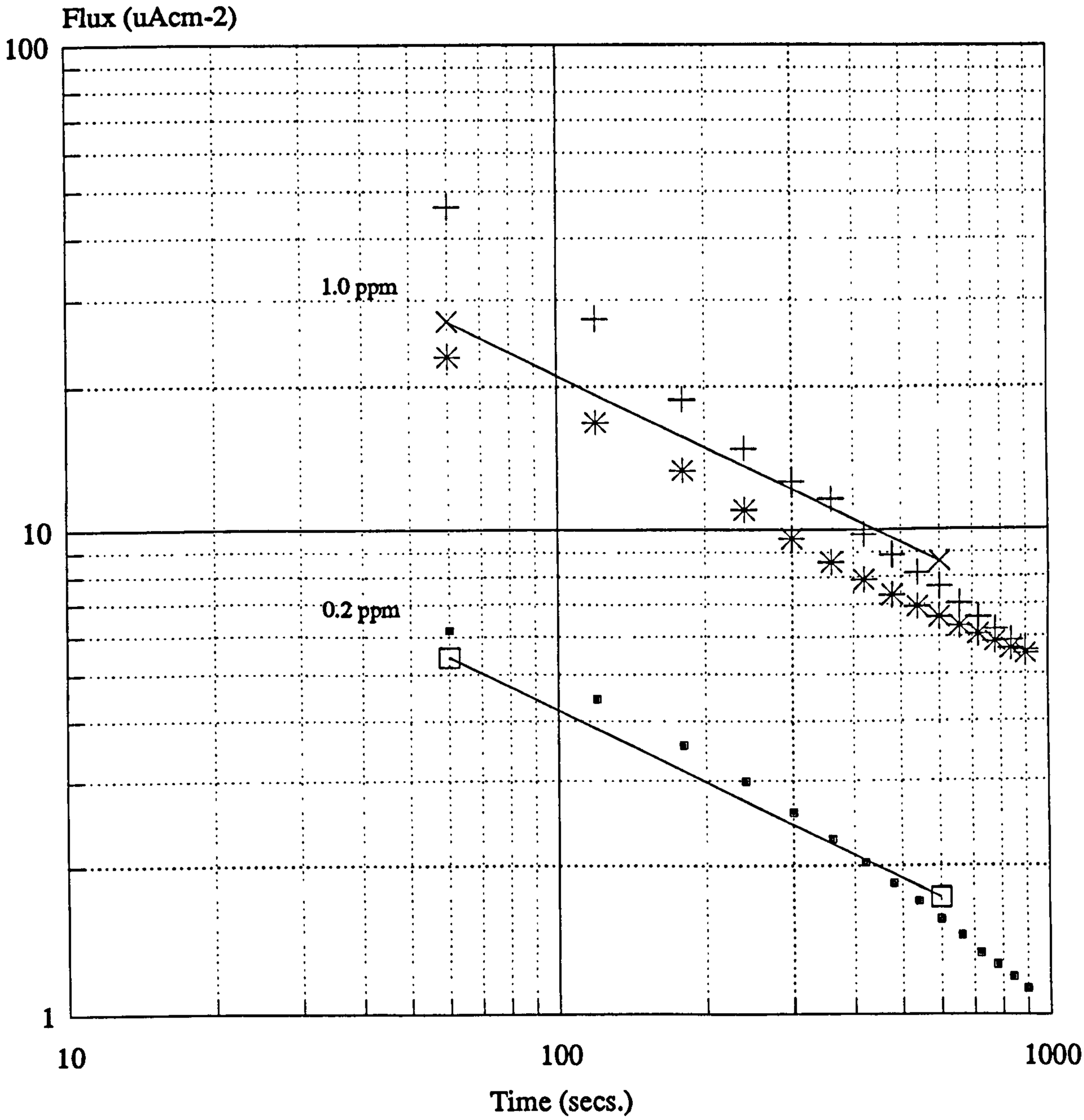

Fig. 4.15 Effect of Post-exposure on the Hydrogen Content of Tempered Specimens. Tempered 20 hours.

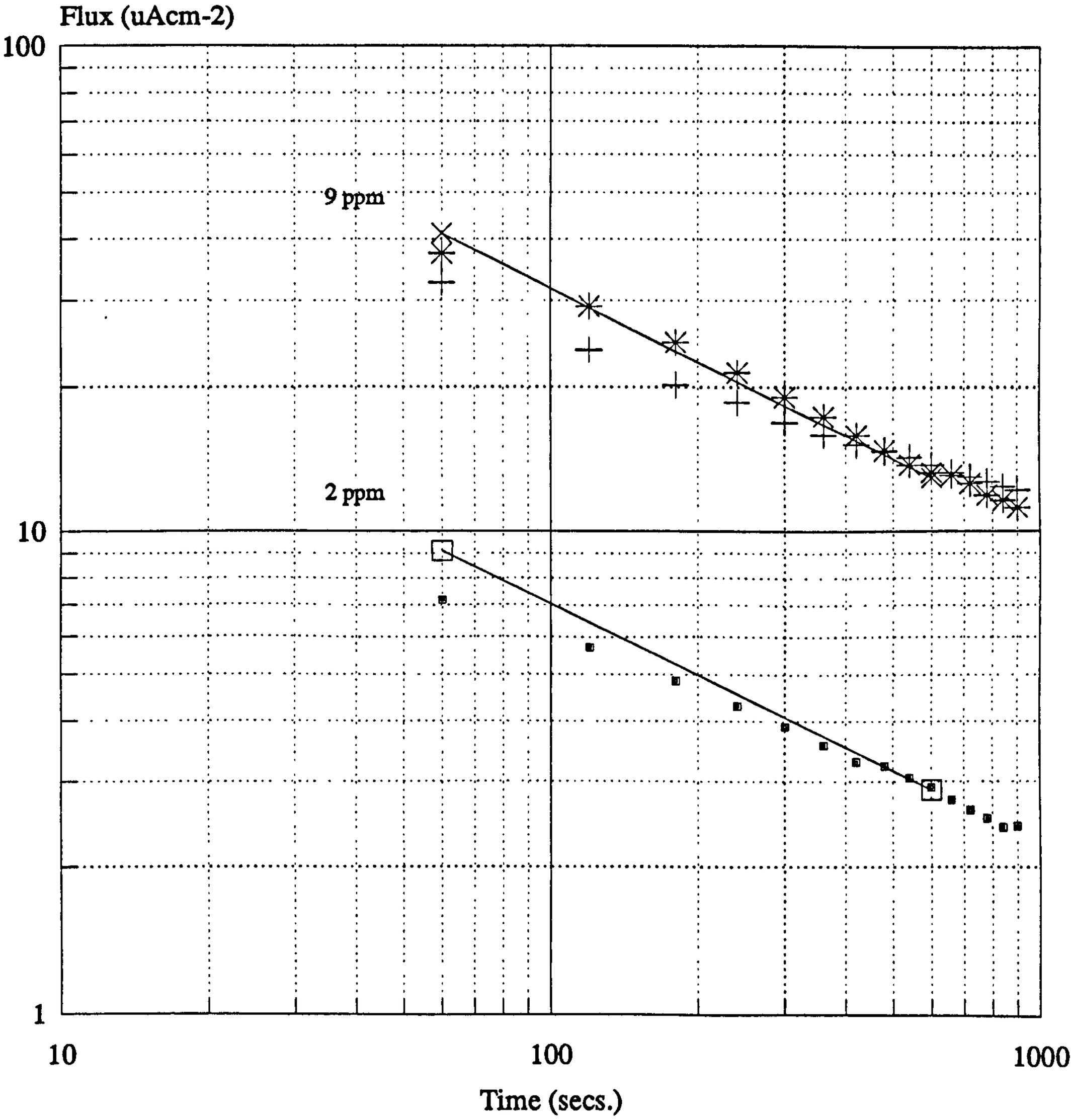

Fig. 4.16. Graphs for Tempered and Plated Specimens Showing the Change in the Hydrogen Determination with Time.

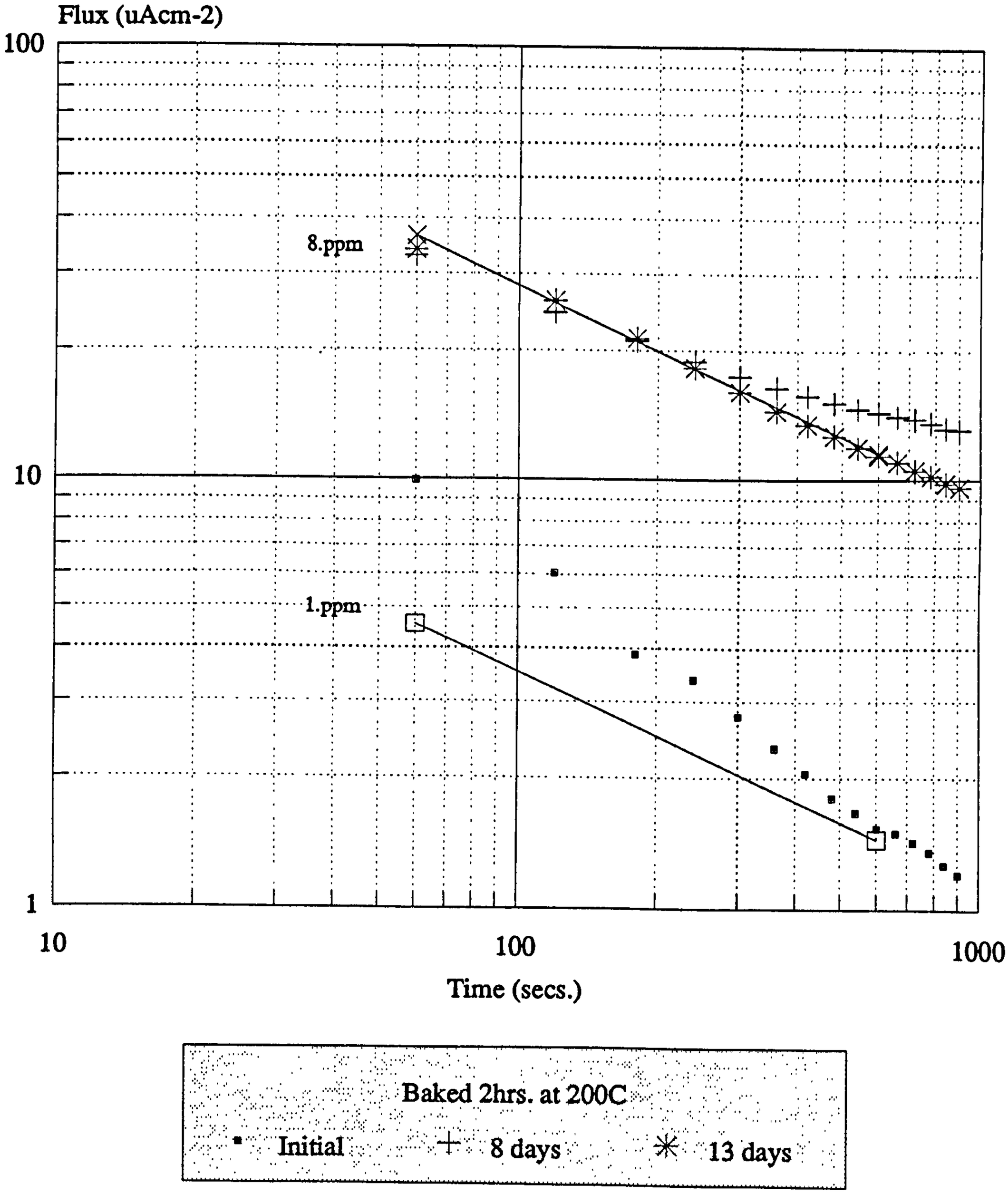

Fig. 4.17 Graphs for Tempered, Plated and Baked Specimens Showing the Change in Hydrogen Determination with Time.

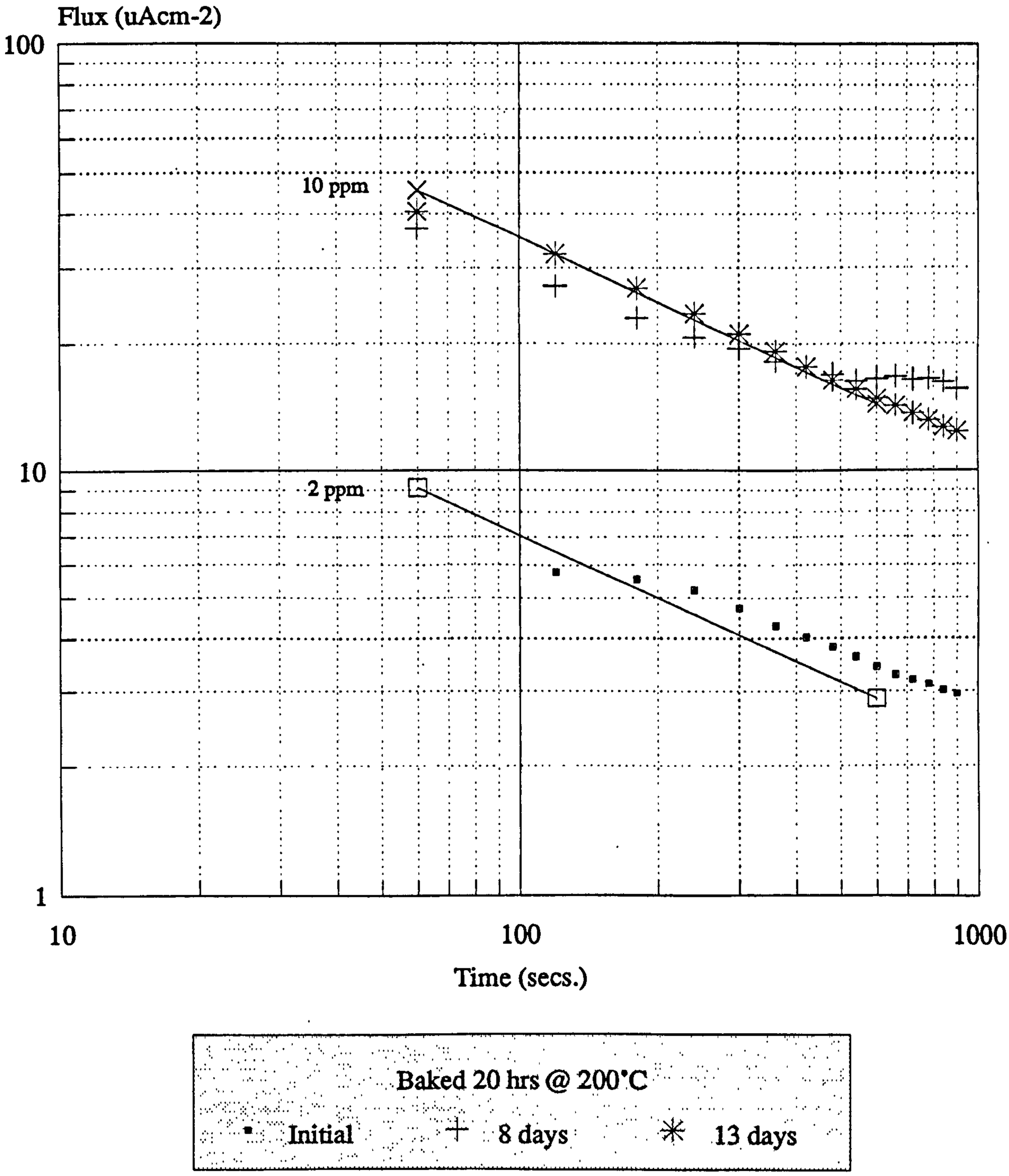

Fig. 4.18 Graphs for Tempered, Plated and Baked Specimens Showing the Change in Hydrogen Determination with Time.

As the diffusion coefficient for nickel plate (taken to be 7 $x10^{-10}$ cm^2sec^{-1}) differed from that of AISI 4340 steel (2.5 $x10^{-7}$ cm^2sec^{-1}), direct comparison of the observed flux would not be valid, and so the information given in Figures 4.15 to 4.18 is displayed in a different way in the charts shown in Figures 4.19 a, b and c. Each block graph in turn compares the initial, 8 day and 13 day hydrogen concentrations for each of the four treatments. Initial concentrations (Figure 4.19 a) for unplated and the specimen which had been baked for 2 hours were very similar (0.2 and 1.0 ppm) and lower than the values for plating, and plating and baking for 20 hours (2.0 and 2.3 ppm). Here it is shown even more clearly that the 20 hour bake has the highest initial value. At 8 days (Figure 4.19 b) the concentration values of the plated specimens are similar to each other; however, referring to Figure 4.18, the flux readings for the 20 hour baked specimen seemed to be less stable. As expected, the unplated specimen has a much lower hydrogen concentration. By 13 days (Figure 4.19 c) the concentrations had stabilised and, as can be seen from Figures 4.15 to 4.18, the depletion flux for each specimen closely followed the theoretical slope.

Whatever the stage of time after treatment the concentration of hydrogen in the plate is an order of magnitude greater than that in the unplated specimen.

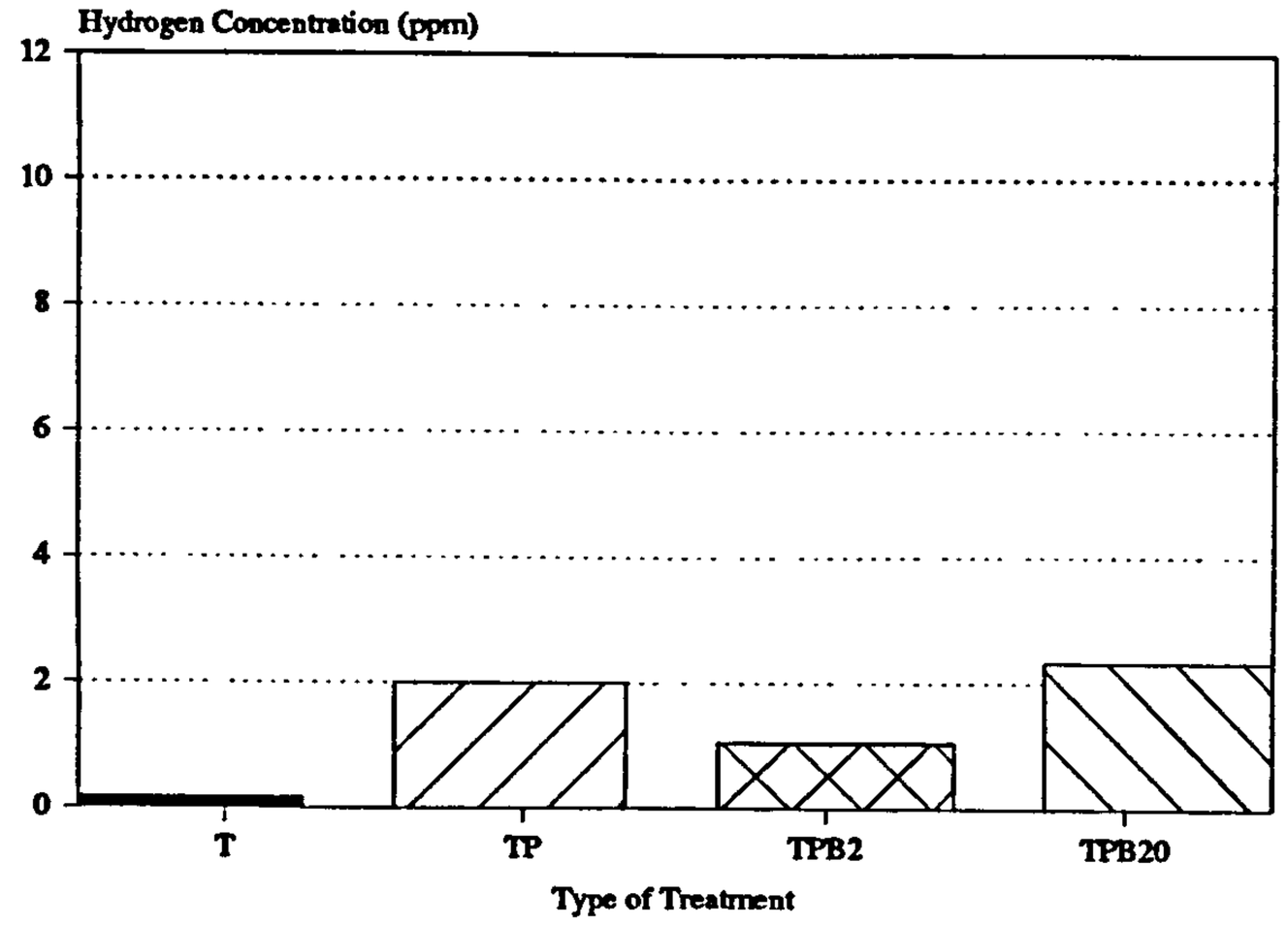

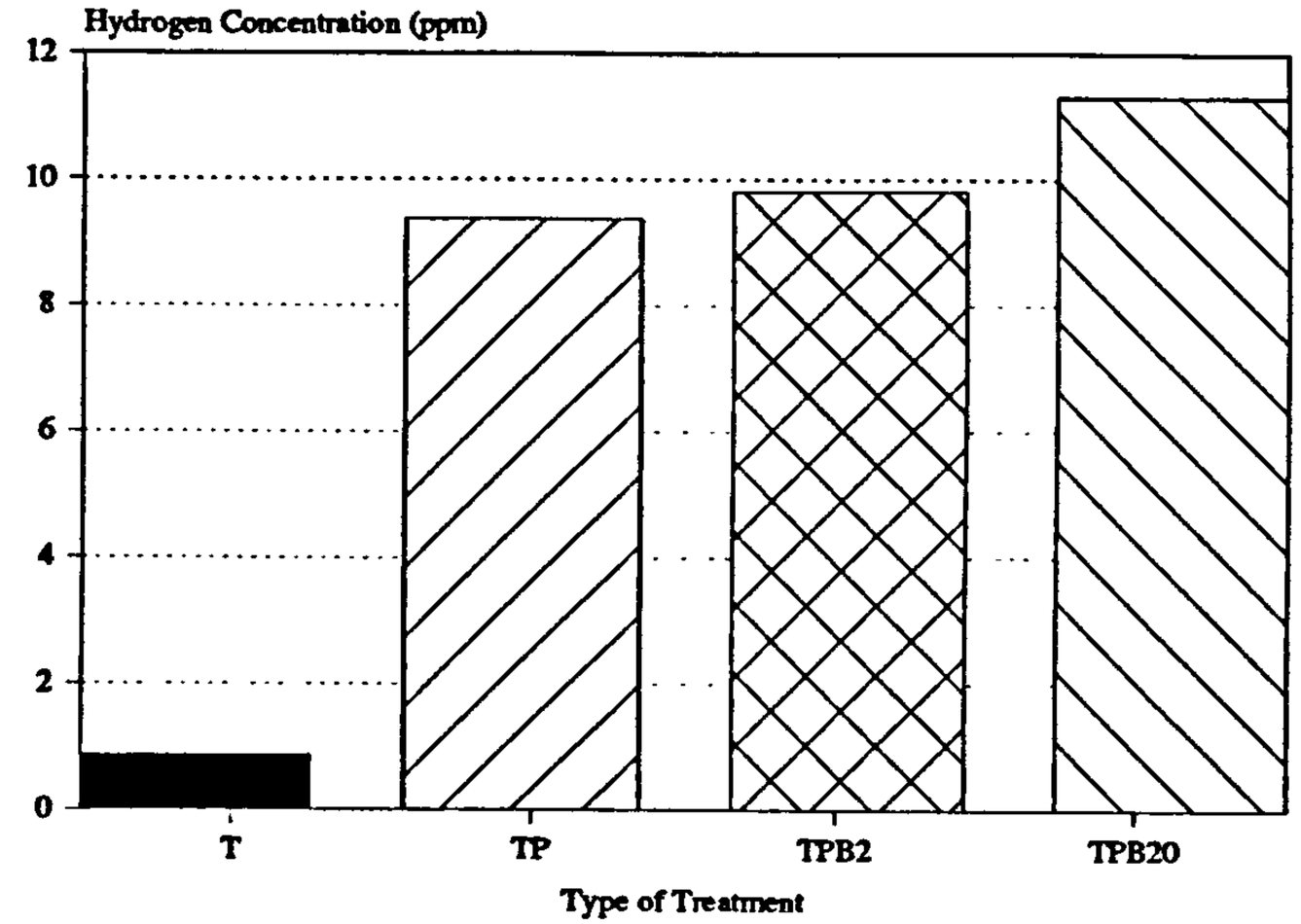

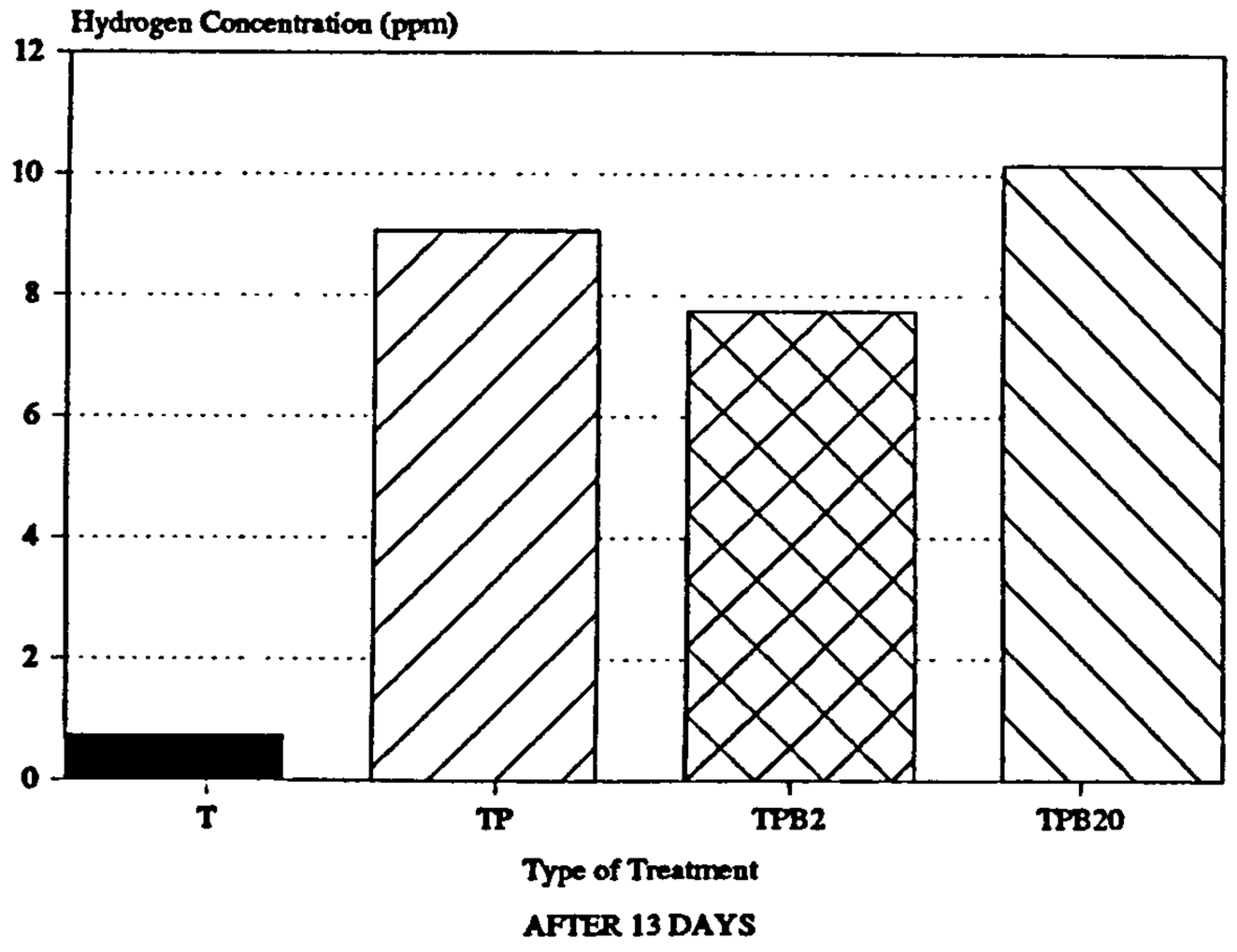

FIG. 4.19

Hydrogen Concentrations after

Four Different Types of Treatment

For Explanation of Codes, see Table 4.6

4.2.2.2.1 Replicate Specimens

Pairs of specimens were checked to see if there was good agreement. These specimens were tempered for 2 hours at 200°C but plating and baking conditions were as previously noted. It can be seen from Figures 4.20 to 4.22 that results were consistent. In all cases the initial values were the lowest. Tempered specimens (Figure 4.20) give similar results for 5 and 10 days, but for tempered and plated specimens (Figure 4.21) the 5 day concentrations seemed to be higher than for the 10 day. This trend was reversed for specimens baked for 2 hours (Figure 4.22) but there was little difference between the 5 and10 day values. Evidently, agreement is good between pairs of specimens treated with identical methods.

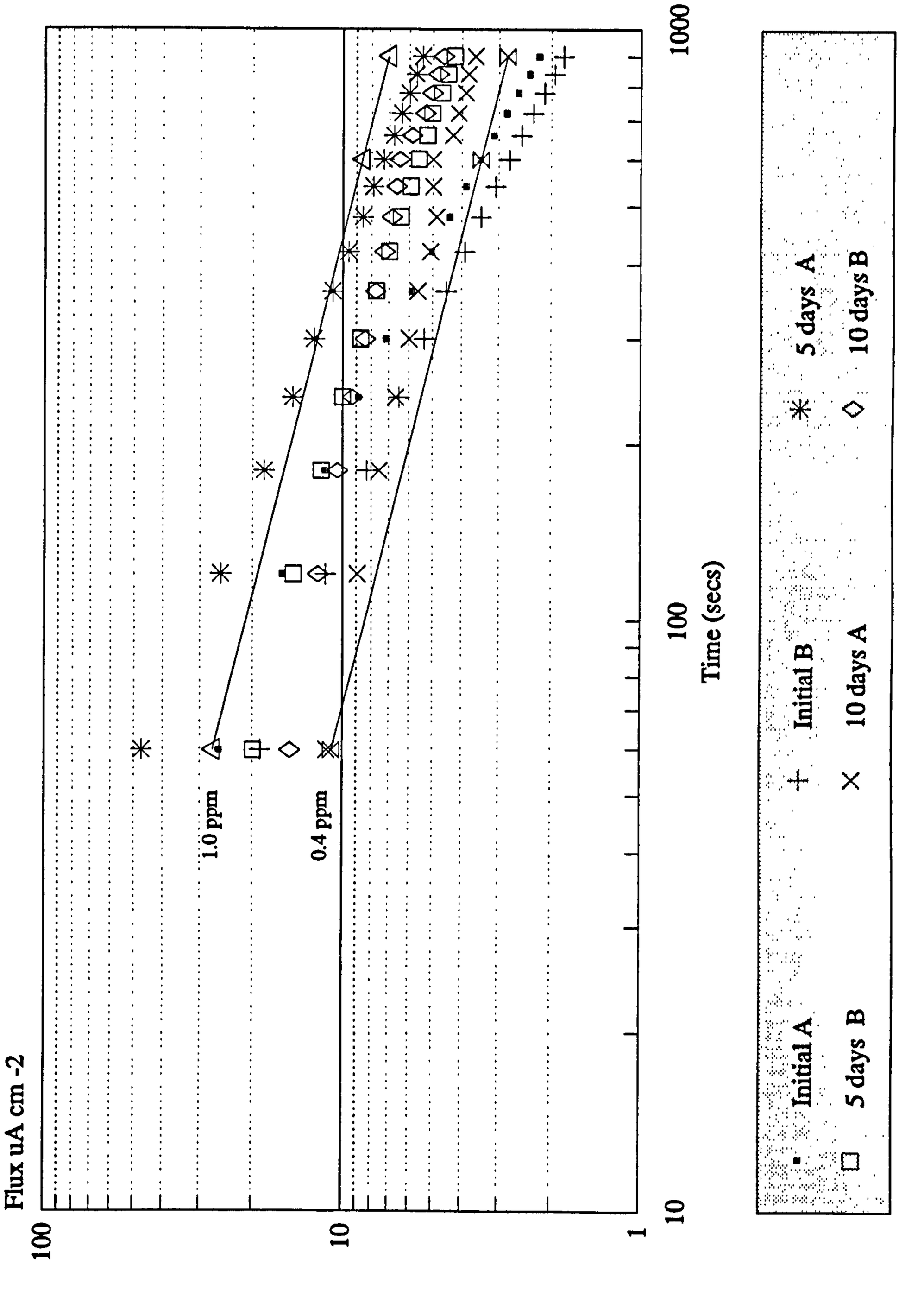
Flux uA cm -2
100
10
1
10
100
1000
Time (secs)
1.0 ppm
0.4 ppm
Initial A
Initial B
5 days A
5 days B
10 days A
10 days B
Hydrogen Determinations on Replicate,
Tempered Specimens.

FIG. 4.20

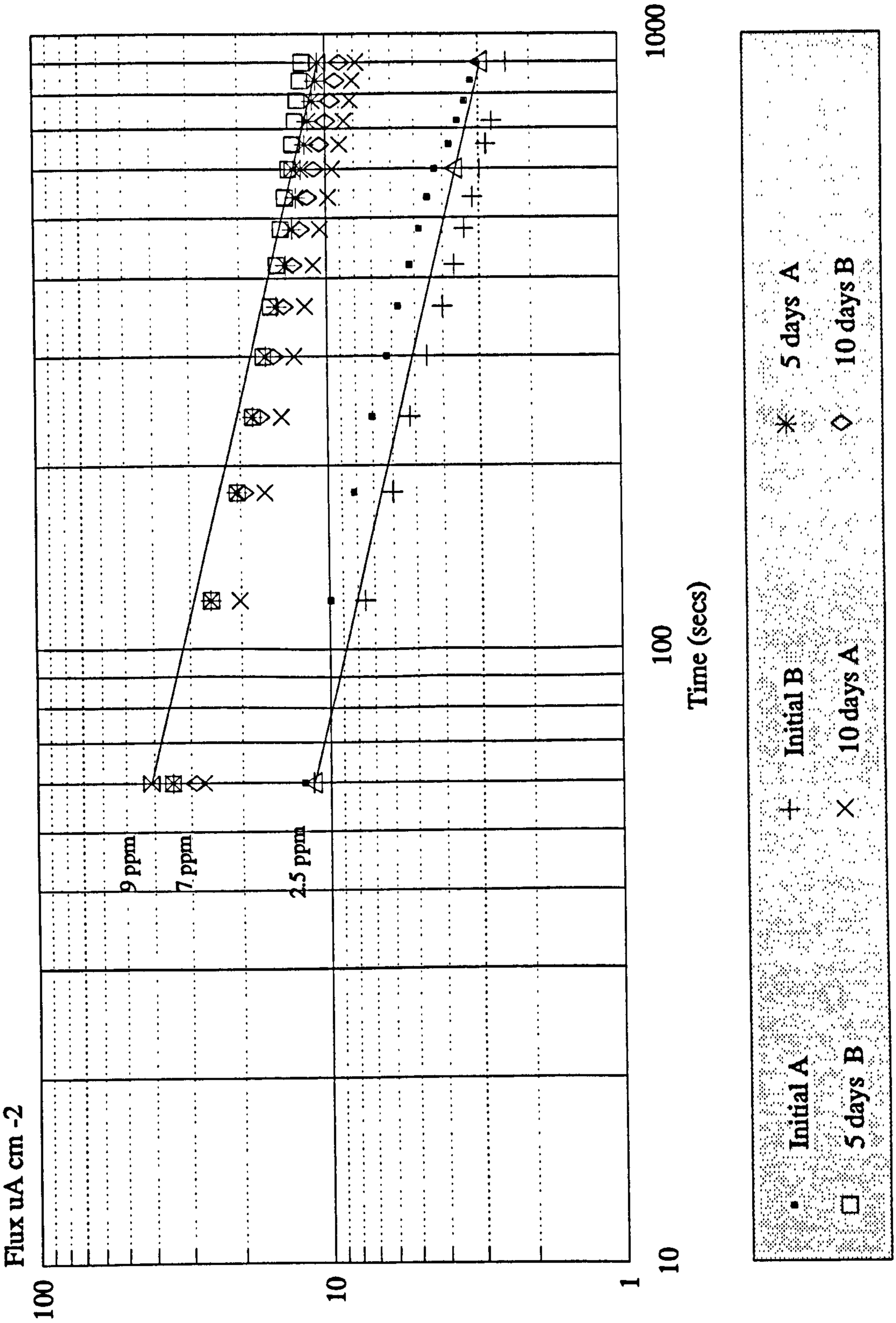
Flux uA cm -2
100
10
1
10
100
1000
Time (secs)
9 ppm
7 ppm
2.5 ppm
Initial A
Initial B
5 days A
5 days B
10 days A
10 days B
Hydrogen Determinations on Replicate
Specimens. Tempered 2 hours and
Plated 2 hours.

FIG. 4.21.

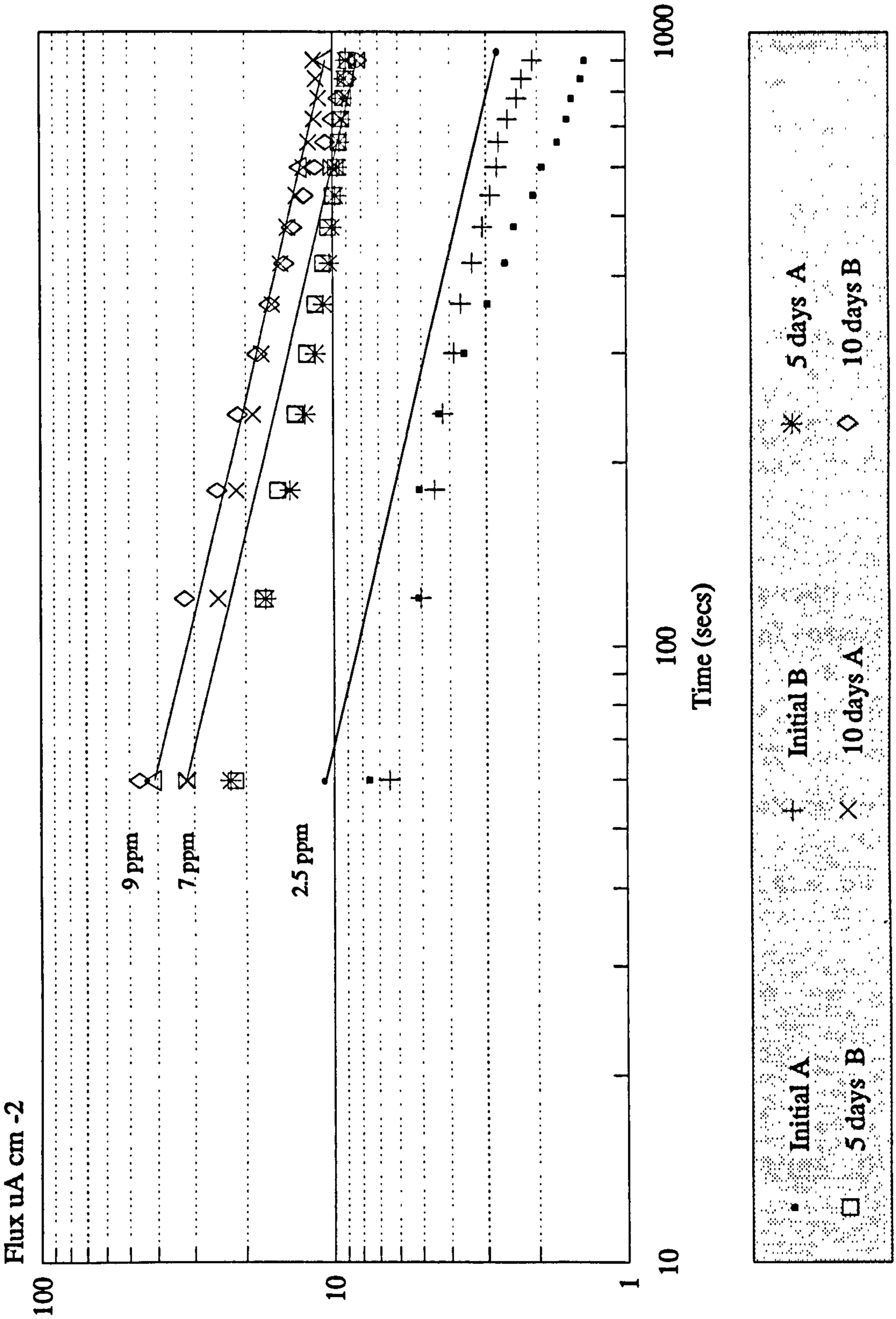
Flux uA cm -2
100
10
1
100
10
1000
Time (secs)
9 ppm
7 ppm
2.5 ppm
Initial A
5 days A
10 days A
Initial B
5 days B
10 days B
Hydrogen Determinations on Replicate
Specimens. Tempered, Plated and
Baked 2 hrs. at 200°C.

FIG. 4.22

4.2.2.2.2 Comparison of Specimens Baked for 2 and 20 hours

It had been noted during experimental work that there seemed to be little difference between baking for 2 or 20 hours and Figures 4.23 to 4.25 confirm this. Daily interval measurements were so similar that only values for initial, 3 days and 5 days are shown for clarity on the graphs. It is puzzling that these specimens did not exhibit the initial low values that had been obtained in earlier experiments. Figure 4.23 shows the initial values for pairs of specimens that had been tempered for 20 hours, plated and baked. The measurements are similar, but baking for 20 hours this time has a slightly lower value of hydrogen content.

Figures 4.24 and 4.25 confirm values of between 8.4 and 11.5 ppm of hydrogen initially falling to between 8.12 and 8.70 ppm after 5 days. Depletion values in the 2 hour baked specimen (Figure 4.24) are very stable but, as has been observed previously, a specimen baked for 20 hours (Figure 4.25) is more difficult to measure. The question that poses itself is, why should this be? The only answer must be, as previously discussed, the effect of the oxide layer.

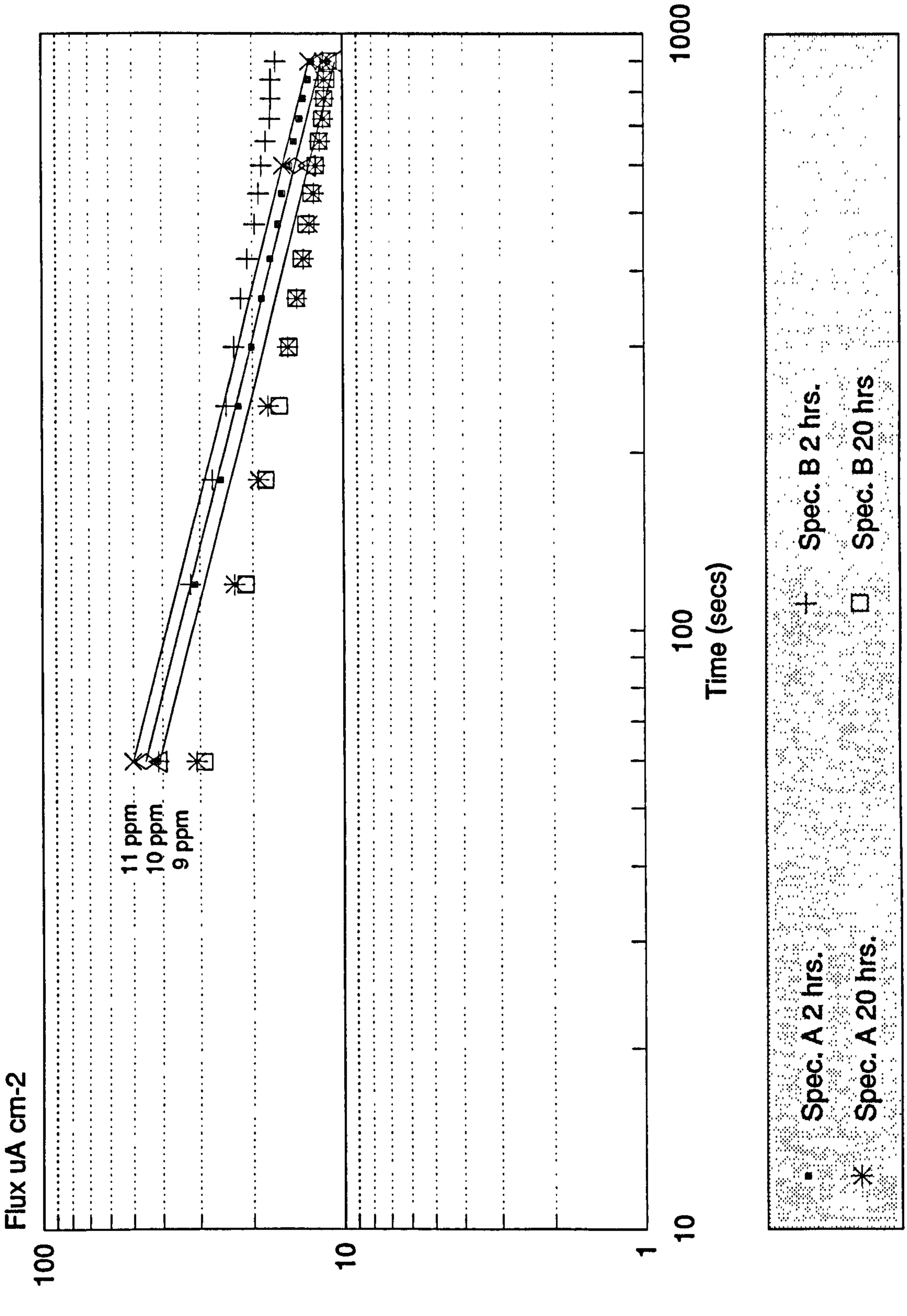
Comparison of Initial Readings
Flux uA cm-2
100
10
1
1000
100
10
Time (secs)
11 ppm
10 ppm
9 ppm
Spec. B 2 hrs.
Spec. B 20 hrs
Specimens Tempered, Plated and Baked
at 200°C for 2 hrs or 20 hrs.
Spec. A 2 hrs.
Spec. A 20 hrs.

FIG. 4.23

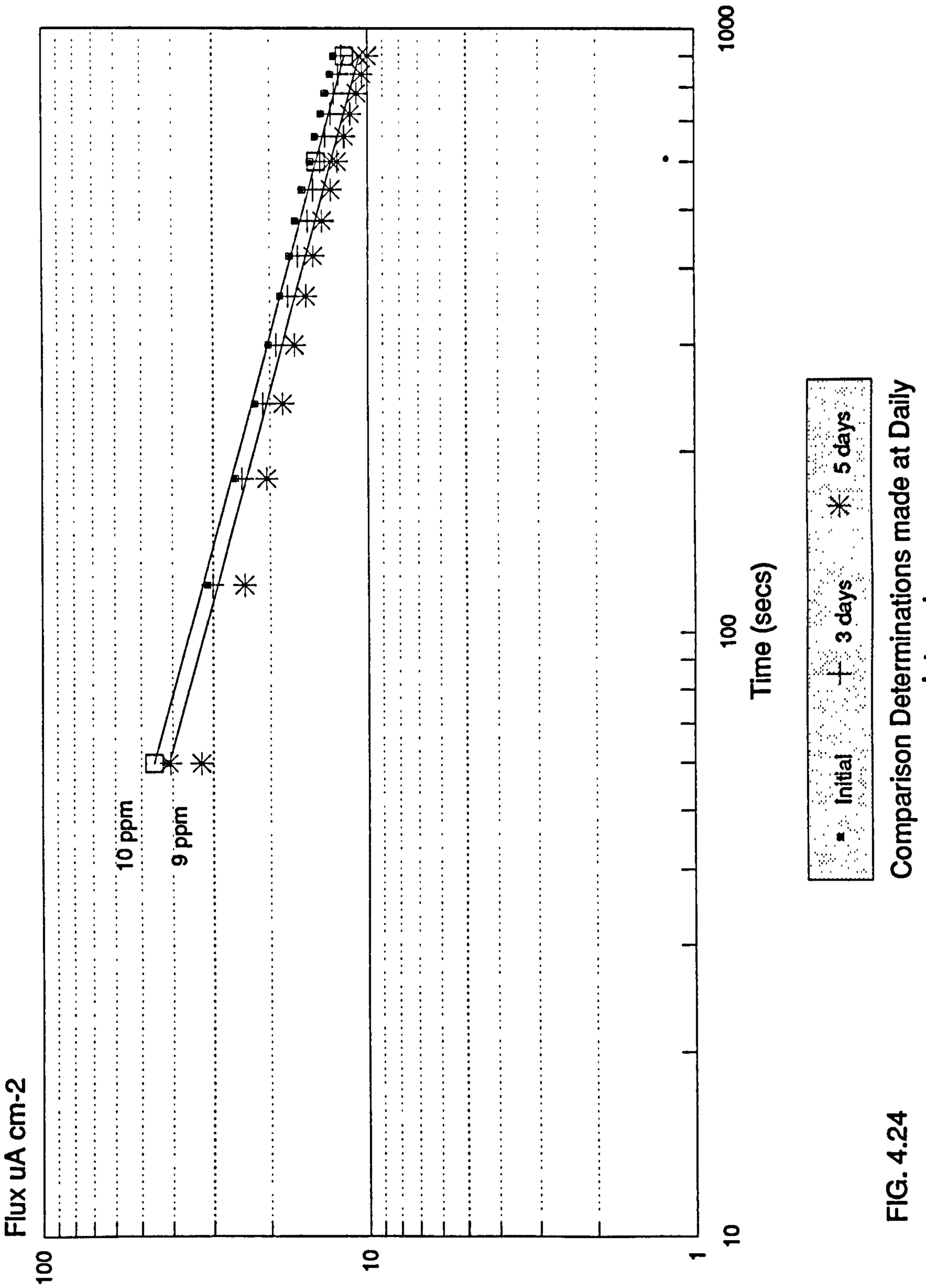

Comparison Determinations made at Daily Intervals.

FIG. 4.24

Tempered, Plated and Baked
Specimens(20 hrs. at 200°C)

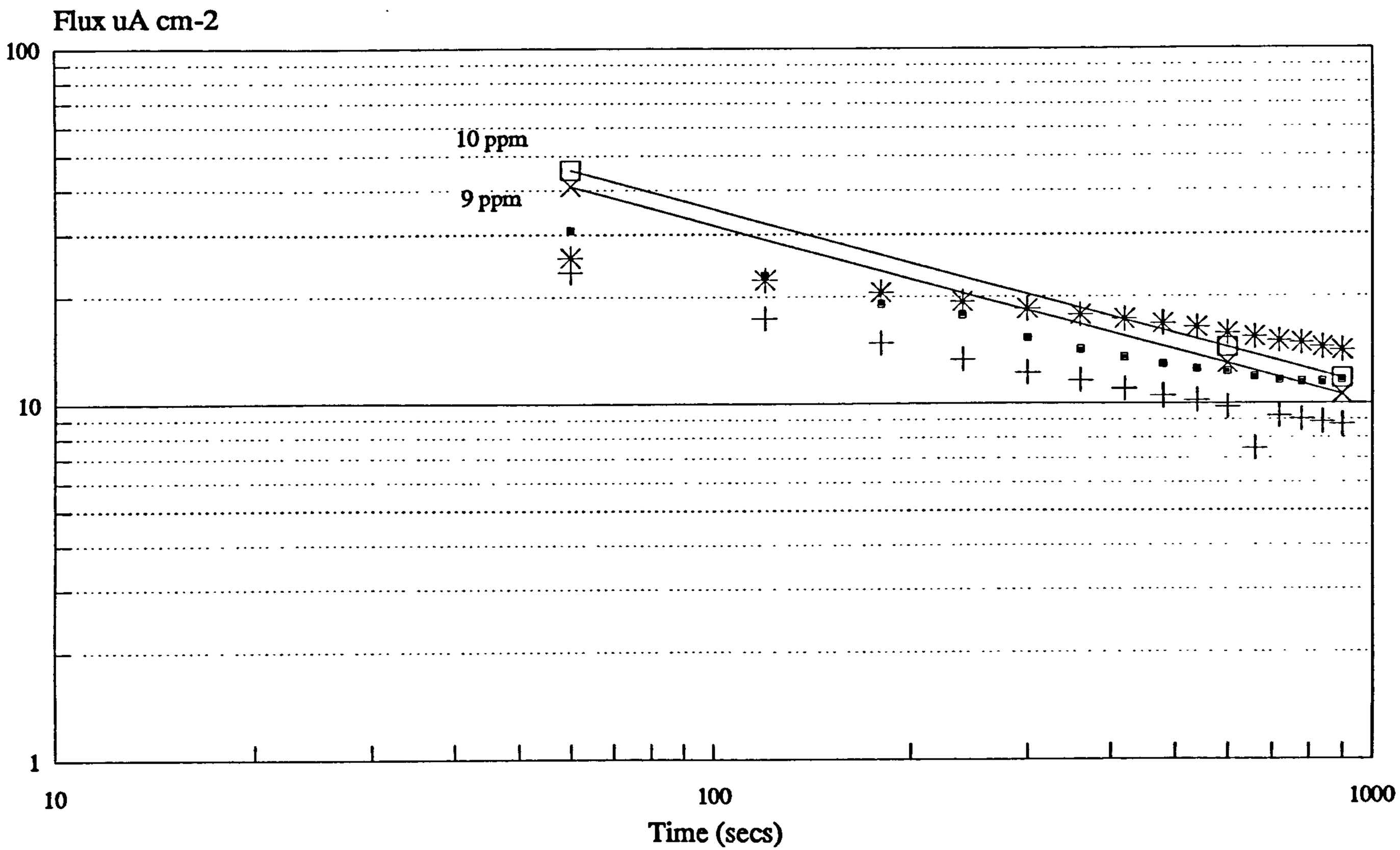

Fig. 4.25

Comparison Determinations made at Daily Intervals.

4.2.2.2.3 Comparison of Frequency of Measurements

Tempered for 2 hours at 200°C, tempered and plated and tempered, plated and baked for 2 hours specimens were tested initially and after 5 and 10 days. Initial readings, shown in Figure 4.26a settle down after 10 minutes to approximately 0.4 ppm for the tempered specimen, 2.46 ppm for the plated and 1.60 ppm for the plated and baked specimen, but after 5 days (Figure 4.26b) the plated specimens are between 6 and 9 ppm whilst the unplated specimen is still below 1 ppm. Indeed, after 10 days, the concentration differences are even more marked; this can be seen in Figure 4.26c, where the unplated specimen is still about 0.7 ppm, whilst the plated specimens range from 7.0 to 8.2 ppm.

Having questioned . . . whether daily measurements were affecting the stability of the hydrogen concentration, a series of measurements was made on two specimens each of the two baking treatments. On one set, daily measurements were made and the second set was left unmeasured for 5 days. The results can be seen in Figure 4.27. As before, the values for the two baking treatments are similar, and it can be seen clearly that there is no significant difference after five days between daily and once only measurements.

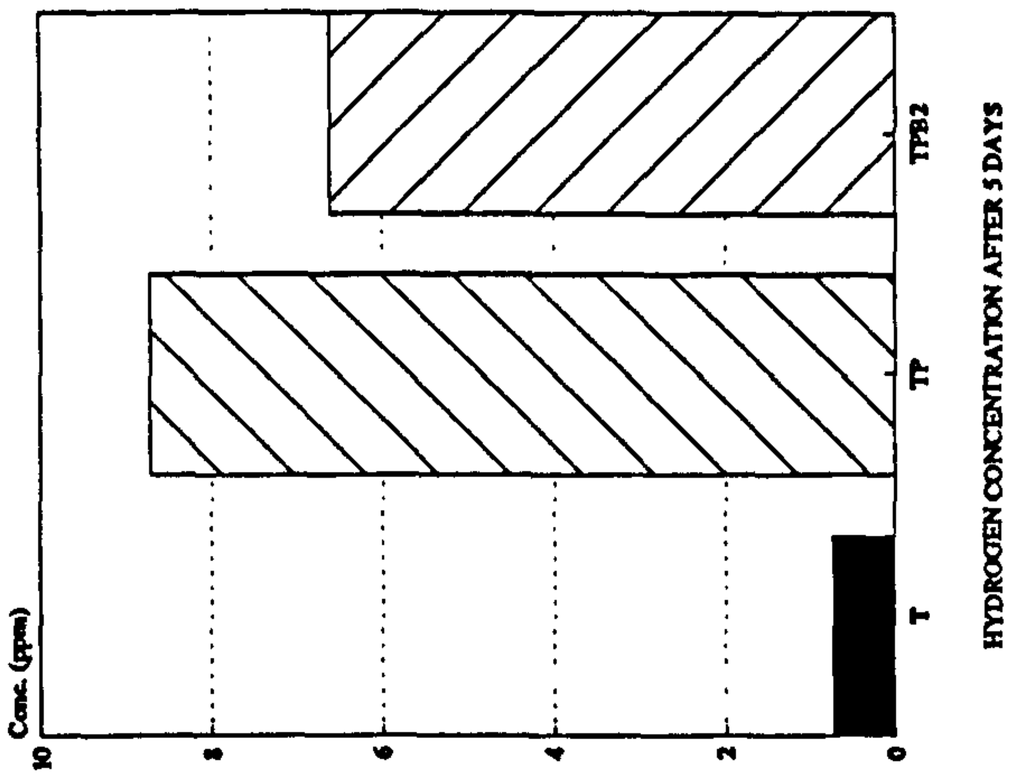

FIG. 4.26

Comparison of Frequency Measurements

For explanation, see Table 4.6

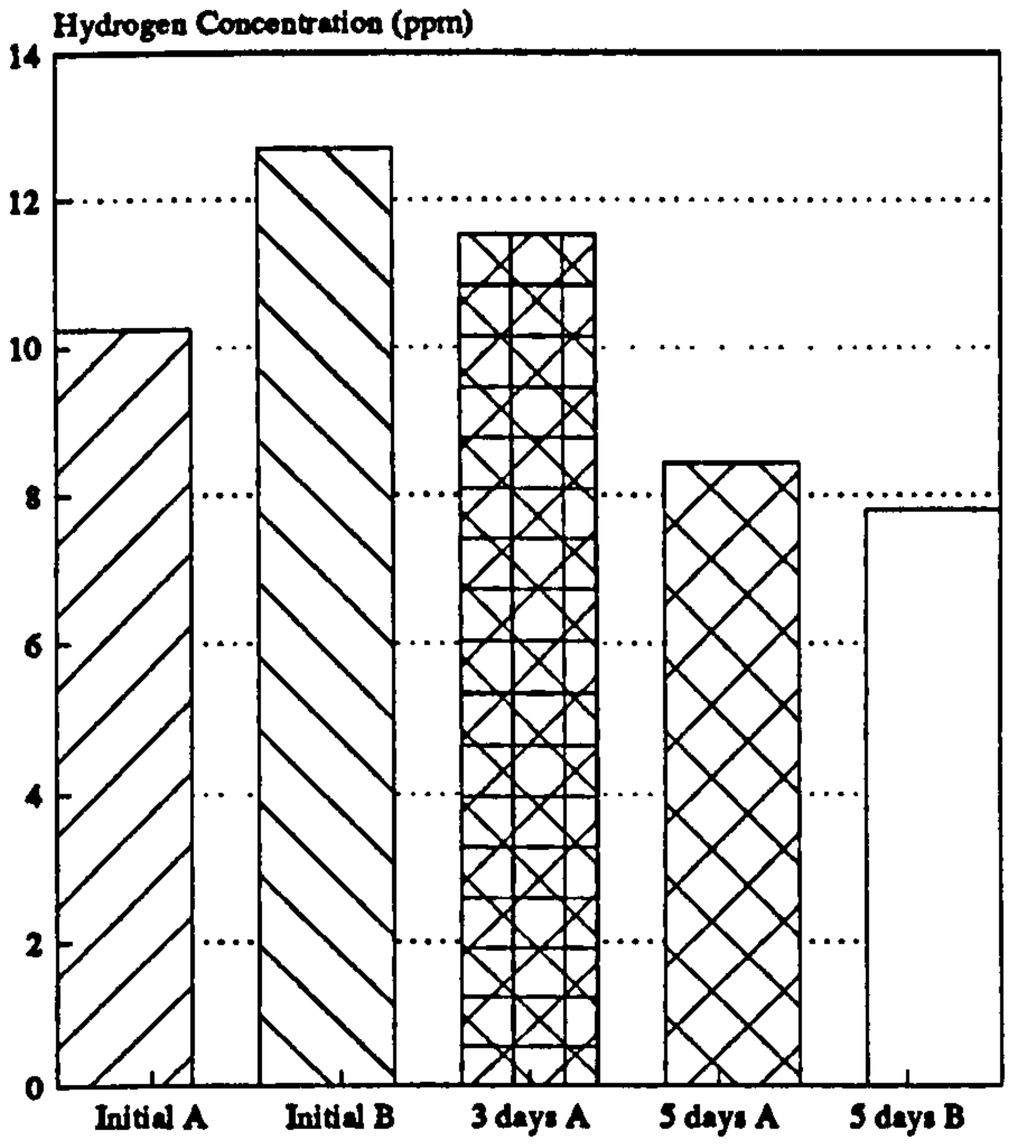

Tempered 20 hrs. at 200°C.
Plated 2 hrs. at5 mAcm2.
Baked 2 hrs. at 200°C.

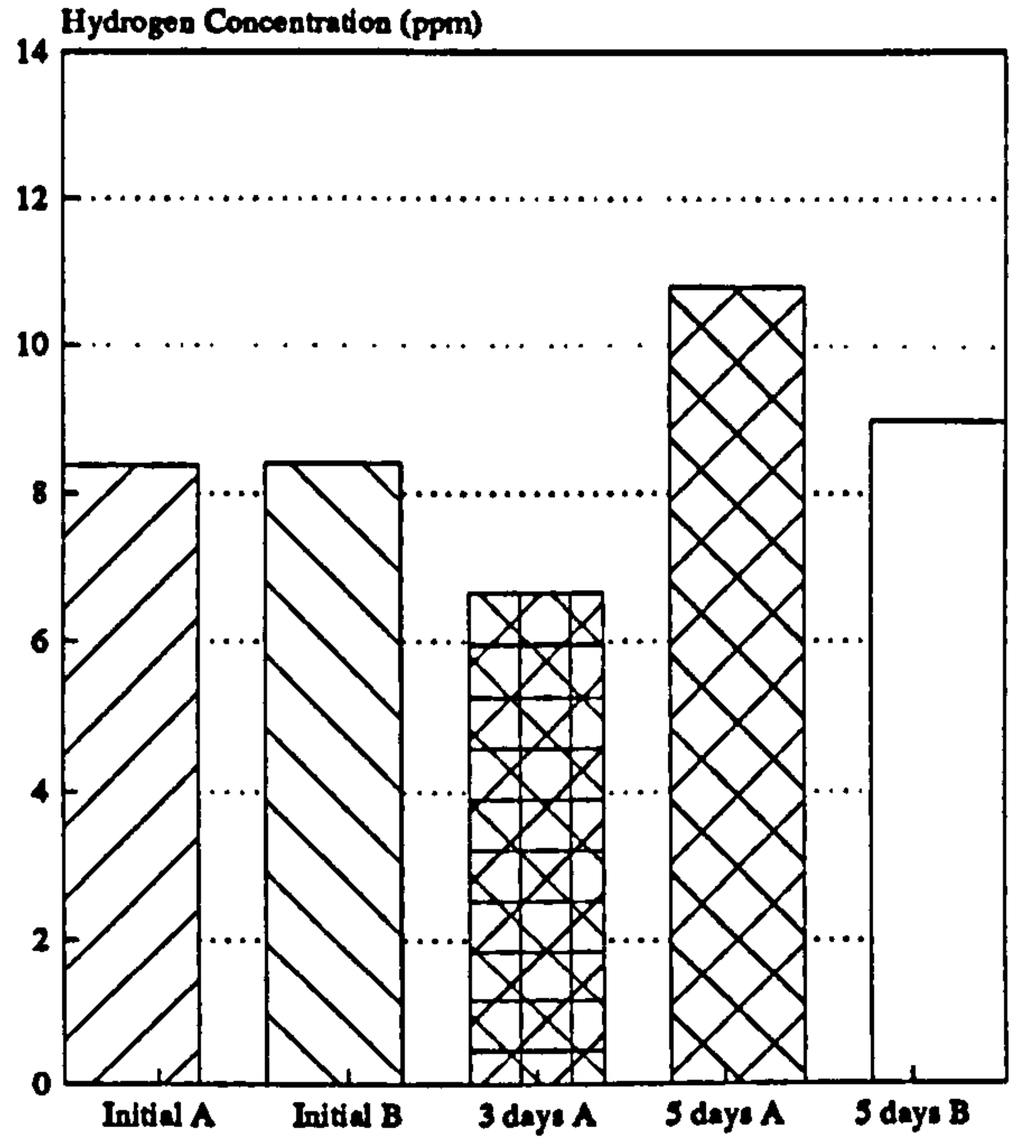

Tempered 20 hrs. at 200°C.
Plated 2 hrs. at 5 mAcm2.
Baked 20 hrs. at 200°C.

FIG. 4.27 Comparison of Daily Measured Specimens with Interval Measured Specimens

4.2.2.2.4 Summary of Results

Table 4.7 summarises the hydrogen contents obtained by probe measurements. It will be seen that there was little difference between specimens tempered at 200°C for either 2 or 20 hours, although Some initial values tended to be higher. Baking plated specimens for 2 hours seemed to be more beneficial than baking for 20 hours.

Table 4.7. Summary of Hydrogen Contents Obtained by Probe Measurements. (ppm)

	Initial	3 days	5 days	8 days	10 days	13 days
T	0.18 * 0.35		0.73	0.87	0.65	0.75
TP	1.99 * 2.46		8.72	9.37	6.97	9.06
TPB2	1.04 * 1.60 11.47	9.55	6.61 8.12	9.81	8.21	7.75
TPB20	2.33 8.39	6.66	8.70	11.31		10.16

KEY

T	Tempered 20 hours at 200°C
TP	Tempered, plated at 5 $mAcm^{-2}$
TPB2	Tempered, plated, baked 2 hrs at 200°C
TPB20	Tempered, plated, baked 20 hours at 200°C
*	Tempered 2 hours at 200°C

4.2.2.3 t-testing using Results Obtained from 6 x 3 cm Sheet Specimens

This section shows the results of two sets of experiments. The first considers specimens that were cathodically charged at 15 $mAcm^{-2}$ and then baked for either 2 or 20 hours at 200°C. The second compares the hydrogen content of the nickel plate with that of the substrate.

4.2.2.3.1 Effects of Baking Cathodically Charged Specimens

Cathodic charging produced initially high hydrogen concentrations (approximately 2.7 ppm) which were significantly reduced by baking at 200°C for 2 or 20 hours. Results are shown in Tables 4.8 and 4.9.

The difference between the baking treatment did not appear significant, as can be seen in Table 4.9. Even after 5 days the loss of hydrogen to the atmosphere by the unbaked specimens was small compared to baking. In all cases except one, ten specimens were tested.

TABLE 4.8 Mean Hydrogen Content of AISI 4340 Steel after Cathodic Charging at 150 $mAcm^{-2}$ and Baking for 2 hrs and 20 hrs at 200°C.

	Initial (ppm)	5 days (ppm)
Cathodic Charging	3.2 (A)	2.5 (D)
2 hrs. at 200°C	1.9 (B)	1.6 (E)
20 hrs. at 200°C	1.9 (C)	1.3 (F)

TABLE 4.9. RESULTS OF THE STATISTICAL 't' TEST

't'	't'	't'
(A)-(B) 2.44*	(D)-(E) 1.55	(A)-(D) 1.09
(A)-(C) 2.15*	(D)-(F) 2.06*	(B)-(E) 1.08
(B)-(C) 0.05	(E)-(F) 1.25	(C)-(F) 1.10

* Readings appear to belong to separate populations

$t_{0.05}$ 1·81

4.2.2.3.2 Hydrogen Content of Plate and Substrate

Initial experiments on the machined specimens involved nickel plate being removed by abrasion and measurements indicated a higher hydrogen content in the substrate. An attempt was made to introduce a graphite layer before laying down the plate, but proved unsuccessful. In both these cases, measurements were erratic; possibly this was due to the many stages necessary in the preparation of the specimens.

The larger specimens were prepared so that more measurements could be made on each. Also the plate was ground off one side to ensure there were fewer stages in specimen preparation. For these specimens, plating was at 2 $mAcm^{-2}$ and not 5 $mAcm^{-2}$. Eight sets of hydrogen measurements were made on one side which was nickel plated and the measurements similarly performed on the steel substrate exposed on the other side. A second set of specimens was plated and then left for seven days before the plate was ground off and a second series of measurements was made. The results are shown in Tables 4.10 and 4.11.

Table 4.10 shows the mean hydrogen contents of the nickel plate and those of AISI 4340 steel substrate and Table 4.11 gives the results of t-tests performed on the values given in Table 4.10.

The nickel plate appears to have a significantly higher value than the substrate (the critical t - value being 2.15) and after seven days the hydrogen content of both plate and substrate had decreased. It is probable that the loss of hydrogen to the atmosphere explained the significant decrease in the nickel ($t > 2.15$).

TABLE 4.10. Mean Hydrogen Contents of Nickel Electrodeposit and AISI 4340 Substrate

	Nickel Plate (ppm)				Steel Substrate (ppm)			
Initial	18.84	19.86	22.22	17.97	0.97	0.93	0.95	1.38
	19.61	19.20	11.16		1.70	1.37	1.39	1.38
	mean (A) 18.41				mean 1.26 (C)			
	S_{n-1} 3.46				S_{n-1} 0.28			
7 days	6.03	6.17	6.12	6.08	1.04	0.94	0.88	0.91
	7.63	6.14	5.99	8.50	1.03	0.90	0.94	
	mean (B) 6.58				mean 0.95 (D)			
	S_{n-1} 0.96				S_{n-1} 0.06			

TABLE 4.11 Results of Statistical t-test

t		t	
(A)-(B)	9.29 *	(B)-(D) *	15.25
(A)-(C)	13.97 *	(C)-(D)	2.67

* readings appear to belong to separate populations.

$t_{0.01}$ 2.65

$t_{0.05}$ 2.15

Finally, five specimens were prepared. First they were quenched and tempered for 20 hours at 200°C, Three specimens were tested immediately and then each was kept under differing conditions:

Specimen A was kept over a desiccant for 5 days
Specimen B was kept under vacuum for 5 days.
Specimen C was left lying on the bench for 5 days.

The remaining two specimens were nickel plated at 2 $mAcm^{-2}$ for 2 hours and then the hydrogen content of the plate was measured. These also were kept under different conditions for 5 days:

Specimen D was kept over a desiccant.
Specimen E was left lying on the bench.

The results for all five specimens are shown in Table 4.12 and Figure 4.28.

TABLE 4.12 Results for Specimens Kept Under Different Storage Conditions

Specimen	Initial	Mean (ppm)	5 Days	mean (ppm)
A	0.18	0.16	0.14	0.15
		>0.140		>0.150
Desiccant	0.05	0.05	0.18	0.13
B	0.15	0.12	0.10	0.10
		>0.108		>0.093
Vacuum	0.08	0.08	0.08	0.09
C	0.11	0.10	0.09	0.09
		>0.095		>0.088
Bench	0.09	0.08	0.09	0.08
D	5.71	5.05	1.58	1.58
Plate		>4.348		>1.715
Desiccant	3.80	2.83	2.00	1.70
E	3.81	4.31	1.57	1.56
Plate		>4.018		>1.583
Bench	3.89	4.06	1.61	1.59

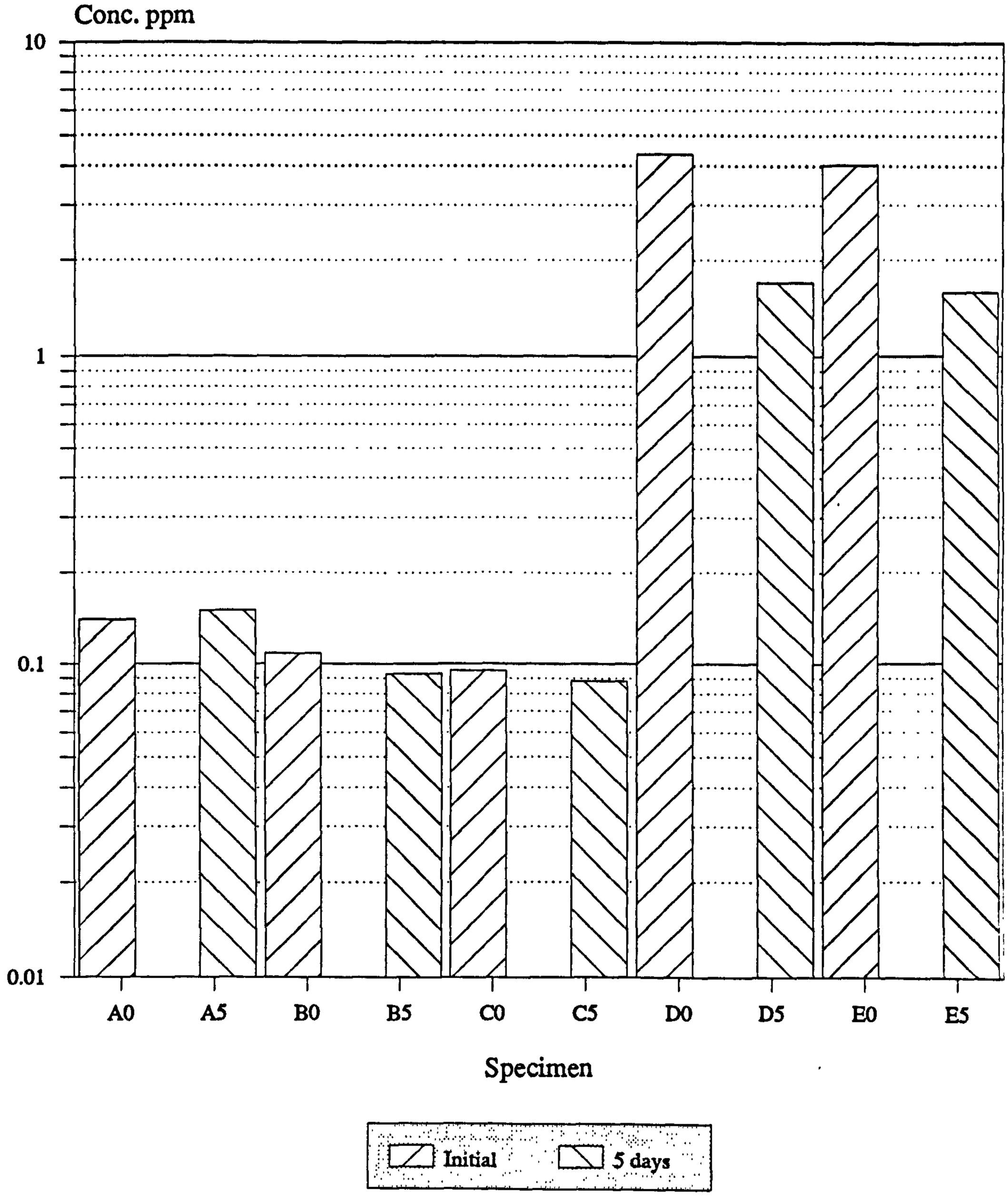

FIG. 4.28 Comparison of Initial and 5 Day Hydrogen Concentration for Specimens under Differing Storage Conditions. (see p 120)

Tables 4.13 to 4.15 show the results of using the t-test to compare the values obtained. From Table 4.13 there is no significant difference between plated and unplated specimens. It is interesting to note that comparing each pair of unplated specimens, A with B and A with C have a t-value less than the critical 95% value of 1.94, yet it is only at the 99% value that B with C are considered to be from the same population. However, it was felt that the three series of readings could be combined so that the comparison could be made with the total readings for the plated specimens where there is no obvious difference.

Table 4.14 shows that there is no significant difference between the 5 day values of the plated specimens which had been kept under differing conditions and no significant difference between those unplated but kept under vacuum or on the bench. Those kept over a desiccant were the only specimens to show an increase in hydrogen content. It is clear from Table 4.15 that there is a highly significant difference between initial and five day values for the plated specimens only. It is also evident that the conditions under which specimens are kept in the short term do not significantly affect the hydrogen content. This compares well with the results obtained in 4.2.2.2.3.

As a result of calculations for both constant load tests and permeation experiments it is clear that statistical t-testing is a valuable aid to the interpretation of the results.

TABLE 4.13 Comparison of Initial Values

Specimens	t
A - B	0.94
A - C	1.61
B - C	2.50
D - E	0.51

Critical values

$t_{0.05}$ 1.94
$t_{0.01}$ 3.14

Combined results

(A + B + C) - (D + E) 16.36 $t_{0.05}$ 1.73
$t_{0.01}$ 2.55

TABLE 4.14 Comparison of 5 Day Hydrogen Concentrations

Specimens	t
A - B	5.08
A - C	5.60
B - C	0.92
D - E	0.05

Critical Values

$t_{0.05}$ 1.94
$t_{0.01}$ 3.14

See p120 for explanation of A, B, C, D and E.

TABLE 4.15. Comparing Initial and 5 Day Hydrogen Concentration

Specimens	t	Storage
A_o - A_5	0.94	desiccant
B_o - B_5	1.86	vacuum
C_o - C_5	1.01	bench
D_o - D_5	4.05*	desiccant
E_o - E_5	21.92*	bench

Critical Values

$t_{0.05}$ 1.94
$t_{0.01}$ 3.14

* These differences are highly significant.

CHAPTER FIVE
DISCUSSION OF RESULTS

5.1 CONSTANT LOAD TESTING

Much valuable information about the susceptibility of high strength steels to hydrogen assisted cracking can be obtained by cathodic charging under load. In such circumstances, the rate of hydrogen generation is controlled, rather than relying upon the corrosion reaction to provide hydrogen.

5.1.1 Methods of Heat Treatment

A literature survey showed that various researchers have used different techniques when heat treating specimens. These are summarised in Table 5.1. Although most authors used an oil quench, it was decided, for practical reasons, to use a water quench after heating the steel into the austenite region and holding the temperature of 830°C for 30 minutes. Specimens of 0.8%C steel were then tempered at a range of temperatures over a range of times; these are fully described in Chapter Three - Methods, whilst AISI 4340 steel was tempered for 20 hours at 200°C as recommended in the Defence Standard (DEF STAN 03-4/2). The tempering treatment was selected to produce a microstructure with a high susceptibility to hydrogen embrittlement and it was hoped that, in later experiments, the effects of post-plating baking on nickel plated steel would be readily detected.

In fact, in constant load testing, specimens of quenched, tempered AISI 4340 steel which had been nickel plated for 2 hours at 5 $mAcm^2$ and tested at 90% σ_f had not failed within 170 hours. It was decided to carry out constant load tests on quenched only steel which was

TABLE 5.1 Treatments used by Various Experimenters

	Quench	Tempered (Degrees C)
Robinson and Sharp	Water	200 for 2 hours
Townsend	Oil	204 for 1 hour 232 for 1 hour
Potak	Oil	200 no time given
Johnson/Morlet/Troiano	Oil	400 for 1 hour
Grundy/Davies/Ryder	Oil	417 for 1 hour
Beachem	Oil	200 for 1 hour each 315 425 538 593
Garber/Bernstein/ Thorpe	Water	685°F for 3 hours. (363°C)

TABLE 5.2 Mechanical Properties of High Strength Steel Specimens

Alloy	Condition	σ_y (MPa)	σ_f (MPa)	Hardness (VPN)
AISI 4340	½ hr.830°C, Q. water Q & T 200°C 3 hours Q & T 200°C 20 hours	1870 1380 1360	2050 1590 1574	385 425 400
0.8%C	As received ½ hr.830°C, Q.water Q & T 350°C 2 hrs. Q & T 400°C 2 hrs.		1910 942 929	560 760 610

susceptible to embrittlement by nickel plating as relatively small concentrations of hydrogen are evolved when plating at a range of current densities compared with the considerably higher hydrogen concentrations obtained when cathodically charging.

Initial work on constant load testing used as-received 0.8%C wire, subjected to cathodic charging under a variety of stresses, in order to test the relationship between stress and time to failure. At the same time, an opportunity to look at the fracture surfaces presented itself and attempts were made to identify possible fracture initiation sites. Effects of heat treatment followed by cathodic charging or nickel plating were also investigated and similar tests were carried out on AISI 4340 steel.

Mechanical properties of both types of steel are listed for comparison (see Table 5.2). It can be seen that the lower carbon steel (AISI 4340) has a much higher strength after tempering but lower hardness values compared to the 0.8%C steel. Published values for the tensile strength of AISI 4340 steel and 300M steel following quenching and tempering are shown for comparison in Figure 5.1 (taken from Sands and Miller, 1956).

FIGURE 5.1 Effects of Tempering Temperature on the Tensile and Impact Properties of Two Medium-carbon Low-alloy Steels Oil-quenched from 855°C

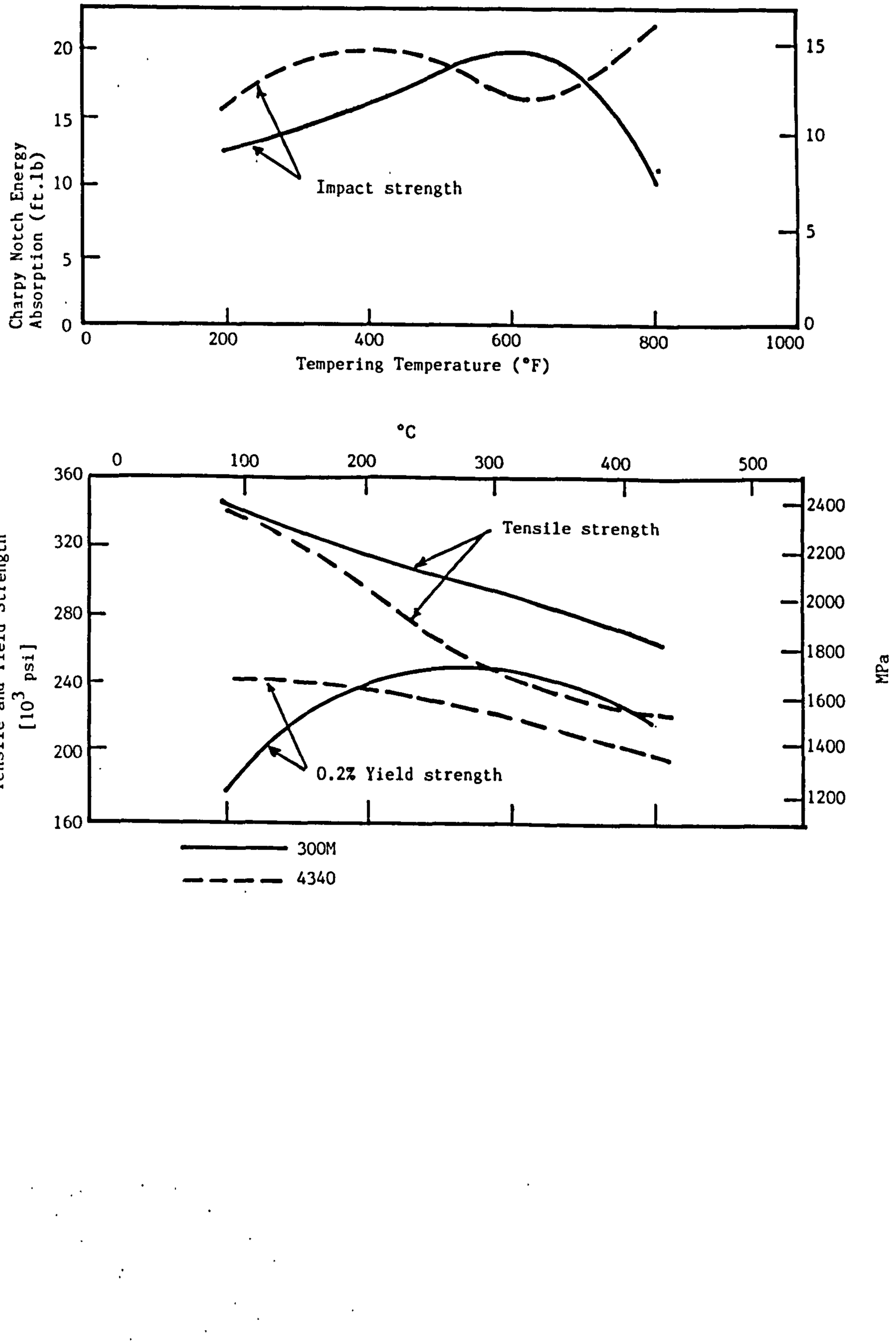

Unfortunately, it was not possible to attain the strength published in the Defence Standard. This is surely due to the fact that there were some residual spheroidal carbides in the microstructure because the temperature during austenising was not sufficiently high to convert the carbides into solid solution and consequently the hardness would be lowered. Evidence of the residual carbides can be seen in the photomicrographs shown in Figure 3.2. Had the austenising temperature been taken up to 1150+ °C before quenching, the recrystallised grain size would reduce the strength to an unacceptable level. However, it should be made clear that the Defence Standard gives recommended baking treatments for steels of a particular strength, but it does not define what the strength of each grade of steel should be. Some doubt is also cast on the use of a spot hardness measurement to indicate the strength of the material as recommended in the Defence Standard. Tensile tests were performed on the AISI 4340 steel used in the experimental work reported in this thesis as can be seen in Table 5.2.

5.1.2. Relationship Between Stress and Microvoid Coalescence

Beachem stated that, as a result of high stress intensity, plastic deformation takes place at a crack tip, causing inclusions present in the plastic region to act as initiation sites for void nucleation and so the fracture process is characterised by microvoid coalescence (MVC). This occurs at low or intermediate stress intensities. Once cracks initiate, further growth appears by intergranular cleavage. These forms of fracture are evident in the scanning electron microscope (SEM) photographs of the fracture surfaces obtained from both types of steel (Figure 5.2 a-c),confirming Beachem's observations noted in Chapter Two - Literature Survey.

FIGURE 5.2 Fracture Surfaces of AISI 4340 Steel

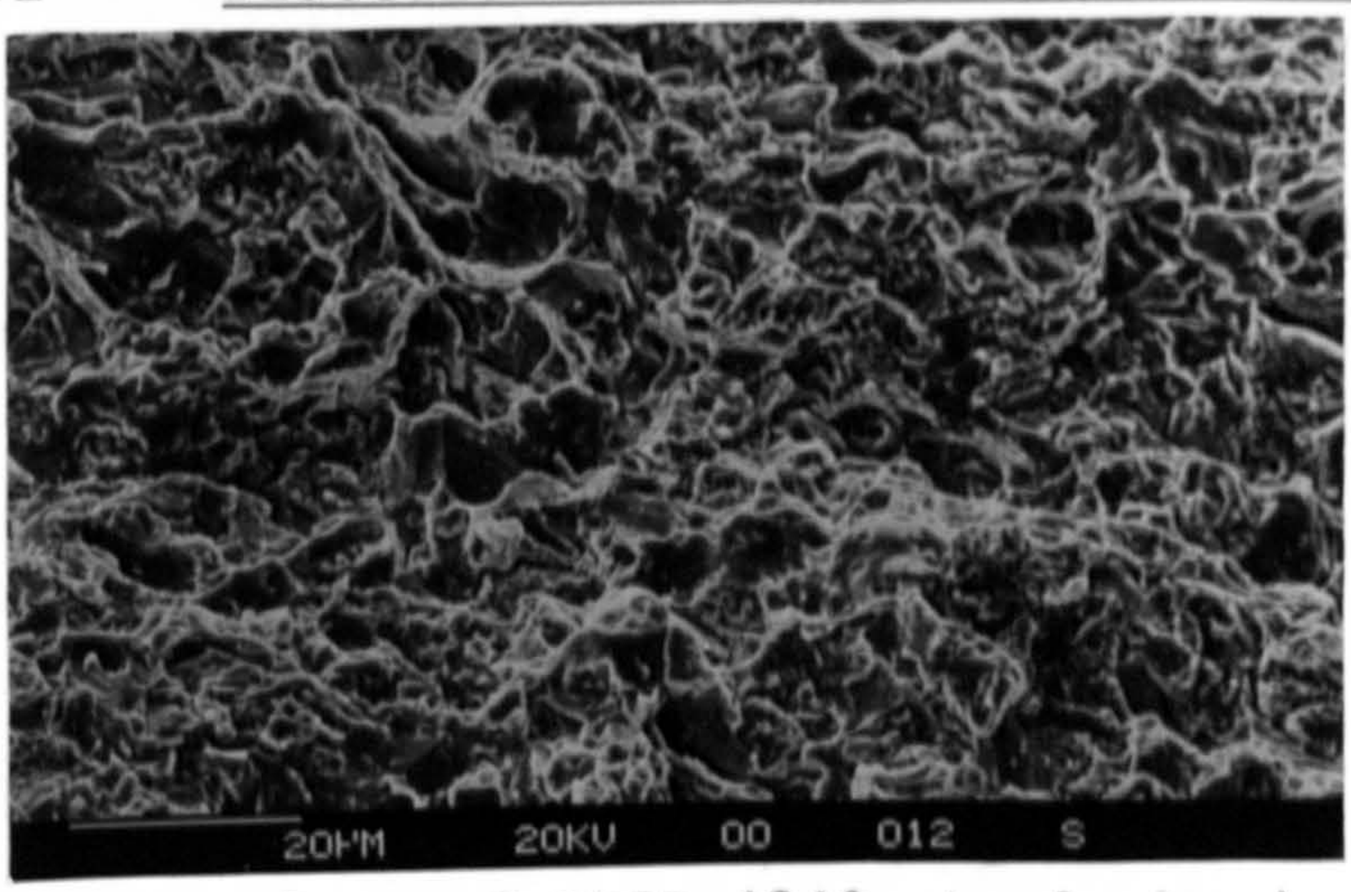

a. Fracture surface of AISI 4340 steel showing microvoid coalescence.

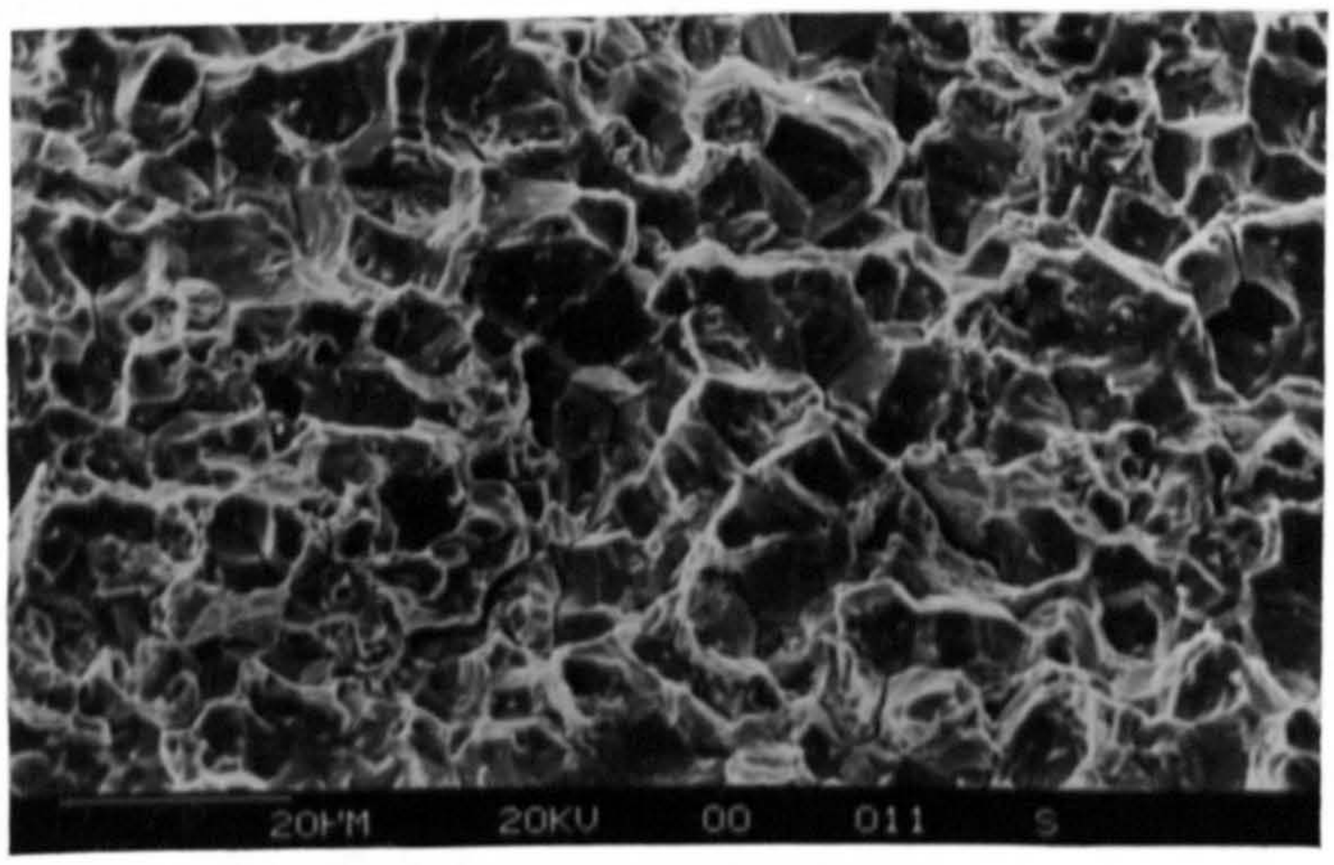

b. Fracture surface of AISI 4340 steel showing inter-granular cracking.

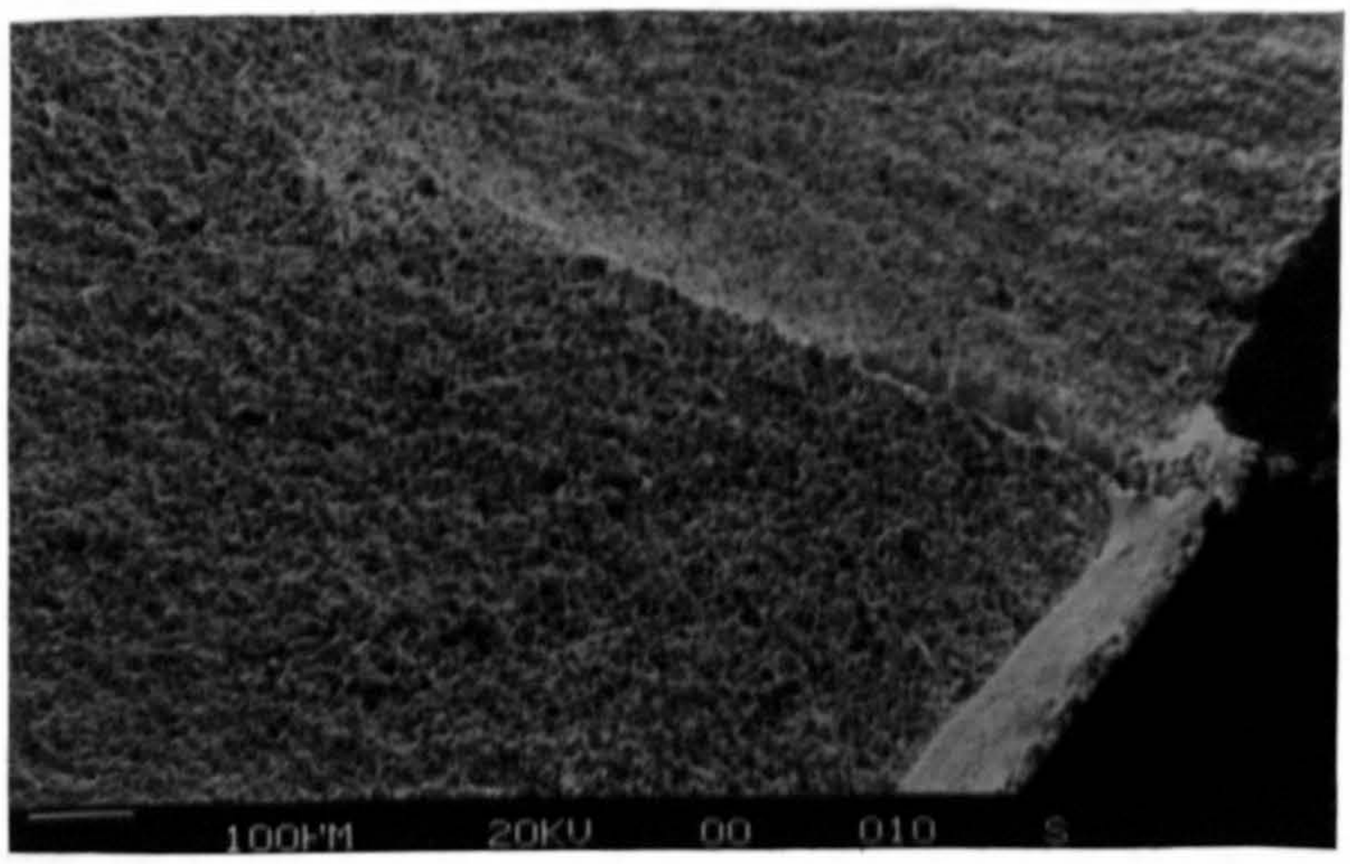

c. Fracture surface of nickel plated AISI 4340 steel.

It was not possible to identify the actual initiation sites but from the photographs of the fracture surfaces seen in Chapter Four (Figure 4.2) it was comparatively easy to estimate the percentage of MVC evident after specimens had fractured after undergoing cathodic charging at a variety of stresses. The results (Figure 4.3) clearly indicate the linear relationship between stress and the extent of MVC. Using the data obtained from Table 4.2, the product-moment correlation coefficient was calculated as r_{xy} = 0.984 and the regression line was of the form

$$y = 0.8x + 1.0$$

Hydrogen embrittlement in the low carbon steel tested would be expected to result in inter-granular (low K) or cleavage (intermediate K) fracture. As the stress increases during tensile testing, then the specimens would finally fail by overload when $\sigma > \sigma_f$ which is characterised by MVC.

The aim of these experiments was to decide between two criteria for overload failure.

There were two possible relationships by which the percentage of MVC affects failure of the wire whilst under stress.

i. Should the relationship obey the equation

$$\% \text{ MVC} = k.\%\sigma_f \qquad \text{where } k \approx 1$$

then the specimen will fail when the stress on the remaining cross-section approaches the fracture stress, i.e. the % MVC increases linearly with σ/σ_f of the initial loading.

ii. When $k_1 \rightarrow k_{1c}$ then k_{1c} = const. $\sigma\sqrt{\pi a}$ where the constant depends on the geometry of the specimen, and is taken to be 1.1 for these calculations, a = crack length, and the % MVC is not linearly related to σ/σ_f. This would mean that at lower stresses (eg 52% σ_f) the value of the constant would be larger and the specimen would fail before reducing to 50% of the cross-sectional area.

It is evident that the linear relationship is applicable and that relationship (i) is more apt, i.e. in all cases $\sigma > \sigma_f$ before 'a' is large enough for $k_1 > k_{1c}$.

5.1.3. Relationship Between Stress and Time to Failure

Quite obviously, for any one stress there would be a wide range of times to failure as the failure sites are undefined and depend on the statistical distribution of defects within the microstructure. This necessitates some form of statistical analysis: Yokoburi (1965) used a Weibull model (see Appendix A) which relates time to failure with the logarithm of the probability of survival.

$$P_s = 1 - P_f = e^{-xt}$$

where P_f is the probability of failure and x is the parameter termed the Weibull slope and is obtained from the negative gradient of the graph of LnP_s against t. The mean failure time $\bar{t}$ is defined as 1/x and can be used as a measure of the susceptibility of the material to hydrogen-induced failure.

Strecker et al (1975) confirmed that the analysis is valid for high carbon wire but Robinson and Sharp (1986) took into account that under certain circumstances there

was a minimum incubation time for failure, t_i, which corresponded to the time necessary for hydrogen to diffuse to a depth where a critical crack was generated. Robinson and Sharp amended the equation above to include this parameter.

$$P_s = 1-P_f = e^{-x\,(t-t_i)}$$

and the mean failure time would now be

$$\bar{t} = t_i + \frac{1}{x}$$

TABLE 5.3 Values of the Minimum Incubation Time, t_i and Mean Failure Time , $\bar{t}$, for Hydrogen Embrittlement of 0.8%C Steel and AISI 4340 Charged at 150mAcm^{-2}

Applied Stress (% σ_f)	t_i (s)	$\bar{t}$ (s)
0.8%C steel		
89.8	131	175
84.5	196	239
78.8	224	393
73.7	312	486
63.0	583	894
52.2	726	2256
AISI 4340		
97.5	18	183
90.0 (Ni plating)	114	620

The various probability plots are shown in Chapter Four - pp 76, 81 Results, and it is clear that the majority of the failures are compressed into the upper part of the graph (due to the logarithmic scale) and so the points obtained in these regions are more significant when determining values of t_i and $\bar{t}$. Comparative values for minimum incubation time and mean failure time can be seen in Table 5.3.

From Figures 4.4 p76 and 4.6 p81 in Chapter Four it can be seen that for most stresses applied, the slopes are similar but transposed along the time axis. This suggests that at lower stresses, not only longer times are necessary before hydrogen concentrations occur which are sufficient to induce failure by initiating a crack which will lead to overload fracture, but also the crack would need to be longer. It is also quite clear that the lower the stress, the longer a specimen will last before failure is likely to occur. From the same graphs, the Weibull plots give a single straight line for stresses in the range 63-90% σ_f but specimens tested at 52% σ_f showed two distinct slopes. For this graph, 54% failed within 100 minutes ($\bar{t}$ 37.6 min) and the rest occurred in times extending over 2800 minutes ($\bar{t}$ = 1120 min). From these observations it is likely that for the higher stresses, a single fracture mechanism takes place but that for low values of applied stress, hydrogen embrittlement either occurs by another mechanism or there is an additional stage which occurs too rapidly to be observed at higher stresses. (See 5.1.4).

The effect of heat-treatment on the embrittlement of the 0.8% steel can be seen in Figure 4.4. In each case, specimens were tested at 80% of the new fracture stress that resulted from the tempering treatment (see Table 5.2). It can be seen that tempering at 350°C lowered the fracture stress and increased the susceptibility to embrittlement. Tempering at 400°C gave a further minor reduction in mechanical

properties but a significant increase in the mean failure time.

From Table 5.3 (p134) and Figure 4.6 (p81)

It can also be seen clearly that cathodically charged AISI 4340 steel which has been quenched only is highly susceptible to hydrogen embrittlement (t_i = 18 sec and $\bar{t}$ = 183 sec) but that nickel plating affords some protection (t_i = 114 sec and $\bar{t}$ = 620 sec) to 0.8C% steel because less hydrogen is absorbed in this process. It will be recalled that quenched and tempered AISI 4340 steel which had been nickel plated had not failed after 170 hours.

5.1.4 Influence of Microstructure on Embrittlement.

Ryder et al (1982) suggested that the relatively low susceptibility of 0.8C% steel to hydrogen embrittlement was due to the cold-worked pearlitic structure containing high concentrations of innocuous traps in the form of carbide/matrix or inclusion/matrix interfaces. Further work by Davies et al (1977) showed that hydrogen diffuses more readily in tempered martensite containing fine carbides rather than in the cold-worked pearlitic material with coarse lamellar carbides. Robinson and Sharp (1986) also demonstrated that carbide interfaces acted as effective traps for hydrogen. They suggested that when tensile stress was removed, hydrogen diffused into innocuous traps at the carbon interfaces and that these traps were irreversible at the testing temperature. Furthermore, the apparent complete recovery from previous hydrogen charging indicates these traps were not significantly filled during 80% of the minimum incubation time.

It has already been stated that, from consideration of fracture mechanics, for a brittle cleavage crack of length, a, to propagate in a stressed specimen the crack stress, σ_n K_{1scc},

must exceed the threshold value K_{th},

where K_{th} = constant. $\sigma\sqrt{\pi a}$.

If, however, there is no prior crack, the size of the stress intensity depends upon the size of the defects present within the microstructure. From fracture mechanics considerations (Brown, 1971), where the crack tip stress intensity, K, must exceed the threshold value, K_{th},

$$K = const.\sigma\sqrt{\pi a}$$

and using the values of 1.1 for the constant and a typical threshold stress intensity of 10 MPa . for high strength steel, Robinson and Evans (1988) calculated that for 0.8%C steel defect sizes would need to be of the order of 7.5 μm before a crack would propagate at 90% σ_f and 25 μm before a crack would propagate at 50% σ_f. However, when defects are of a similar size to the grain size of the material, fracture mechanics criteria do not necessarily hold true.

This would probably explain the reason for the apparent two-stage Weibull plot for specimens stressed at 52% σ_f whilst being cathodically charged. It is suggested that defects of the size necessary for K_{th} to be exceeded were present within the steel in all specimens subjected to the higher stresses and consequently crack propagation took place once the local hydrogen concentration, C_{th}, exceeded the critical value. However, it is postulated that at the lower stress of 52% σ_f, defects of sufficient size were present in only 50% of the specimens and that a greater length of charging time was essential in the remaining specimens before sufficient hydrogen migrated to internal voids large enough for K_{th} to be attained.

5.1.5 Influence of Alloying Techniques.

Interesting work is being done at present by Paatsch (1988), who is investigating the avoidance of hydrogen embrittlement by thermal alloying techniques. He has shown that the hydrogen evolved during the plating process is outgassed during alloying heat treatment which occurs simultaneously as de-embrittling baking. Once the plating has occurred, the samples were heat-treated in the temperature range of 700 - 950°C for up to one hour in an argon atmosphere. He found that just ten minutes of heat treatment at 850°C would be sufficient to form a nickel-iron diffusion zone which would have a diffusion coefficient of less than 10^{-10} cm^2sec^{-1} (see Figures 2.4 and 2.5) which reduces the hydrogen diffusion considerably. Furthermore, the low alloyed steel that Paatsch used showed that it could be nickel plated without any embrittlement if the plating process is followed by heat treatment of 850°C and succeeded by a quench and temper process, and that the newly formed diffusion barrier allows the additional deposition of a zinc layer improving the good corrosion resistance.

It will be interesting to see how this work progresses.

5.2 PERMEATION EXPERIMENTS

5.2.1 Introduction

The theory behind the double-cell method of Devanathan and Stachurski is discussed in Chapter Two - Literature Survey (ρ^{35}) Applying Bockris's equation for calculating the breakthrough time.

$$t_b = \frac{L^2}{15.3D}$$

where D, the diffusion coefficient, was taken to be 2.5 x 10^{-7} cm^2s^{-1}, to AISI 4340 steel of thickness 2 mm gave a breakthrough time of 10,500 seconds, i.e. nearly 3 hours. Quite clearly this time was unsatisfactory for the experiments concerning this steel to take place under laboratory conditions using Devanathan and Stachurski's double cell technique. Bearing in mind that the main interest was the hydrogen being absorbed during the plating process, it was decided that a thin steel shim should be used as a substrate for plating.

The micro-structure of the shim is shown in Figure 3.3.ρ^{45} The larger grain size and the thinness of the membrane (57 μm) meant that the calculated breakthrough time would be less than 9 seconds if the value of D had been similar to that taken above. It would also be a good base for depositing nickel plate and measuring the hydrogen absorbed during, and after, deposition. Since much of the work involved comparison of rates, then it was not necessary that the value of D (the diffusion coefficient) should be known precisely.

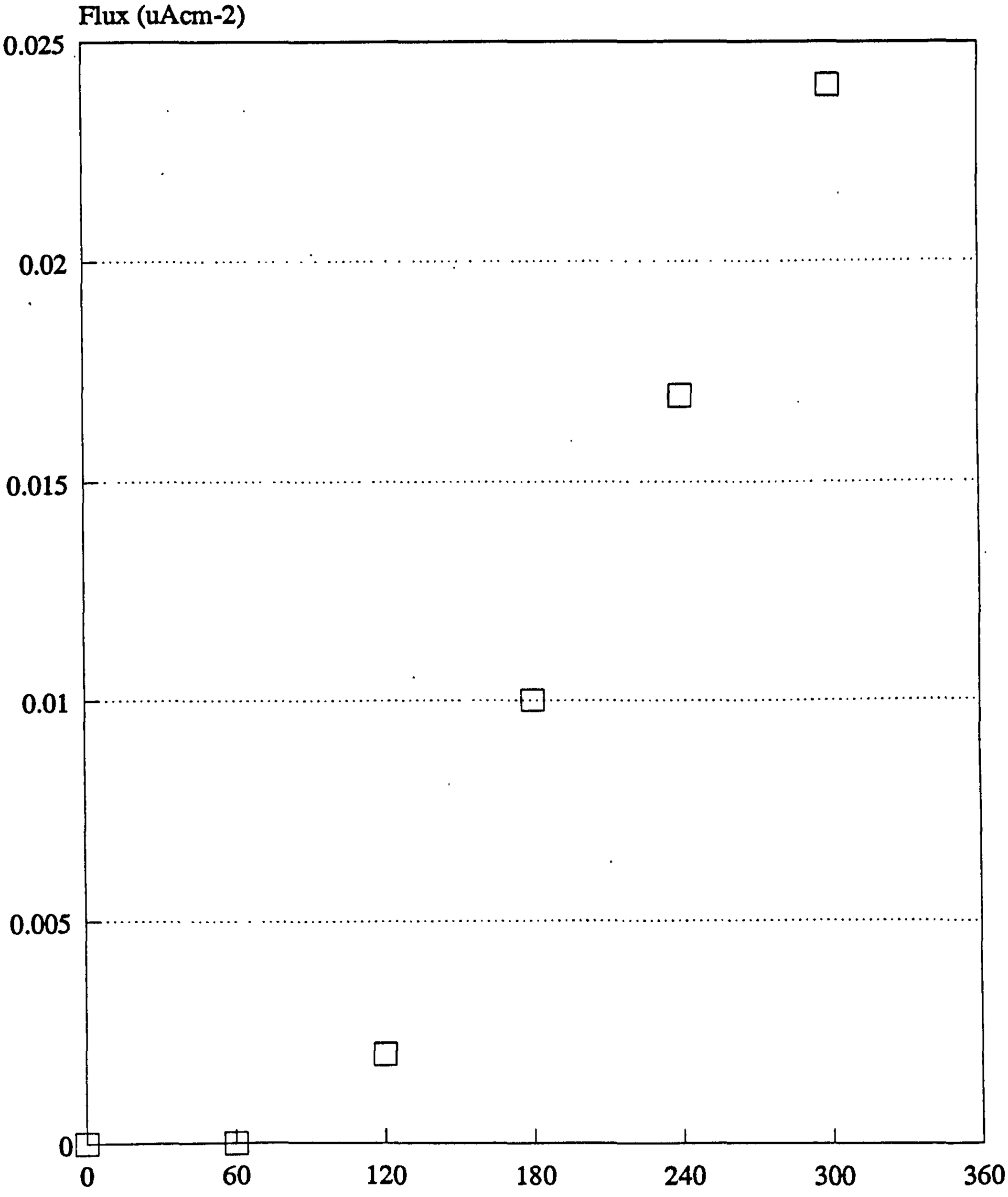

FIG 5.3 Estimation of Breakthrough Time (t)

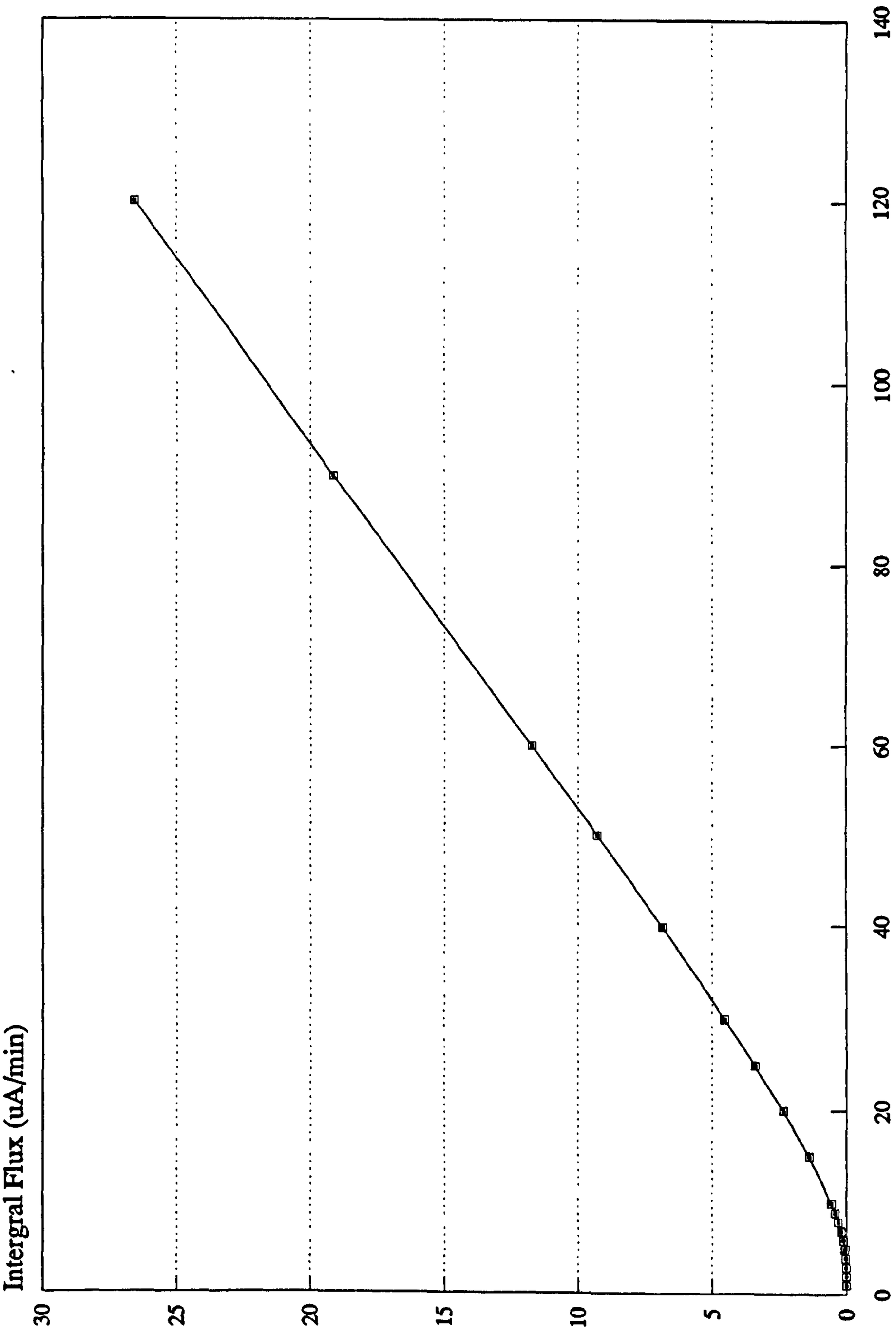
Integral Flux versus Time Plot to show Time-lag Characteristics
Intergral Flux (uA/min)
Time (mins)
0
5
10
15
20
25
30
0
20
40
60
80
100
120
140

FIG. 5.4

5.2.1.1 Calculation of the Diffusion Coefficient for the Steel Foil

Having assumed D to be 2.5 x 10^{-7} cm^2s^{-1} and expecting a breakthrough time of about 9 seconds, it was noted that the breakthrough time ranged from 30 to 225 seconds. In Figure 5.3 it can be seen that by plotting the initial rapid rise in flux over the first ten minutes, when the transient resembles a straight line, and extrapolating back, it was possible to estimate the breakthrough time with some degree of accuracy. Over 24 measurements of this type yielded a mean breakthrough time of 104 seconds with a standard deviation of 52 seconds. Using t_b = 104 seconds in the formula given in the section above (5.2.1), D was calculated to be 2.04 x 10^{-8} cm^2s^{-1}.

A similar method can also be used by plotting the cumulative hydrogen concentration over the whole plating time. Taking data obtained when plating at 5 $mAcm^{-2}$ the cumulative area under the flux/time curve was calculated. For the curve shown in Figure 5.4, the time-lag was shown to be 265 seconds, and using the formula for diffusion under potentiostatic control given in Devanathan and Stachurski (1962),

$$t = L^2/6D$$

the diffusion coefficient is shown to be 2.04 x $10^{-8}cm^2sec^{-1}$.
Over repeated measurements performed in the laboratory at Cranfield, the value of D obtained (2.08 x $10^{-8}cm^2sec^{-1}$) was sufficiently close to that obtained by the first method, and it was decided to use the value of 2 x $10^{-8}cm^2sec^{-1}$ in relevant calculations.

5.2.2 Effect of Plating at Different Current Densities

The recommended range of plating current densities is 5 - 20 $mAcm^{-2}$. Standards recommend that there should be an initial "flash-plating" at the high current density and then the current should be reduced to give a more even plating. Experimental results indicate that this would ensure a fast protective layer being in position to deter ingress of the higher concentration of hydrogen evolved at the lower current density. For all experiments, the plating was done at a constant rate for a constant period of time (2 hours).

The most even coatings were obtained at rates of 5 $mAcm^{-2}$ and 10 $mAcm^{-2}$ and Figure 5.5 shows the effect of plating quality on hydrogen absorption. Transients for poor and uneven coating continue to rise but the effect was negligible when plating at 5 and 10 $mAcm^{-2}$. When plate was deposited at 20 $mAcm^{-2}$, two effects were observed:

1. uneven plating and
ii pitting

These effects were even more evident when plating at 30 and 40 $mAcm^{-2}$. It was clear that the uneven plating was caused by the tensile forces acting on the shim as the plate was rapidly deposited on bubble-free areas of shim. Indeed, once specimens were removed from the double-cell the shim was quite crumpled despite being smooth at the beginning of the experiment.

It was wondered if the pitting was caused by small bubbles of hydrogen being trapped on the surface of the steel, preventing protective plate being deposited. In fact, at 40 $mAcm^{-2}$ the pitting was so severe that the permeation transient continued to rise rather than settle to a plateau similar to those observed for specimens plated at lower rates. (See Figure 5.6).

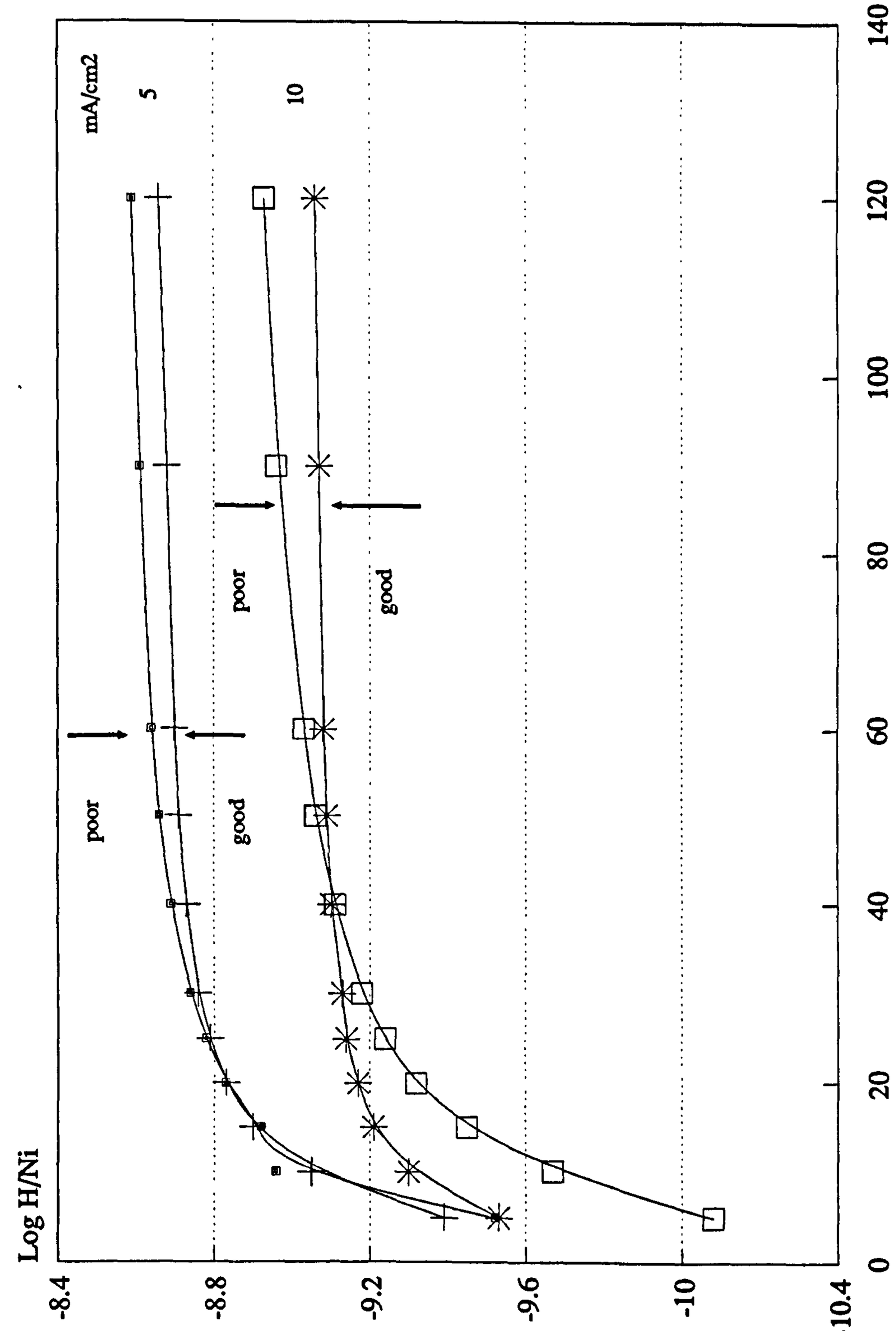

FIG 5.5 Graphs Showing the Effect of Plating Quality on Hydrogen Absorption During Electro-deposition of Nickel.

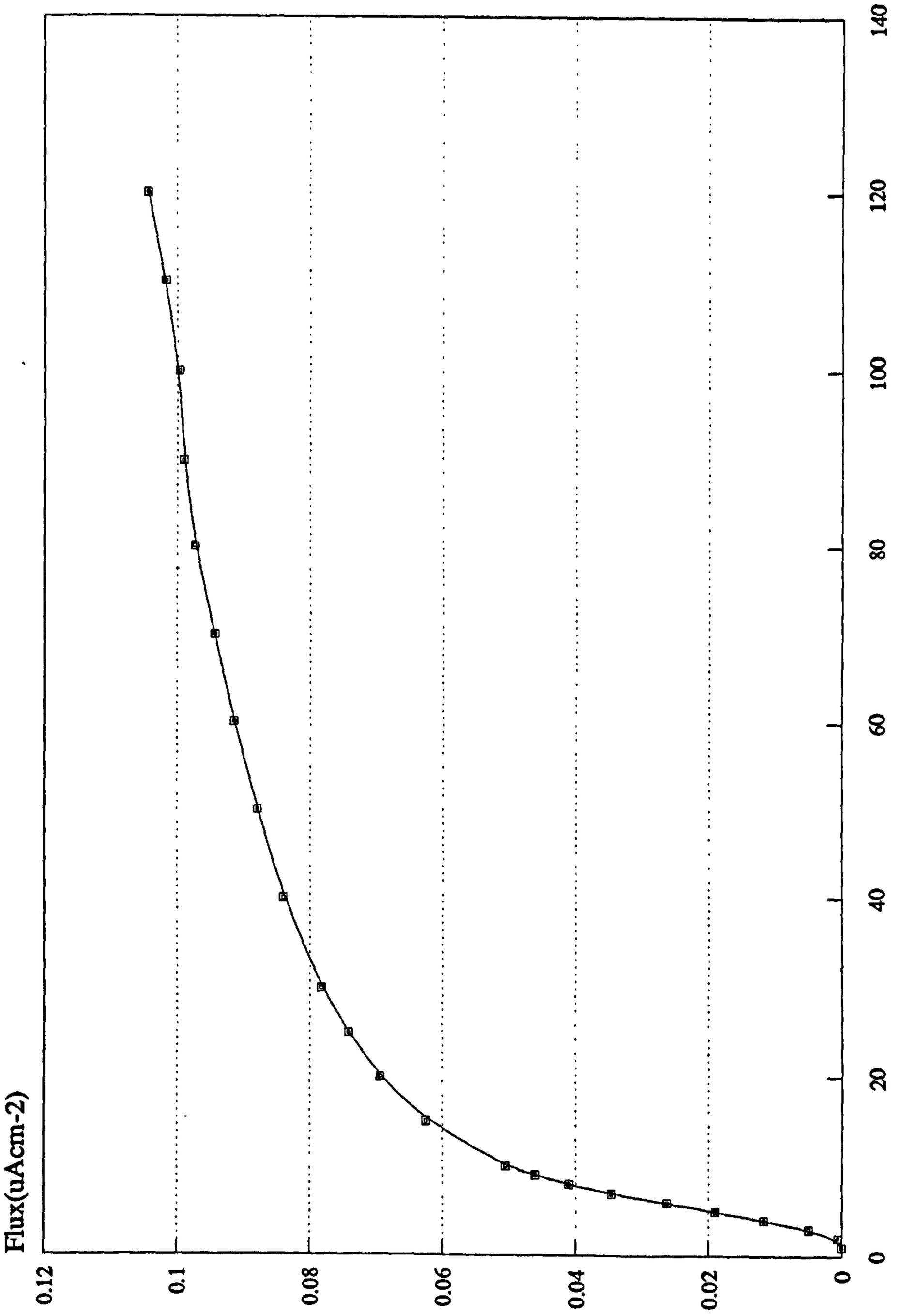
Permeation Transient Obtained when Plating at 40 mA/cm2
Flux(uAcm-2)
0.12
0.1
0.08
0.06
0.04
0.02
0
Time(mins)
0
20
40
60
80
100
120
140

FIG. 5.6

Experiments were repeated effectively, using a small motorised stirrer to discourage formation, and encourage dispersion, of the bubbles. However, the flux increased, possibly due to there being no polarising concentration of hydrogen in solution at the surface of the metal. As can be seen in Figures 4.10 and 4.11, stirred solutions and unstirred solutions plated at rates of 5 and 10 $mAcm^{-2}$ gave similar profiles, but the stirred solutions indicated a higher flux of hydrogen. Stirring seemed to have no effect on the formation of pits when higher plating rates were used, and no explanation is yet offered.

"Out-of-range" high current densities were no longer investigated and at the other extreme it had also been noted that at the low plating current density of 2 $mAcm^{-2}$, the plate was so thin that it did not form a coating of sufficient thickness to protect the steel from the hydrogen being evolved at the interface of the plate and the plating solution. Consequently, it was decided to concentrate on plate deposited at 5 or 10 $mAcm^{-2}$.

5.2.3 Hydrogen Absorption During Plating

As can be seen in Figure 4.7, hydrogen flux permeating the steel during electro-plating with nickel rose rapidly at first and then settled to a plateau value after about 30 minutes, suggesting that the hydrogen concentration was then uniform throughout the plate. As it is generally considered that the plateau would be reached after about 30 x t_b, this appears to be consistent. More hydrogen is permeated whilst plating at 5 $mAcm^{-2}$ than at 10 $mAcm^{-2}$. However, even after plating has ceased, hydrogen continues to diffuse through the steel (Figures 4.8, 4.9) It is suggested that any delay in post-plating heat treatment to disperse the hydrogen from the nickel plate would result in even higher concentrations of hydrogen accumulating in the

steel. Indeed, when testing the effect of post-plating baking (see Chapter Four - Results 4.2.1.4) the indications were that the treatment does remove some hydrogen from the plate as the transient was much lower (Figure 4.12).

Quite obviously, the nickel is being deposited at a faster rate with a higher current density, and so it would be easier to compare the effect if the same mass of plate is being considered in each case. Figure 5.7 shows the transients obtained when the mass of hydrogen permeating the foil per unit mass of nickel being deposited is plotted against time. The mass of hydrogen was calculated from the area beneath each flux curve whilst the mass of nickel deposited per second was obtained from weight gain measurements.

The Defence Standard generally accepts that the lower the plating current density, the greater the hydrogen permeation during plating, and this is confirmed by the H/Ni values shown in Figure 5.7. The benefit of "flash-plating" at a high current density is also evident from this figure.

5.2.4 "Reservoir" Effect

Surface hydrogen concentration, C_0, is obtained from the equation

$$J_\infty = \frac{C_0 . F . D}{L}$$

where J_α is the equilibrium flux of hydrogen
F is Faraday's constant
D is the apparent diffusion coefficient of hydrogen in steel
and L is the thickness of the permeating membrane.

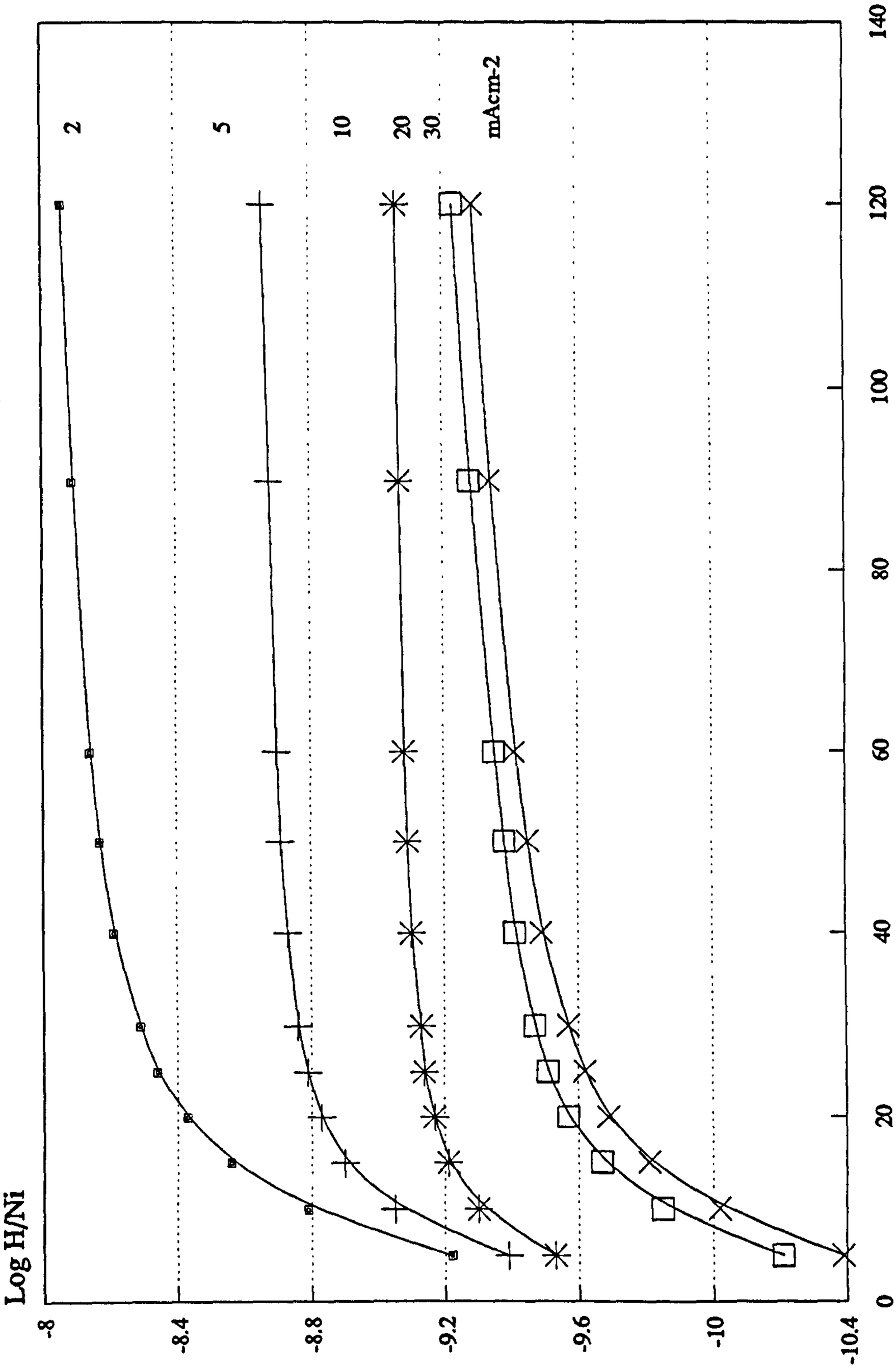

FIG. 5.7 Graphs Showing the Influence of Current Density on Hydrogen Permeation during Electroplating of Nickel

For plated steel, there are several possible concentration gradients, and these are expressed in diagrammatic form below. (Figure 5.8). In each case, C_0 is the initial surface hydrogen concentration and the line joining C_0 to 0 is the concentration gradient.

Figure 5.8 Possible Concentration Gradients for Nickel Plated Steel

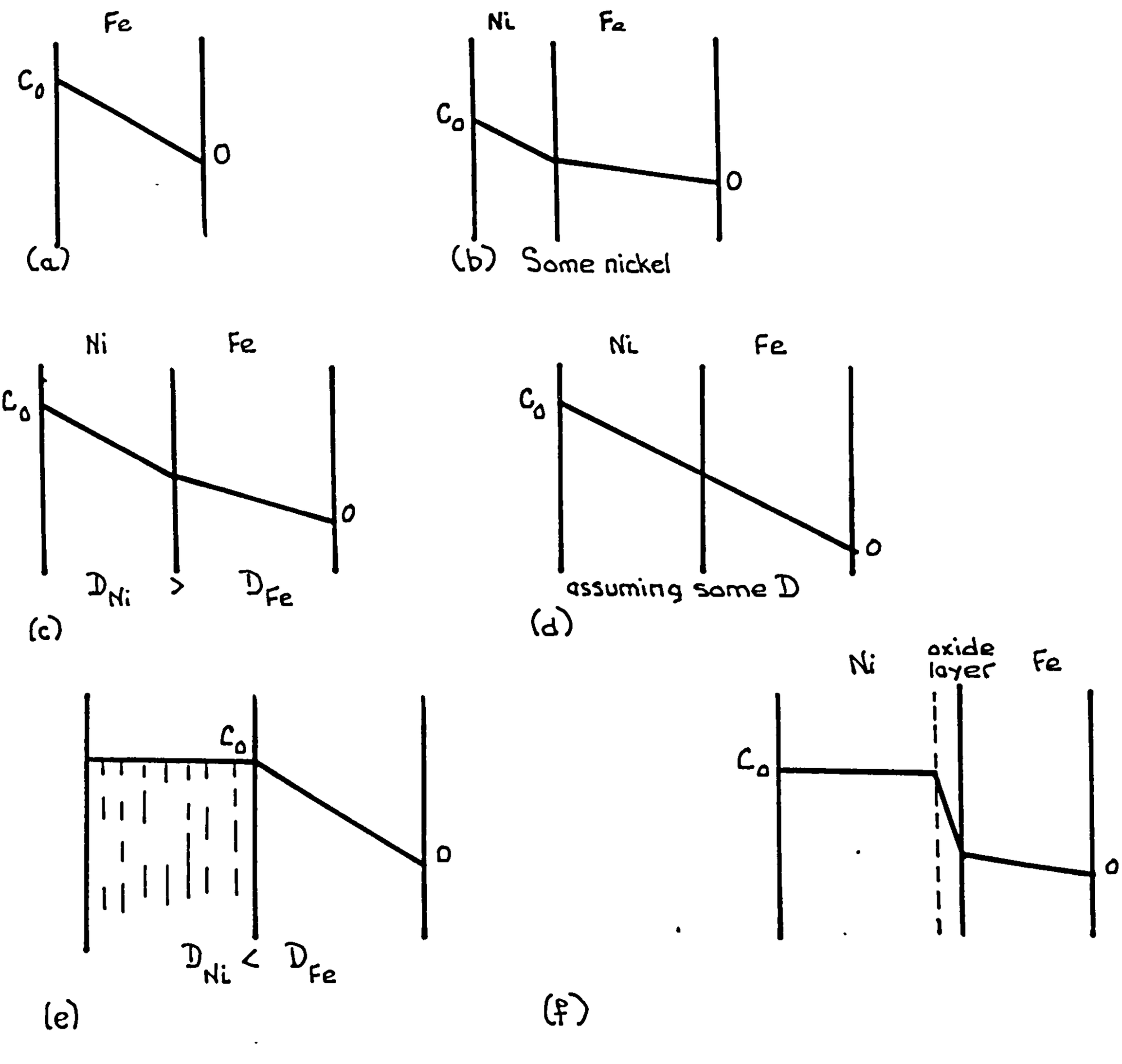

As J_{Fe} must equal J_{Ni}, the concentration gradients would depend upon the individual diffusion coefficients for the two metals.

$$i.e.\ \frac{(C_0 - C_1)FD_{Ni}}{L} = \frac{(C_0 - C_1)FD_{Fe}}{L}$$

Figures 5.9 and 5.10 consider calculations based on two extreme cases, that shown in Figure 5.8 (b and c) and that shown in (e). Should the highest hydrogen concentration occur at the nickel/solution interface, then the diffusion distance, L, would increase as the thickness of the plate increases and the permeation transients would continue to rise, as shown in Figure 5.9. However, should the hydrogen remain at a constant level in the nickel, causing L to remain constant at the thickness of the steel, then the theoretical transients shown in Figure 5.10 will occur.

Referring to the permeation transients shown in Figures 4.7 and 4.9, all transients shown reached plateaux, implying that C_0 eventually reached constant values. Comparing these figures with Figures 5.9 and 5.10, it would appear that situation (e) is more likely to occur and that there is a uniform hydrogen concentration in the nickel, or expressed another way, the nickel seems to act as a reservoir providing a constant concentration of hydrogen available to diffuse into the steel.

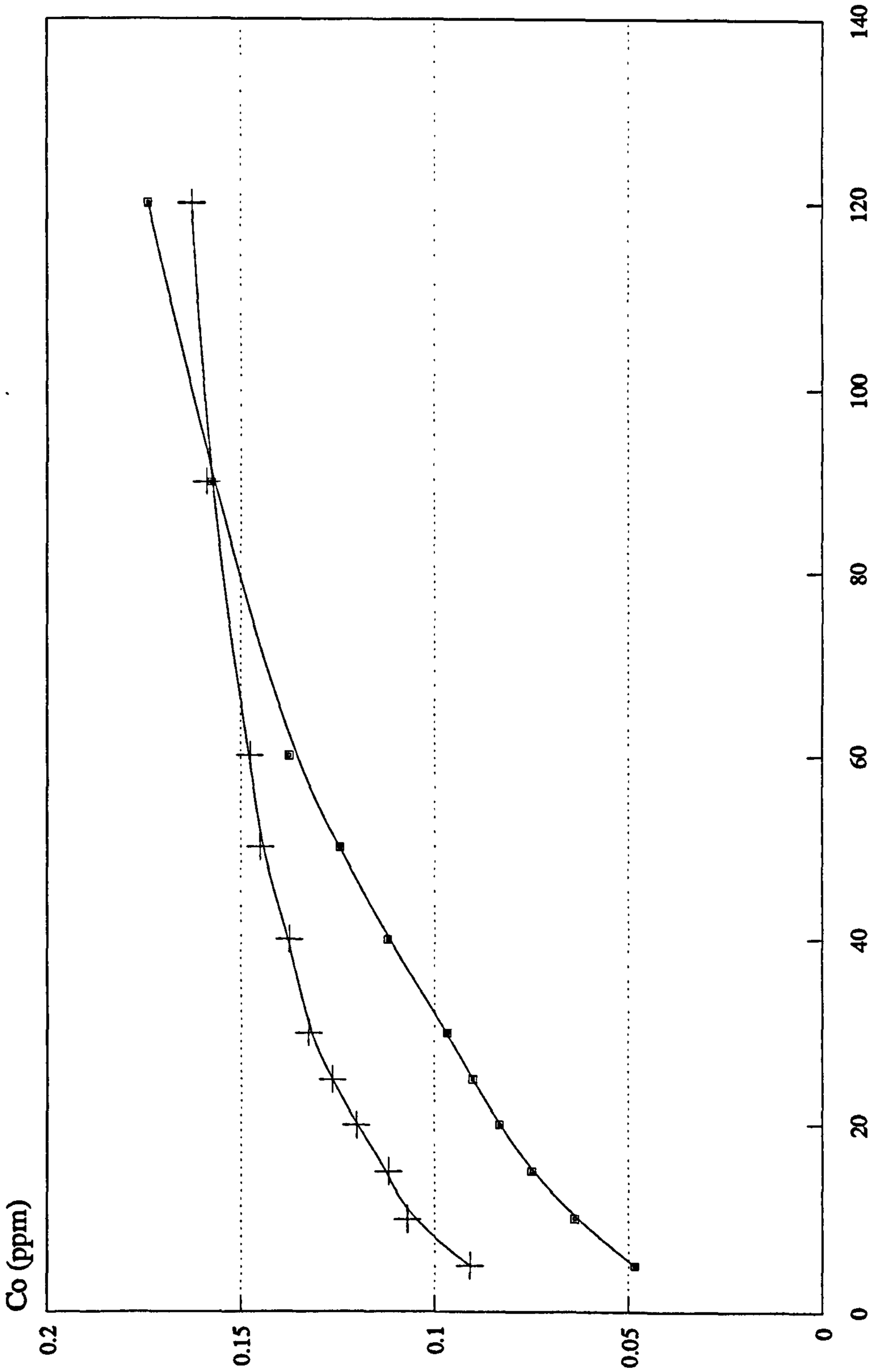

FIG. 5.9 Co v Time for Varying L

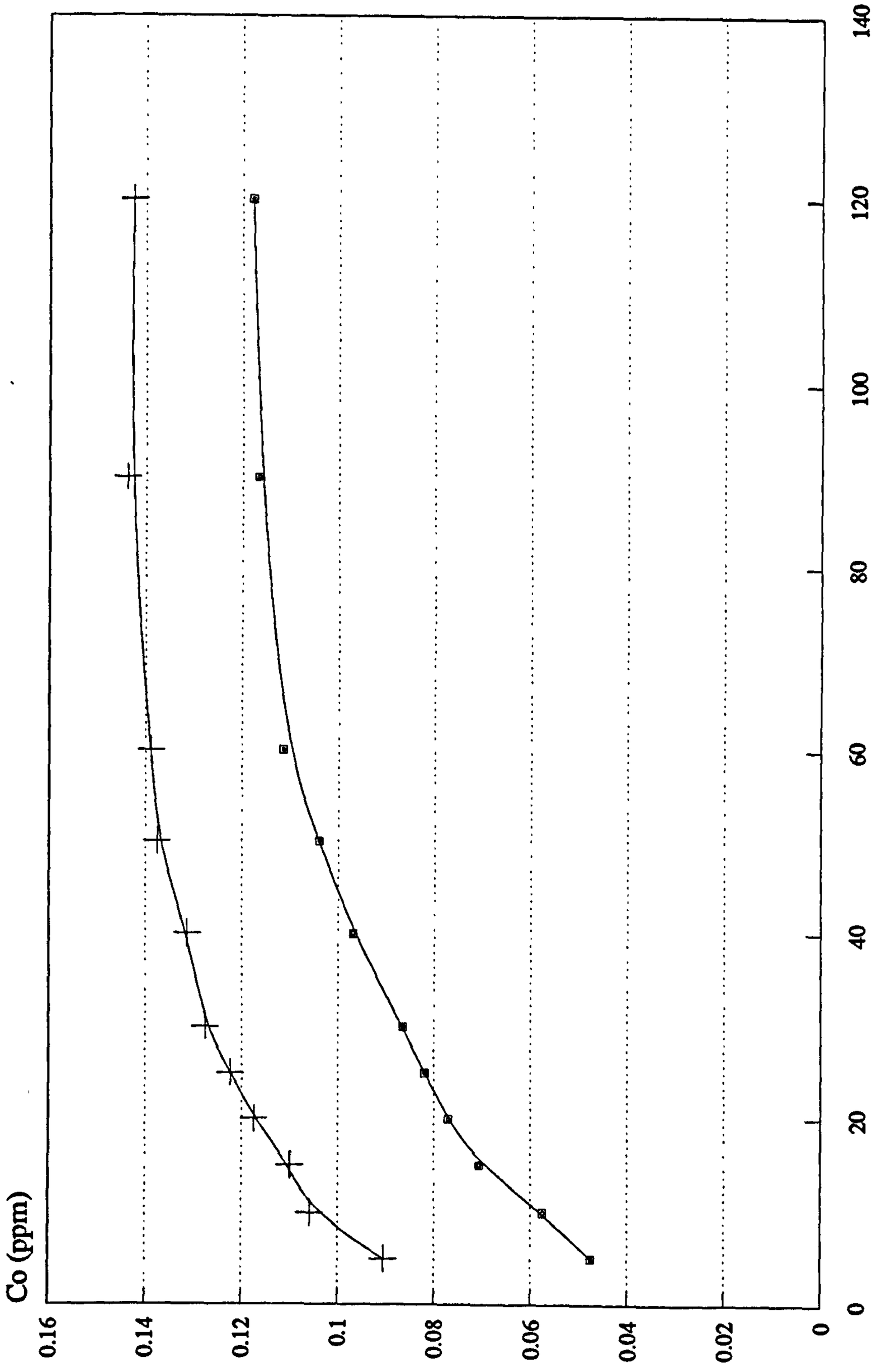
Co v Time for Constant L
10 mAcm-2
5 mAcm-2
Co (ppm)
Time (Mins)
0
0.02
0.04
0.06
0.08
0.1
0.12
0.14
0.16
20
40
60
80
100
120
140

FIG. 5.10

5.2.5 Calculations of C_0

The C_0 value for each plating current density was obtained using Bockris's (1977) equation

$$J_\infty = \frac{FD(C_0 - C_1)}{L}$$

and these values are shown in Table 5.4.

TABLE 5.4. C_0 Values for Nickel Plating and Cathodic Charging

	Current Density ($mAcm^{-2}$)	C_0 (ppm)
Nickel Plating	2	13.0×10^{-3}
	5	6.5×10^{-3}
	10	5.9×10^{-3}
	20	10.1×10^{-3}
	30	12.6×10^{-3}
Cathodic Charging	150	1.1

From the table, it can be seen that during nickel plating, the highest hydrogen concentration occurs at 2 $mAcm^{-2}$ and 30 $mAcm^{-2}$. It is thought that the high values for 20 and 30 $mAcm^{-2}$ are probably due to the influence of defects within the plating. However, it is known that plating within the recommended range results in improved plating efficiency followed by less hydrogen absorption (see Figure 5.5) p144

It is also clear from the table that nickel plating affords protection from hydrogen ingress as the unprotected

steel, cathodically charged at 150 $mAcm^{-2}$, permeates two orders of magnitude more hydrogen.

At first, the puzzling factor appears to be the low hydrogen concentration compared to that obtained by Townsend. He showed that the concentration of hydrogen in the nickel plate was considerably higher than that in the steel substrate, and gave figures of 270 ppm and 1.3 ppm respectively. However, Townsend used high temperature vacuum extraction to analyse the hydrogen content and this method would detect the total hydrogen present, including that trapped innocuously in irreversible traps, whereas the technique used for this thesis would detect only mobile hydrogen. It will be seen during the discussion on probe measurements, that substrate values are not too dissimilar to those obtained by Townsend, and it is this evidence that suggests example (f) is the most likely with a higher hydrogen concentration in the nickel.

This is not at odds with the conclusions reached in Section 5.2.4 since the profiles shown in Figures 5.8e and 5.8f are similar, and it would be unrealistic to deny the presence of an oxide layer between the two metals.

5.3 GEL-FILLED HYDROGEN PROBE MEASUREMENTS

5.3.1 Introduction

In the previous section on permeation, the transients obtained showed the amount of hydrogen generated at the surface of, and available for entry into, the specimen, whereas in this section, the transients obtained should give the concentration of the actual diffusible hydrogen present in the material.

The theory behind the Barnacle Cell technique variation, using a gel-filled probe, has been discussed in Chapter Two. For AISI 4340 steel which has a diffusion coefficient of 2.5 x $10^{-7}cm^2s^{-1}$ the permeation current equation shown below will hold true when using the simplified first term solution to the diffusion equation.

For a sample of thickness L = 2mm.

$$t\ max = L^2 / 4D$$
$$= 4 \times 10^{-2}/(4 \times 2.5 \times 10^{-7})$$
$$= 4 \times 10^4 \text{ seconds}$$

All experimental probe measurements were made over periods of not more than 15 minutes (900 seconds) and, as stated in Chapters Three and Four, four main heat treatments were used, not only to assess the hydrogen content of electroplated specimens but also to compare the efficacy of post-plating de-embrittlement baking.

Using the equation $J_t = FC_0\ (D/\pi t)^{\frac{1}{2}}$ and by plotting log J_t against log t, the graph should have a gradient of -½. Theoretical decay transients can be seen on the graphs which show experimental results (Figures 4.14 to 4.30) and these results, in general, lie parallel to the theoretical transients.

In most cases, the permeation current took some time to settle down. This compares with the results obtained by Bockris in 1977 (see Figure 5.11), where he showed that, using the double-cell method of Devanathan and Stachurski, for various charging rates the current density - time transients separate after about five minutes. Although the techniques involving the probe and the double-cell differ in some respects, it is likely that a similar time-lag occurs. Consequently, it was decided that the hydrogen concentrations should be assessed from the flux value recorded at ten minutes.

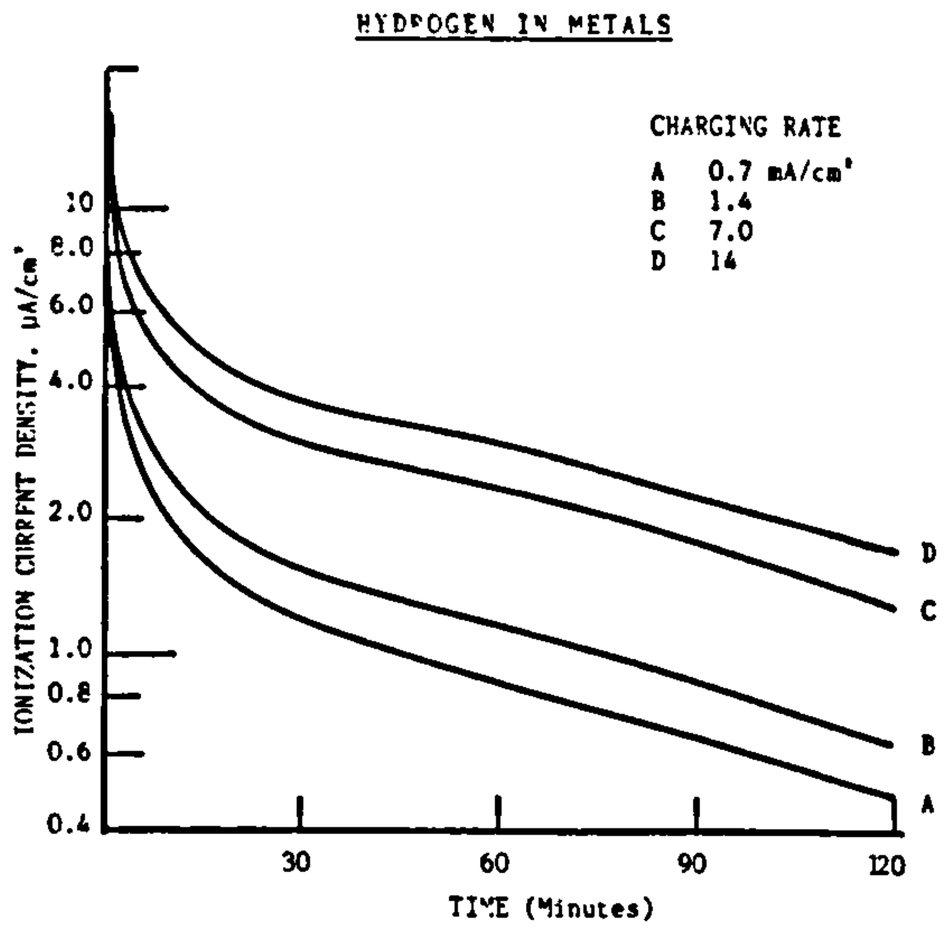

FIG. 5.11 Extraction Transients for AISI 4340 Steel in 0.2M NaOH after Charging at Different Rates.

5.3.2. Effects Caused by Nickel Plating on "Tensile" Specimens

5.3.2.1 Post-exposure Effects

pp 98 →

Figures 4.14 to 4.20 compare tempered (T), tempered and plated (TP), plated and baked 2 hours (TPB2) and tempered, plated and baked 20 hours (TPB20), and it is evident that nickel plating increases the level of hydrogen by as much as an order of magnitude but still does not

approach that achieved whilst cathodically charging with a cathodic poison, Sn, at 150 $mAcm^{-2}$. These values can be seen in Table 4.7. However, it was clear that the hydrogen values gradually increased over a period of days, the initially low values being due to the effects of the quenching. It was considered that exposure to the atmosphere caused some corrosion to occur and that hydrogen absorption consequently increased until an equilibrium was reached.

Two other possible explanations were considered. The first was that when atmospheric corrosion occurred, an oxide layer would be formed which, in turn, would react with the sodium hydroxide gel in the probe, and this reaction would increase the current, causing the gradient to alter due to the current sustained by the reaction. This increase could be misinterpreted as an increase in hydrogen. However, as mentioned in Chapter Three - Methods, each specimen was carefully abraded before any measurements were made and so this suggestion could be dismissed.

The second explanation needs to be carefully considered. It concerns the possibility of a hydrogen concentration gradient existing near the surface immediately after plating. Due to the higher concentration of hydrogen at the surface, this would be very rapidly depleted by the probe and give a low measurement. Equilibrium would occur after several days and a higher, more stable value would be attained. Calculations by Devanathan and Stachurski and by Crank suggest that about 11 hours would need to elapse before the hydrogen would be uniformly distributed in 2 mm thick specimens. Since the probe measurements assume that the hydrogen concentration profile is uniform then it is possible that the initial measurements are of dubious

accuracy. This seems highly pertinent until the same argument is used for the quenched, tempered but unplated specimen. This specimen also gave initially lower hydrogen measurements and yet there is no reason for there to be anything other than a uniform concentration gradient from the beginning. Since the amount of hydrogen removed over a period of 600 seconds of the probe measurement is small to that removed during the previous treatment, the only explanation for the unplated specimen is that given originally - atmospheric corrosion occurring, leading to eventual equilibrium.

5.3.2.2 Reproducibility of Results

Bearing in mind that the gel-filled probe is a new variation of an established technique, it is essential that reproducibility of results is established. When pairs of specimens subjected to identical treatments (Chapter 4.2.2.2.1) were measured, it was clear that agreement was good. However, for tempered and plated specimens which were not subjected to de-embrittling baking (Figure 4.21), the 10 day hydrogen concentration was lower than that for the 5 day value. It is thought that this is due to the loss of hydrogen to the atmosphere outweighing the ingress of hydrogen due to corrosion. This trend was reversed for the baked specimens (TPB2 and TPB20) where it is to be expected that outgassing had already occurred to some extent due to the de-embrittling treatment.

However, when determinations were made on different specimens, there was considerable scatter in the results (see 5.3.3), and it was thought that this was due to the measure of variability in each of the steps, and with many steps the results would show increased scatter. For this reason, repeated measurements were made on the same specimens.

5.3.2.3 Comparison of Specimens Baked for 2 and 20 hours

Figures 4.23, 4.24 and 4.25 indicated that there was very little difference between baking treatments. It had been observed that at times it was difficult to measure effectively specimens that had been baked for 20 hours but it is possible that a greater depth of oxide layer would be obtained after 20 hours as compared with 2 hours and consequently it is likely that abrasion did not always efficiently remove all of this layer, thus making it more difficult to obtain stable measurements. However, after

five days hydrogen concentrations are so similar that it seems unnecessary to bake for longer than 2 hours and, indeed, Table 4.7 (p115) indicates that the 2 hour bake is more beneficial.

5.3.2.4 Frequency of Measurements

It is clear from results obtained in Chapter 4.2.2.2.3 (p112) that there was no significant difference between daily measurements over 5 days and a once-only series after 5 days. It is not necessary for frequent measurements to be made since it is clear that the probe measurements do not adversely affect the hydrogen concentration in the sample.

5.3.3 Effects of Plating using "Sheet" Specimens

All tests carried out so far concerned only the hydrogen present in the nickel plate. Careful study was made of the work by Townsend who compared the hydrogen concentrations in the plate and the underlying substrate. He, too, found the effect shown in the permeation studies that the nickel acts as a reservoir of mobile hydrogen and that this hydrogen continues to diffuse into the steel substrate.

It was considered in this work that the most consistent results would be obtained by using single 6 cm x 3 cm specimens of the 2 mm thick sheet steel on which five or more replicate measurements could be performed without the need to prepare individual test pieces. This also made it easier to remove the nickel plate by abrasion.

Results shown in Table 4.10 (p119) show that initially, the nickel plate has a much higher concentration of hydrogen (18.41 ppm) than the underlying steel (1.26 ppm) but after seven days, the concentrations had fallen to 6.58 ppm and

0.95 ppm respectively.

These values are treated statistically to give the t-values shown in Table 4.11. Comparing the concentrations initially for the nickel plate (A) and the substrate (C), the critical t value which must be exceeded for the two groups to be considered significantly different is 2.16 at the 95% level and 2.65 at the 99% level and as the calculated value is 13.97, the difference between the two concentrations is highly significant. This agrees with work published by Townsend. After seven days the hydrogen content measured in the nickel (B) and the steel (D) were lower at 6.58 ppm and 0.95 ppm respectively. The decrease in the nickel was highly significant ($t_{0.95} > 2.15$) and probably represented the loss of hydrogen to the atmosphere, since if there had been diffusion from the nickel into the steel, the concentration within the substrate would have increased rather than been observed to decrease. However, the t value for initial and seven day quantities of measured hydrogen within the substrate is 2.67, very close to the 99% critical value of 2.65, although greater than the 95% value of 2.15. This indicates that the measured values could possibly be from the same population and that the slight drop is due to the redistribution of hydrogen to deeper layers within the steel over seven days.

Cathodically charged specimens, as expected, gave much higher hydrogen values which were significantly reduced by baking. The figures given in Tables 4.8 and 4.9 were (p117) those obtained for measurements made on sheet specimens. Those obtained on replicate specimens were similar. Initially, the hydrogen concentration obtained from cathodic charging (A) was 3.2 ppm and this was significantly reduced by baking for either 2 hours (B) or 20 hours (C); the concentrations measured at 1.19 ppm in

both cases. The critical $t_{0.05}$ value is 1.81 and comparing A-B and A-C, the calculated t values were 2.44 and 2.15 respectively, confirming the reduction by baking as significant. The differing values are due to the different standard deviations obtained.

After five days, the hydrogen concentrations had all reduced; cathodic charging (D) 2.5 ppm, cathodic charging followed by baking for 2 hours (E) 1.6 ppm and cathodic charging followed by baking for 20 hours (F) 1.3 ppm. However, these reductions were small compared to the effects of baking and in each case except one (D-F), the lower values were not significant. Whilst baking for 2 hours and for 20 hours were efficient in reducing hydrogen concentration, there seemed to be little difference in effectiveness between the two baking times.

5.3.3.1 Reproducibility of Results

As with tensile specimens, measurements on the sheet specimens varied. On individual specimens repeated measurements were consistent but between each set there is a statistical variation. It is considered that a combination of factors will determine this variation i.e. the basic nature of the steel, the heat-treatment, pre-plating preparation and the plating process itself. When t-testing, several measurements should be made and the mean value used when comparing the results with those of other specimens.

5.3.4 Methods of Storage

Some concern had been expressed as to the effects on hydrogen concentration caused by different methods of storage. Five specimens were prepared by heat-treating

and tempering at 200°C for 2 hours; two of the five specimens were then plated at 5 $mAcm^{-2}$ and baked for two hours again at 200°C. All five were measured for hydrogen content and then kept under differing conditions for five days. Hydrogen contents were then measured again. The results are shown in Tables 4.12 to 4.15. pp 121-5

Specimens A, B and C gave initial results which were very similar, as was to be expected from all having received identical heat treatment. Specimens D and E were both nickel plated and also gave similar measurements. Results from all five are shown in Table 4.12 and Table 4.13. Specimens A and D were kept over a desiccant, specimen B was kept under vacuum and specimens C and E were left lying on the bench. Table 4.12 lists the measurements for all five specimens, whilst Table 4.15 compares the differences between the initial and five day results for each type of specimen. Table 4.14 compares the five day measurements with each other in the group. For instance, after five days there is a highly significant difference between A and B and between A and C whereas there is little difference between B and C. This seems rather odd as it would be expected that the two stored under moisture restricted conditions, A and B, would be expected to differ from that left on the bench (C) and exposed to the atmosphere in the laboratory. However, there was little difference in the five day measurements for the plated specimens (D and E) which were kept over a desiccant and on the bench respectively. It is also interesting to note that the values for B and C tend to approach each other after five days.

However, it is Table 4.15 which is the most significant since it compares initial and five day measurements for each separate specimen. For those unplated specimens the differences were not significant,

being well inside the 95% critical value for A and C and just inside for specimen B which was kept under vacuum, whereas, as to be expected, the hydrogen content of the plated specimens had decreased in a highly significant manner. Figure 4.28 displays the results in graphical form. (p122)

It would seem that the best method of storage is that used throughout the experimental work i.e. stored over a desiccant.

5.3.5. Conclusions

The probe can be considered to be a quick and easy way of measuring the concentration of diffusible hydrogen within a metal. It is this mobile hydrogen within the lattice which can cause embrittlement if it diffuses to areas of high triaxial stress.

Since the new design uses an electrolytic gel this results in less likelihood of leakage and/or bubbles and so it is possible to make in situ measurements which is a major advantage over the method used by Townsend. The high temperature extraction method used by Townsend measures the total hydrogen present including that irreversibly trapped at grain boundaries, carbide interfaces, etc. As only the mobile lattice hydrogen is likely to cause embrittlement it is useful to differentiate between mobile and total hydrogen content.

The best method of storage of laboratory specimens would appear to be over a desiccant.

It should be noted that the probe method gives reproducible results and these are repeatable on the same specimens but there is some variability between specimens.

Due to the nature of the material, the heat-treatment used, pre-plating preparation and the electro-plating technique itself, it is necessary to make several measurements and take the mean value but, despite this, the technique is rapid and easy to apply not only in the laboratory but also in the factory and in the field.

CHAPTER 5.4

MATHEMATICAL MODELLING

5.4.1. Introduction

This section attempts to relate results obtained for constant load testing and for diffusion experiments by simple mathematical modelling. Although it is based on the embrittlement of AISI 4340 steel resulting from nickel plating, it is clear that the method could be applied to other systems.

It is generally accepted that the concentration profiles for hydrogen of a fixed surface concentration, C_o, diffusing into a steel specimen of thickness, L, will resemble that shown in Figure 5.12.

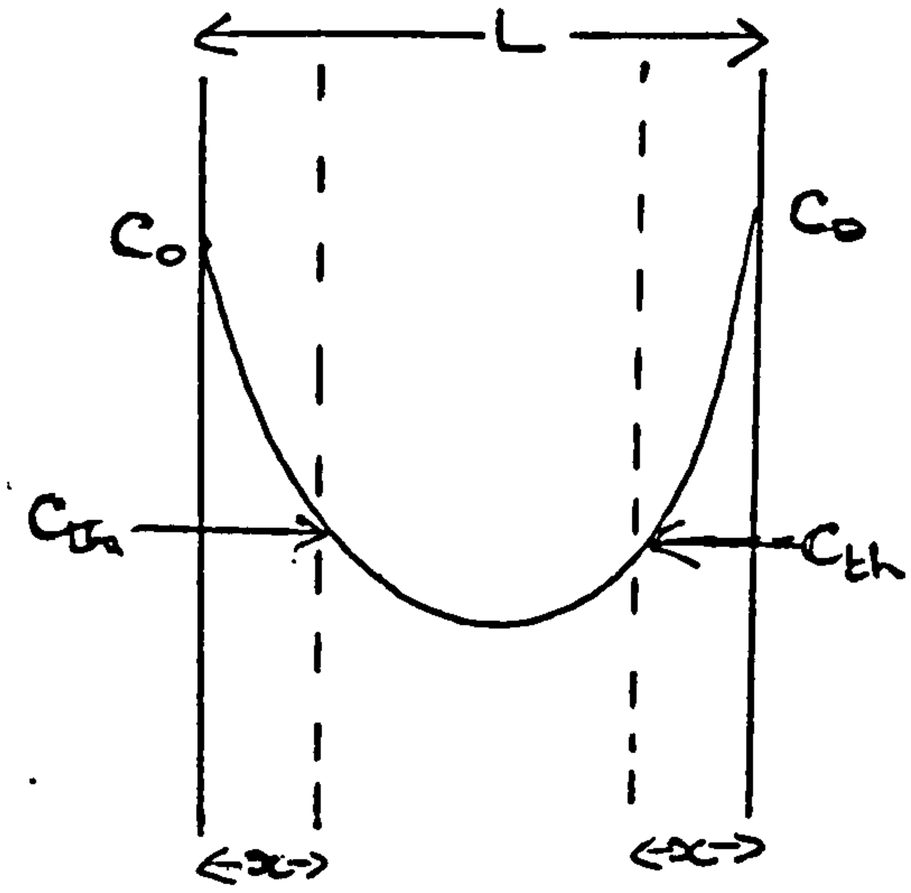

Figure 5.12. Hydrogen concentration profile

It is considered that hydrogen diffuses into the steel during exposure time, t, at a surface concentration, C_o. At a depth, x, the hydrogen reaches a threshold concentration, C_{th}.

5.4.1.1 Basic assumptions

It is assumed that:

(i) Hydrogen will diffuse into steel and, after a time, t, it will have reached a hydrogen concentration, C_{th}, at a depth, x, (as shown in Figure 5.12).

(ii) Any steel will contain defects which will act as internal stress raisers. These defects have a range of sizes and are randomly distributed throughout the specimen.

(iii) These defects will grow provided the stress intensity, K, at the defect exceeds a threshold value, K_{th}. At the same time, the local hydrogen concentration, [H], must also exceed a threshold concentration, C_{th}.

Referring to Figure 5.12, within the region bounded by the surface and depth, x, the hydrogen concentration exceeds the threshold concentration. If any defect is contained within this region then, provided $K > K_{iscc}$, the defect will grow.

(iv) Defects will grow in the brittle manner which is associated with hydrogen assisted cracking i.e. showing cleavage fracture.

(v) Final failure occurs in a ductile mode when the applied true stress, o, exceeds the fracture stress, o_f. This is characterised by microvoid coalescence, (MVC), and extreme ductility. As was observed with constant load testing, final failure occurred by this mode once the defect had propagated over 10% of the cross-section in specimens loaded to 90% o_f.

(vi) All defects grow perpendicular to the applied

stress.

The depth at which [H] exceeds C_{th} can be modelled with respect to time using Fick's second law of diffusion. Crank (Methods and Diffusion) used this law and applied the method of separating the variables to give the equation for these hydrogen concentration curves as:

$$C = C_0[1 - 4 \sum_{k=1}^{\infty} \frac{1}{(2k - 1)\pi} \sin \frac{(2K - 1)\pi x}{L} \exp \left(\frac{-(2k - 1)^2\pi^2 Dt}{L^2}\right.$$

(13)

EQUATION A

where the symbols represent the following:

C_0 surface concentration of hydrogen
k dummy variable
x Distance from the surface of the specimen
D diffusion coefficient for the specimen
t time
L thickness of the specimen,

Pressouyre and Bernstein (1979) found that, for long times, the equation could be re-written as

$$C = C_0 \left[1 - \frac{4}{\pi} \sin \frac{\pi x}{L} \exp \left(\frac{-\pi^2 Dt}{L^2}\right)\right]$$

EQUATION B

and initial calculations were made using this approximation. However, the experimental mean times to failure suggested it was necessary to use Equation A and sum the first fifty terms of each sequence.

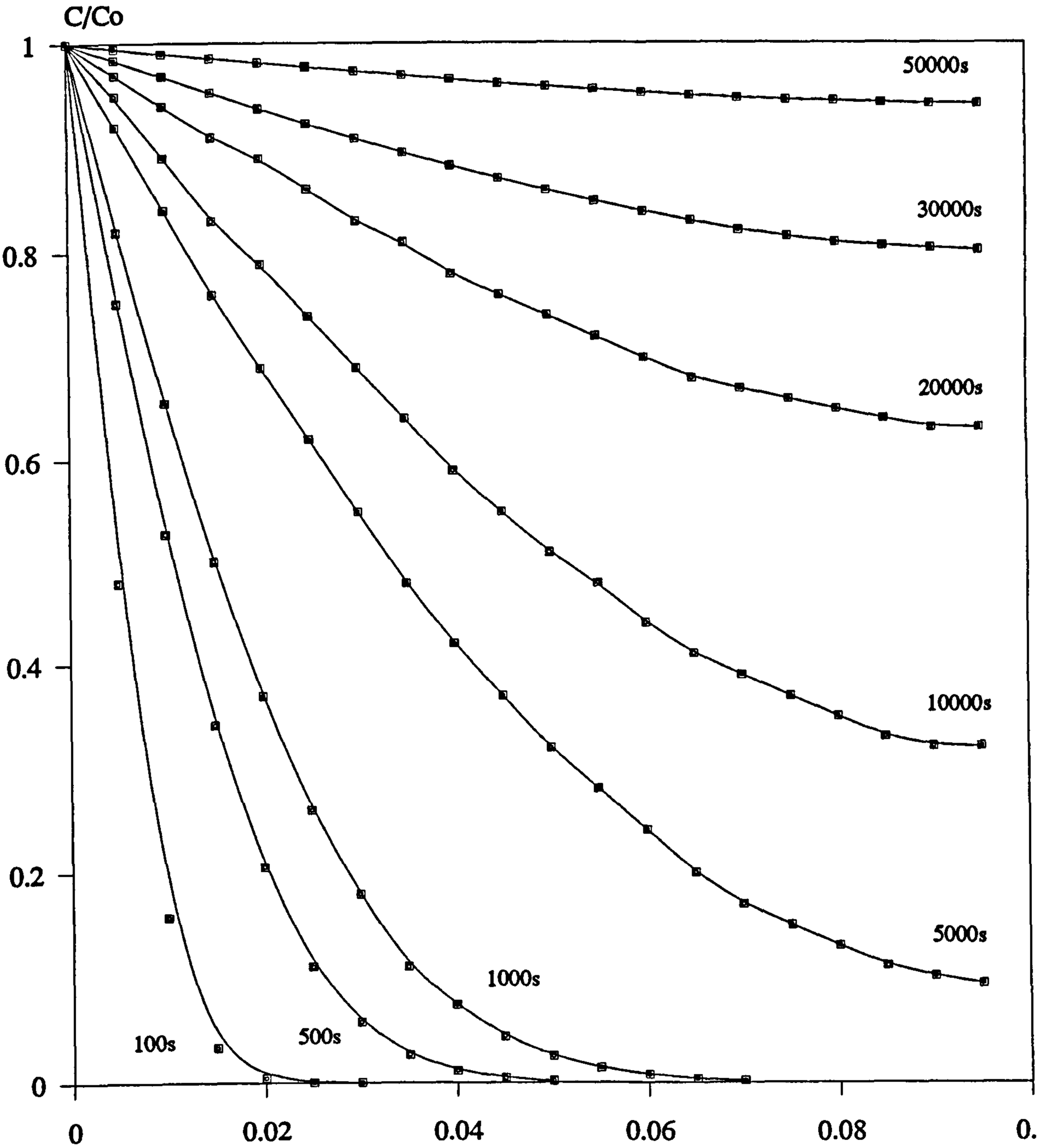

FIG. 5.12 Calculated hydrogen concentration profiles for a 0.2 cm thick specimen after a range of exposures times.

Using L = 0.2 cm and D = 2 x 10^{-8} cm^2s^{-1} C/C_0 was calculated for various lengths of exposure times and thus theoretical hydrogen concentration profiles were obtained. Figure 5.13 shows the profiles obtained for a range of exposure times. It can clearly be seen that over the range of experimental times to failure (345 - 695 seconds) virtually no hydrogen has penetrated deeper than 0.05 cm (less than 23% of the thickness of the specimen) and that, indeed, for a uniform profile, exposure times would need to exceed 50,000 seconds.

Despite this, the model can give predictions of times to initiate a failure that may result from a range of plating parameters. Figure 5.14 shows two conditions for hydrogen penetration by diffusion. Using the above equations A and B it is possible to calculate [H] at any depth, x. However, $K_{i.cc}$ depends upon C as shown in Yamakawa's Equation E on page 191.

The fact that brittle cleavage occurs means that the fracture mechanics Equation D on page 186 may be used to evaluate the following:

(i) The maximum size defect which should remain stable.

(ii) The minimum size defect which could initiate failure.

(iii) The theoretical size defect which is on the point of initiating failure.

The consequence of initiation is taken to be that the whole area with [H] exceeding C_{th} is regarded as potentially failed and the initial conditions are set up so that the remaining ligament is now just unstable from plastic overload.

Figure 5.14

a. Side diffusion

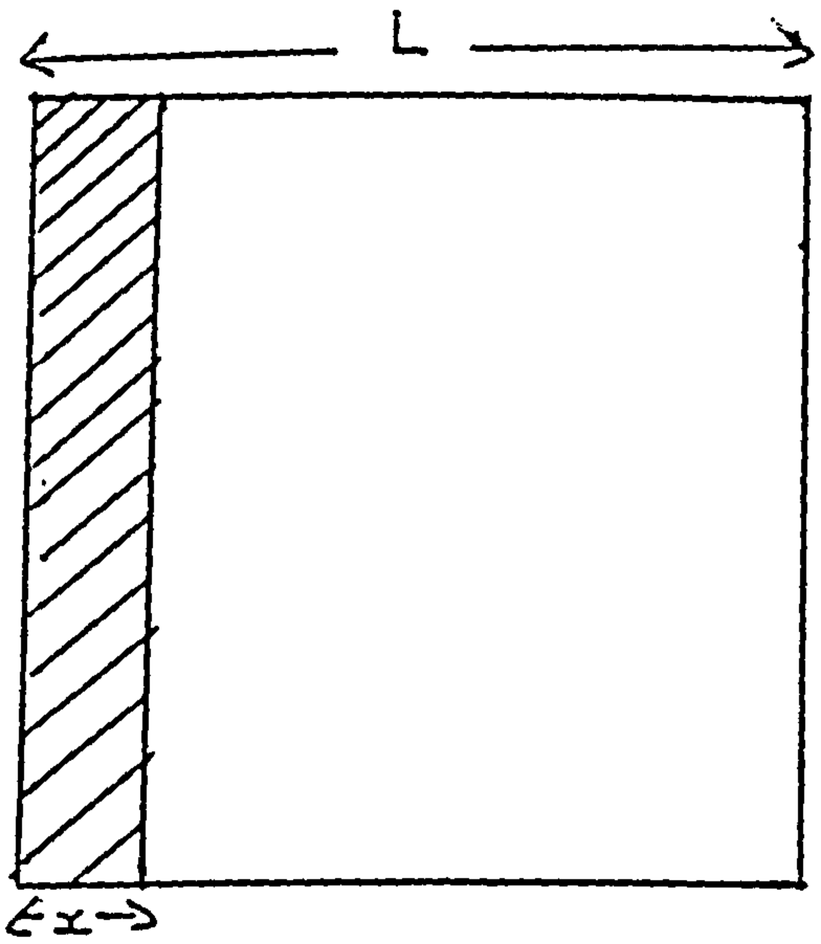

Hydrogen Enriched Zone

b. Peripheral diffusion

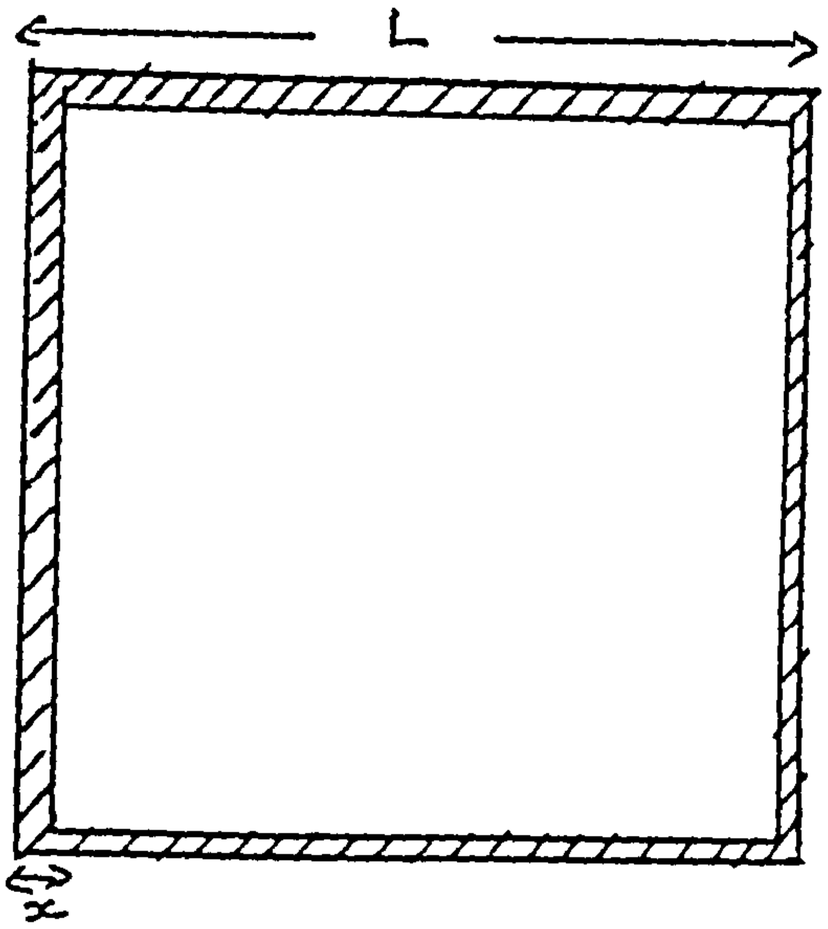

Figure 5.15

Growth of defect within hydrogen enriched zone.

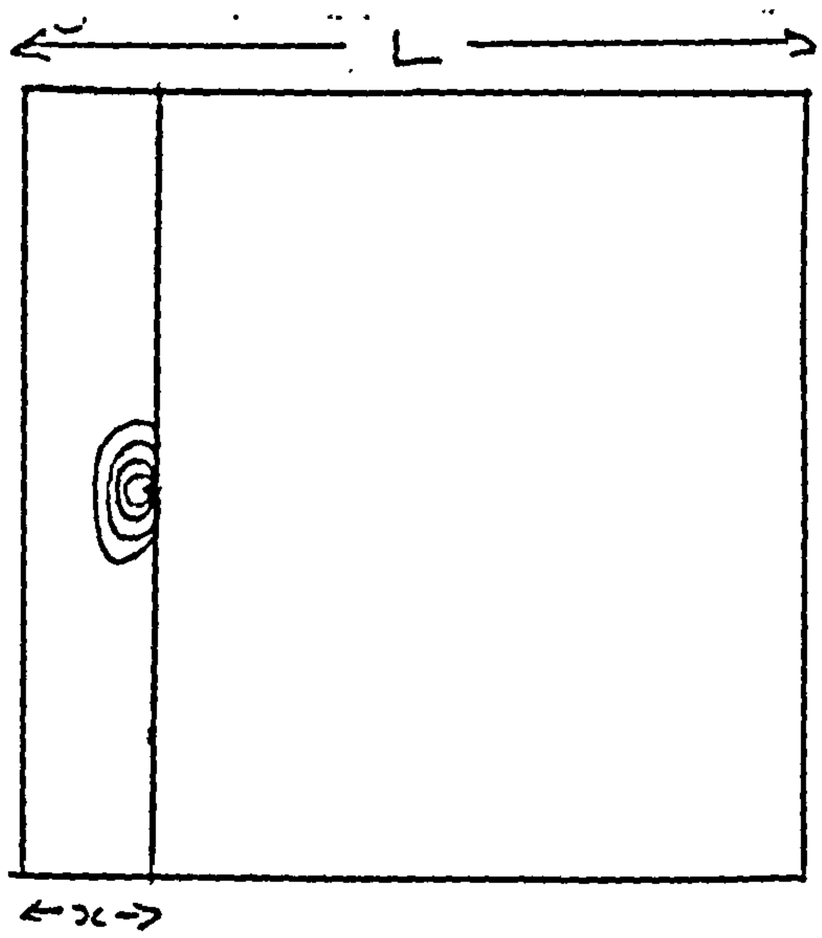

However, from SEM observations. it is quite obvious there is not a single initiation event. The model does not consider the consequences of initiation but, in practice, initiation and arrest do occur. Hence the model can consider a distribution of internal defects (of equivalent crack dimensions, a) sited randomly throughout the material.

The event is then linked to a critical defect, of size a, in stress chosen as 90% o_f at a depth where the hydrogen concentration is lower over 90% of the cross section.

The model was first used to consider the likelihood of failure initiated with point-sized surface defects growing in areas affected by peripheral or side diffusion as shown in Figure 5.14. Having found this was suitable, by fixing C_0 and t for values obtained when plating at 5 $mAcm^{-2}$, (from Tables 5.3 and 5.5), it was possible to consider whether or not plating time affected time to failure as well as the stress applied after plating.

Having assumed all failure was initiated by point size surface defects the model was then adapted to consider the effects of identical defects at various depths for various hydrogen concentrations. Then the effects of different size defects at constant depths of 0.01 cm and 0.02 cm were considered.

Figure 5.15 shows a defect at the limit of the hydrogen embrittled zone. A defect at this position is assumed to grow outwards into the zone of higher hydrogen concentration until again it occupies 10% of the cross-sectional area when final ductile overload will occur.

There were two equations connecting stress and hydrogen concentration and these were compared. Having

decided which equation was the most likely for AISI 4340 steel the effects of different stresses on various defects sizes were modelled.

5.4.2. Consideration of Peripheral and Side Cracks in Calculating C_{th}

In the first part of this chapter - Discussion of Results - C_0 values were calculated for each plating condition using the equation in Bockris

$$J = FD(C_0 - C)/L \qquad \text{EQUATION C}$$

and these values are reproduced below for ease of reference.

TABLE 5.5 C_o Values Obtained at Various Plating Current Densities

	Current Density (mA/cm^2)	C_o (ppm)
Ni Plating	2	13.00×10^{-3}
	5	6.50×10^{-3}
	10	5.88×10^{-3}
	20	10.10×10^{-3}
	30	12.60×10^{-3}
Cathodic Charging	150	1.1

When comparing the two extreme cases of peripheral and side diffusion first considered in Chapter Four the approximated equation B was used. For nickel plated quenched AISI 4340 steel plated at 5 $mAcm^{-2}$ stressed at 90% σ_f the mean failure time was 620 seconds (See Table 5.3 on page 134). The two extreme cases of critical defect sizes would be 0.02 cm in the case of side diffusion and 0.00513 cm in the case of peripheral diffusion.

Equation B was solved for a time of 620 seconds to give a C/C_o value at 0.02 cm from the surface and this gave a value of 0.256. However, from the permeation studies, the C_o value for nickel plating at a current density of 5 $mAcm^{-2}$ was shown to be 6.5×10^{-3} ppm (see above-Table 5.5). This means that if the C/C_o value is to be 0.256 at the critical defect size of 0.02 cm then C_{th} must be 0.256 C_o or 1.664×10^{-3} ppm.

Similarly it can be shown for the case of peripheral growth C/C_o will be 0.7708 and that C_{th} will be 5.01×10^{-3} ppm.

TABLE 5.6. Calculated Values of Mean Time to Failure for AISI 4340 Stressed at 90% σ, and Nickel Plated at a Range of Current Densities

(SIDE DIFFUSION)

Current Density ($mAcm^{-2}$)	Co (ppm)	C_{th}/Co	t (seconds)
2	13.0×10^{-3}	0.1278	345
5	6.5×10^{-3}	0.2560	620
10	5.88×10^{-3}	0.2830	695
20	10.1×10^{-3}	0.1640	413
30	12.6×10^{-3}	0.1317	352

TABLE 5.7. Calculated Values of Mean Time to Failure for AISI 4340 Stressed at 90% σ_f and Nickel Plated at a Range of Current Densities

(PERIPHERAL DIFFUSION)

Current Density ($mAcm^{-2}$)	Co (ppm)	C_{th}/Co	t (seconds)
2	13.0×10^{-3}	0.3855	70
5	6.5×10^{-3}	0.7710	620
10	5.88×10^{-3}	0.8522	1540
20	10.1×10^{-3}	0.4951	113
30	12.6×10^{-3}	0.3970	74

Assuming that C_{th} is a constant property of the steel and not related to the rate of plating then the value of C_{th} will apply for each of the current densities used. Taking values of C_0 given in Table 5.5 values of C/C_0 were calculated for each. Table 5.6 gives the values obtained assuming one extreme of side growth and Table 5.7 gives the values assuming the other extreme of peripheral growth. Each C/C_0 value was substituted in Equation B to give the expected mean failure times; these also are shown in Tables 5.6 and 5.7.

Figures 5.16 and 5.17 show the calculated hydrogen concentration for the two extreme conditions of side and peripheral diffusion.

The model so far seems to hold true and, subsequently, it was necessary to consider plating time, size of defects, depth of defects and how each parameter affects time to failure.

FIG. 5.16 Calculated Hydrogen Concentration Profiles giving the Threshold Concentration at a Depth of 0.02 cm.

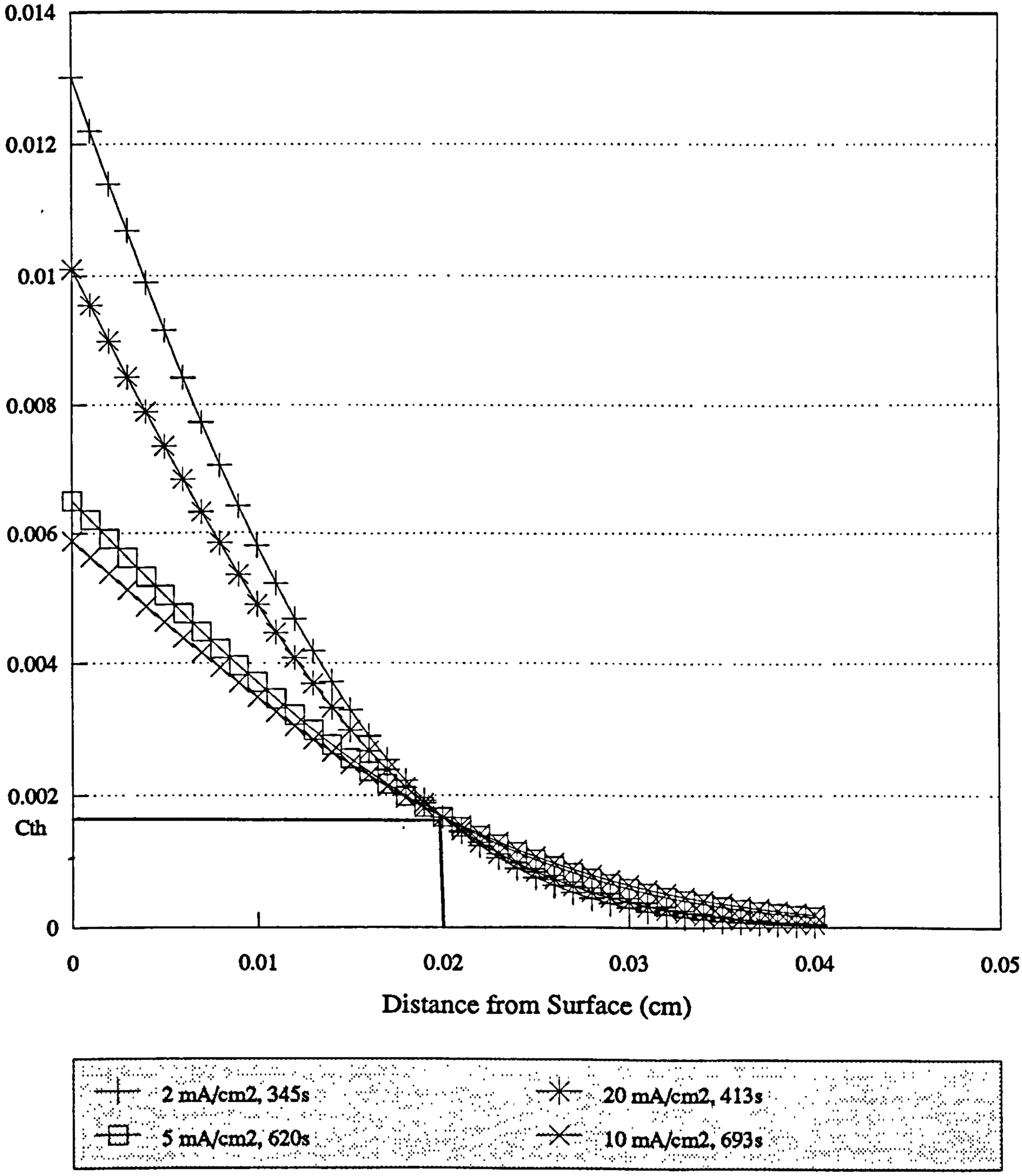

FIG. 5.17 Calculated Hydrogen Concentration Profiles giving the Threshold Concentration at 0.00513 cm. depth.

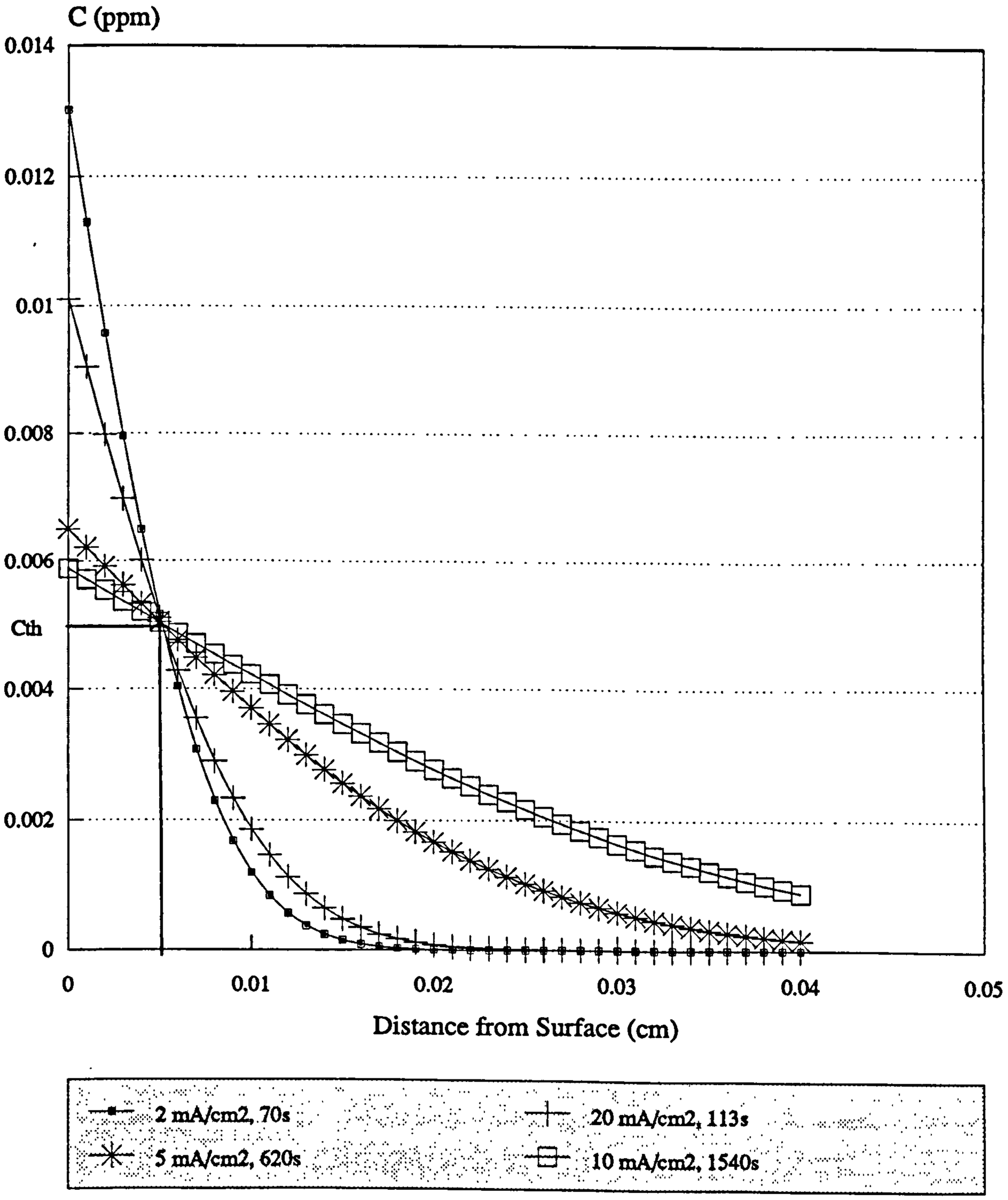

5.4.3 Effect of Plating Time

In Chapter Four comparisons were made regarding the hydrogen diffusion occurring during plating and after plating but under stress and it was evident that it was only while the specimen was under stress that hydrogen ingress was significant. The opinion that plating time was comparatively irrelevant is confirmed by calculating hydrogen concentration profiles for specimens nickel plated at 5 $mAcm^{-2}$ considering 2 hours plating time only and 2 hours plating time plus 620 seconds under stress. The results are shown in Figure 5.18 where it is evident that the hydrogen concentration per unit depth of specimen increases at a faster rate once the specimen is under stress.

When experimenting with 0.8%C steel, Robinson and Sharp found that it was likely that during the time under stress hydrogen diffused to microstructural defects until there was a sufficient concentration to initiate failure, but during unloading the hydrogen tended to diffuse to innocuous irreversible traps. On reloading the mobile atomic hydrogen once more diffused to defects. Should 0.4%C steel of the type AISI 4340 behave in a similar fashion then it is unlikely that diffusion during plating would help initiate failure and that only time under stress would significantly affect the liability for a crack to be initiated and grow until ultimately fracture occurs.

The modelling done so far would tend to support this proposal. Indeed, Figure 5.19 compares the two conditions when looking at the influence of defect depth on time to failure. This is discussed more fully in the next section, 5.4.4.

FIG 5.18 Calculated Hydrogen Concentration Profiles for Nickel Plating at 5mAcm-2.

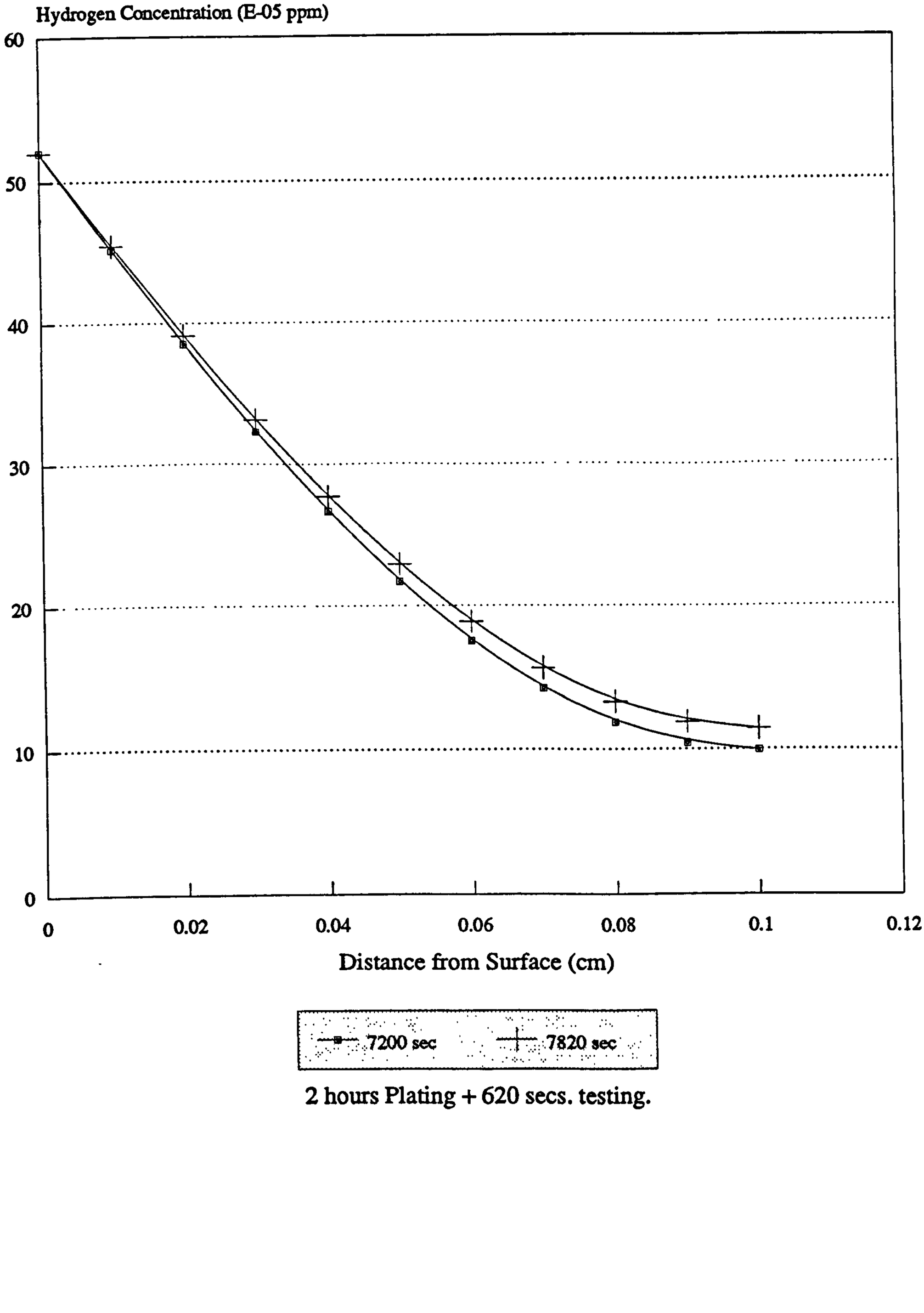

2 hours Plating + 620 secs. testing.

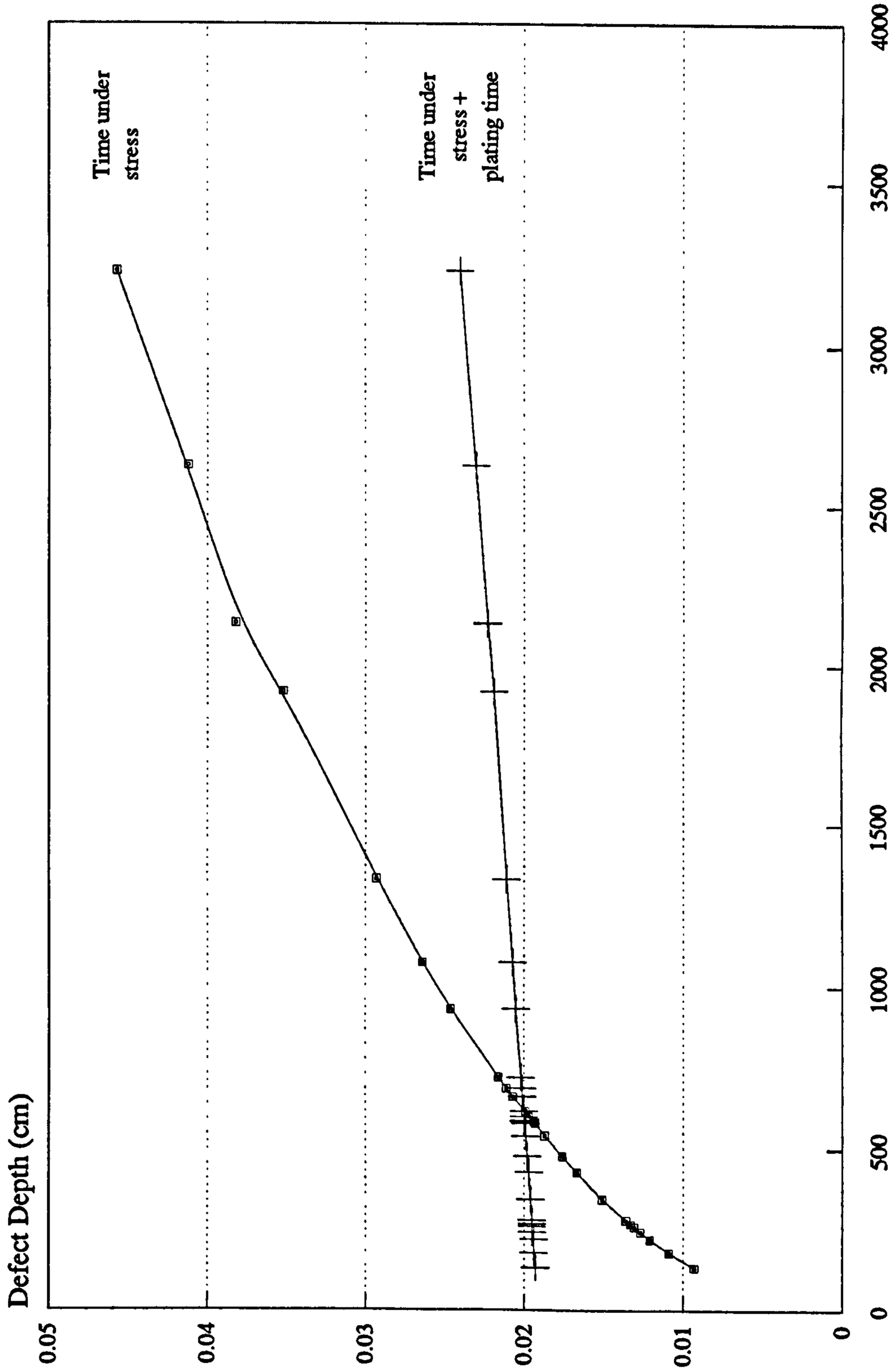

FIG. 5.19 Graph Showing how the Theoretical Timeo to Failure is Influenced by the Depth of the Critical Defect.

5.4.4 Effect of Depth of Microstructural Defects

So far the modelling has assumed that all cracks are initiated by point size defects at the surface only. It is obvious that, in any steel specimen, defects will vary in size and be scattered randomly throughout the specimen and that it is likely that crack initiation will occur more rapidly at a large sub-surface defect than at a very small surface defect, since the local stress intensity at the larger defect may well be greater than that of the surface defect despite the fact the concentration of hydrogen is greater at the surface.

The model now encompasses the effect of the depth of the microstructural defects which, for ease of calculation, are assumed to be of the same size. It is also assumed that once C_{th} is reached at any one of these defects, a crack will be initiated. From Chapter 5.4.2, C_{th} was calculated as 1.66×10^{-3} ppm for a side crack initiated in a specimen plated at 5 $mAcm^{-2}$ for two hours and then stressed at 90% σ_f. The mean time to failure was 620 seconds but, from embrittlement tests (Chapter 5.4.2), a range of failure times was obtained. For each failure time, it was calculated at which depth C_{th} would be reached.

This same set of calculations was repeated to include the 2 hours plating time added to each failure time and the results are shown in Figure 5.19. Again it would seem that time under stress is more significant. Indeed, only the first seventeen values of the time under stress ~~&~~ plus plating are shown since the other seven values extend well beyond the scale of the graph.

Having established that only time under stress need be considered, the calculations were repeated for each of the failure times obtained when the specimens were loaded after being plated at current densities of 2, 5, 10 and 20 $mAcm^{-2}$ The results can be seen depicted in Figure 5.20. With the same distribution of defects, specimens plated at 2 $mAcm^{-2}$ are likely to fail more rapidly than those plated in the recommended range of 5 - 20 $mAcm^{-2}$, but the best range would appear to be 5 - 10 $mAcm^{-2}$. This agrees with the practical recommendations (DEF Standard 03 - 01) that the optimum plating rate should be in the range 5 to 10 $mAcm^{-2}$.

5.4.5 Effect of Defect Size

As indicated in Chapter Two it is likely that the concentration of hydrogen necessary to initiate cracking will depend upon the stress which is exerted upon the material; consequently, the larger the stress intensifier or defect, the lower the effective concentration of hydrogen needed.

Figure 5.21 (reproduced from Lucas and Robinson, 1986) shows the influence of lattice hydrogen on K_{th} for 50D steel. Yamakawa et al (1984) compiled results obtained by Yoshizawa et al., Endo et al., and Salb et al. who all looked at the effects on high strength steels. This compilation is shown in Figure 5.22. Both sets of results confirm that the higher the stress intensity, the lower the concentration of hydrogen necessary to initiate cracks.

Earlier modelling in this chapter assumed the size of each defect was the same, thus there would be no variation in local stress intensity for each defect. This, in turn, allowed C_{th} to be calculated as a constant value of 1.33 x 10^{-4} ppm. The model now assumes a more logical range of defect sizes, all of which would have its own K_{iscc}.

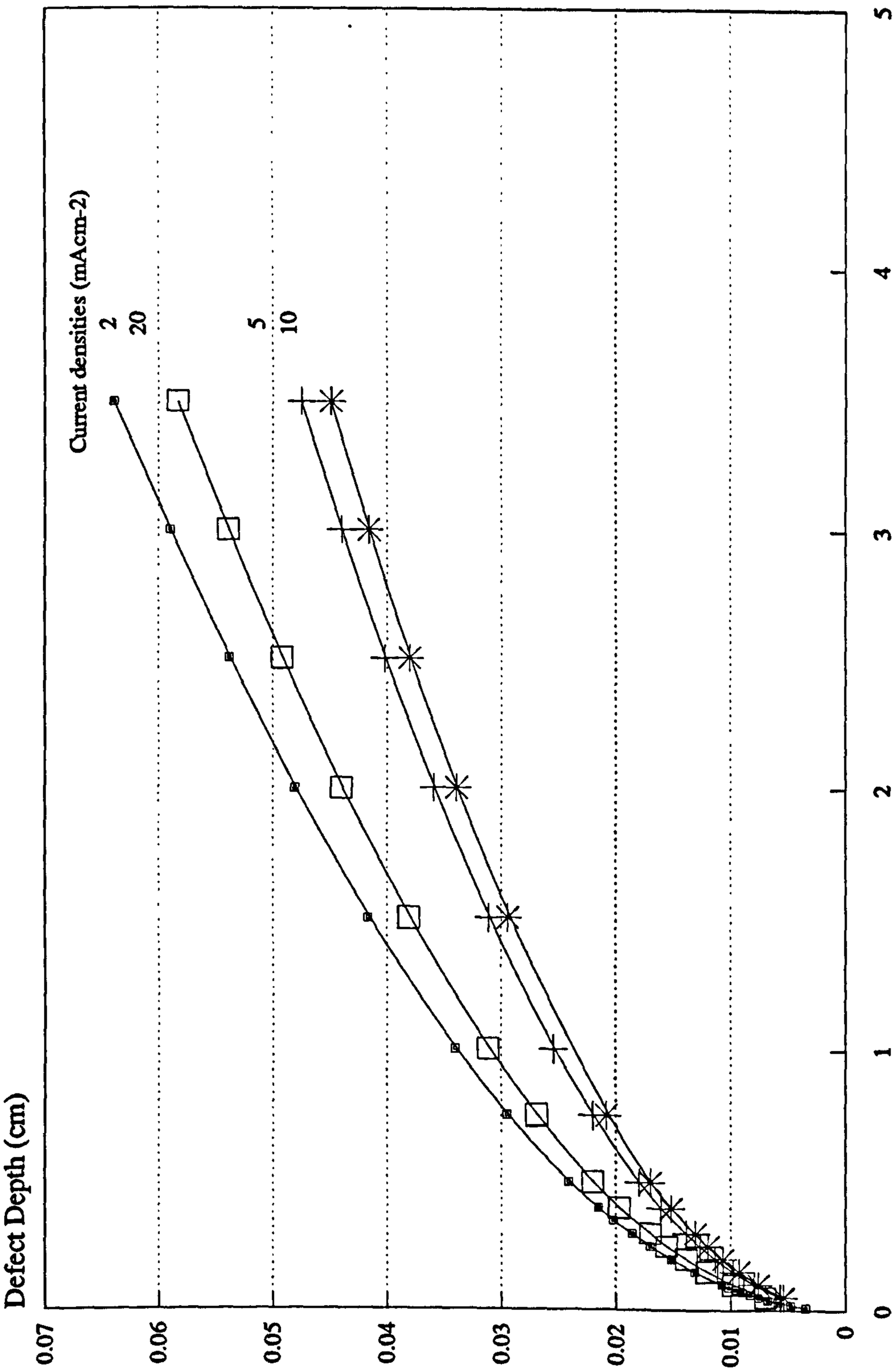

Graph Showing Theoretical Times to Failure for each Critical Depth in Specimens Plated at Various Rates.

FIG. 5.20

FIGURE 5.21 Influence of Lattice Hydrogen on K_{th} for 50D Steel

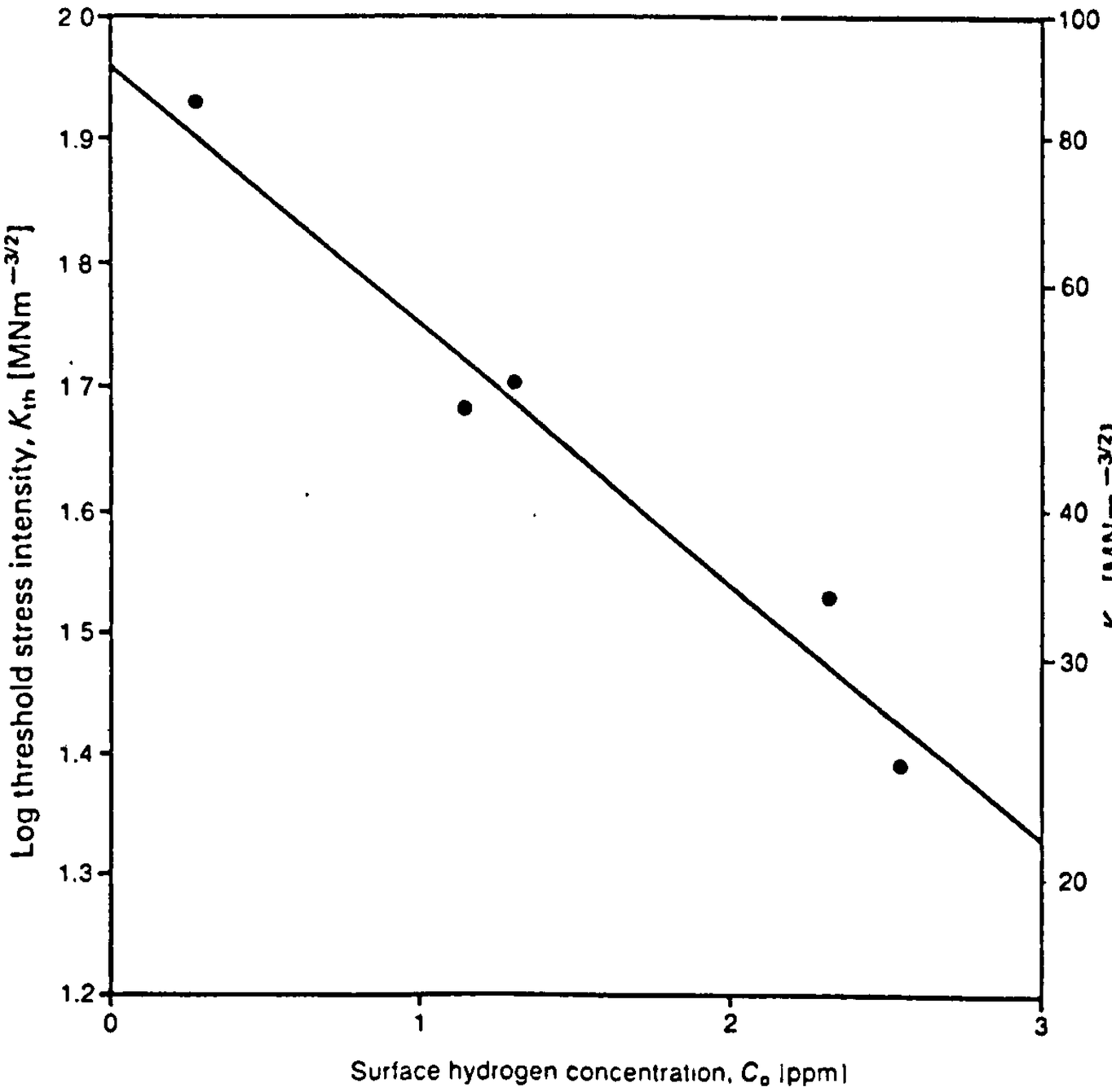

FIGURE 5.22 Relationship between K_{Iscc} of High Strength Steel and Hydrogen Content

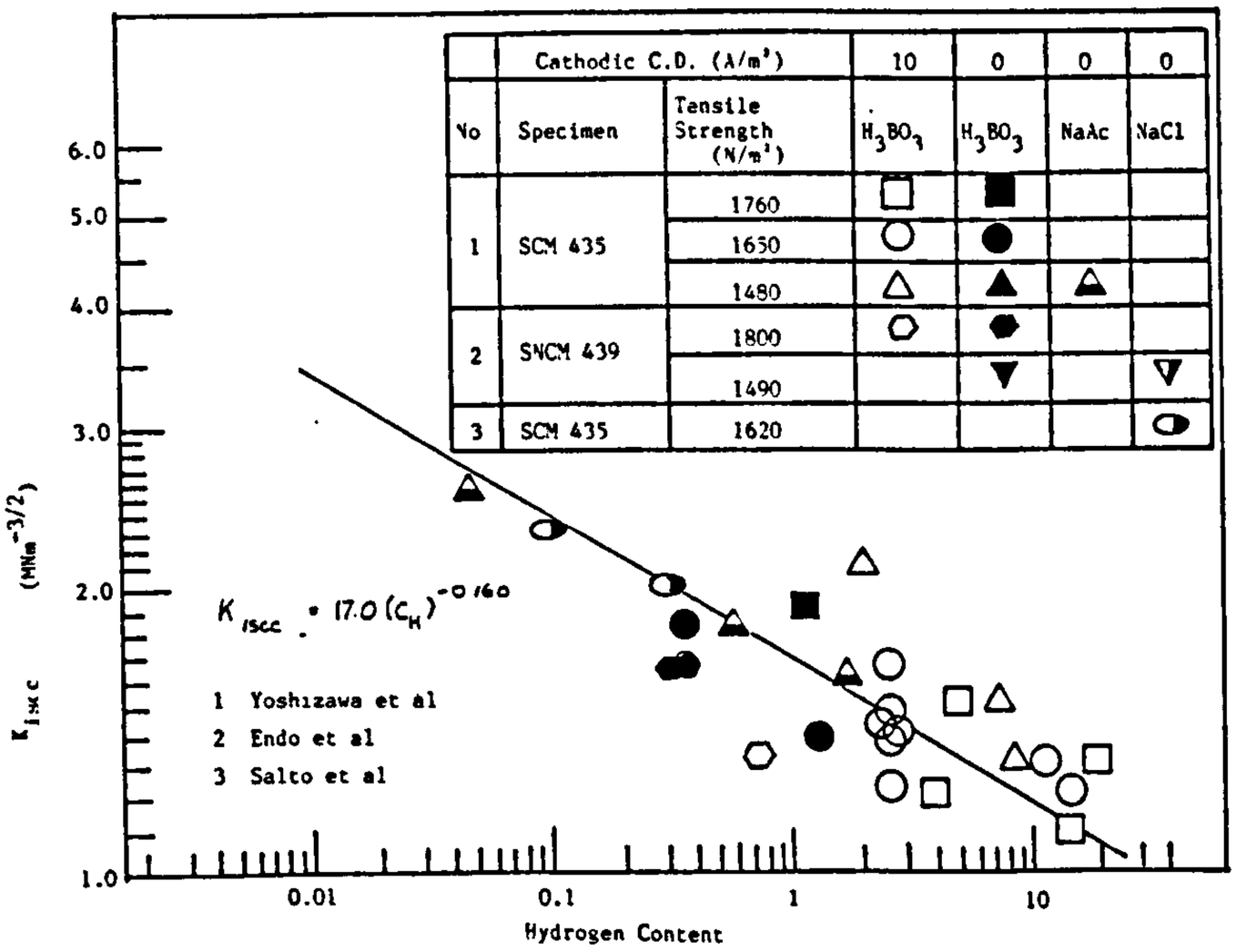

Values for K were calculated using the established formula

$$k = constant.\sigma\sqrt{\pi a} \qquad \text{EQUATION D}$$

where a is the defect size and σ is the applied stress. It was again assumed that the defects were two-dimensional in the plane perpendicular to the applied stress. This allowed for the constant value of 1.1 to be used in the equation. The value for o was taken to be 1380 (from Table 5.2 on page 127).

TABLE 5.8. Calculated Crack Initiation Times for Defects with a Range of Sizes, Located at a Depth of 0.2 mm and a Surface Hydrogen Concentration of 20 ppm

a mm.	K	H ppm.	C/C_o	t sec.
1.6E-2	10.762	17.4	0.871	18020
1.7E-2	11.094	14.4	0.720	6200
1.8E-2	11.415	12.1	0.603	2950
1.9E-2	11.728	10.2	0.509	1835
2.0E-2	12.033	8.7	0.43	1304
3.0E-2	14.737	2.4	0.122	335
4.0E-2	17.017	0.99	4.97E-2	207
5.0E-2	19.025	0.49	2.47E-2	158
6.0E-2	20.841	0.28	1.4E-2	133
7.0E-2	22.511	0.17	8.65E-3	116
8.0E-2	24.065	0.11	5.7E-3	105
9.0E-2	25.525	7.9E-2	3.94E-3	97
0.10	26.906	5.7E-2	2.84E-3	91

Knowing the measured $C_{th}/K_{i_{scc}}$ behaviour of the steel, easy steps can be made from 'a' to the required hydrogen concentration and thence, using Fick's Law, to calculate

the likely time to failure. Table 5.8 shows one set of values for the range of defect sizes where the defects are at a depth of 0.02 cm with a surface hydrogen concentration of 20 ppm.

The value for K was determined from equation D. The the value for [H] was obtained using Yamakawa's equation E on page 191 where C_H is the same as [H]. Hence C/C_o was calculated. Crank's equation (Equation A on page 168) was applied in an iterative mode to decide which value of 't' would give the calculated C/C_o value.

First calculations were made using the experimentally obtained value C_0 = 0.086 ppm (see Table 5.5) and assuming constant depths of 0.01 cm and 0.02 cm. These can be seen graphically as part of Figure 5.23. However, for times to failure obtained experimentally, the calculations indicate that the defect sizes would need to be over 1 mm in size and defects of that order would be visible. Referring to the published results (Figure 5.22 reproduced from Yamakawa) it was felt that a more realistic C_0 value would be of the order of 20 ppm and so all subsequent calculations used this value. Figure 5.23 includes calculated failure times assuming C_0 to be 20 ppm for defects ranging from 0.02 mm to 0.1 mm. The indication is, that for microscopic defects of less than 0.02 mm, even at 90% σ_f, failure would be unlikely to occur before 1 hour for a near surface defect (0.01 mm depth).

Indeed Figures 5.24 and 5.25 show enlargements of the corresponding section of Figure 5.23. These indicate the effect of defect size on failure time when the defect is at depths of 0.01, 0.02, 0.05 and 0.1 cm (i.e. halfway through the thickness of the specimen). The figures confirm that, for defects of less than 0.002 cm, times greater than 5 hours would pass before failure was likely to occur.

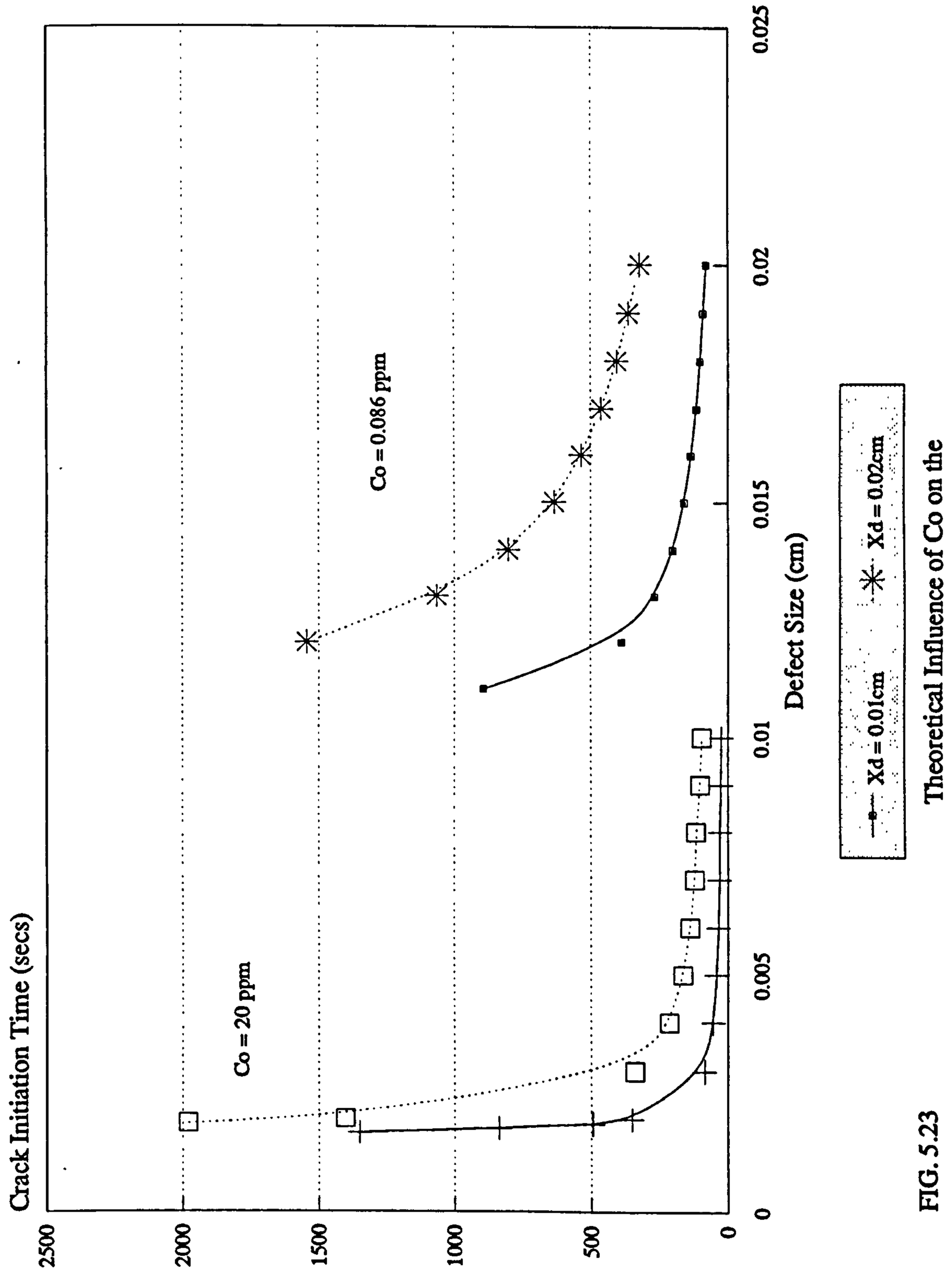
Crack Initiation Time (secs)
2500
2000
1500
1000
500
0
Co = 20 ppm
Co = 0.086 ppm
0
0.005
0.01
0.015
0.02
0.025
Defect Size (cm)
Xd = 0.01cm
Xd = 0.02cm
Theoretical Influence of Co on the
Crack Initiation Time

FIG. 5.23

FIG. 5.24 Theoretical Results Showing the Effect of Defect Size on Crack Initiation Time.

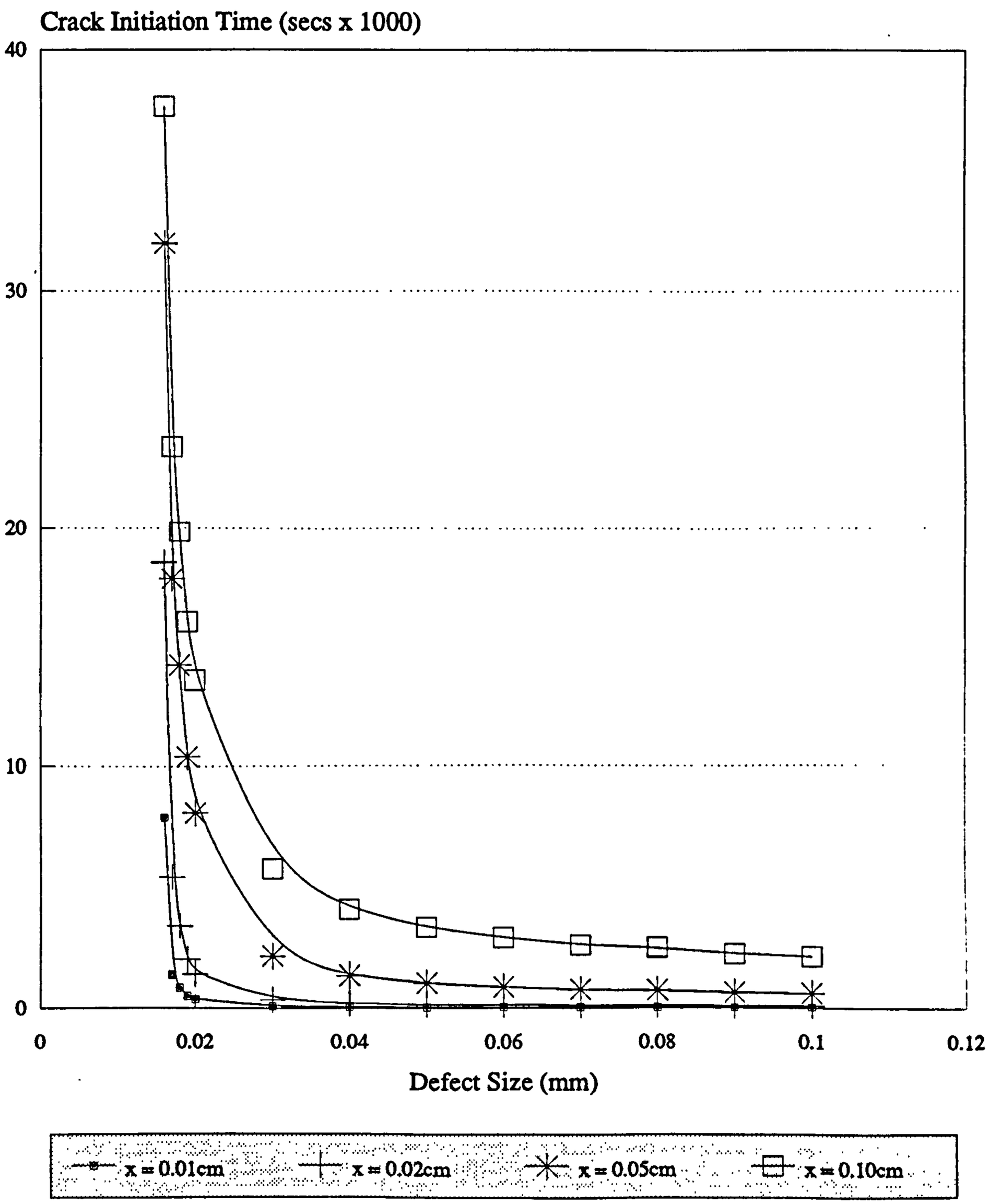

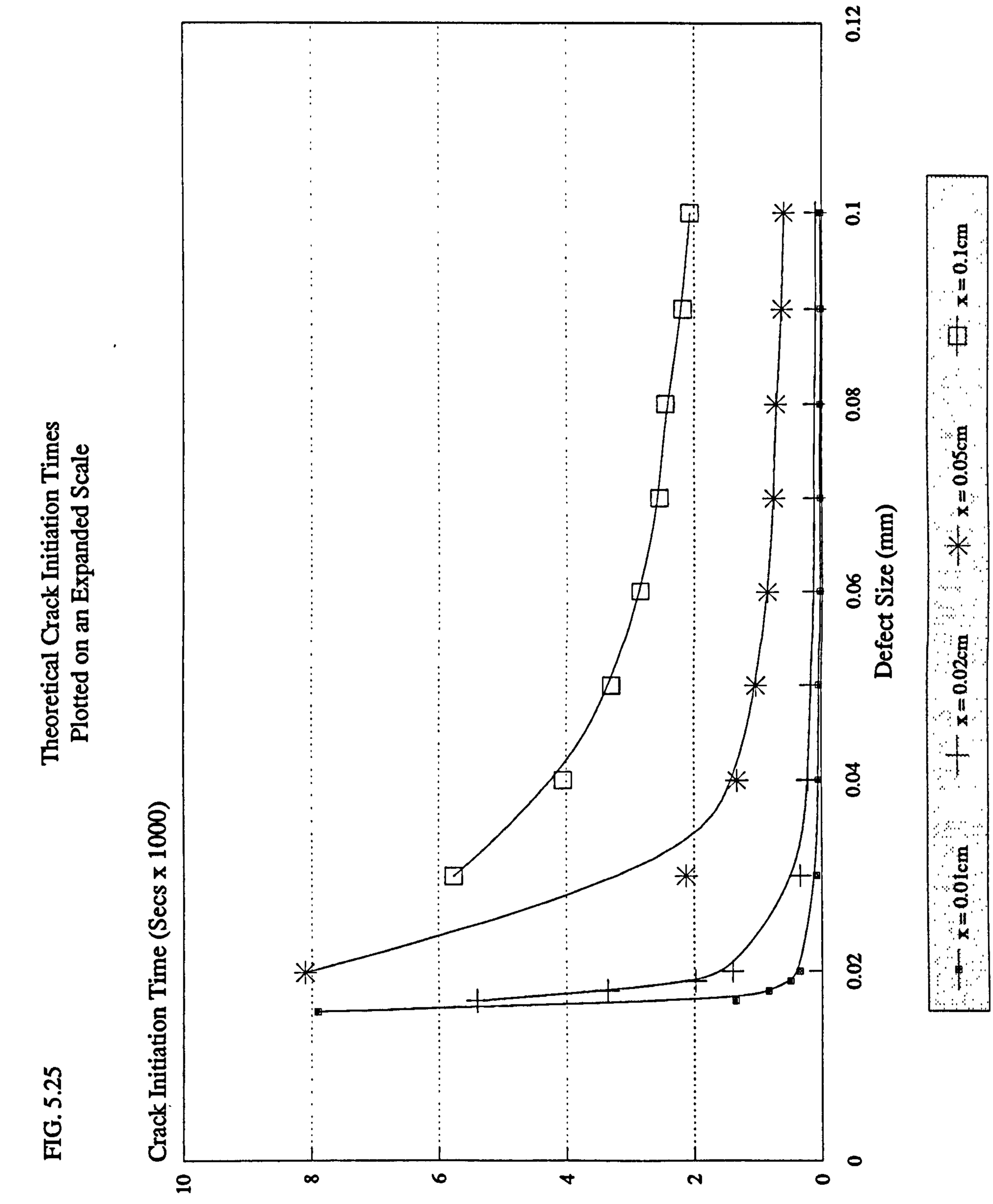
Theoretical Crack Initiation Times
Plotted on an Expanded Scale
Crack Initiation Time (Secs x 1000)
10
8
6
4
2
0
0.02
0.04
0.06
0.08
0.1
0.12
Defect Size (mm)
x = 0.01cm
x = 0.02cm
x = 0.05cm
x = 0.1cm

FIG. 5.25

5.4.6 Comparison of Two Equations Linking K_{Iscc} and C_0

Mathematical modelling so far has made use of Yamakawa's equation (1984) to connect K_{Iscc} and the hydrogen concentration

$$K_{Iscc} = 17.0\ C^{-0.160} \qquad \text{EQUATION E}$$

but an alternative equation is to be found in Lucas and Robinson (1987)

$$K_{Iscc} = 91.2\ e^{0.49C_0} \qquad \text{EQUATION F}$$

Figure 5.26 compares the two equations; Yamakawa's equation is represented by the line, and the points superimposed upon it are from Lucas and Robinson's equation. It is evident that the log-log scale is not suitable for the latter equation.

When the calculations regarding defect size using Yamakawa's equation were repeated using the second equation the results did not appear to be realistic. With a hydrogen concentration of 20 ppm and at a depth of 0.01 cm the defect would need to range in size from 1 to 11 μm with corresponding times to failure ranging from 85 to 21 seconds. At a defect depth of 0.02 cm the defect size would still need to lie between 1 and 11 μm and cracks would be initiated within the range of 340 to 85 seconds. Any defect larger than 12 microns would cause instant failure.

Indeed, repeating the calculations using a concentration of 1 ppm gave even less realistic values (see Figure 5.27)

FIG. 5.26 Comparison of Yamakawa's Equation with that of Lucas and Robinson.

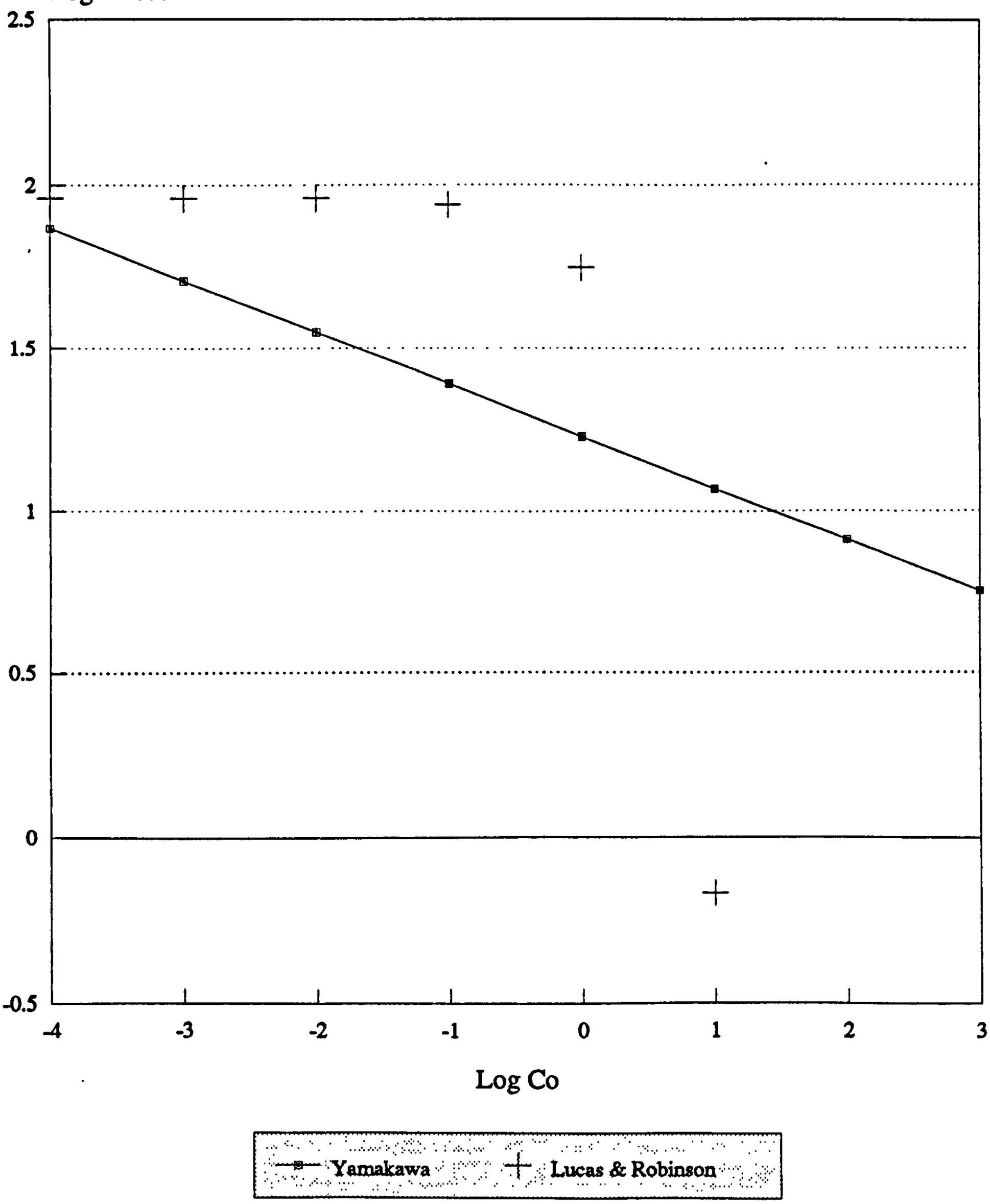

FIG. 5.27 Time to Failure using Lucas and Robinson's Equation for a Hydrogen Concentration of 1 ppm.

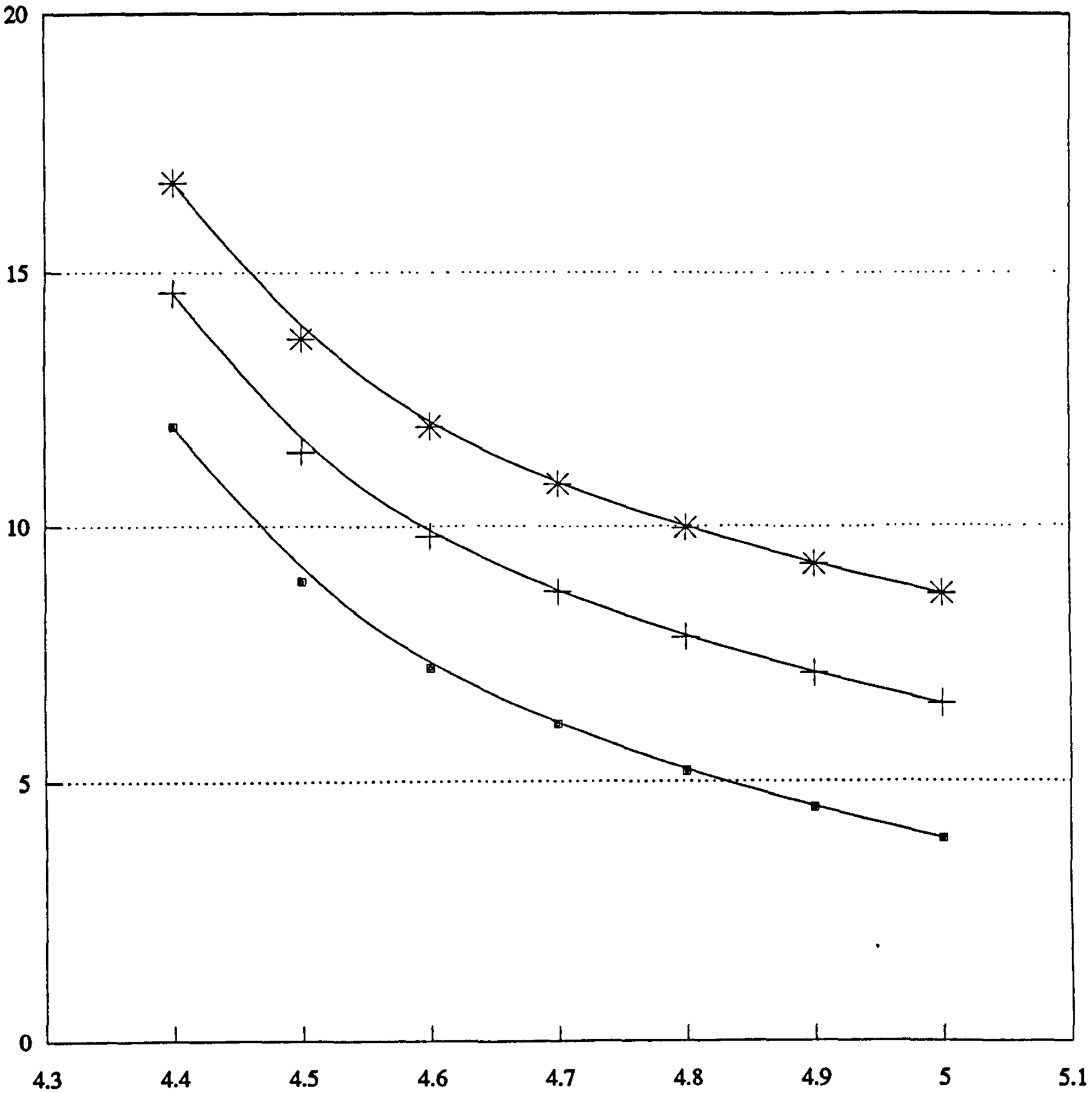

However, it should be stressed that Lucas and Robinson were referring to low carbon medium strength steels whereas Yamakawa and his associates had collated results relevant to high strength steels similar to, and including, AISI 4340. Obviously it makes more sense to use Yamakawa's equation but the main problem would appear to be the actual concentrations found by him. This could possibly be explained by the method of hydrogen determination used.

5.4.7. Comparison of the Effects of Different Stresses

The final part of the modelling process was to compare the effects of stress. All calculations so far have assumed the material to be stressed at 90% σ_f; these calculations were repeated for 80% and 50% σ_f at the various depths of 0.01, 0.02 and 0.05 cm and at C_0 values for 1.5, 10 and 20 ppm. In each case there was a wide range of values for both crack lengths and times to initiate the cracks. It was observed that the lower stress leads to longer times before failure is likely to occur.

Table 5.9 shows for a range of hydrogen concentrations the minimum defect size at which it is theoretically possible to initiate a crack.

Evidently at a hydrogen concentration of 1 ppm and a stress intensity of 50% σ_f a defect would have to be of the order of 200 microns in size before a $K_{i_{scc}}$ sufficient to initiate a crack would be reached, but, if the stress were 90% σ_f, then a much smaller defect of 40 μm would be a potential cause of failure by hydrogen embrittlement. Similarly at a concentration of 20 ppm the defects would need to be a minimum of 50 μm and 20μm, respectively.

TABLE 5.9. The Theoretical Defect Size and Fracture Stress Necessary to Initiate Cracking at Various Hydrogen Concentrations.

ppm	% UTS	0.01cm	0.02cm	0.05cm
1	50	200		200
	80	60	60	60
	90	40	40	40
5	90	30	30	30
10	90	20	20	20
20	50	50		50
	80	20	20	20
	90	20	20	20

It would seem quite possible for this model to be used to predict, for any given concentration of hydrogen, the likely minimum size of defect that would be necessary for hydrogen embrittlement failure to occur and also predict the likely minimum time before which failure would occur.

5.4.8 Summary

Use of $K_{i_{scc}}$ data is based on the relationship between stress intensity, K, nominal stress, σ, and crack size, a. A knowledge of $K_{i_{scc}}$ and either σ or a permits one to calculate either the allowable crack size a or the allowable stress, σ, below which cracking is not expected.

5.5 GENERAL SUMMARY

It is clear that the level of hydrogen arising from nickel plating is smaller by at least two orders of magnitude compared to that of cathodically charged steel. Yet each of the three experimental techniques used in this thesis is of value in detecting the very small quantities

generated.

The well-established constant load test sensitively detects embrittlement in cathodically charged steel but, when used while nickel plating, does not readily detect the much smaller hydrogen increase unless the steel is in the very highly susceptible condition of being quenched and not tempered.

Diffusion into steel is determined by the type and distribution of reversible and irreversible trapping sites within the micro-structure (Ryder et al, 1982). Other factors influencing crack propagation are the concentration of hydrogen and size and location of defects present. It is well-known that the wide range of failure times under constant load testing, albeit under apparently identical experimental conditions, is due to the statistical variation of each of the factors. Yokobori (1965) used a Weibull model which has been used extensively by other researchers including Strecker et al (1969, 1975) and Robinson and Sharp (1982).

This analysis has been corroborated by the mathematical modelling used in this thesis where the theoretical relationships between various parameters fit closely the observed experimental behaviour of cathodically charged or nickel plated steel under stress. Assuming cracks initiate at microstructural defects which have a range of sizes and are distributed over a range of depths below the surface, it is possible to calculate the minimum size defect for a crack to initiate. If it were possible to produce a steel with no defects above this minimum size then, theoretically, embrittlement would not occur.

Using the double-cell technique, Berman, De Luccia and Mansfield (1979) found that constant load failure data

correlated with cathodically charged flat tensile specimens of AISI 4340 steel. It has not been possible to directly correlate hydrogen concentrations measured using the double-cell technique with those obtained using the probe. The double-cell imposes a diffusion gradient by cathodically producing hydrogen at one side whilst simultaneously removing the hydrogen from the other side by oxidising it. The probe makes use only of the oxidation process; a potential is imposed on the surface of the part which is made the anode of the electro-chemical cell causing mobile hydrogen in the part to emerge and be oxidised at the surface. Figure 5.28 shows a schematic representation of the difference: 5.28a shows that the double-cell technique measures the constant concentration of hydrogen at the surface whereas 5.28b shows that the concentration at the surface being measured varies as the hydrogen diffuses to that surface.

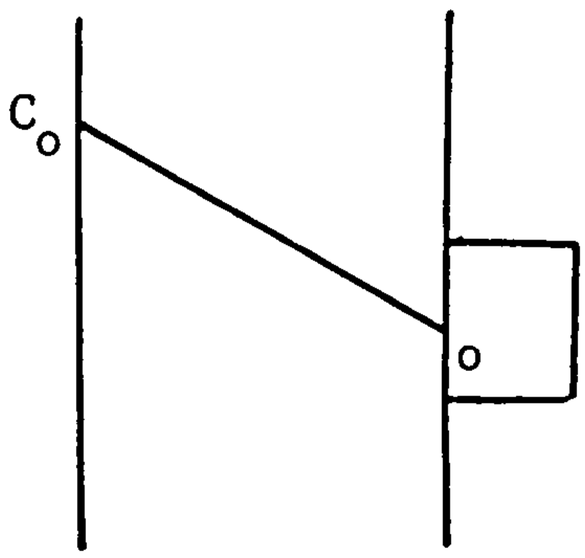

a. 2nd cell used to infer C_o on influx side

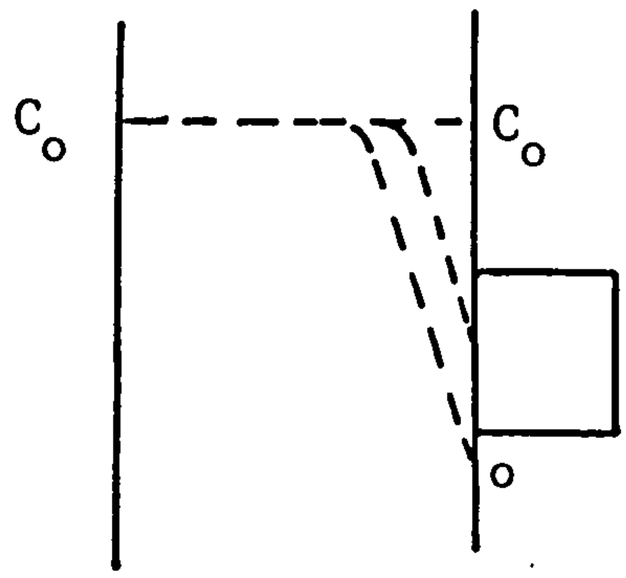

b. Probe infers C_o throughout

FIGURE 5.28

In decay a continuous ionisation current is set up during and after charging (or plating) and the total

hydrogen permeated is obtained from the area under the graph. However, there is a distinct separation between charging (or plating) and the extraction phase when using the gel-filled probe and the hydrogen content is established from the flux value after ten minutes. Figures 2.9b and 2.10a show the ionisation curves for both techniques. (They are both shown underneath for ease of reference.)

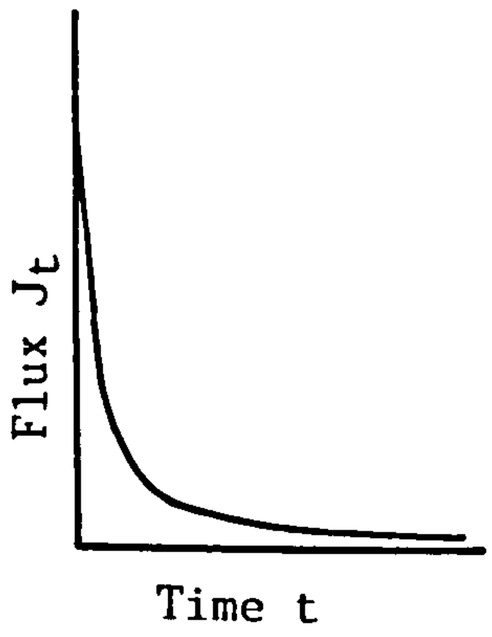

Fig. 2.9b. Decaying current transient resulting from hydrogen diffusion from the specimen surface

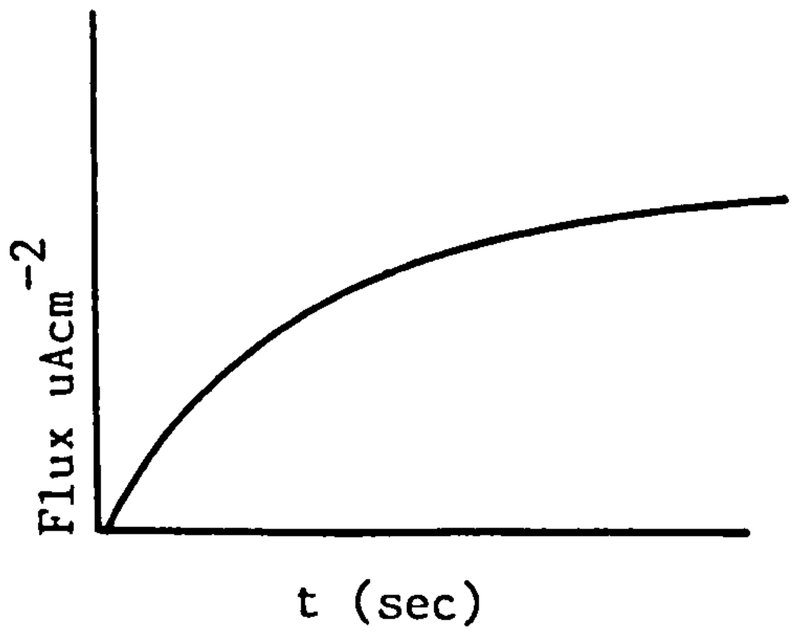

Fig 2.10a Double-cell Permeation

The only realistic comparison can be made between cathodically charged specimens. The hydrogen concentration of 1.1 ppm for 0.04%C foil ($D= 2 \times 10^{-8} cm^2 s^{-1}$) using the double-cell technique is similar to that obtained, 3.2 ppm, for 0.4C% AISI 4340 steel ($D = 2.5 \times 10^{-7} cm^2 s^{-1}$ using the gel-filled probe.

Both of these values are similar to those obtained by Townsend (1981). His measurement of 1.5 ppm was that obtained after nickel plating and removing the plate, and this figure is compares well with that resulting from a similar technique in the work done for this thesis.

It is interesting to note that, although the level of hydrogen decreases on exposure to the atmosphere for cathodically charged steel it increases for nickel-plated

and unplated steel. This increase is contrary to the effect found by Robinson and Hudson (1990) where they demonstrated that for welded 50D steel plate there was a decrease in hydrogen content over several days. Figure 5.29 shows the comparative effects which tend towards a common value of approximately 1 ppm. This increase, sufficient to counter the effects of de-embrittling treatment, is possibly due to corrosion.

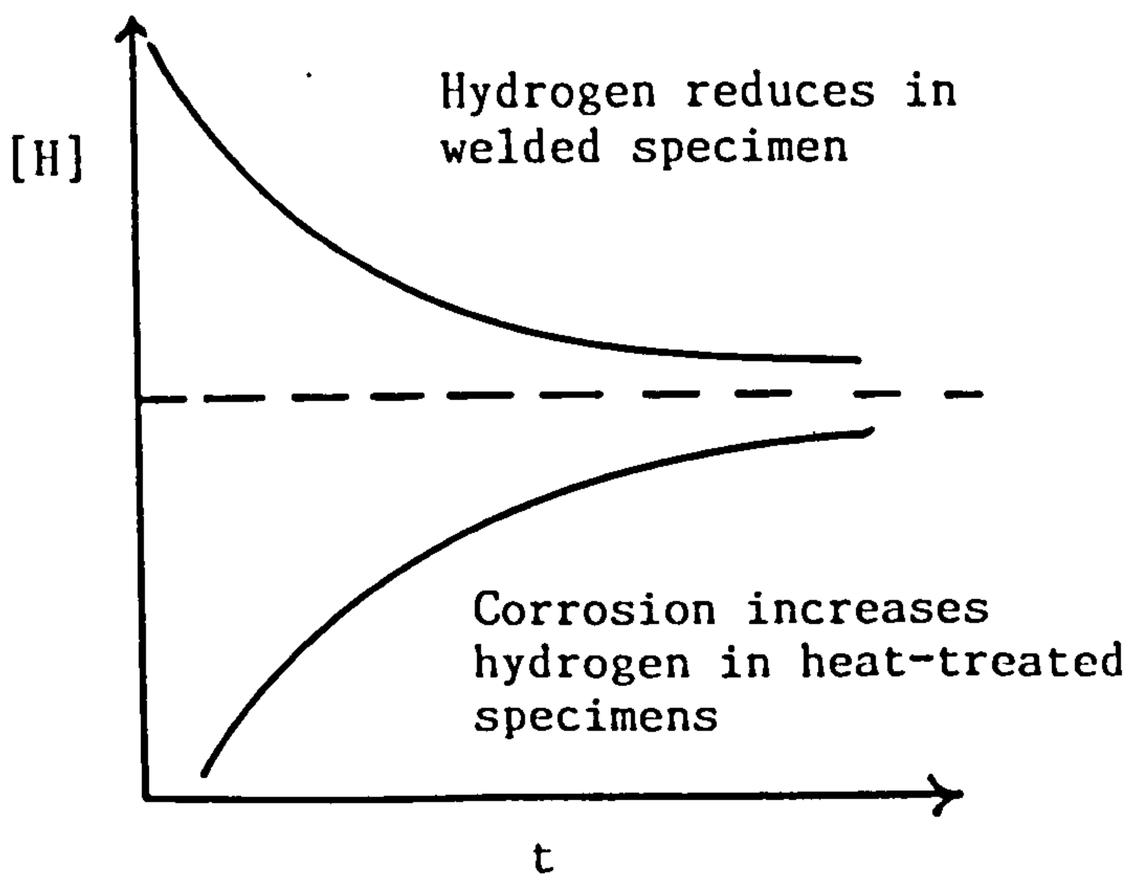

FIG 5.29 Schematic representation of hydrogen concentrations in welded 50D steel and heat-treated AISI 4340 steel.

Levels of hydrogen obtained for specimens plated at 5 $mAcm^{-2}$ were 6.5 $x10^{-3}$ ppm and 18.4 ppm using the double-cell and probe techniques respectively. It should be noted that the "probe concentration" had fallen to 6.6 ppm after five days. These values are considerably at odds with those measured by Townsend (270 ppm) but, as has been stated previously, this figure represents the total hydrogen present.

Berman et al (1979) found that after electroplating (using cadmium) and then baking, the hydrogen remaining varied considerably depending on the porosity of the plate. This seems to partly explain the variation of results

obtained in both permeation techniques. An additional explanation would include the basic nature of the steel, heat-treatment and pre-plating preparation.

For practical purposes the probe may be considered a quick and easy way to measure concentration of diffusible hydrogen within a metal. Once the relationship between double-cell measurements and those obtained using the probe have been clearly established the value of C_0 may be obtained. From this it will be possible to use the mathematical model based on the equation obtained by Yamakawa (1984) to make predictions concerning the likelihood of cracking due to hydrogen embrittlement for AISI 4340 steel.

CHAPTER SIX
CONCLUSIONS

1. The results of hydrogen embrittlement testing can be treated by Weibull statistical analysis to give a minimum incubation time, t_i, and mean time to failure, $\bar{t}$.

2. Quenched and tempered 0.8%C steel exhibits a higher susceptibility to hydrogen embrittlement than cold-worked pearlitic steel of the same composition. It is probable that the reduced susceptibility is due to the coarse lamellar carbide interfaces in the pearlite acting as particularly innocuous traps for mobile hydrogen.

3. At low applied stresses the mechanism of hydrogen embrittlement contains an additional initiation step which is thought to be due to the formation of internal voids of sufficient size for the threshold stress intensity, K_{th}, to be exceeded.

4. Electro-deposited nickel acts as a reservoir of hydrogen which continues to diffuse into the steel substrate after the cessation of electroplating. This implies that a delay in post-plating baking treatment would increase the amount of hydrogen absorbed by the steel.

5. The lower the plating current density the higher the concentration of hydrogen within the nickel deposit. The use in industry of "flash-plating", using an initially high current density, is confirmed to be beneficial.

6. The effect of post-plating baking treatment is clearly seen using the double-cell permeation technique. Specimens which have been plated for 2 hours, removed from the cell, subjected to post-plating heat treatment and replaced in the cell exhibited a much lower decay transient, indicating that the post-plating baking does remove hydrogen from the plate.

7. The gel-filled electrochemical probe can be used to measure the hydrogen content of a specimen in situ.

8. t-testing is a valuable aid to the interpretation of results.

9. Reproducibility of the probe technique is good for specimens prepared in the same batch. However the many stages involved in preparing specimens can cause variation of the hydrogen concentrations between batches.

10. For cathodically charged AISI 4340 steel, similar reductions in hydrogen concentration are obtained after baking for 2 or 20 hours.

11. Equilibrium in hydrogen content was reached several days after exposure to the atmosphere. However, the initial hydrogen concentrations affected the approach to equilibrium. If the initial concentration was high it decreased with time but if the initial concentration was low there was an increase. This increase was probably due to atmospheric corrosion.

12. Mathematical modelling explains the variation of time to failure caused by cracks initiating from microstructural defects distributed over a range of depths below the surface of the specimen.

13. It is important that the maximum defect sizes should be correctly assessed as it is at these defects that the shortest crack initiation times would occur.

14. Defects comparable in size to the grain size of the material could cause problems when applying fracture mechanics equations.

15. It is possible to predict crack initiation times when the relationship between K_{th} and the hydrogen content is known.

16. For a specific hydrogen concentration in steel and given a particular heat treatment or plating process, there is a minimum defect size within the microstructure at which a crack can initiate. Below this size embrittlement is not expected to occur.

APPENDIX A
Statistical Methods

This appendix describes a) Student's t-test
and b) Weibull Analysis

a) Student's t-test

This test is made when results are obtained from very small samples and it is intended to determine whether or not different sets of sample results belong to the same parent population.

The Central Limit Theorem states that the population formed by the means of a large number of small samples will always be normally distributed. However, Student (the pseudonym of William Gosset) noted that the estimated value of the standard deviation ($\hat{s}$) was a poor comparison with the true value (σ).

. In fact, $\hat{s}$ tends to underestimate σ for more than half the time. Consequently the test statistic

$$z = \frac{\bar{x} - \mu_0}{\left(\frac{\hat{S}}{\sqrt{N}}\right)}$$

will tend to be more spread out than the normal Gaussian distribution and [illegible] a t-curve would be more appropriate.

Knowing the means of two samples, it is necessary to estimate whether they are likely to be representative of a single parent population. The assumption is made that any difference between the means of two samples is due purely to chance and that there is no significant difference

between them. By calculating the relevant t-statistic, and referring to tables of critical values appropriate to the number of degrees of freedom and accuracy, it is possible to make an informed decision.

The term "degrees of freedom" refers to the number of values which are free to vary after certain restrictions have been placed on the data; thus, if the sample size is n, the number of degrees of freedom would be n - 1. If two samples of sizes n_A and n_B are being compared, the number of degrees of freedom would be $n_A + n_B - 2$.

The test statistic "t" is calculated using the following information:

	Sample A	Sample B
Size of sample	n_A	n_B
mean of results	$\bar{x}_A$	$\bar{x}_B$
variance	s^2_A	s^2_B
degrees of freedom	$v = n_A + n_B - 2$	

$$t = \frac{|\bar{x}_A - \bar{x}_B|}{\sigma\sqrt{\frac{1}{n_A}+\frac{1}{n_B}}}$$

where:

$$\sigma = \sqrt{\frac{n_A s_A^2 + n_B s_B^2}{n_A + n_B - 2}}$$

If t exceeds the appropriate critical value then it is assumed that the two sets of results differ significantly and belong to two separate populations.

b) Weibull Analysis

The Weibull Distribution is probably the most popular model used in industry to describe failure times. The curve varies according to specific parameters and, in the case of stress failure times, is a stochastic (time-based) process and is exponential in form. Several researchers, including Yokoburi (1965), Strecker et al (1975) and Grundy et al (1982, 1983) have used the model to explain the wide range of failure times in delayed fracture tests. Their Weibull model treats the scatter in failure times as a probability distribution generated by time where the number of failures which have occurred by time, t, is dependent on chance.

The researchers mentioned above have shown that the probability of a specimen NOT failing within time, t, is given by:

$$P_s = e^{-xt}$$

where x is the probability per unit time that a crack of sufficient size to cause failure will occur during time, t. The value of x can be obtained from the negative slope of the graph of lnP against time, t. The mean failure time, $\bar{t}$, is defined as 1/x and this quantity is a sensitive measure of susceptibility to hydrogen induced failure.

Robinson and Sharp (1986) found that for specimens being charged and loaded simultaneously there was a minimum incubation time, t_i, corresponding to that time, in the most susceptible specimen tested, for hydrogen to diffuse to the depth where a critical crack length was generated. They accordingly modified the equation above to:

$$P_s = e^{-x(t-t_i)}$$

and redefined $\bar{t}$ as $\bar{t} = t_i + 1/x$

REFERENCES

ADLER, P.N., KAMYKOWSKI, E.A. and PADAWER, G.M. (1974). Localized Hydrogen Measurements in Surfaces using the Lithium Nuclear Microprobe. Hydrogen in Metals. pp.623-630. Eds. Bernstein & Thompson ASM (1974).

ADAIR, A.M. and HOOK, R.E. (1962). Acta Met. (1962). Vol.10, pp.741-743.

AHMAD, S.A., RYDER, D.A. and DAVIES, T.J. (1975). Eng. Fracture Mech. (1975) Vol.7, pp.357-65.

ARCHER, M. and GRANT, N. (1984). Achievable Boundary Conditions in Potentiostatic and Galvanostatic Hydrogen Permeation through Palladium and Nickel foils. Proc. R. Soc. London. A395. pp.165-183 (1984).

ASANO, S., SUGIMOTO, T. and OHTANI, N. (1973). Bull Nagoya Inst. Tech. (1973). Vol.25, p.361.

BARANOWSKI, B. (1972). Berichte der Bunsen - Gesellschaft fÜr Physikalïsche Chemie. ed. E. Wicke. (1972). Vol.76. pp.714-723.

BASTIEN, P. and AZOU, P. (1951). Effect of Hydrogen on the Deformation and Fracture of Iron & Steel in Simple Tension Proc. First World Metallurgical Cong. Am. Soc. Metals, Cleveland, Ohio. (1951).

BEACHEM, C.D. (1972). New Model for Hydrogen - Assisted Cracking (Hydrogen Embrittlement). Met. Trans. Vol.3. (February 1972). pp.437-451.

BEACHEM, C.D. (1977). Proc. NACE Conf. France June 1973. Eds. Staehle, Hochmann, McCright and Slater. Pub. 1977. pp.376-381.

BERMAN, D.A. BECK, W. and de LUCCIA, J.J. (1974). The Determination of Hydrogen in High Strength Steel Structures by an Electrochemical Technique. Hydrogen in Metals. pp.595-607. Eds. Bernstein and Thompson ASM (1974).

BERMAN, D.A., de LUCCIA, J.J. and MANSFIELD, F. (1979). Barnacle Electrode: New Tool for Measuring Hydrogen in High Strength Steels. Metal Progress. May 1979. pp.58-61.

BERNSTEIN, I.M. (1970). Mat. Sci. Eng. (1970) Vol.6. pp.1-19.

BERNSTEIN, I.M., GARBER, R. and PRESSOUYRE, G.M. (1976). Effect of Dissolved Hydrogen on Mechanical Behaviour of Metals. Effect of Hydrogen on Behaviour of Materials. Proc. Int. Conf. Metallurgical Soc. AIME. 1976. Eds. Thompson and Bernstein.

BERNSTEIN, I.M. and THOMPSON, A.W. (1976). Int. Met. Rev. 1976. Vol.21. pp.269-287.

BIDMEAD AND DAVIES. (1978). The Potentialities of Electrodeposition and Associated Processes in Engineering Practice. Trans. Inst. Met. Fin. 1978. Vol.56. pp.97-106.

BOCKRIS, J. O'M. (1977). On Hydrogen Damage and the Electrical Properties of Interfaces. Proc. NACE 5. 1977. pp.286-305.

BROWN, B.F.(1971). Strength Corrosion Cracking of High Strength Steels. NATO Conf. The Theory of Stress Corrosion Cracking in Alloys. Ed. J.E. Scully. (1971).

CARTER, V.E. (1977). Metallic Coatings for Corrosion Control. Newnes - Butterworth 1977.

CRANK, J. (1956). The Mathematics of Diffusion. OUP 1956. p.60.

CREIGHTON AND KOEHLER. (1950). Electrochemistry. Electroplating Solutions. Vol.2. Applications. John Wiley & Sons (1950).

DAVIES, T.J., GRUNDY, R. and RYDER, D.A. (1983). A Statistical Treatment of Hydrogen Induced Delayed Failure. Jour. Mat. Sc. Vol.18. 1983. pp.3128-3136.

DAVIES, T.J., HAYES, F.H., STRECKER, E. AND RYDER, D.A. (1977). Proc. 2nd. Int. Conf. Hydrogen in Metals. July 6-11. 1977.

DEVANATHAN, M.A.V. and STACHURSKI, Z. (1962). Proc. Roy. Soc. 1962. Vol. A270. p.90.

DEVANATHAN, M.A.V., STACHURSKI, Z. and BECK, W. (1963). A Technique for the Evaluation of Hydrogen Embrittlement Characteristics of Electroplating Baths. Jour.Electrochem. Soc. Aug. 1963. pp.886-890.

DIBARI, G.A. (Nickel Plating. International Nickel Co. Inc. Suffern. N.Y. p.270.

DINI, J.W. and JOHNSON, H.R. (1977). Electrodeposition of Zn - Ni Alloys and Coatings. Presented at the Government Industries Workshop on Alternatives for Cadmium Electroplating in Metal Finishing. Galthersburg. M.D. 4-6 Oct. 1977.

FIDELLE, J.P. (1988) Discussion of New Theory of Hydrogen Effects on the Mechanical Properties of Metal Systems based on Mendeleev's Table. Quote on p.750. re. FeH. Proc. Conf. Hydrogen and Materials. Beijing. 9-13 May. 1988.

FLOREEN, S.F. (1985) Hydrogen Cracking in Speciality Steels. Hydrogen Degradation of Ferrous Alloys. pp.799-821.

FONTANA and GREEN. Corrosion Engineering. McGraw-Hill. 1978.

GABE, D.R. (1978). Principles of Metal Surface Treatment and Protection. 2nd. Edition. Pergammon Press (1978). p.68.

GARBER, R., BERNSTEIN, I.M. and THOMPSON, A.W. (1981). Hydrogen Assisted Ductile Fracture of Spheroidised Carbon Steels. Met. Trans. Vol.12A. Feb. 1981. pp.225-235.

GAHR, S., GROSSBECK, M.L. and BIRNBAUM, H.K. (1977). Acta. Met. Vol.25. 1977. pp.125-134.

GERBERICH, W.W., GARRY, J. and LESSER, J.F. (1977). Grain Size and Concentration Effects in Internal and External Hydrogen Embrittlement. Hydrogen in Metals. Eds. Thompson and Bernstein. 1977.

GIBALA. R. (1977). As J.J. Gilman NACE 5. pp.244-271.

GILEADI, E. and FULLENWIDER, H. (1966). Univ. of Pennsylvania. Final Report to Naval Air Engineering Centre. Contract No. N156-46659. Sept. 1966.

GILEADI, E., FULLENWIDER, M. and BOCKRIS, J.O'M. (1966) Journal Electrochemical Society. Vol.113, p.926.

GILMAN, J.J. (1977). Proc. NACE Conf. France. June 1973. Eds.Staehle, Hochman, McCright and Slater. Pub. 1977. pp.57-60.

GRUNDY, T., DAVIES, T.J. and RIDER, D.A. (1983). A New Statistical Model of the Hydrogen Embrittlement of Steel. Jour. Mat. Sc. 18 (1983). pp.3128-3136.

GRUNDY, T., RYDER, T.J. and STANLEY. (1982). A New Statistical Model for the Hydrogen Embrittlement of a Quenched and Tempered Steel. Inst. Met. Hydrogen in Steel Conf. 14 - 16 July 1982. Bath.

HANCOCK, G.G. and JOHNSON, H.H. (1965). Trans TMS - AIME. 1965. Vol.236. pp.513-516.

HARRIS, T.M. and LATANISION, R.M. (1990). Grain Boundary Diffusion of Hydrogen in Electrodeposited Nickel. Hydrogen Effects on Material Behaviour. Eds. Moody and Thompson. 1990.

HIROSE, A., ARAKI, T. and KIKUTA, Y. (1988). Effect of Nonmetallic Inclusions on Behaviour of Hydrogen Diffusion and HAC. Proc. Conf. Hydrogen and Materials. Beijing. 9-13 May. 1988. pp.554-561.

HIRTH, JOHN P. (1980). Effects of Hydrogen on the Properties of Iron and Steel. ASMMS. Met. Trans. Vol.11A. June 1980. pp.861-890.

HOLZWORTH, M.L. and LOUTHAN, M.R. (1968). Corrosion 24. 1968. p.110.

HSIAO, C. (1988). Some Critical Issues of Hydrogen Induced Cracking. Proc. Conf. Hydrogen and Materials. Beijing. 9-13 May. 1988. pp.502-515.

HUDSON, D.R. (1987). Development of a Hydrogen Probe. M.Sc. Thesis. Cranfield. Sept. 1987.

IINO, M. (1988). Hydrogen - Defect Interactions and Hydrogen Induced Embrittlement in Iron, Steel and Other Metals. Proc. Conf. Hydrogen and Materials. Beijing. 9-13 May. 1988.

JOHNSON, H.H. and HIRTH, J.P. (1976). Met. Trans. A. Vol.7A. Oct 1976. pp.1543-1548.

JOHNSON, H.H., MORLET, J.G. and TROIANO, A.R. (1958). The Effect of Baking on Fracture Characteristics of Cathodically Charged 4340 Steel. Trans. AIME. 1958. Vol.212. pp.528-536.

KAMITANI, M., KOQA, T. and TSUJI, H. (1985). Electrodeposition of Bright Zn - Ni Alloys. Sur. Fin. 85. Ann. Tech. Conf. Procs. Detroit 15 - 18 July 1985.

KERNS, G.E., WANG, M.T. and STAEHLE, R.W. (1977). Proc. NACE Conf. France. June 1973. Eds. Staehle, Hochman, McCright and Slater. Pub. 1977. p.700.

KIMURA, H. and MATSUI, H. (1979). Scr. Met. 1979. Vol.13. pp.221-224.

KIUCHI, K. and McLELLAN, R.B. Diversity in Hydrogen Diffusion Coefficients from Various Laboratories with Different Methods. Acta Met. Vol.31(7). 1982. pp.961-984.

KOSCO, T.J. and THOMPSON, A.W. (1982). The Effect of Hydrogen on Constrained Yielding and Fracture in a Spheroidized Medium - Carbon Steel. Scripta Met. Vol.16. 1982. pp.1367-1371.

LACOMBE, P., AUCOUTURIER, M., LAURENT, J.P. and LAPASSET, G. (1973). Proc. NACE. Conf. France. June 1973. Eds. Staehle, Hochman, McCright and Slater. Pub. 1977. pp.423-431.

LEE, T.D., GOLDENBURG, T. and HIRTH, J.P. (1979). Met. Trans A. 1979. Vol.10A. pp.439-448.

LESLIE, W.C. The Physical Metallurgy of Steels. McGraw Hill. p.290.

LOUTHEN, M.R. and McNUTT, R.P. (1977). The Role of Test Technique in Evaluating Hydrogen Embrittlement Mechanisms. Proc. Int. Conf. on Hydrogen on Behaviour of Materials. Eds. Thompson and Bernstein 1977. pp.496-506.

LUCAS. K.A. (1985). The Hydrogen Assisted Cracking of Steel. M.Sc. Thesis. Cranfield. Oct. 1985.

LUCAS, K.A. and ROBINSON, M.J. (1986). Corrosion Science. Vol.26. No. 9. 1986. pp.705-717.

LUCAS, K.A. and ROBINSON, M.J. (1987). Prediction of Hydrogen Assisted Cracking of Steels. Plant Corrosion-Prediction of Materials Performance. Ellis Howards Ltd. 1987. Eds. J. Strutt and J. Nichols. pp.181-192.

LYNCH, S.P. (1979). Metals Forum. 1979. Vol.2. pp.189-200.

LYNCH, S.P. (1981). Hydrogen Effects in Metals. Eds. Bernstein and Thompson. Met. Soc. AIME. New York. pp.863-871.

McBREEN, J., NANIS, L. and BECK, W. (1966). Journ. Electrochem. Soc. 1966. Vol.113. pp.1218-1222.

McINTYRE, P. Hydrogen Effects in High Strength Steels. Hydrogen Degradation of Ferrous Alloys. pp.763-798.

MAHKLOUI, M.M. and SISSON, R.D. (Jnr). (1990). Hydrogen Uptake During Cadmium Plating. Hydrogen Effects on Material Behaviour. Eds. Moody and Thompson. The Minerals, Metals and Materials Soc. 1990.

MANALATOS, P. and LeCOZE, J. (1988). Electrochemical Permeation of Hydrogen in Pure Iron and Low Alloy Steels. Influence of the Passive Layer formed on the Exit Side. Proc. Conf. Hydrogen and Materials. Beijing 9-13 May. 1988. pp.577-589.

MANSFELD, F., JEANJAQUET, S. and ROE, D.K. (1982). Barnacle Electrode Measurement System for Hydrogen in Steels. Materials Performance. Feb. 1982. p.35.

MATUSIEWICZ, G. and DUQUETTE, D.J. (1985). Diffusion Coefficient of Hydrogen in Nickel. Acta Met. Vol.33. p1637. 1985.

MURDOCH, J. and BARNES, J.A. Statistics. MacMillan Press. 1973. p.170.

NAIR, S.V., JENSON, R.R. and TIEN, J.K. (1983). Metall. Trans. A. 14A (1983). p.385.

NANIS, L. (1964). Proposal on Hydrogen Embrittlement to Naval Air Engineering Centre. Univ, of Penna. Oct 1964.

NELSON, H.G. and WILLIAMS, D.P. (1977). Quantitative Observations of Hydrogen Induced Slow Crack Growth in a Low Alloy Steel. Stress Corrosion Cracking and Hydrogen Embrittlement of Iron Base Alloys. Eds. Staehle, Hockman, McCright and Slater. NACE 5. 1977. pp.390-404.

NELSON, H.G., WILLIAMS, D.P. and TETELMAN, A.S. (1971). Metall. Trans. 2. 1971. p.953.

NICHOLS, J.R. and HANCOCK, P. (1983). Proc. Conf. "High Temperature Corrosion". NACE 6. San Diego. pp.198-210. Ed. R. Rapp. Pub. NACE. 1983.

ONYEKPE, B.O. (1988). Trapping Theory of Hydrogen Damage due to the Shape and Distribution of Cavities. Proc. Conf. Hydrogen and Materials. Beijing. 9-13 May. 1988. pp.626-628.

ORIANI, R.A. (1969). Fundamental Aspects of Stress Corrosion Cracking. Eds. Staehle, Forty and von Rooyan. Pub. NACE. (1969) p.32

ORIANI. R.A. (1970). Acta Met. 1970 Vol.18. p.147.

ORIANI. R.A. (1977). A Decohesion Theory for Hydrogen Induced Crack Propagation. NACE 5. Pub. NACE. 1977. pp.351-358.

ORIANI, R.A. (1978). Ann. Rev. Mater. Sci. 1978. Vol.8. pp.327-57.

ORIANI. R.A. (1987). Hydrogen - The Versatile Embrittler. Whitney Award Lecture 1987 - NACE. pp.390-397.

ORIANI, R.A. and JOSEPHIC, P.H. (1972). Scripta. Met. Vol.6. 1972. pp.681-688.

ORIANI, R.A. and JOSEPHIC, P.H. (1979). Environment Sensitive Fracture of Engineering Materials. ed. Z.A. Foroulis. TMS - AIME. Warrendale Pa. 1979. pp.232.

PAATSCH, W. (1988). Influence of Alloying Techniques on Hydrogen Embrittlement of Electroplated Steel. Proc. Conf. Hydrogen and Materials. Beijing. 9-13 May 1988.

PAGE, R.A. and GERBERICH, W.W. (1982). Met. Trans. A. Vol.13A. 1982. pp.305-312.

PEI, X., LIU, Y. and CHEN, C. (1988). A New Mechanism of Hydrogen Assisted Cracking. Proc. Conf. Hydrogen and Materials. 9-13 May. Beijing. 1988. pp. 287-293.

PETCH, N.J. and STABLES, P. (1952). Nature. Vol.169. (1952). p.842.

POLLOCK, W.J. (1988). Application of Slow Strain Rate Testing to Assess the Degree of Hydrogen Damage in Low Alloy High Strength Steel by Aircraft Maintenance Chemicals. Beijing. 9-13 May. 1988. pp.775-784.

PRESSOUYRE, G.M. and BERNSTEIN, I.M. (1978). Met. Trans. Acta. Vol.9A. Nov. pp.1571-80. 1978.

PRESSOUYRE, G.M. and BERNSTEIN, I.M. (1979). Acta Met. 1979. Vol.27. pp.89-100.

PYUN, SU-IL and ORIANI, R.A. (1989). The Permeation of Hydrogen through the Passivating Films on Iron and Nickel. Corrosion Science. Vol.29. No. 5. (1989). p.485-496.

RHINES, F.N. (1970). Commentary on Hydrogen Embrittlement in Steels. Corr. Sc. 10. 839 (1970).

RICE, J.R. (1977). Corrosion Cracking and Hydrogen Embrittlement of Iron Base Alloys. NACE 5. (1977). p.11.

ROBINSON, M.J. and EVANS, J.M. (1988). A Quantitative Study of the Effects of Electroplating on Hydrogen Absorption and Embrittlement in High Strength Steels. Hydrogen and Materials. Beijing. 9-13 May. 1988.

ROBINSON, M.J. and EVANS, J.M. (1989). Probe Measurements to Determine the Hydrogen Content of Electroplated Steel. Trans. Inst. Met. Finishing. 1989. Vol.67. pp.78-81.

ROBINSON, M.J. and HUDSON, D.R.J. (1990). Measurement of Hydrogen Concentrations in BS4360 Grade 50D Carbon-Manganese Steel using an Electrochemical Probe. Br. Corros. J. 1990. Vol.25. No. 4. pp.279-284.

ROBINSON, M.J. and SHARP, R.M. (1986). Corrosion. Vol.41. No. 10. pp.582-586. 1986.

RYDER, D.A., GRUNDY, T. and DAVIES, T.J. (1982). Proc. Conf. "Current Solutions to Hydrogen Problems in Steel". 1st. International Conf. ASM. Washington. Nos. 1-5. (1982). pp.272-275.

SANDS, J.W. and MILLER, O.O. (1956). Effects of Tempering Temperature on the Tensile and Impact Properties of 25 mm. Round Bars of Two Medium-Carbon Low Alloy Steels Oil-quenched from 855°C. Mater. Methods 43:94 (3).

SHUBINSKY, Y. DAVIES, T.J. and RYDER, D.A. (1982). Hydrogen in Steel Conference. Inst. Met. Bath. 14 - 16 April 1982.

SMIALOWSKI, M. (1962). Hydrogen in Steel. Addison-Wesley. Reading. Mass. 1962. p.16.

SMITH, C.J.E. (1985). Current Requirements for the Design and Maintenance against Corrosion of UK Military Aircraft. AGARD. (NATO). Lecture Series. 141.

SPIEDEL. M.O. (1984). Stress Corrosion Cracking and Corrosion Fatigue Fracture Mechanics. Corrosion in Power Generating Equipment. eds. M.O. Spiedel and A. Atrens. Plenum Press. New York. 1984. pp.85-132.

STANDARDS:

DEF STAN 00-970. Leaflet 406/1. Design Requirements for Service Aircraft. Vol.1. No. 4. Steels.

F 519-577. ASTM. Mechanical Hydrogen Embrittlement Testing of Plating Processes and Aircraft Maintenance Chemicals.

DTD 905a. FEB. 1955. Ministry of Aviation. Nickel Plating (Heavy). Process Specification.

BS. 1224:1970. Electroplated Coatings of Nickel and Chromium.

DEF STAN 03-01. Electrodeposition of Nickel and Chromium.

DEF STAN 03-2/2. Cleaning and Preparation of Metal Surfaces.

DEF STAN 03-4/2. Pre-Treatment and Protection of Steel Parts of Specified Maximum tensile stress exceeding 1450 N/m^2.

STEIGERWALD, E.A., SCHALLER, F.W. and TROIANO, A.R. (1959). Trans Met. Soc. AIME. Vol.215. Dec 1959. pp.1048-1052.

STEIGERWALD, E.A., SCHALLER, F.W. and TROIANO, A.R. (1960). Trans. Met. Soc. AIME. Vol.218. Oct 1960. pp.832-41.

STRECKER, E., RYDER, D.A. and DAVIES, T.J. (1969). Jour. Iron & Steel Inst. Vol.207. 1960. pp.1639-1641.

STRECKER, E., RYDER, D.A. and DAVIES, T.J. (1975). Met. Tech. May 1975.

THOMPSON, A.W. (1979). Ductile Fracture Topography: Geometrical Contributions and Effects of Hydrogen. Met. Trans. Vol.10A. June 1979. pp.727-731.

THOMPSON. A.W. (1983). The Relation between Changes in Ductility and in Ductile Fracture Topography: Control by Microvoid Nucleation. Vol.31. No. 10. pp.1517.

THOMPSON, A.W. AND BERNSTEIN, I.M. (1979). Adv. Corros. Sci. Technol. (1979). Vol.7. pp.53-175.

THOMSON, R. and LIN, I.H. (1985) Fundamentals of Fracture. Hydrogen Degradation of Ferrous Alloys. eds. Oriani, Kirk and Smialowski. Noyes Pub. Park Ridge. New Jersey. 1985 pp.454-511.

TIEN, J.K., THOMPSON, A.W., BERNSTEIN, I.M. and RICHARDS, R.J. (1976). Met. Trans. A. Vol 7A. June 1976. pp.821-829.

TOWNSEND, H.E. (1981). A Study of the Entry and Removal of Hydrogen During Coating and Thermal Treatment of Steel. NACE. 1981. Vol.37. No. 2. pp. 115-119.

TROIANO, A.R. (1959). Corrosion 15. (1959). 207t.

TROIANO, A.R. (1960). Trans. ASM. 1960. Vol.52. p.54.

VEHOFF, H. and ROTHE. W. (1983). Acta. Met. Vol.31. pp.1781-1793.

WEST, A.J. and LOUTHAN, Jnr.M.R. (1979). Met. Trans. A. Vol.10A. 1979. pp.1679-1682.

WESTLAKE, D.G. (1969). Trans. ASM. 1969. Vol.62. pp. 1000-1006.

WHITE. P.E. (1987). Plated Coatings for Stainless Steel. Seminar - Engineering Coatings. CIT(SIS) Nov. 1987.

WILLIAMS, D.P. and NELSON, H.G. (1970). Met. Trans. Vol.1. 1970. p.63.

XIAN, A., HU, X., LI, P and WANG, Y. (1988). Hydrogen Trapping in Low Carbon Steels. Proc. Conf. Hydrogen and Materials. Beijing 9-13 May.1988.

YAMAKAWA, K., TSUBAKINO, H. and YOSHIZAWA, S. (1984). A New Electrochemical Hydrogen Probe. Corrosion Monitoring in Industrial Plants using Non Destructive Testing and Electrochemical Methods. ASTM. STP 908. Philadelphia 1984. pp.221-236.

YOKOBORI, T. (1965). Strength, Fracture and Fatigue of Materials. Eds. Groningen and P. Noordhoff. 1965. pp.22-28.

ZAKROCZYMSKI, T. (1985). An Electrochemical Method for Hydrogen Determination in Steel. NACE. 1982. Vol.38. No. 4. April 1982. pp.218-223.

ZAKROCZYMSKI, T. (1982). The Effect of Straining on the Transport of Hydrogen in Iron, Nickel and Stainless Steel. NACE. Vol.41. No. 8. Aug. 1985. pp.485-489.

ZAPPFE, C.A. and. SIMS, C.E. (1941). Hydrogen Embrittlement. Internal Stress and Defects in Steel. Trans. AIME. 1941. Vol.145. pp.225-261.